Stressed Astrocytes:

Insights on the Pathology of Alexander Disease

Eileen Guilfoyle

Submitted in partial fulfillment of the
requirements for the degree of
Doctor of Philosophy
in the Graduate School of Arts and Sciences

COLUMBIA UNIVERSITY

2013

ABSTRACT

Stressed Astrocytes: Insights on the Pathology of Alexander Disease

Eileen Guilfoyle

Alexander disease (AxD) is a rare and fatal neurological disorder caused by mutations in the gene that encodes glial fibrillary acidic protein (GFAP), an intermediate filament protein found in astrocytes in the central nervous system. The clinical presentations of AxD are diverse, ranging from onset in infancy to onset in early adulthood, and include seizures, psychomotor retardation, ataxia, and a variety of neurological signs related to abnormal brain stem function. The defining neuropathological hallmark is the presence of cytoplasmic, proteinaceous inclusions called Rosenthal fibers in astrocytes. Although *GFAP* expression is astrocytic, AxD patients also show de/dysmyelination and variable amounts of neuronal loss, most severely in infantile-onset patients. Astrocytes undergo severe morphological changes, beyond that of typical reactive astrocytes, and develop several forms of cell stress. However, how stressed astrocytes cause the loss of myelin in this disease is unknown. In this work I have conducted a largely immunohistological investigation of AxD patient tissue, model mice, and primary astrocytes cultured from the AxD model mice, focusing on factors that might provide insight into the pathological manifestations of AxD and paying particular attention to those factors which might contribute to de/dysmyelination.

To gain insight on the morphological transformation of astrocytes in AxD, I analyzed GFAP in the hippocampus of the most severely affected AxD mouse. Astrocytes in these mice lose their star-like shape, and become hypertrophic and often multinucleated. They accumulate large amounts of GFAP. Subsequent study of primary cultured astrocytes from AxD mice revealed that these cells have perinuclear inclusions of GFAP surrounded by displaced microtubules and displaced Golgi.

I next investigated another mechanism of stress that may affect astrocyte function in AxD. Work in our lab and others' has demonstrated proteasomal inhibition in AxD astrocytes. Because the unfolded protein response in the endoplasmic reticulum (ER) can be enacted by proteasomal inhibition, I examined the immunohistochemical expression of two proteins commonly increased under conditions of ER stress. We found BIP/Grp78, an ER chaperone, increased in AxD patient astrocytes and model mice. Additionally, the CCAAT enhancer binding protein homologous protein (CHOP) was expressed by a small subset of astrocytes in the AxD mouse hippocampus, unveiling ER stress as a potential contributory factor in AxD pathology.

Work in other labs has found iron in astrocytes in AxD model mice. To further elucidate mechanisms of cellular stress in AxD, I conducted an immunohistochemical analysis of iron and several regulatory proteins in AxD patients and found, by enhanced Perls' staining, Fe3+ in Rosenthal fibers and iron and ferritin accumulated in astrocytes. This finding is in marked contrast to what one sees in the normal CNS, with little staining of astrocytes, and easily detectable staining of oligodendrocytes.

Finally, I examined the localization of the cell surface glycoprotein CD44, along with several related proteins, including its ligand hyaluronan. I found CD44 protein expression greatly increased in the white matter, cortex and hippocampus of AxD patients and in the hippocampus of AxD mice. Additionally, through use of a biotinylated hyaluronan binding protein, I found abnormally high levels of hyaluronan in the hippocampus of AxD mice in the same areas where increases in CD44 were found. Work elsewhere has found CD44 and hyaluronan in other disorders that affect myelination, and experiments have revealed an inhibitory effect of hyaluronan on oligodendrocyte development and myelination.

The studies in this thesis contribute novel stressors to the list of those that impact astrocytes in AxD and, in particular, suggest the accumulation of iron in astrocytes as potentially important to the pathological manifestations of AxD. Additionally, my research has revealed dramatic increases in the expression of

CD44 in AxD astrocytes which, in conjunction with widespread increases in hyaluronan, may be critical to understanding the mechanisms underlying the de/dysmyelination that occur in this disease.

Table of Contents

Table of Figures

Chapter 4 Figures

Acknowledgements

I deeply thank my Ph.D. advisor and mentor, Dr. James E. Goldman, for his patience, support, encouragement and contribution to my scientific education. Though I had little previous experimental experience, Jim generously accepted me into his lab and allowed me to develop the technical skills I need in order to properly address scientific questions. His knowledge of biochemistry, neurobiology, medicine and glial cells were invaluable to my education, and his pleasant disposition made time in the lab enjoyable.

My work could not have been undertaken without the invaluable help of my collaborator and good friend, Sasha Sosunov. Sasha is a true genius with confocal miscroscopy and he took all of the confocal images within this thesis. Sasha's training as a neuropathologist, unflagging interest in Alexander disease and easy sense of humor made the hours at the confocal enjoyable and immensely educational. I thank also Xioping Wu and Guy McKhann for their collaboration and helpful conversations.

A special thanks to Markel Olabarria, whose own recent experience defending his Ph.D. made him an invaluable source of advice and encouragement. Markel helped me with cell counts and densitometry measures for this thesis, and I could not have completed the project without his help.

I thank my committee members Lloyd Greene, Ron Liem and Serge Przedborski for their constructive criticism, interest in my project and especially for their dedication to my training as a scientist, and Wilma Friedman for agreeing to serve as an outside examiner and for her enthusiasm for my topics. I also thank Ron in his role as director of the Integrated Program for allowing me the opportunity to study here at Columbia. I am indebted to Zaia Sivo and Ron for keeping me on track and moving me towards completion of my degree.

I am very grateful to Mika Melikyan and Carol Mason for generous donations of WT mice. Special thanks to Mika for training and for her always pleasant demeanor – I am deeply appreciative of her help. Carol Mason offered very generous encouragement and guidance to me and served on my qualifying exam committee, I thank her.

A very special thanks to Bernetta Abramson, our lab manager, who was always willing to extend a hand in times of need and whose sense of humor and friendship I have valued. Thanks also to all the current and former lab members and associates of the Goldman lab, especially Marisa Cotrina, Eunie Jang, Angelina Mela and Grace Lin, under whom I trained as a rotation student. Goumei Tang and Rujin Tian are former lab members who also studied Alexander disease and offered helpful suggestions – I am grateful for their guidance.

I am grateful to Peter Canoll and the Canoll lab members with whom we share lab meetings. Peter's attentiveness, insight and good humor were a reason to look forward to presenting at lab meeting. Thanks to Richard Valley and the Valley lab, for friendship and antibodies towards Golgi and microtubules that were used for this thesis work. Steven Spitalnik and Eldad Hod generously gave reagents for collaborations on cytokine assays. Eldad in particular has been extremely helpful and I am grateful to him for his guidance. For helpful discussions about iron and kind gifts of antibodies, I thank Jonathan Barasch and Neal Paragas. For initial aliquots of P-ERM and total ERM and helpful protocols, I thank Qin Wang. A special thanks to high school student Gabriella Carr for her expert technical help.

Bruce McEwen gave me generous and kind advice and offered invaluable opportunity to volunteer in his lab, I thank him and Gwen Wood for generously serving as my supervisor while in the McEwen lab.

Tim DeVoogtd encouraged me to applying to graduate school, and has been a critical point of support and guidance for me over these years. Thank you Tim! A very special acknowledgement to my good friends at Columbia, Shahrnaz Kemal, Punita Bhansali, and CaitlinLazar.

My two wonderful children Sophie and Gus Moody, are beacons of joy which guide me home I am deeply grateful for their their encouragement, love, and support over, especially over this past year.

Finally, I could not have even contemplated entering a full-time graduate program or completed the work required for this thesis without the loving support and unwavering encouragement of my husband, David Moody. He bore much of the responsibilities at home while having his own very demanding career. I am a fabulously lucky woman to have him in my corner.

Dedication

All of the work behind this thesis was completed in dedication to and loving memory of my mother, Patricia A. Guilfoyle.

Chapter 1

Introduction

Alexander Disease: a brief history

In 1949 W. Stewart Alexander, an Australian physician, described a case of a 15 month old boy who was admitted to the hospital presenting with progressive megalencephaly, hydroencephalus, frequent vomiting, psychomotor delays and almost continuous screaming and who died 4 weeks later of massive pulmonary emboli. Remarkably, the pathological examination revealed abundant inclusions in hypertrophic astrocytes that stained brightly for eosin and were located throughout the white matter and in subpial locations, especially surrounding blood vessels (Alexander, 1949). Pathologists would later identify these protein aggregates found within astrocytes as Rosenthal fibers (Eng et al., 1998), first described a case of syringomyelia (Rosenthal, 1898; Wippold et al., 2006).

Additional cases in infants and children were described, and although a range of clinical presentations were noted, all cases shared extensive, especially frontal, white matter loss or deficiency and the presence of Rosenthal fibers (Crome, 1953; Friede, 1964; Wohlwill et al., 1959). Authors of these papers and Alexander himself had proposed disease names, but in 1964 Friede jettisoned these and established "Alexander Disease" (AxD) eponymously honoring the physician who first described it (Friede, 1964).

Rosenthal fibers were also reported in cases involving older children and adult patients who presented with less severe features and had a slower clinical course (Herndon et al., 1970; Pridmore et al., 1993; Russo et al., 1976;Seil et al., 1968). Eventually, three clinical subtypes based upon age of onset were suggested to characterize AxD – infantile (onset within 24 months of birth), juvenile (onset from ages 2 through 14) and adult (onset over age 14) (Borrett and Becker, 1985; Pridmore et al., 1993; Russo et al., 1976). Infant patients typically suffer a disease course which includes seizures, megalencephaly, developmental delays and a leukodystrophy associated with severe loss of myelin in the frontal lobe. Death usually occurs within the first decade of life. The progression and clinical manifestations of juvenile and adult forms are usually less severe, but vary widely with bulbar symptoms, spasticity and

ataxia being common between them. While the disease course is sometimes slower in these AxD patients, it too is usually fatal.

Rosenthal fibers

Description

In reporting the sixth case of AxD, Friede stressed that the most consistent feature of all of the cases described were what we now know as Rosenthal fibers and this has held (Friede, 1964; Gorospe et al., 2002; Herndon et al., 1970; Li et al., 2005). These astrocytic inclusions are most easily found around blood vessels and at the pial and subependymal surfaces (see Fig 3A) and in infant cases predominate in the subcortical white matter (WM), but can be found in all regions of the CNS. Irregular in shape, some bead-like and others elongated, Rosenthal fibers have a distinct hyaline or glassy appearance, staining bright pink with eosin (Alexander, 1949; Crome, 1952; Wohlwill and Paine, 1958). Light and electron microscopic studies of patient tissue have reported a range of sizes, most between 10μm-40μm in length, but as small as 0.2 μm, and others as large 100μm in size (Herndon et al., 1970; Towfighi et al., 1983).

Ultrastructurally, Rosenthal fibers are electron-dense, granular and membraneless aggregates, which are in close association to intermediate filaments – many seeming to radiate from the electron dense core(s) (see Fig3B)(Borrett and Becker, 1985; Gullotta and Kuchelmeister, 1986; Herndon et al., 1970; Seil et al., 1968; Tihen, 1972; Tomokane et al., 1991; Towfighi et al., 1983; Walls et al., 1984; Wippold et al., 2006). Electron dense material can be a solid mass or loosely scattered deposits or a combination where a core (or cores) is surrounded by smaller deposits (Tomokane et al., 1991). Small deposits are thought to be an initial stage of Rosenthal fiber formation and these can sometimes be found in perinuclear locations (see Fig 3B) (Eng et al., 1998; Herndon et al., 1970; Townsend et al., 1985). Because some of these have been found in biopsies of children in early stages of diseases, it has been

hypothesized that Rosenthal fibers s start at this location and eventually travel to a resting location at astrocyte endfeet (Messing and Goldman, 2004).

There seems to be no correlation between numbers of Rosenthal fibers and extent of demyelination at autopsy (Friede, 1964). In general, the distribution of Rosenthal fibers correlates with GFAP levels, which are highest in the white matter and subpial locations.

Components of Rosenthal fibers

Immunohistochemical studies of AxD patient tissue have shown anti-GFAP staining around the periphery of Rosenthal fibers, corresponding to where filaments are seen ultrastructurally (Borrett and Becker, 1985; Goldman and Corbin, 1988; Janzer and Friede, 1981; Towfighi et al., 1983). However, immunogold electron microscopy studies have demonstrated that GFAP is a component of electron dense cores of Rosenthal fibers (Dinda et al., 1990; Johnson and Bettica, 1989; Tomokane et al., 1991), along with alpha B-crystallin and HSP27 (Tomokane et al., 1991). By this method, ubiquitin was found in the cores of smaller and scattered osmiophilic clumps while in larger cores, ubiquitin was found primarily in the outermost positions (Tomokane et al., 1991).

Rosenthal fibers were partially purified biochemically from the AxD brain by the Goldman lab using 2% SDS and found to contain GFAP, ubiquinated alpha B-crystallin and HSP27 (Goldman and Corbin, 1991; Iwaki et al., 1989; Iwaki et al., 1992). By immunostaining, Rosenthal fibers were also found to contain the S20 proteasome (Tang et al., 2010), p62, LC3 (Tang et al., 2008), p-JNK (Tang et al., 2006) and Plectin, a cytoskeletal linker (Tian et al., 2006).

Rosenthal fibers are not unique to AxD

While AxD is best defined from a pathologist's perspective by the presence of Rosenthal fibers, these inclusions are not unique to the disease and are also found surrounding reactive lesions such as slow growing tumors, cysts, vascular malformations and in some cases of chronic inflammation like glial scars

in multiple sclerosis. They are perhaps best known in pilocytic astrocytomas, but have also be found in other neoplasms such as ganglioglioma (for more complete list, see Fig 4) (Wippold et al., 2006).

Nickel implantation controversy

Intriguingly, Rosenthal fiber-like structures also have been found in the endfeet of astrocytes in the rat brain after nickel implantation (Kress et al., 1981). Because blood brain barrier disruption was also found in these rats, the authors hypothesized that Rosenthal fibers contained plasma proteins engulfed under circumstances of chronic blood brain barrier disruption. This was a controversial proposal, but there was support (Herndon, 1999). While there have been reports of lymphocyte invasion in AxD, especially in the brain stem (Rankin et al., 1977; Russo et al., 1976; Soffer and Horoupian, 1979; Towfighi et al., 1983), widespread inflammation or blood barrier disruption has not been suggested and at least one of these reports may be due to reported concomitant viral infection (Soffer and Horoupian, 1979). Subsequent to the Kress et al. publication, Rosenthal fibers were found negative by immunostaining for serum proteins such as globulins, albumin and fibronectin (Seil et al., 1968; Tomokane et al., 1991; Towfighi et al., 1983). Moreover, subsequent research does not support that Rosenthal fibers are due to disruption of the blood brain barrier, and the Rosenthal fiber-like structures found by Kress et al. were determined not to be Rosenthal fibers (J. Goldman, unpublished observation).

GFAP protein and *GFAP* mutation

GFAP protein

GFAP was first purified from plaques obtained from post-mortem tissue from multiple sclerosis patients (Eng et al., 1971). The human gene resides on chromosome 17q21 and encodes a 432 amino acid long polypeptide with a molecular weight of 55 kDa (Bongcam-Rudloff et al., 1991; Reeves et al., 1989). The gene has nine exons and shows high homology between species (Isaacs et al., 1998; Reeves et al., 1989). Specifically, human and mouse *GFAP* show high homology (Brenner et al., 1990). GFAP shares the highly conserved structure of other intermediate filament proteins – a central alpha-helical rod domain flanked

by a non-conserved n- terminal head and c-terminal tail which allow many of these proteins to interact and form the characteristic approximately 10nm diameter filaments (Geisler and Weber, 1982; Parry and Steinert, 1992; Steinert and Roop, 1988). Intermediate filament proteins have been classified into subtypes based upon similarities in the amino acid composition of the rod domain, the overall charge of the protein and the predicted structure and ability to co-assemble with other intermediate filaments (Steinert and Roop, 1988). Using these classifications, GFAP is a type III intermediate filament protein, along with vimentin, with which it can interact.

In the mature CNS, GFAP is expressed in astrocytes of the white matter and hippocampus and in those found at the sub-pial and sub-ependymal areas. They are also found in neuronal precursor cells in the subgranular zone of the hippocampus (Doetsch et al., 1999) and subependymal layer of the cerebral cortex (Roelofs et al., 2005). Outside of the CNS, GFAP is found in the perisinusoidal stellate cells of the liver and its expression decreases as these cells differentiate (Buniatian et al., 1996a; Buniatian et al., 1996b).

GFAP has several splice isoforms. Astrocyte lineage cells express GFAP alpha predominantly. GFAP beta is found mainly in the peripheral nervous system, expressed at low levels by Schwann cells (Hagiwara et al., 1993), whereas GFAP gamma is found both in the CNS and in mouse bone marrow and spleen (Brenner, 1994; Zelenika et al., 1995). Delta GFAP (Condorelli et al., 1999), also known as epsilon GFAP (Hol et al., 2003; Nielsen et al., 2002a), is also expressed in the CNS, varies from the other isoforms in that its c-terminal tail is almost entirely unique in amino acid sequence (Hol et al., 2003).

GFAP Mutations

Background

Prior to the events which led to the discovery that *GFAP* mutations were the basis of most AxD cases, thought on the origin of the disease were mixed. Rare familial cases were identified, but the majority of

reported disease cases did not appear to be passed on from parents (Johnson et al., 1996; Pridmore et al., 1993; Schwankhaus et al., 1995). The sporadic nature of the disease with its wide range of clinical manifestations and ages of onset (Borrett and Becker, 1985; Herndon et al., 1970; Pridmore et al., 1993; Russo et al., 1976; Springer et al., 2000; van der Knaap et al., 2001) made it unclear if AxD was genetic or environmental (Pridmore et al., 1993), though if genetic, it was postulated to be a recessive mutation based upon the number of unaffected parents and family members (Reichard et al., 1996).

An unexpected and monumental leap in the understanding of the origin of AxD was made by Messing et al. with the development of a glial fibrillary acidic protein (GFAP) transgenic mouse (Messing et al., 1998). This mouse carries several copies of the human *GFAP* gene driven by its own promoter in addition to the endogenous murine *GFAP* and was developed to study the role of elevated GFAP levels in reactive gliosis (Messing et al., 1998). Concomitant with very high levels of GFAP, these mice were found to have astrocytes with enlarged cell bodies and, by GFAP immunostaining, hypertrophic cell processes. Surprisingly, some astrocytes were found to contain Rosenthal fibers. Ultrastructurally, these Rosenthal fibers were found to be identical to some found human AxD patients. Cultured primary astrocytes from these mice displayed perinuclear inclusions that bore high similarity on an electron-microscope level to similarly-located Rosenthal fibers from a 17-month old infant (Eng, 1985). These findings made a powerful case that Rosenthal fibers were a cell autonomous response to excess GFAP and that AxD was, in fact, a primary disorder of astrocytes.

GFAP had been earlier been proposed as a candidate gene responsible for AxD (Becker and Teixeira, 1988). It was not until Rosenthal fibers were found in GFAP transgenic mice, and DNA sequencing became feasible that the gene for this intermediate filament protein gene became the prominent candidate for AxD and the *GFAP* gene from patients was probed for mutations. In 2001 Brenner et al. significantly advanced the field by reporting they had amplified and sequenced each exon and several

adjoining introns of the *GFAP* gene from 11 AxD patients whose diagnosis had been confirmed at autopsy and found that 10 of 11 contained non-conservative, heterozygous missense mutations in *GFAP* while two control leukodystrophy cases were found be normal. The heterozygosity of the mutation suggested that the *GFAP* mutation was acting in a dominant fashion. The missense mutations all affected Arginine residues at four different positions, which were located on both the rod and tail regions of the protein. Parental DNA, where available, was analyzed specifically for the mutations found in their children and all were found to be normal, demonstrating that these particular mutations arose sporadically and thus the disease was not genetically based(Brenner et al., 2001).

A total of 78 unique mutations in the coding region of GFAP account for most of the currently diagnosed cases of AxD (Prust et al., 2011) (see Fig 5). Most of AxD mutations allow the mutated proteins to dimerize and assemble into 10nm filaments with the exception of R416W, which aggregates into broader and shorter configurations (Nielsen et al., 2002b). The mutated proteins, however, have been found to form aggregates in cells and in primary culture, which inhibits proteasome activity (as reviewed by Brenner et al., 2008).

Gain-of-function mutation

The full role of GFAP has not been fully elucidated, so it is impossible to rule out the possibility that AxD pathology comes from a loss-of-function. Arguments that disease mutations are gain of function have predominated in reviews in the literature (Messing et al., 2001a; Messing et al., 2001b; Messing et al., 2012b; Quinlan, 2001). The first argument proposed is that GFAP null mice do not have Rosenthal fibers or any pathology resembling AxD. The phenotype of GFAP null mice is extremely subtle – they have full lifespans, reproduce normally and have unimpaired gross motor skills (Pekny et al., 1995; Shibuki et al., 1996) and are no different than wild type mice (WT) in response to several injury paradigms including kainic acid administration and stab wound (Gomi et al., 1995), but do show susceptibility to blunt head

injury (Nawashiro et al., 1998), ischemia (Nawashiro et al., 1998; Tanaka et al., 2002) and hypotonic stress (Anderova et al., 2001), though mechanisms are unknown. Minor changes in astrocyte morphology vis-a-vis shortened processes were shown with ultrastructural and dye injection studies (Anderova et al., 2001; Liedtke et al., 1996; McCall et al., 1996). Other studies suggested primary astrocytes from *GFAP*-null mice had altered expression of extracellular matrix (ECM) components, but this isn't entirely clear from *in vivo* studies (Wang et al., 1997). Additionally, blood brain barrier alterations were found *in vivo* and suggested in a cell culture model (Liedtke et al., 1996; Pekny et al., 1995). The second argument is that only overexpression of *GFAP* or missense mutations of the disease can cause Rosenthal fibers or other pathology seen in AxD (Quinlan, 2001). Finally reviewers make the case that most of the missense mutations in AxD allow for filament formation are not like null, nonsense or frameshift mutations that may occur in other intermediate filament disorders where there is loss of function.

GFAP mutations alone do not seem sufficient for the phenotype

Two arguments have been raised in support of the proposition that *GFAP* mutations alone may not be sufficient for the phenotypic expression of the disease and that genetic or environmental modifiers may be necessary to trigger the disease in affected individuals. First, there are adult individuals who have *GFAP* mutations but who are as of yet asymptomatic. These were identified as part of analysis of the DNA of relatives of patients in the three familial cases of AxD (as reviewed by Messing et al., 2012a). While some have suggested inherited *GFAP* mutations act at nearly 100% penetrance (Messing et al., 2012a; Stumpf et al., 2003), this estimate seems questionable because it is based only on the percentage of individuals whose DNA was analyzed, while more than half of unaffected siblings of affected individuals in these families have not been tested for *GFAP* mutations. Two adult siblings in these families whose ages have not been revealed to protect their identity are positive for the mutations of their siblings but as of publication of the review in early 2012, are unaffected.

The second argument that there may be additional factors at hand other than *GFAP* mutations in AxD is that identical genetic mutations of GFAP rarely produce common ages of onset, clinical symptoms or disease courses. This has been most frequently noted in the R416W mutations which can be both type I and type II (or Infant, Juvenile and Adult onset) (Brenner et al., 2001; Gorospe et al., 2002; Li et al., 2006; Thyagarajan et al., 2004). It should be noted that the leukodystrophies express similar variables in expression.

Support for this argument comes from the fact that AXD cases have been found to present with other genetic mutations or after illnesses. For example, laboratory testing of an infant onset type I patient who presented with refractory epilepsy and hypotonia found increased concentrations of lactate in the plasma, mitochondria with structural abnormalities and decreased cytochrome-c oxidase activity – collectively suggesting mitochondrial disease. MRI examination was conducted at 5 months and while the child showed some WM abnormalities, AxD was not suspected. At 14 months the changes were consistent with diagnosis of AxD and the child was subsequently found to have a unique mutation (N386I) in the tail region of GFAP (Caceres-Marzal et al., 2006). Neither parent bore a *GFAP* mutation. This child suffered a severe course of progress of the disease and died at the age of 22 months. While some cases of AxD and intermediate filament diseases may cause apparent mitochondrial abnormalities, the nature of the defects found in this child were very unlikely secondary to AxD (Brenner et al., 2008). Another patient was found to have one of twelve reported R88C mutations and also had a rare polymorphism of mitochondrial DNA which had been previously found in a patient with mitochondrial myopathy. Although this patient was reported to undergo a less severe course of AxD than most others with this mutation and still lives (Brenner et al., 2008), it is plausible that the mitochondrial dysfunction in this case may have contributed to the onset and the severity of the disease.

Potential environmental triggers may be ones that can produce increased levels of GFAP, such as brain trauma, high fever and infection which push GFAP levels over a threshold. This may be the case in a patient whose onset of seizures symptomatic of AxD occurred after receiving a polio vaccine at four and a half months an experiencing a high fever. Other cases have been reported which presented after brain trauma (Namekawa et al., 2002) and high fever and /or infection (Herndon et al., 1970; Kyllerman et al., 2005; Shiroma et al., 2003), and several adult cases have presented after prolonged medical illness (Mastri and Sung, 1973; Riggs et al., 1988; Schwankhaus et al., 1995)

AxD is an astrogliopathy

Because heterozygous mutations in the gene encoding the intermediate filament GFAP have been found in most cases of AxD (Brenner et al., 2001; Li et al., 2005; M et al., 2009), and this protein is predominantly expressed in astrocytes, the disease is considered the best example of a disorder that is primary to these glial cells, or an astrogliopathy. Upon observing what we now know as Rosenthal fibers in astrocytes, Alexander presciently predicted the disease to be an astrocytic disorder. While this was later opposed (Crome, 1953; Herndon, 1999; Vogel and Hallervorden, 1962), the concept of an astrocytic disease gained support when Friede's pathological study showed a consistent involvement of "eosinophilic deposits" in astrocyte endfeet (Friede, 1964). While *GFAP* is expressed in neural stem cells and in non-myelinating Schwann cells of the peripheral nervous system, none of these cells have Rosenthal fibers nor are tissues where these cells types reside affected with any pathology, possibly suggesting that to manifest itself, GFAP levels in cells need to reach a certain threshold (as reviewed by Messing et al., 2012a).

Though AxD is a primary disease of astrocytes, astrocyte loss has not been extensively documented. Pathological examinations of patient tissue have noted a loss of oligodendrocytes, CA1 neurons and axonal degeneration and the activation of microglia (Gorospe et al., 2002; Walls et al., 1984).

AxD and other leukodystrophies

De/dysmyelination in AxD

The mechanism by which this primary disease of astrocytes causes de- and dysmyelination is not known. Diseased astrocytes may be deficient in their ability provide oligodendrocytes or lineage cells with essential trophic factors or impaired in their ability to make contact with these cells. Astrocytes could themselves be the source of inflammatory or toxic factors or activate other cells such as microglia to become toxic to oligodendrocytes. One major mechanism by which astrocytes in AxD could damage other cells in the CNS, including oligodendrocytes, is through the loss of normal function in glutamate uptake and potassium and other ion buffering. Deficits in astrocytic ability to perform normal regulatory functions in the CNS could create a toxic environment and be damaging to oligodendrocytes and neurons.

Leukodystrophies

AxD is classified as a leukodystrophy, however there are two distinct patterns of myelination defects in this disease that can be detected by Magnetic Resonance Imaging (MRI). The first, which occurs in infant onset, type I patients, is characteristic of a leukodystrophy and involves a symmetric loss and frontal predominance (See Fig 1 and Fig 7, right). The other is that more typical for type II patients and involves the brain stem and cerebellum.

Genetic disorders which cause a defect directly related to the synthesis and maintenance of myelin are called leukodystrophies, while disorders causing secondary myelin damage are called leukoencephalopathies (Kohlschutter and Eichler, 2011). The former term, however, is used more broadly to describe hereditary or metabolic white matter abnormality (Barkovich and Messing, 2006). AxD shares with other leukodystrophies variable age of onset – infant, juvenile and adult - and a variety of manifested phenotypes, sometimes based upon the severity of mutation, but also within identical genetic mutations (as reviewed by Kohlschutter and Eichler, 2011). The variable age of onset for

leukodystrophies is most likely is due to the fact that while the majority of myelination occurs during the first two years of life, the process in some parts of the brain may not be complete until adolescence or young adulthood (as reviewed by Baumann and Pham-Dinh, 2001; Gorospe and Maletkovic, 2006). Like Canavan disease, megalencephalic leukodystrophy with cysts and vanishing WM disease, AxD shows a frontal predominance. And like X-linked adrenoleukodystrophies and megalencephalic leukodystrophies, "U fibers," or the white matter just under the cortex, are often spared (Friede, 1964; Kohlschutter and Eichler, 2011). However, while other leukodystrophies, like X-linked adrenoleukodystrophies and megalencephalic leukodystrophies are active demyelinating, AxD does not show similar progression on an MRI, so appears to perhaps be a dysmyelinating disorder (van der Voorn et al., 2009). While Leigh's syndrome does not produce typical frontal myelin loss, it is symptomatically similar to AxD and before genetic testing the two diseases were sometimes confused.

Diagnostic tools

Because the most common mutations in GFAP have been identified, DNA sequencing for mutations in GFAP has been established as the gold standard to confirm a diagnosis for AxD (Brenner et al., 2001). While there are no molecular markers specific for AxD that are currently known, laboratory tests are helpful in the context of ruling out other disorders, especially leukodystrophies, which do possess specific or suggestive molecular markers. While GFAP has been found in the CNS of three out of three patients tested (Takanashi et al., 1998), the intermediate filament is similarly found in a wide range of neurological conditions and is not specific to AxD (Liem and Messing, 2009). Early in the disease, an extremely reliable diagnostic tool was brain biopsy and histological examination for the presence of Rosenthal fibers, but this has been largely done away with in favor of genetic sequencing.

MRI patterns of AxD

MRI is a highly sensitive and specific tool for analyzing deficits in myelin and myelination and has proved powerful in diagnosing AxD (Hess et al., 1990; Takanashi et al., 1998; van der Knaap et al., 1996; van der

Knaap et al., 2001; van der Knaap et al., 1995). For a disease of such diverse clinical features, MRIs of type I cases are remarkably consistent (Prust et al., 2011; van der Knaap et al., 2001) and have a characteristic frontal predominance of white matter loss (see Fig 6) and symmetric white matter abnormalities (see Fig 1, center), however, this is shared with other leukodystrophies, especially ones with a metabolic basis like metachromatic leukodystrophy.

Diagnosis of the disease took a significant leap in 2001 when van der Knaap et al. established criteria to be used for MRI diagnosis of AxD. The authors analyzed the MRIs of three AxD patients who had autopsy confirmation of diagnosis, and established five MRI criteria for AxD – four of which had to be met to establish diagnosis. They then applied these to 217 cases of children with leukoencephalopathy of unknown origin and 19 cases fulfilled these criteria. Four of these children were subsequently tested by biopsy and all were confirmed as AxD (van der Knaap et al., 2001). These criteria were a significant advance in the field (Gorospe et al., 2002; Prust et al., 2011) and are considered highly reliable for diagnosis (Barkovich and Messing, 2006; Kohlschutter and Eichler, 2011).

Because adult patients have less regular and often focal demyelination, their cases have been cases have been confused with Multiple Sclerosis (Herndon et al., 1970; Li et al., 2005; Schwankhaus et al., 1995; Seil et al., 1968) or low grade gliomas (Duckett et al., 1992), especially pilocytic astrocytomas, putatively because the presence of Rosenthal fibers creates similar spectra on MRIs (van der Voorn et al., 2009). And in fact diagnostic distinction between reactive gliosis and low-grade infiltrating gliomas sometimes presents a pathological challenge (as reviewed by Rivera-Zengotita and Yachnis, 2012)

Age of onset: an important indicator of AxD severity

From the identification of the first Infant, Juvenile and Adult cases, age of onset has been recognized as an important indicator of AxD severity (Borrett and Becker, 1985; Pridmore et al., 1993; Russo et al., 1976). However, recently, Prust along with 33 co-authors published an impressive study which reviewed

185 previously reported cases of AxD along with 30 new cases, assessing clinical and radiologic data (Prust et al., 2011). They assessed the relationship between age of onset and clinical data, and used Wilcoxan rank sum tests to identify variables associated with survival. Not surprisingly, these authors found that earlier age of onset was a strong predictor of severity of both a patient's clinical manifestations and the results of MRI. The authors found onset earlier than the age of four was predicted by seizures, febrile seizures, motor delay, cognitive delay, history of failure to thrive, history of paroxysmal deterioration (that associated with an illness or injury), macrocephaly and classical MRI features of AxD as defined by van der Knapp (see diagnosis, above) except for those related to brain stem abnormalities. Clinical phenotypes that predicted late onset (greater than the age of four) were bulbar symptoms, autonomic dysfunction, gait disturbance, ataxia, dysarthria, dysphonia, ocular movement abnormalities and palatal myoclonus and MRI being "atypical," with respect to van der Knaap et al. criteria (van der Knaap et al., 2001). The abnormalities most commonly seen through magnetic resonance imaging MRI in adult patients were posterior white matter fossa abnormalities and atrophy of the brain stem, atrophy of the cerebellum or atrophy of the spinal cord (see Fig 1).

Classifications of AxD – type I and type II

While acknowledging age of onset as an important predictor, Prust et al. argue for a more nuanced view of AxD. Using statistical methods to analyze the age of onset in 215 cases and 6 dichotomous variables that the authors judge to represent the phenotypic spectrum of AxD expressed across the lifespan, as well as an assessment of MRI data as being typical or not according to accepted standards set by van der Knapp (van der Knaap et al., 2001) to fit a latent class analysis, Prust et al. identified "type I" as a more severe form of the disease and "type II" as a less severe form (Prust et al., 2011). (See Fig 2). They obtained admirable correct class membership assignments with 0.96 for type I and 0.90 for type II. Post hoc analysis showed that patients with type I AxD usually presented before the age of 4, while type II patients developed clinical signs and symptoms throughout their lifespans. Survival analysis predicted

that there was a 2.0 fold increase in incidence of mortality for type I patients (mean survival 17.3 +/- 3.6) over type II patients (mean survival 25.0 +/- 1.9). This study significantly simplified classification of disease severity among the many ages of patients it affects and will be useful to describe patients who are symptomatically more like patients who typically present at other ages of onset. For example for the 10% of patients assigned to type I who presented after the age of four and the approximately 28% of type II patients presented before this age. This classification will be especially useful in conjunction with age-of-onset and, where applicable, age at death to give a concise, if not altogether thorough understanding of a patient's disease course.

AxD mouse models

Several lines of GFAP transgenic mice have been developed which have the WT, human *GFAP* expressed in several copies and driven off of its own promoter (Messing et al., 1998). Lines of this mouse expressing the highest levels of human *GFAP* died by 14 days postnatal of unknown causes and these contained more Rosenthal fibers than did lines which expressed less human *GFAP* and had a normal lifespan. The current transgenic mouse line that is used (73.7) is less in body weight than its normal counter parts but lives a normal lifespan (Hagemann et al., 2005). In addition to the human GFAP transgenic 73.7 (**Tg**) mouse, several knock-in lines have been developed (Hagemann et al., 2006) which reproduce the genetic modifications found in AxD by expressing missense mutations in one copy of the mouse *GFAP*. The R76H mouse carries the mouse homologue to human R79H while the R236H mouse carries a genetic change analogous to R239H in AxD patients – the most lethal of all AxD mutations (Hagemann et al., 2006). Because the R236H mouse has the most severe phenotype and because it is the only knock-in mouse I use for our studies, I will limit all further references to knock-in (**KI**) mice to it, unless otherwise specified.

Both the KI and Tg mice have increased levels of GFAP protein as determined by ELISA and have Rosenthal fibers, though fewer Rosenthal fibers than is typically seen in patients and not generally at blood vessels (Hagemann et al., 2006; Hagemann et al., 2005; Messing et al., 1998). However, the mice have relatively normal lifespans, show no show detectable myelin loss, and appear to have normal levels of myelin basic protein (Hagemann et al., 2006). KI mice were found to be substantially more susceptible to Kainic acid induced seizures and subsequent neuronal damage compared with WT mice (Hagemann et al., 2006). Additionally they die after seizure at much greater numbers than do WT mice.

A third type of mouse is derived from mating the TG mouse with the KI mouse (**Tg/KI**). This mouse has a particularly severe phenotype and dies between four and five weeks, from seizures, but like the Tg and KI mice, the Tg/KI mouse is reported to show no indication of myelin abnormalities (Hagemann et al., 2006; Hagemann et al., 2012). It is also known that there is a synergistic increase in the amount of GFAP protein they produce and the insoluble fraction of GFAP protein almost doubles over that of the Tg mouse (Hagemann et al., 2006).

AxD and cellular stress

AxD patients and model mice, flies and primary astrocytes and cell lines expressing mGFAP and/or transgenic GFAP have been found to undergo many biochemical changes, which may involve or are indicative of a stress response as they accumulate high levels of GFAP. Some of these are discussed below.

Heat shock proteins

One of the first indicators of a stress response in AxD was the discovery that the heat shock proteins alpha B-crystallin (Iwaki et al., 1989) and HSP27 (Iwaki et al., 1992) are major constituents of Rosenthal fibers. Furthermore, the mRNA transcript and protein expression of these heat shock proteins by Western blot were both found elevated in brains of AxD patients (Head et al., 1993).

Proteasomal inhibition in AxD

The ubiquitin-proteasome pathway is the primary pathway for elimination of cytosolic proteins. The proteasome is composed of a 20S core where proteins are degraded via three catalytic enzymatic activities – trypsin-like, chymotrypsin-like and peptidyl-glutamyl peptide hydrolase-like (PGPH) (Pickart and Cohen, 2004) – and the 19S lid that possesses ubiquitin receptors and ATPase activity, which strips ubiquitin from substrates before they are presented to the 20S proteasome (Vembar and Brodsky, 2008). Accumulation and aggregation of misfolded proteins associated with pathological conditions, including CNS disorders, have been hypothesized to occur because of defects in either the ability of mutant proteins to bind the proteasome or the impaired proteolytic capacity of the cell (as reviewed by Johnston, 2006).

Inroads leading to an understanding of how a mutation in an intermediate filament protein can be so pernicious have been made by the Goldman lab. Tang et al. demonstrated that there is decreased proteasomal activity in AxD patient tissue by showing significantly decreased degradation of chymotrypsin and PGPH substrates in lysates of frozen autopsy tissue obtained from the white matter of patients with the R239C, R239H and the R416W mutations versus controls (Tang et al., 2006). The authors also suggest that astrocytes may be involved in this impairment as that the 20S proteasome and ubiquitin are localized to Rosenthal fibers in patient tissue immunohistochemistry (Tang et al., 2006). Additional support for proteasomal inhibition in AxD astrocytes comes from Cho et al., who found proteolytic activity impaired in primary astrocytes from Tg and KI mice (Cho and Messing, 2009).

In vitro experiments by Tang et al. demonstrated that, like other intermediate filament proteins, both WT human GFAP and R239C are able to bind the 20S proteasome in both the Triton-X soluble (or "unassembled") and the pellet (or "assembled") fraction via reciprocal co-immunoprecipitation and *in vitro* co-sedimentation assays in transfected COS7 cells (Tang et al., 2010). The "unassembled" mutant GFAP significantly inhibited proteasome activity *in vitro*. Furthermore the "unassembled" mutant GFAP

comprised a collection of oligomers, the largest ones not seen in the "unpolymerized" WT GFAP. The addition of alpha B-crystallin to the mutant GFAP oligomers returned the size distribution of the population to the WT GFAP distribution and also relieved the proteasome inhibition. Additionally Tang and colleagues showed that U251 cells stably expressing WT or R239H GFAP and exposed to the proteasomal inhibitors MG132 and lactacystin show an increase in GFAP by Western blot indicating a feed forward mechanism by which GFAP is increased in AxD (Tang et al., 2006). Proteasomal inhibition in these cells activate the mitogen-activated protein kinase stress pathways leading to the activation of JNK and p38 map kinases and these in turn activate AP-1 transcription factors, increasing the transcription of GFAP.

Autophagy is indicated in AxD

Autophagy is another means by which Rosenthal fibers in AxD patient tissue are surrounded by positive signal for an antibody against LC3, a marker for autophagosomes (Tang et al., 2008). Electron microscopic images of AxD patient tissue and AxD mice show double membraned autophagosomes in close proximity to Rosenthal fibers (Tang et al., 2008). These results suggest that autophagy may b**e** increased in AxD astrocytes in order to degrade GFAP and other proteins associated with Rosenthal fibers or these characteristic protein inclusions themselves.

Oxidative stress

AxD patients, model mice and model flies all have indications of oxidative stress. Rosenthal Fibers were found to contain a pyrrole modification arising from the lipid peroxidation product 4 hydroxy-2-nonenal (HNE) (Castellani et al., 1998). Both Tg and KI mice crossed to a reporter mouse expressing a transgene consisting of the core antioxidant response element (ARE) from the NADH quinone oxidoreductase (Nqo1) promoter placed in front of the human placental alkaline phosphatase gene (ARE-hPAP) showed robust antioxidant gene expression (Hagemann et al., 2006; Hagemann et al., 2005). In the KI mice these ARE-hPAP expressing cells were found in the hippocampal fissure, corpus collosum, cingulum, rostral

migratory stream, lateral olfactory tract and glomerular layer of the olfactory bulb. Interestingly, the only subset of GFAP positive cells in these mice expressed ARE-hPAP (Hagemann et al., 2006).

Inducible expression of ARE-driven genes is thought to be largely mediated through Nrf2 (Chan and Kan, 1999; Itoh et al., 1997; Itoh et al., 1999), a transcription factor activated under conditions of oxidative stress (as reviewed by Hayes and McMahon, 2001) and which mediates many phase II detoxification response genes. In a microarray gene expression analysis of the olfactory bulb of the AxD Tg mice, at 3 week (early) and 4 month (late) time points, many genes driven by Nrf2 were found upregulated both early and late, indicating that oxidative stress response is an early phenomena (Hagemann et al., 2006). It should also be noted that in addition to Nrf2, other nuclear transcription factors including c-Jun, Nrf1, Jun-B, and Jun-D can bind to the ARE and regulate expression and induction of NQO1 gene (Jaiswal, 2000)

Oxidative stress may also be indicated by the presence of iron found increased in astrocytes of AxD model mice, where it is normally found in oligodendrocytes. Fe3+ iron was found by modified Perls' stain to be greatly increased in astrocytes of the olfactory bulb and hippocampus in AxD KI and Tg mice, and this was also found true for ferritin by immunostaining (Hagemann et al., 2006; Hagemann et al., 2005; Hagemann et al., 2012).

Primary astrocytes from AxD KI and Tg mice are more susceptible to H_20_2 toxicity than those from wild-type counterparts, and this may be an indication that that iron is too elevated in these cells, making Fenton chemistry possible (Cho and Messing, 2009).

In a Drosophila model of AxD, expression of human R79H GFAP (and to a lesser extent, WT hGFAP) in glia produces Rosenthal fiber-like aggregates, and a non-cell autonomous oxidative stress response that is toxic, through glial glutamate transporters, to neurons (Wang et al., 2011). Overexpressing heat shock proteins/chaperones ameliorates both Rosenthal fiber-like aggregation and the neuronal lethal

phenotype, while overexpressing antioxidant genes or treating with oral antioxidants attenuates the lethal phenotype, but have no effect on aggregates (Wang et al., 2011). These data suggest oxidant stress as a primary mechanism in AxD neurotoxicity (Wang et al., 2011).

Impaired glutamate uptake and astrocyte coupling in AxD

AxD KI mice lose expression of Glt-1 and have compromised glutamate uptake (Tian et al., 2010). Both Glt-1 protein and transcript are found reduced in the Tg/KI mice (Hagemann et al., 2009), and collaborative work on Tg/KI mice that will be published along with some of the work in this thesis has confirmed and extends this, demonstrating not only impaired glutamate uptake and loss of GLT-1 in Tg/KI mice, but also loss of coupling of astrocytes (Sosunov et al., 2013).

Reactive astrocytes

The condition of reactive astrocytes – astrogliosis, or reactive astrocytosis – has many defined characteristics, but is often detected by an increase in the amount of GFAP immunoreactivity (GFAP-IR) (as reviewed by Eddleston and Mucke, 1993). The hypertrophied or enlarged appearance of GFAP processes on astrocytes is a characteristic response to injury, inflammation, viral infection and degenerative diseases of the CNS. The expression of GFAP can be induced by cytokine production by infiltrating mononuclear cells and/or resident microglia and autocrine stimulation by factors such as LCN2 (Zamanian et al., 2012).

Astrocyte proliferation during astrogliosis

Astrocytes have been shown to proliferate during models of astrogliosis. Stab wound induces [3H]thymidine incorporation into cells that also expressed GFAP (Miyake et al., 1988). More recently, fate mapping studies have shown that while most reactive astrocytes are derived from phenotypic transformation of existing astrocytes, a small subset of astrocytes do in fact divide after stab wound (Buffo et al., 2008) and after the induction of experimental autoimmune encephalomyelitis (EAE) (Guo

et al., 2011). In the EAE spinal cord only fibrous astrocytes in the white matter divide and proliferate while the reactive astrocyte population in the grey matter is derived exclusively from phenotypically transformed protoplasmic astrocytes.

The detrimental effects of reactive astrocytes have been especially noted with respect to myelination, perhaps because they are more apparent, but more recently reactive astrocytes have been shown to be essential for the beneficial effects of withstanding CNS injury, and improving recovery after experimental autoimmune encephalomyelitis, particularly in their ability to prevent invasion by inflammation producing cells (Bush et al., 1999; Faulkner et al., 2004; Voskuhl et al., 2009).

Expression of stem cell-like or early genes in reactive astrocytes

Subsets of reactive astrocytes are able to show features of stem and progenitor cells (Buffo et al., 2010). Reactive astrocytes re-express many proteins present in high amounts during development in precursor cells such as, vimentin and nestin, but are absent or less present in mature cells (Fawcett and Asher, 1999; Ridet et al., 1997). The reactive response in terms of gene expression is heterogeneous to specific type of CNS insult at an early timepoint after injury (Zamanian et al., 2012). The morphological transformation of reactive astrocytes also varies in severity, as well as upon distance from the wound or neuropathological lesion.

Reactive astrocytes are not homogeneous

A recent and microarray study used GFP transgenic mice driven from the Aldh1l1 promoter, a gene which codes formaldehyde dehydrogenase 1 family, member L1, a protein found in all astrocytes, unlike GFAP. The authors identified a set of genes differentially regulated by astrocytes isolated from mice one day after undergoing reactive gliosis in two separate models of brain injury – ischemia produced by middle cerebral artery occlusion and intraperitoneal lipopolysaccharide (LPS) injection. While approximately half of the genes differentially expressed were common to both models of reactive

gliosis, the other half was unique to each injury model, indicating that while reactive astrocytes have common markers, astrogliosis, at least in the one day post injury timeframe the authors chose to document, is a heterogeneous response specific to the injury type (Zamanian et al., 2012).

The transcripts that were most highly induced and common to both models of injury were Lcn2 and Serapina3n. Lcn2 codes for lipocalin2, a secreted protein which has increased expression in a wide variety of pathological states and which has bacteriostatic effects through its capture and depletion of iron binding molecules called siderophores that are used by some bacteria as a means of iron acquisition and which may be involved in cellular iron acquisition and/or depletion (Goetz et al., 2002; Schmidt-Ott et al., 2007; Yang et al., 2002). Lcn2 has recently been implicated as an autocrine mediator of reactive gliosis through upregulation of GFAP in astrocytes (Chia et al., 2011; Lee et al., 2009). Serapina3n is an inhibitor of peptidase activity and its expression is increased after nerve injury and inflammation (Gesase and Kiyama, 2007; Takamiya et al., 2002).

Thesis overview

In **Chapter 2**, I undertake an immunohistological examination of GFAP expression in astrocytes in mouse models to gain insight on how their transformed shape and other endogenous stressors might impact other cells in the CNS.

In **Chapter 3**, I explore the causes of demyelination more directly by examining the expression of CD44, a cell surface glycoprotein that is specifically expressed by astrocytes in the white matter and sub-pial and subventricular regions, where Rosenthal fibers are found in abundance. We also examine several of its binding partners -the extracellular matrix molecule hyaluronan, its principal ligand, and the ezrin/radixin/moesin proteins, which link CD44 to the cytoskeleton.

In **Chapter 4**, I briefly introduce iron's importance to the brain and its regulation in the CNS. Additionally I reviews the ways that iron can be toxic to cells and potential destructive. I then present the results of a

brief histochemical analysis of two infant onset, type 1 AxD patients and a control patient using a modified Perls' iron stain for Fe3+ and antibodies to ferritin, ferroportin and ceruloplasmin to examine these iron related proteins.

In **Chapter 5**, I review the results of these experiments and relevant discussion points and discuss their interpretation and significance. I also put forth future directions that are suggested as a result of my work. **Chapter 6** provides a detailed description of the materials and methods utilized to carry out this thesis project.

Tissue used in these studies

Where possible, I used AxD patient tissue for immunostaining and Western blot. Human autopsy tissue, however, is limiting because it often represents the end course of a disease, and therefore I also used AxD mice. Very few studies have been conducted using the mice produced as a cross between the Tg and KI AxD strains. As described above, it is known that these mice do not show any overt loss of myelin and die between 30—35 days, most likely from seizures (Hagemann et al., 2006). The increased lethality of these mice whose individual strains show normal lifespans suggest that the synergistic increase in levels of GFAP leads to overwhelming astrocyte dysfunction and subsequent lethality (Hagemann et al., 2006).

In autopsy tissue I mainly examine the subcortical white matter, where there is extensive demyelination and Rosenthal fibers in type I patients. However, because in the mouse the amount of subcortical white matter is small and because early studies did not show demyelination in these animals, I chose to focus on the hippocampus in the mouse for several reasons: first, unlike protoplasmic astrocytes of the cortex, astrocytes in the hippocampus express high levels of GFAP; particularly in the stratum lacunosum; second, the hippocampus is a major locus for seizure activity and AxD type I patients suffer from seizures while the Tg/KI mice die of seizures; third, CD44, a protein we examine later in this thesis, is

expressed abundantly in the stratum lacunosum-moleculare, a hippocampal layer that contains myelinated fiber projections from the entorhinal cortex that synapse on dendrites of pyramidal and dentate neurons (See Fig 7).

Chapter 1: Figures

Figure 1. Typical MRI of AxD

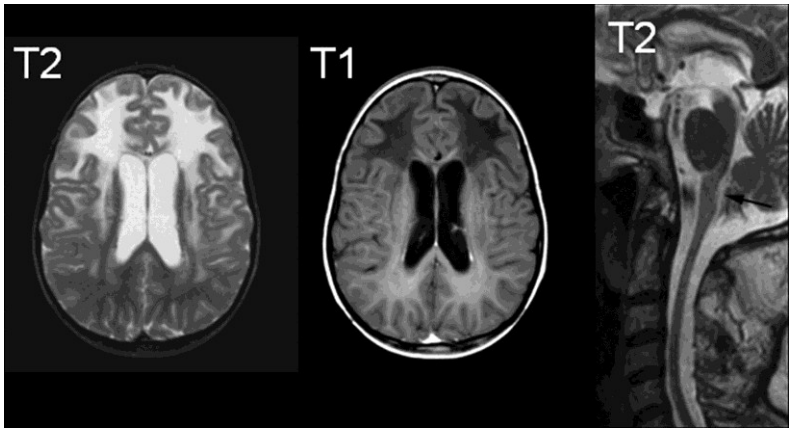

Magnetic Resonance Images (MRIs) typical for an infant onset, type I patient show symmetrical white matter abnormality. (Image from Messing A et al. J. Neurosci. 2012; 32:5017-5023).

Figure 2. Type I and Type II AxD– Comparison of age of onset, clinical features, radiological features and survival

	Type I	Type II
Age of onset	Before age 4	Across lifespan
Clinical features	Seizures Macrocephaly Encephalopathy Sudden deterioration after insult or injury Failure to thrive Developmental delay	Autonomic dysfunction Bulbar symptoms Ocular movement abnormalities Palatal myoclonus (muscle spasms in palate which make noise in ears) Few or no neurocognitive or development deficits
Radiological features	Classical radiological features	Atypical radiological features
Survival	Survival 2 years +/- after diagnosis	Survival as long as 25 years after diagnosis

(from Prust et al. Neurology 2011; 77:1287-94)

Figure 3. Morphological features of Rosenthal fibers

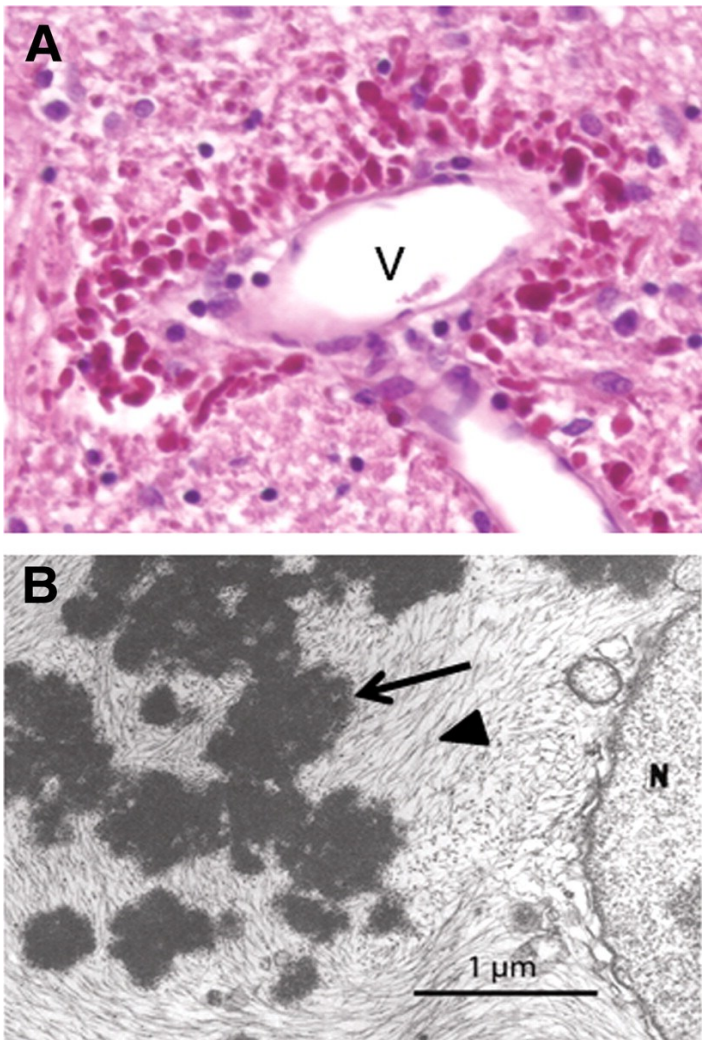

(A) Hematoxylin and eosin stain of the brain stem of a 1-year-old child shows abundant Rosenthal fibers (arrows), stained darker pink, in perivascular astrocyte endfeet surrounding a blood vessel (V). (B) Loosely scattered electron positive deposits (arrow) surrounded by intermediate filaments (arrowhead) form a perinuclear Rosenthal fiber in the astrocyte of a 17 month old child. (N) nucleus. Transmission electron microscopy.

(Modified from: Messing A et al. J. Neurosci. 2012; 32:5017-5023).

Figure 4. Lesions demonstrating Rosenthal fibers

Category		Examples
Reactive Lesions	Parenchyma surrounding slowly growing, low-grade tumors	Hemangioblastoma, craniopharyngioma
	Parenchyma surrounding cysts	Syringomyelia, pineal cyst
	Parenchyma surrounding vascular malformations	Arteriovenous malformations, cavernomas
	Parenchyma surrounding chronic inflammation	Multiple sclerosis
Neoplastic		Pilocytic astrocytoma
		Ganglioglioma
Genetic/Metabolic		Alexander disease

(Wippold FJ et al. Am. J. Neuroradiol. 2006; 27:958-61).

Figure 5. Reported AxD associated GFAP mutations as of 2011

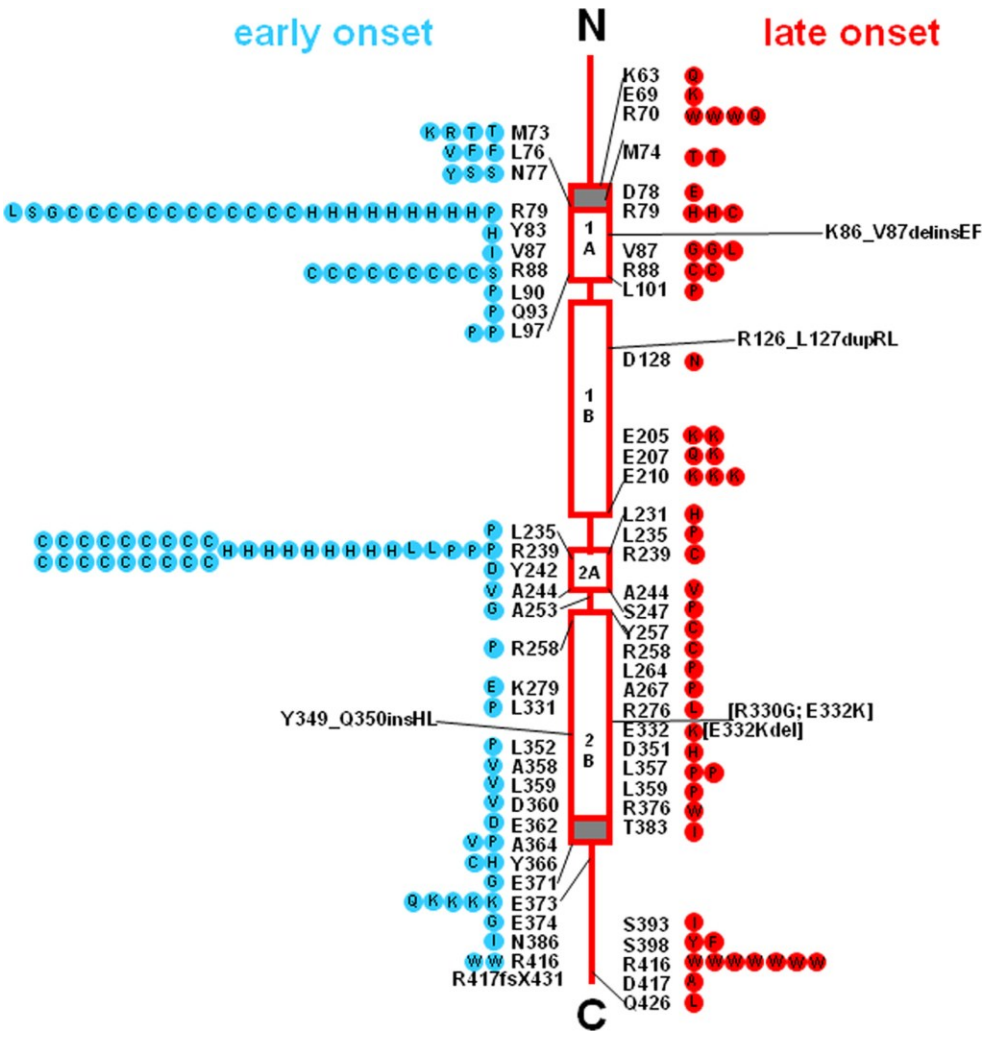

(Messing A et al. J. Neurosci. 2012; 32:5017-5023)

Figure 6. Extensive demyelination in type I infant onset AxD

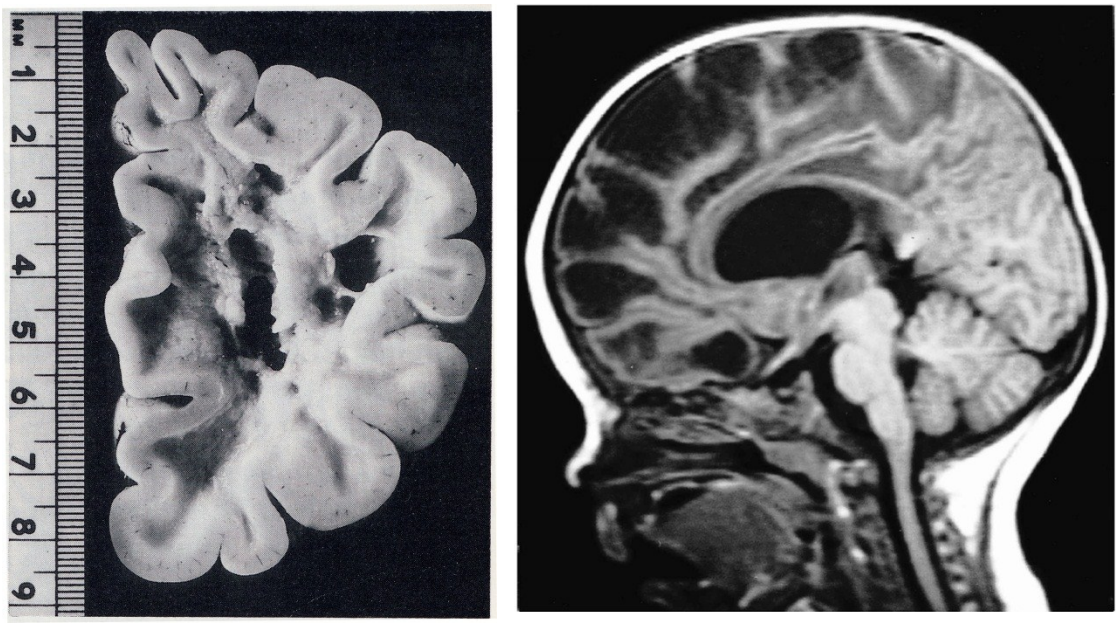

(A) Coronal section showing a cavitation and near total loss of white matter. (B) T1-weighted MRI of an 8-month-old patient showing cystic degeneration in the frontal and parietal lobes.

Figure 7. Hippocampus

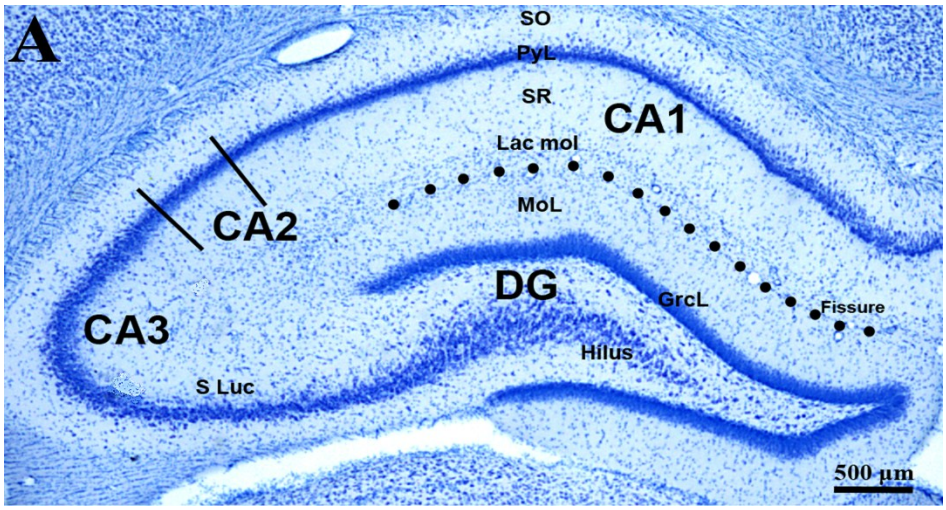

Markel Olabarria 2011

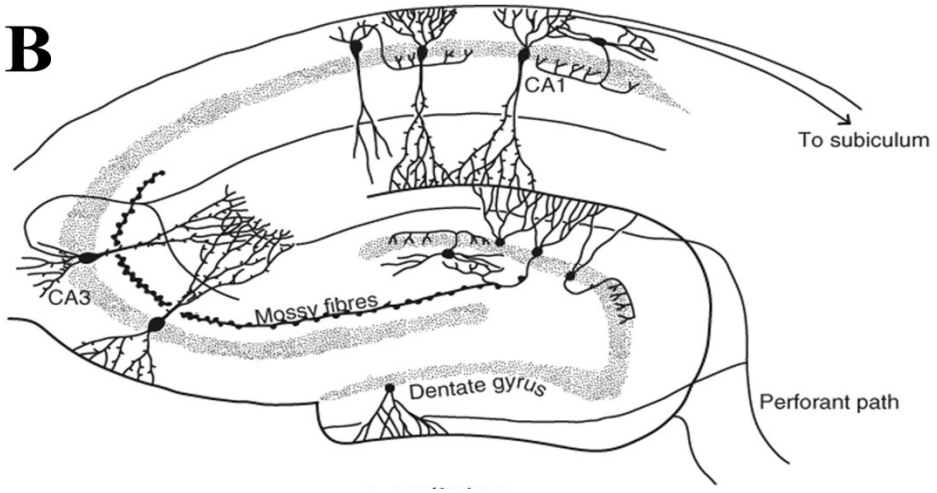

(A) Toluidine blue stained rat hippocampus showing the distribution of different layers. Key: DG: Denate Gyrus; GrcL: Granular cell layer; MoL: Molecular cell layer; S Luc: Stratum Lucidum; Lac mol: Lacunosum Moleculare; SR: Stratum Radiatum; SO: Stratum Oriens (adapted from Rodríguez- unpublished photograph courtesy of Markel Olibarria) (B) Scheme of the hippocampus illustrating the main types of neurons of the principal layers: Granular cell neurons populate the Grcl extending the dendritic tree to the MoL and projecting mossy fibers the pyramidal neurons of the CA3. Both pyramidal neurons in the CA3 and CA1 display apical and basal dendritic trees (Adapted from Rolls, 2009).

Chapter 2

Alexander disease astrocytes:

morphologically and ER stressed

Introduction

In this chapter, through immunoanalysis and Western blot of AxD mice and patient tissue, I explore manifestations of morphological stress in astrocytes and a novel stressors to which AxD astrocytes might be subject. Astrocytes and cell lines expressing mGFAP and/or transgenic GFAP have been found to undergo many biochemical changes, which may involve or are indicative of a stress response as they accumulate high levels of GFAP. These include an inhibition of proteasomal activity, induction of autophagy, activation of mitogen-activated protein kinase stress pathways leading to the activation of JNK and p38 kinases, upregulation of small heat shock protein genes encoding alpha B-crystallin and Hsp27, and loss of GLT-1, a major glutamate transporter in astrocytes (Cho and Messing, 2009; Tang et al., 2010; Tang et al., 2006; Tang et al., 2008; Tian et al., 2010). Oxidant stress is indicated by iron accumulation in astrocytes of KI and Tg mice, vastly increased expression of genes driven by antioxidant response element (Hagemann et al., 2006; Hagemann et al., 2005) and the presence of advanced glycation end products and 4-hydroxynoneal in Rosenthal fibers (Castellani et al., 1998; Castellani et al., 1997).

Astrocytes in AxD patients experience severe morphological transformation, beyond that of a typical reactive astrocytes, including formation of Rosenthal fibers, hugely distended cell bodies, greatly hyperphotried processes and binucleated and otherwise abnormal nuclei. In the first part of this chapter, I use AxD model mice and primary cells to explore phenotypic changes in astrocytes that might lend insight to the changes we see the astrocytes of patients. I find that along with an almost 4-fold increase in GFAP protein in the hippocampus, there are profound changes in astrocyte phenotype, especially in the s stratum lacunosum moleculare. GFAP immunostaining reveals hypertrophied processes on many of these cells, and additional some processes which appear retracted or “collapsed.”

BIP. In the second part of this chapter, I examine the endoplasm reticulum (ER) and the unfolded protein response (UPR) in AxD. The ubiquitin proteasome system is important for clearance of proteins marked for degradation by ER quality control mechanisms, and proteasomal inhibition can induce ER stress (Mancini et al., 2000; O'Hare et al., 1999; Ward and Kopito, 1994). Because there are many indicators of proteasomal inhibition in AxD, I hypothesize that the ER stress pathways are activated in AxD. BIPI conducted an immunohistological examination of AxD patients and mice, and found increased expression of BIP/Grp78 in astrocytes. Additionally I found present the CCAAT enhancer binding protein homologous protein (CHOP) in some astrocytes of the Tg/KI mice.

ER has essential roles in lipid and sterol synthesis, intracellular calcium homeostasis and protein secretion (as reviewed by Ma and Hendershot, 2004). In this last role, roughly one third of all proteins enter the endoplasmic reticulum as part of the secretory pathway (as reviewed by Kanapin et al., 2003). Here, they are folded to their native conformation and acquire post-translational modifications that include lipidation, glycosylation and formation of intra and inter-molecular disulfide bonds (as reviewed by Ma and Hendershot, 2004). Quality control is maintained in the ER by a set of resident chaperones and multiple check points that assure only properly folded proteins exit the ER while unfolded proteins are retained in the ER, remaining associated with chaperones before they are degraded (as reviewed by Fewell et al., 2001; Hammond and Helenius, 1995). This degradation process for failed proteins is termed endoplasmic reticulum associated degradation (ERAD) (Werner et al., 1996). Much work has been conducted in yeast elucidating mechanisms of ERAD, but it is unknown whether mammals share all of these mechanisms with yeast (as reviewed by Vembar and Brodsky, 2008). It is known that some proteins marked for ERAD are ubiquinated and degraded by the proteasome, that chemical inhibitors of the proteasome can inhibit this process, and that the activity of the proteasome is required for some ERAD designated proteins to leave the ER (Mancini et al., 2000; O'Hare et al., 1999; Ward and Kopito, 1994). Experiments have demonstrated that specific ERAD designated proteins can leave the ER under

condition of proteasomal inhibition. These are transported on microtubules to perinuclear organelles called aggresomes where they are then degraded by autophagosomes (as reviewed by Johnston, 2006). ER stress is known as any process that disrupts the balance between the folding load and the capacity of the folding machinery (as reviewed by Ron and Walter, 2007). The term "unfolded protein response" (UPR) grew out of several proof-of-principle experiments establishing that folding-incompetent proteins could induce a response that induced transcriptional and translational increases in ER resident chaperones (Adams and Rose, 1985; Gething et al., 1986; Kozutsumi et al., 1988; Zimmer et al., 1999). It has since been established that pathways activated by as part of the UPR, however, can also be caused by conditions other than excess or folding-incompetent proteins, such as those that interfere with ER calcium stores (Paschen et al., 2003; Sambrook, 1990), nutrient stress (Harding et al., 2005; Scheuner et al., 2001; Schroder et al., 2000), viral infection, iron deprivation, hypoxia/ischemia and oxidative stress, as well as differentiation of cells to highly secretory types (Calfon et al., 2002; Iwakoshi et al., 2003). This has led to the introduction of the more inclusive term "integrated stress response" (ISR) in addition to unfolded protein response (as reviewed by Markowitz et al., 2007).

Under conditions of ER stress, a set of coordinated transcriptional responses are introduced to bring the ER back to homeostasis and proper protein folding. These activities are mediated by three transcriptional pathways, which are transduced by the proteins PERK, IRE1 and ATF6. These proteins are located in the ER membrane facing the lumen and, under normal physiological conditions, are bound by the ATP-dependent ER chaperone BIP (immunoglobulin heavy-chain binding protein). During conditions of ER stress, BIP dissociates from these proteins and functions in protein chaperone activity in the lumen, freeing PERK, IRE1 and ATF6 to mediate transcriptional events. ATF6 translocates to the Golgi where it is processed to an active form that then functions as a transcription factor. IRE1 dimerizes and, through subsequent activation of RNase activity, splices the transcription factor XBP1 to a form that is potent for transcriptional activation. PERK is unique in that it participates in three UPR/ISR-mediated

events, both translational attenuation and activation and additionally, through activation of Nrf2, antioxidant response (as reviewed by Cullinan and Diehl, 2006). Transcriptional attenuation occurs via phosphorylation and subsequent inactivation of the elongation factor, eif2alpha, and during this process genes that respond to transcription factor ATF 4 are preferentially transcribed (as reviewed by Schroder and Kaufman, 2005). PERK phosphorylation of bZIP transcription factor Nrf2 allows it to translocate to the nucleus and activate transcription through the ARE (antioxidant response element) (Jian et al., 2008; Schroder and Kaufman, 2005) (Fig A).

In Chapter 1, studies conducted by the Goldman lab were described that suggest that proteasomal inhibition is a major contributor to the pathology caused by AxD. In vitro and cell culture experiments have demonstrated that mutant and human WT GFAP cause proteasomal inhibition and the 20S proteasome is associated with Rosenthal fibers in patient tissue (Tang et al., 2010; Tang et al., 2008). Additionally, primary cells from Tg and KI mice show impaired proteolysis by the proteasome (Cho and Messing, 2009). Because inhibition of the proteasome was found to impair the ERAD process (as reviewed by Vembar and Brodsky, 2008) and there is strong evidence for proteasomal inhibition in AxD astrocytes, I hypothesized that ER stress might be a factor in AxD.

Results

GFAP is increased in AxD Tg/KI mice at 2 and 4 weeks

Because accumulated GFAP in astrocytes is thought to trigger many pathological manifestations of AxD, I first examined GFAP distribution and levels in the most severely affected of AxD mice, the Tg/KI mouse that has a lifespan of less than 30 days, and found, as expected, a dramatic increase in the GFAP protein in Tg/KI animals over controls at both time points because these mice carry extra copies of human *GFAP* and its promoter in addition to their endogenous WT and mutant GFAP genes (Messing et al., 1998). In the WT hippocampus at 2 weeks, most of the immunostaining for GFAP could be seen in the stratum lacunosum moleculare (str. lac.-mol.) (Fig 1A, left), while in the 4 week old WT more GFAP

immunoreactivity was apparent in the stratum radiatum (str. rad.), which contains the dendrites of the CA1 pyramidal cells, and the stratum moleculare (str. mol.), which contains the dendrites of the granule cells of the dentate gyrus (See Chapter 1 Fig 7 for anatomy of the hippocampus). Tg/KI animals, in contrast, had already, by 2 weeks, immunoreactivity for GFAP in both the str. rad. and the str. mol. in addition to that in the str. lac.-mol. (Fig 1A, right) and in the 4 week old Tg/KI mouse this appeared to greatly increased (Fig 1B, right). The increases in GFAP in the Tg/KI mice that were observed by immunofluorescence, were also observed by Western blot analysis (Fig 1C). Note that for Tg/KI animals there are many faint bands at upper levels in the gel that may represent ubiquitinated GFAP protein and, likely, dimers (~100kDa) and tetramers (~200kDa) (Fig 2C). In addition there is a band migrating at a faster rate immediately below the major band at approximately 49 kDa, which may represent a proteolytically or otherwise cleaved species that is not present in WT animals (Fig 2C). Quantification of the GFAP protein levels of three independent experiments using densitometric analysis demonstrated a roughly 3-fold increase in GFAP expression in Tg/KI mouse at two weeks (***$p < 0.0005$) and a 4 fold increase at 4 weeks (****$p < 0.00005$) (Fig 1D). GFAP levels in the Tg/KI animals also increased significantly between 2 and 4 weeks (*$p < 0.05$), while there was no significant increase in WT GFAP (Fig 1D).

Severe morphological changes are seen in astrocytes in the str. lac. of 4 week old Tg/KI mice

We noticed that astrocytes in the str.lac.-mol., which appeared to be the first of the regions we examined to become immunoreactive to GFAP in the WT animals, are severely morphologically affected, characterized by hypertrophic processes and cell bodies. To assess the morphological changes that may ensue from increased GFAP expression, we first examined astrocytes in this severely affected portion of the hippocampus. In 4 week old Tg/KI mouse, the str. lac.-mol. contains many cells that appear to have lost processes and have a rounded appearance (Fig 2A right, arrow). Similar cells examined at high magnification (Fig 2B and C), have greatly accumulated GFAP in the cell body and display single

hypertrophied processes (Fig 2C, arrow), and what appear to be retracted or "collapsed" GFAP+ cell processes (Fig 2B, arrow). Nuclei are often abnormal or binucleated (Fig 4B, arrowheads).

GFAP and Alpha Tubulin are found together in perinuclear inclusions

In order to obtain another perspective on the morphologically transformed cells in the Tg/KI mouse, I turned to cell culture and examined primary astrocytes from. Both Tg and Tg/KI cells in culture show perinuclear inclusions. In these experiments, I used Tg cells due to their resilience, and the fact that their inclusions are similar to those seen in Tg/KI mice, though less numerous. I examined these cells for the expression of GFAP, along with alpha tubulin to visualize microtubules. WT cells at low magnification (Fig 3A) show few GFAP+ cells – a commonly reported observation for mouse primary astrocytes. Tg cells (Fig 3B) show many cells with perinuclear ring-like inclusions; arrows point to three. We were surprised to see microtubules in close association with these ring-like inclusions (Fig 3B). When examined by high magnification, WT cells (Fig 3C) had filamentous GFAP+ and alpha tubulin + processes, while Tg cells (Fig 3D) show ring-like inclusions of GFAP around centers that lack immunofluorescence. GFAP is in the innermost part of these inclusions, while alpha tubulin is at the outermost part and the periphery (Fig 3D, arrows).

Golgi is mislocalized in Tg primary astrocytes with perinuclear inclusions

Positioning of the Golgi is impacted by microtubule stability (Hehnly et al., 2010), therefore I next examined several organelle markers with GFAP to determine if they also might be impacted by perinuclear inclusions. I used a cis Golgi marker GM130, along with GFAP, to immunostain Tg primary cells, and found that in cells with perinuclear inclusions the golgi appeared mislocalized in comparison to neighboring cells with normal filamentous GFAP expression (Fig 4A and B, arrows). We examined these cells with high magnification and confocal 3D reconstruction to better understand these inclusions and found the cis Golgi appeared associated with or underneath a GFAP "cap" (Fig 4D and F).

AxD patients show accumulated BIP expression in white matter astrocytes

In order to determine if ER stress pathways are part of the pathology of AxD, I used immunohistochemistry to examine the expression of the ER chaperone BIP in AxD patient cortex and underlying white matter. I began my investigation with BIP because the antibodies were available and reported to be successful for immunostaining of both mouse and human tissue (Kovacs et al., 2009). At low power, I immediately saw a significant contrast between control (Fig 5A) and AxD R416W (Fig 5B) immunostains. While the control patient had high levels of BIP immunoreactivity in the cortex flanking the WM, and light immunostaining within the WM (Fig 5A, arrows), the R239H patient showed the reverse – WM with high levels of BIP immunoreactivity (Fig 5B, arrows) and cortex with low levels. The R416W patient WM (Fig 5C, arrows) did not show more immunostaining than in the cortex but did show less of a contrast between the WM and grey matter than control. Upon higher magnification (Fig 5D, E, F, G, H and I) differences between AxD and control became far clearer. The control WM showed many oligodendrocytes with BIP immunoreactivity in small cell bodies some with characteristic lacey processes (Fig 5G, arrows) and astrocytes with discrete, compact perinuclear BIP staining (Fig 5G, red asterisk) are displayed. Almost all oligodendrocytes cell bodies, which have small nuclei, show BIP immunoreactivity (some marked with black arrows) and BIP immunostaining can be observed into lacey processes (Fig 5G, black arrow, top). The tissue section from the AxD R239H patient displays hypertophic astrocytes and many Rosenthal fibers that immunostained a very light blue with hemotoxylin. In the WM of the AxD R239H patient, almost all astrocytes have granular deposits of BIP in their cell bodies (Fig 5H, red asterisks). Especially coarsely stained astrocytes can be seen at lower right. Some oligodendrocytes cell bodies can be observed with a tight ring of immunostaining to around their cell bodies, and several seem to have very little or no reactivity to BIP (Fig 5H, black arrows). The R416W patient has a relatively well-preserved cortex and astrocytes are striking in their accumulation of BIP, which often appears slightly granular. Several perinuclear Rosenthal fibers can be seen in the tissue

(Fig 5I, lower right red asterisk) and the more lightly immunostained Rosenthal fibers are surrounded by darker, granular BIP immunostaining here.

BIP is significantly elevated at 2 weeks and 4 weeks in AxD Tg/KI mice

To study further the role of BIP in AxD astrocyte pathology I turned to AxD model mice to determine if BIP was increased in these animals. First, I looked at the most severely affected animal, the Tg/KI mouse which dies at about 30-35 days. I examined the total hippocampus for BIP immunostaining at low magnification (Fig 6A and B) and there appeared to be some increases in Tg/KI animal, especially in the CA1 in the 4 week old Tg/KI.

Because neurons stain for BIP, it would be difficult to measure astrocyte-specific BIP levels by Western blot, so we counted BIP positive and GFAP+ astrocytes on images and found significant increases in BIP already in 2 week-old mice (*p=0.037, Fig 6C), progressing to a more dramatic difference at 4 weeks of age (**p=0.008; Fig 6C). Layer specific analysis showed that changes at 2 weeks of age only take place in the str. lac.-mol. (*p=0.041; Fig 7C and D) while at 4 weeks of age differences in BIP expression become striking and is significantly higher in both str. lac.-mol. and stratum radiatum (str. rad.) (**p=0.008 and *p=0.041; Fig 7C and D).

Expression of BIP in astrocytes of one year old Tg Mouse

Having observed a widespread increase in BIP among most astrocytes in the 4 week old Tg/KI mouse, I examined the one year old mice. WT mouse GFAP positive astrocytes showed very low levels of BIP immunostaining (Fig 8A, arrows). Likewise, in the Tg animal some GFAP positive astrocytes were observed with very little or no expression of BIP (Fig 8B and C, arrows), but strikingly some GFAP positive astrocytes in the one year old Tg mice showed very high and aberrantly localized expression of BIP, an ER resident protein (Fig 8B and C, yellow arrowheads). Thus, in contrast to the Tg/KI mouse, there is a

heterogeneous pattern of BIP immunostaining among the GFAP positive population of cells in the TG mouse hippocampus.

CHOP is co-expressed with BIP in a subset of astrocytes

Both BIP and CHOP are regulated downstream of the three main initiators of the unfolded protein response. However, while BIP is a generally thought a pro-survival chaperone, CHOP is induced when the balance between folding demand and capacity cannot be resolved favorably by the UPR. In four week old Tg/KI animals, I consistently saw several GFAP positive astrocytes with CHOP staining in nuclei (Fig 9B-F, small yellow arrowheads) and, to a lesser extent, in the cell body immediately adjacent to the nucleus (Fig 9B, F, large yellow arrowheads). While induction of BIP was widespread in the 4 week old Tg/KI mouse, I observed only a few CHOP positive astrocytes. I generally saw more CHOP positive astrocytes close to the pyramidal layer in the CA1, however only four animals were examined. WT animals (Fig 9A, top panels) show little or no CHOP labeling at 4 weeks of age. 2 week Tg/KI animals show a variable number of CHOP positive astrocytes ranging from 1 to 6 counts per analyzed hippocampus.

A note: I attempted to immunostain patient tissue with an antibody for CHOP, but I found no reactivity in either AxD patient or control (data not shown).

Discussion

In this chapter I revealed severe phenotypic changes in astrocytes in the Tg/KI mice that resulted in the conversion of star-like protoplasmic astrocytes in WT mice to cells that have hypertrophied or "collapsed" GFAP positive cell bodies and are multinucleated or have other nuclear abnormalities in connection with the accumulation of GFAP (Figs 1 and 2) (Sosunov et al., 2013). I next found that primary Tg astrocytes in culture have large perinuclear rings of GFAP filaments and a disrupted microtubule network and Golgi apparatus (Figs 3 and 4). Additionally, I present strong

immunohistological evidence that supports my hypothesis that ER stress in astrocytes is a component of the fatal pathology of AxD: first, I found BIP at higher levels in astrocytes in AxD patient tissue; second, I found significantly higher reactivity to BIP in astrocytes in the Tg/KI mouse at both 2 and 4 weeks; third, in the Tg/KI mice I found CHOP in astrocytes of the hippocampus at 4 weeks. While I have not explored the mechanism by which these proteins are induced, these results support a role for the induction of the unfolded protein response.

High levels of GFAP expression in AxD mice coincide with morphological transformation of astrocytes

The expression of mutant GFAP in AxD patients causes massive increases in the levels of GFAP in astrocytes both by immunofluorescence and by Western blot. Viewed at a terminal stage, these diseased astrocytes gain thick processes, exhibit distended cell bodies and display abnormal nuclei which are sometimes multinucleated. Morphologically they undergo dramatic changes to reach this end state.

I examined the most severely affected AxD mice, the Tg/KI for GFAP expression and immunoreactivity. We found GFAP to be increased almost 4 fold over WT mice by Western blot at both 2 weeks and 4 weeks (Fig 1D). By immunofluorescence for GFAP, these cells at 4 weeks displayed an extremely reactive phenotype. Some, especially in the str. lac.-mol., had undergone what seemed to be "collapsed" cell bodies (Fig2B, arrows) and others had greatly hypertrophic processes (Fig 2C, arrows).

Astrocytes of the hippocampus, like other protoplasmic astrocytes, form a highly organized network with individual cells regulating and integrating neuronal and vascular interactions within discrete regions (Bushong et al., 2004; Tout et al., 1993). In order to carry out these functions astrocytes must be able to extend fine processes into small domains between cells. The loss of thin GFAP+ processes we saw in 4 week old Tg/KI mice (Fig 2B, C), may be indicative of loss of the fine processes. In fact, collaborative work with the Tg/KI mice where astrocytes from the str. lac.-mol. were injected with Lucifer yellow

demonstrated loss of fine processes in these astrocytes, which may have severe consequences for the surrounding cells with respect to uptake of glutamate and potassium. AxD KI mice have compromised glutamate uptake (Tian et al., 2010) and collaborative work on Tg/KI mice that will be published along with some of the work in this thesis has confirmed and extends this demonstrating not only impaired glutamate uptake in Tg/KI mice, and loss of GLT-1 in these mice, but also loss of coupling of astrocytes and impaired potassium uptake in some more phenotypically transformed cells (Sosunov et al., 2013).

The results in this chapter and these collaborative studies suggest AxD astrocytes are extremely transformed and differ in morphology from "typical" reactive astrocytes. For example, the cell morphology of astrocytes after an electrically-induced cerebral cortex lesion was studied by Wilhelmsson et al. (Wilhelmsson et al., 2006). The authors injected reactive astrocytes with dye in the tissue surrounding, but not immediately adjacent to, the lesion. These astrocytes showed hypertrophic processes by reactivity to GFAP antibodies, and dye injection demonstrated that the soma and main processes were thicker, however these cells retained their bushy morphology and fine processes (Wilhelmsson et al., 2006). Similar injury models have been employed that demonstrate that concomitant with glial scarring of the lesion, reactive astrocytes not immediately adjacent to the lesion itself eventually return to normal levels of GFAP reactivity (Mathewson and Berry, 1985), and this has been found to be true in other models of CNS injury, allowing investigators to conclude that the glial reactions not involving astrocytes within the glial scar itself, are reversible upon removal of the stimulus for reactivity (Kalman, 2004). Because AxD is an astrogliopathy, the initial reactivity stems from the cell itself and therefore there is no resolution.

Binucleation of astrocytes

The presence of multiple nuclei on astrocytes in the Tg/KI mice (Fig 2A) suggests that they are driven to proliferate, but cytokinesis is inhibited. Phosphorylation of intermediate filaments by Cdk1, Plk1, Rho-kinase and Aurora-B kinases is required during cytokinesis (Izawa and Inagaki, 2006). The accumulation

of GFAP in AxD astrocytes may in some way interfere with intermediate filament phosphorylation at a critical time in mitosis, leading to failure of cytokinesis and a polyploid state. A polyploidy state may in turn dramatically increase the amount of GFAP produced by any given cell, thus contributing to a feed-forward mechanism of cellular stress.

Perinuclear rings of GFAP and microtubules in primary Tg astrocytes

Transgenic human GFAP mice express several copies of human GFAP in addition to their endogenous GFAP. In the cultured astrocytes from the Tg mice, I observed in some cells large perinuclear inclusions, composed on the exterior by caged or capped GFAP (Fig 3D, 4C-F). The GFAP inclusions are surrounded by rings of disrupted microtubules. The "rings" of GFAP proteins are reminiscent of intermediate filament expression in astrocytes after microtubule network disruption using drugs, such as colchicine (Sotelo et al., 1980). These experiments demonstrated that organized intermediate filaments require assembled microtubules and these interactions were found to not be direct, but to occur via intermediate filament linking proteins (as reviewed in Sonnenberg and Liem, 2007). Plectin is one such linker protein and has been found in AxD patient Rosenthal fibers (Tian et al., 2006). The overexpression of plectin rescues aggregated mutant GFAP in co-transfected cells, restoring a filamentous phenotype (Tian et al., 2006). There are several possibilities of why plectin has this effect: aggregation of proteins in AxD may be caused by an insufficient linker protein to intermediate filament protein ratio; alternatively, phosphorylation status of intermediate filament proteins may also impact plectin binding (Foisner et al., 1991). Conversely hyper-phosphorylation of intermediate filaments is known to induce cytoplasmic aggregates of disassembled intermediate filaments (Chou et al., 1990), some of which are distributed around the centrosome during early mitosis. It is possible then that the perinuclear inclusions observed in the Tg cells may be caused by insufficient plectin or altered phosphorylation of GFAP, vimentin or nuclear lamins.

Aberrant expression of BIP in ER of AxD Patients

In AxD patient tissue, I observed both increased expression and a grainy appearance to BIP immunoreactivity. The R239H patient, in particular, shows an overwhelmingly high level of immunostaining of BIP in the white matter and grain expression in astrocytes (Fig 1H), which was also observed in the R416W patient, where a distinct, perinuclear accumulation of BIP appears in a granular pattern. Although the literature does not readily suggest what these grainy bodies may be, perhaps they are accumulated proteins in the ER.

BIP expression has been found protective to cells (Yu et al., 1999), and this has been demonstrated in astrocytes. In a model of ischemia, transient transfection of BIP into mouse primary astrocytes is protective against cell death through Ca+ stabilization and suppression of mitochondrial-produced oxidative stress (Ouyang et al., 2011).

ER stress is an early and widespread response in Tg/KI animals

We found that WT mice expressed BIP at relatively high levels in pyramidal and granular cell neurons and in scattered cells that appeared to be neurons throughout the hippocampus. Some WT astrocytes also showed detectable levels of BIP, but were low in immunoreactivity in comparison to neurons. Because the basal expression of BIP by neurons precluded accurate measurement of BIP by Western blot, we counted BIP positive and GFAP positive cells to quantitate astrocytic expression of BIP. The increase in the total number of Tg/KI astrocytes with BIP expression versus WT was found significant at both 2 and 4 weeks Fig 6C). While the number of BiP positive and GFAP positive cells in the str. lac.-mol., an area of the hippocampus where there is early GFAP expression, appeared to reach its highest level at 2 weeks of age and remain at this level (Fig 7D). However, the decrease in expression by WT astrocytes, in comparison to the unchanged levels of BIP, accounted for the large increase in BIP expression between 2 weeks and 4 weeks (Fig 3D). This effect was also true for overall expression of BIP in the hippocampus – while numbers of BIP positive and GFAP positive cells are approximately equal at 2

weeks and at 4 weeks, the overall fold change over WT expression increases considerably – a 3.5-fold change in the 2 week Tg/KI animal and an 8-fold change its 4 week counterpart (Fig 6C). There is not a significant change in BIP reactivity in the str. rad. of the 2 week old Tg/KI animal and this most likely reflects the low relative level of GFAP reactivity at this age, in comparison to the 4 week old animal (Fig 6A and B).

These results suggest that the induction of BIP in the hippocampus of Tg/KI mice is a response to tremendous increases in levels of GFAP. By 4 weeks many astrocytes in the hippocampus are undergoing a stress response, in contrast to the one year old Tg mouse, where only occasional very high GFAP expressing, morphologically aberrant astrocytes experience the same stress.

ER stress and KI mouse mortality after Kainic Acid induced stress

Kainic acid administration to rodents causes cell death of neurons and is accompanied by an increase in the number of GFAP-positive astrocytes in the hippocampus (Yang et al., 1997). While AxD KI mice have little discernible pathology, they were found to be substantially more susceptible to Kainic acid induced seizures and subsequent neuronal damage compared with WT mice (Hagemann et al., 2006). Additionally they die after seizure at much greater numbers than do WT mice. More recently, Kainic acid administration to mice was shown to upregulate ER stress markers BIP and OASIS in astrocytes in the str. rad. and str. lac. (Chihara et al., 2009). The authors found more neuronal death in OASIS-/- mice after kainic acid insult, suggesting OASIS as the protective proteins in astrocytes. Astrocytes from OASIS-/- mice express less BIP than WT mouse primary astrocytes after ER stress (Kondo et al., 2005). OASIS is a less well-characterized ER stress protein, most likely due to the fact that there are no functional commercial antibodies available. Like IRE1 and ATF6, OASIS is a transcription factor and is expressed in astrocytes (Kondo et al., 2005). OASIS null mice have shown more neuronal damage after kainite acid administration and less GFAP expression. The authors concluded that the reduction in the number of GFAP-positive cells in OASIS -/- mice is not due to the degeneration of GFAP-positive cells following

kainic acid treatment, but from lack of cell division as measured by dUTP labeling. Taken together, these results suggested that the increased presence of astrocytes in the kainic acid induced brain is protective as is BIP induction. Taking these data into consideration it is possible that the high mortality observed in the KI mice after kainic acid exposure may be due to increased sensitively to ER stressors, due to high basal activation levels. However, if exacerbated by other stressors that require a functioning ERAD system, such as the protection astrocytes confer to neurons, under conditions of kainic acid exposure the system could potentially fail and cell death could ensue.

BIP in 1 year Tg animal suggests unresolved ER stress

In WT 1 year old animals, immunostaining for BIP in GFAP positive cells was limited to a small area close to the nucleus (Fig 8A, arrows), while in one year old Tg animals BIP protein expression was heterogeneous among GFAP+ cells. Some cells some had very low or no immunoreactivity (Fig 8B and C, arrows) while others had strong but rather diffuse BIP immunostaining that appeared to occupy a large volume around the cell body of extremely pathological-appearing astrocytes, by GFAP expression (Fig 8B yellow arrowheads). This was a consistent observed feature. While study of a wider range of ages of both Tg and KI animals is necessary in order to more fully understanding the UPR/ISR in these animals, the high consistency of BIP immunostaining in these very morphologically aberrant astrocytes that have accumulated high levels of GFAP, along with what appears to be a potentially enormously distended ER, suggests, first that accumulated GFAP may be linked to accumulation of BIP. Second, if BIP expression is denoting the physical location of the ER, then some Tg astrocytes have an abnormally large ER and perhaps correspondingly high numbers of proteins within. Finally, the potentially abnormally large ER in these animals suggests chronic ER stress, yet the UPR/IPR has favorably enacted adaptive mechanisms and by-passed apoptosis. This may be an intrinsic quality of astrocytes to withstand greater levels of stress than other cells, a quality of astrocytes in culture (Goldbaum et al., 2006; Griot et al., 1990; Husain and Juurlink, 1995). In cells, adaptation to short term demands of increased protein synthesis and

folding are part of normal ER function, and studies have shown that the volume of the ER necessary to accommodate an accumulation of unfolded protein will expand with need while other systems are put in place to enhance degradation of proteins (Menzel et al., 1997; Takewaka et al., 1999).

Possible causes of UPR in In AxD

Inferring that the large increases we see in BIP by immunostaining in astrocytes in AxD patients and mice indicates the UPR/ISR is enacted, I suggest three possible events in AxD that might converge to causing ER stress in astrocytes – increased protein processing through the ER, proteasomal inhibition and inhibition of autophagy. First, in AxD it is likely that increased protein synthesis and therefore increased protein trafficking through the ER is taking place. Studies in our lab have shown that both mGFAP and GFAP can cause proteasomal inhibition and that this in turn activates JNK and p38 kinase (Tang et al., 2010; Tang et al., 2006) which can activate AP-1 mediated transcription. Another gene transcription pathway that is activated in AxD mice, and that likely contributes to increased processing of genes through the ER, is gene expression driven by the ARE (Hagemann et al., 2006; Hagemann et al., 2005).

The ERAD pathway targets proteins rejected from ER quality control mechanisms to the proteasome. In AxD there is abundant evidence that the proteasome is inhibited in astrocytes (Cho and Messing, 2009; Tang et al., 2010). Therefore, this means of potential ERAD inhibition seems likely in AxD, however the activation of the UPR may also be caused, or at least aggravated, by possible inhibition of autophagy. Alternate methods of ERAD associated proteolysis occur through trafficking of proteins to aggresomes where they can be degraded by autophagosomes – double-membraned structures that engulf substrates and deliver them to lysosomes for degradation (as reviewed by Vembar and Brodsky, 2008). A third event can be enacted to degrade both the ER and accumulated substrate in case of ERAD failure and this too involves autophagy-mediated degradation of accumulated proteins and portions of the ER itself (Ogata et al., 2006).

Inhibition of mTOR induces autophagy in animal models of Huntington disease (Ravikumar et al., 2004), and pS6, a well-known marker for mTOR activation, is abundantly expressed in the Tg/KI mice (Sosunov et al., 2013). Stress pathways enacted by proteasomal inhibition, in tandem with a demonstrated oxidative stress response, may increase protein processing through the ER and elevate the volume of ERAD-destined proteins. Meanwhile, the mechanisms responsible for the degradation of these proteins, proteasomal clearance on one hand, and aggresomes to autophagosomes on the other, are or may be impaired. These are likely contributors to the induction of the UPR in AxD astrocytes and the ability of the Tg animal to withstand this level of ER stress, may lie in the relatively few astrocytes with high levels of BIP in comparison to that which were demonstrated in the Tg/KI mouse (Fig 6C).

BIP loss in patient oligodendrocytes may signal impaired myelination

In both AxD patients I examined, there appeared to be less BIP in oligodendrocytes than in control tissue. Humans have many more oligodendrocytes than do rodents. In human white matter, these cells can often be identified by their small, compact cell bodies. In control patient tissue, oligodendrocytes were of note because they seemed to exhibit a substantial level of endogenous BIP (Fig 5G). Oligodendrocytes possess huge membrane areas that can outweigh their cell bodies by up to 100 fold (Wiggins et al., 1974) and thus their metabolic demands are high for protein and lipid synthesis. While the transcript for myelin basic protein is transported to distal tips of cell processes and translated locally (Ainger et al., 1993), other myelin proteins such as proteolipid protein (PLP), myelin-associated glycoprotein and myelin oligodendrocyte glycoprotein are processed through the ER. Therefore, the ER of oligodendrocytes may be under considerable demand, especially during myelination, which occurs through childhood, and thus during the age of our patients, and requires the assistance of additional chaperones. Along these lines, the induction of components of the ER stress response pathway in oligodendrocytes via IFN gamma administration was found protective to oligodendrocytes in mouse models of MS (Lin et al., 2007).

We observed a decrease in BIP immunostaining in oligodendrocytes in one AxD patient (Fig 5I, black arrow), and what appeared to be a decrease in the pattern of perinuclear expression of BIP in another (Fig 5H, black arrows) in contrast to control counterparts (Fig 5G). This may be indication that they have decreased synthesis of myelin-related proteins, and may serve as a useful marker to assess in understanding the de/dysmyelination that occurs in AxD.

CHOP expression may not be pro-apoptotic

I found CHOP in a small subset of BIP positive and GFAP positive astrocytes in the Tg/KI mice. CHOP was detected either in the nucleus or the cytoplasm, but not in both of these areas together (Fig 8 and 9). If expressed under conditions of ER stress, CHOP is generally thought to be proapoptotic (as reviewed by Kim et al., 2008; Maytin et al., 2001; Wang et al., 1996) and this was demonstrated in primary rat astrocytes undergoing oxygen glucose deprivation (Benavides et al., 2005). In this model of cell stress, CHOP was found expressed in the nucleus of astrocytes that eventually underwent apoptosis (Benavides et al., 2005). CHOP expression, however, may not necessarily be demonstrative of cells undergoing apoptosis. In neonatal rats presenting with virus infection of the CNS, CHOP was detected in both neurons and astrocytes in the hippocampus and cerebellum, but subsequent cell death occurred only in neurons (Williams and Lipkin, 2006). Of note was that no BIP was found in neurons, but astrocytes in these same animals co-expressed BIP and CHOP, which may be one reason they were able to withstand infection (Williams and Lipkin, 2006).

Chapter 2: Figures

Figure A. The unfolded protein response / integrated stress response (UPR . ISR)

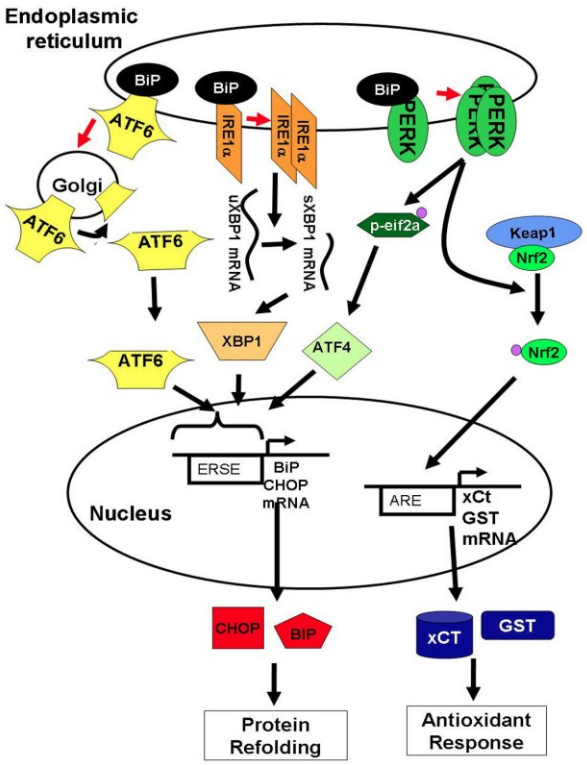

In response to stress, the endoplasmic reticulum chaperone protein BiP utilization by unfolded proteins frees the 3 initiators of the ISR: ATF6, IRE1α, and PERK. ATF6 is translocated to the golgi and cleaved releasing ATF6-p50, a transcription factor. Free IRE1α splices uXBP1 to sXBP1 which can now be translated. PERK phosphorylates 2 known substrates, eIF2α and Nrf2. eIF2α depresses general translation initiation, but favors translation of ATF4. ATF6-p53, sXBP1, and ATF4 translocate to the nucleus and activate transcription of chaperone proteins like BiP to re-establish homeostasis. Concomitantly, phosphorylation of Nrf2 by PERK disrupts interaction between Keap1 and Nrf2 leading to translocation of Nrf2 to the nucleus and transactivation of antioxidant genes including GST and xCT. Together, these responses reduce oxidative stress and establish protein refolding. (Markowitz, White, Kolson, & Jordan-Sciutto, CellScience, 2009).

Figure 1. GFAP is significantly increased in Tg/KI mice

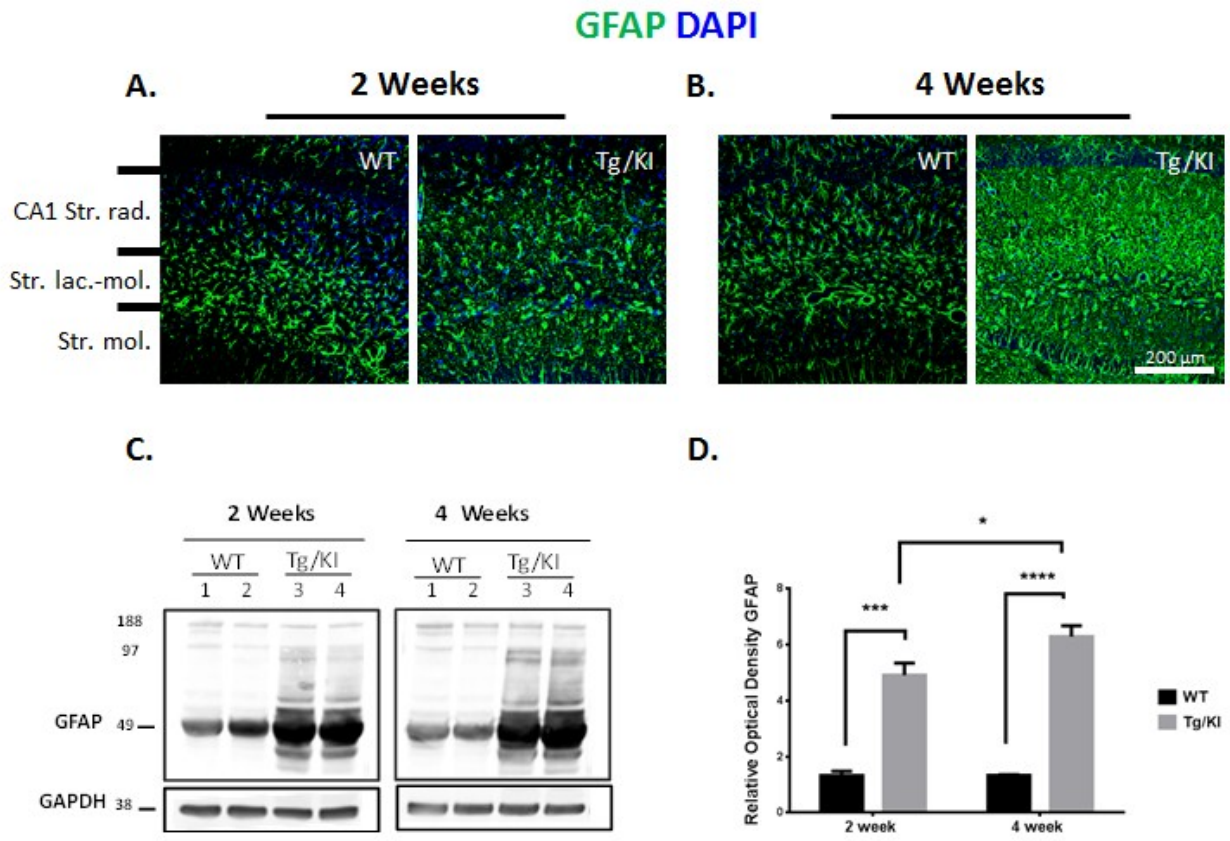

(A, B) GFAP Immunofluorescence in hippocampus of Tg/KI mice at 2 and 4 weeks of age. Tg/KI mice at 2 weeks (A, right) and 4 weeks (B, right) show high reactivity with antibodies for GFAP when compared to age-matched WT. (C) Western blot analysis of GFAP in hippocampi (10ug total protein/lane) of 2 and 4 week WT and Tg/KI mice. GAPDH is assessed as a loading control. One blot of three shown. (D) Quantitative evaluation of GFAP levels based upon optical densities normalized to the level of GAPDH, shows GFAP is significantly higher in Tg/KI hippocampus than in WT hippocampus at both 2 weeks (***$p < 0.0005$) and 4 weeks (****$p < 0.00005$). Additionally the there is a significant difference in the increase in GFAP between 2 weeks and 4 weeks (*$p < 0.05$). Note that all GFAP immunoreactive bands were scanned for optical density evaluation, not only the 50 kDa band. Data are mean +/- standard

error of mean (SEM) of 3 independent experiments. Two way ANOVA with Tukey test; *$p < 0.05$, ***$p < 0.0005$, ****$p < 0.00005$.

Figure 2. Phenotypic changes in astrocytes in 4 week Tg/KI str. lac.-mol.

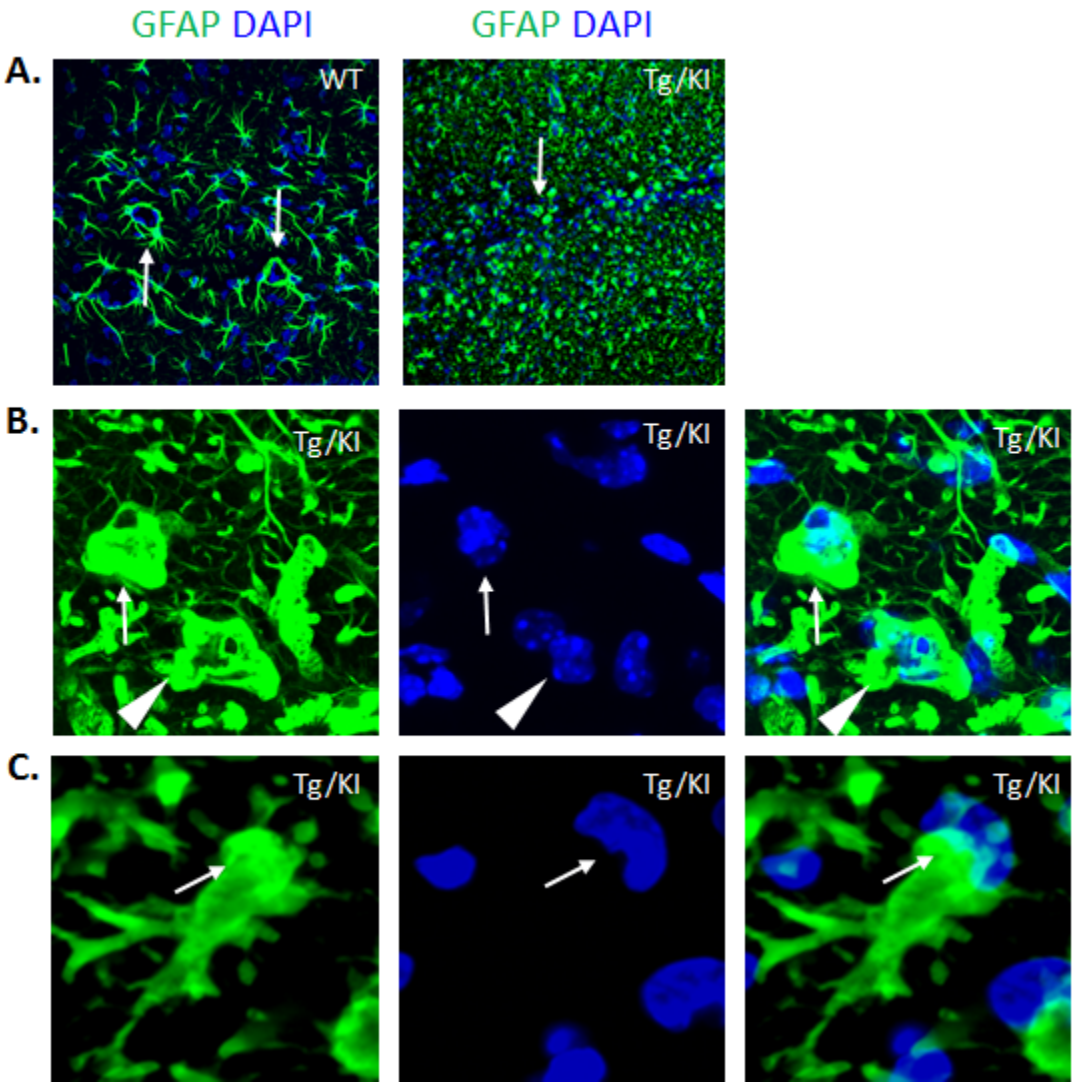

Morphological changes to astrocytes in the 4 week Tg/KI mouse hippocampus are especially apparent in the str. lac.-mol. (A) Low magnification image of str. lac-mol. in WT and Tg/KI mouse with immunofluorescence for GFAP. DAPI is used to visualize nuclei. (A) WT mice show many GFAP+ astrocytes that display thin GFAP+ processes extending from cell bodies in a star-like manner. Some GFAP+ processes collect around the blood vessels of the str. lac.-mol. (A, left arrow). In Tg/KI str. lac.-mol., GFAP+ immunoreactivity reveals rounded, large cells lacking main branches (A, arrow). (B, C) High magnification images of the str. lac.-mol. reveal astrocytes with greatly diminished numbers of GFAP+

cell processes and hypertrophied appearance of those that remain (C, arrows) and cells that have seemed to have had their GFAP processes retract or “collapse” to entirely fill cell bodies with GFAP immunoreactivity (B, arrows). Many of these astrocytes have binucleated (B, arrowheads), lobulated or otherwise abnormal nuclei. Confocal microscopy.

Figure 3. Primary astrocytes from Tg mice form perinuclear inclusions of GFAP and microtubules

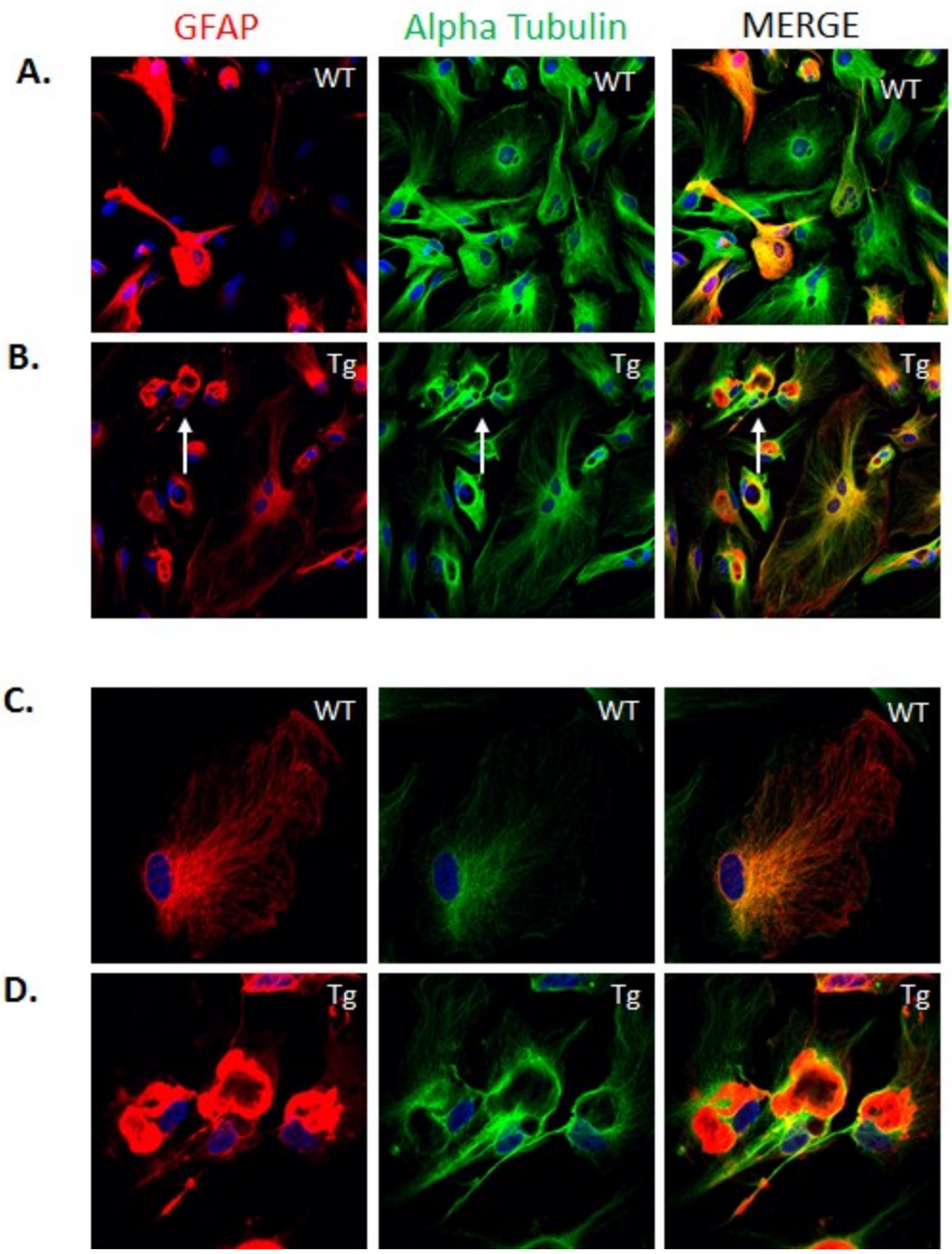

Primary Tg astrocytes triple stained for the expression of GFAP (red), alpha tubulin (green) to visualize microtubules and DAPI (blue) for nuclei. (A) WT cells at low magnification display few GFAP+ cells – a commonly reported observation for mouse primary astrocytes. (B) Most Tg cells show GFAP expression and many cells contain perinuclear ring-like inclusions, arrow point to three. Microtubules (green) are in

close association with these inclusions. (C) WT cell at high magnification display lacey, filamentous GFAP+ and alpha tubulin+ processes. (D) Tg cells at high magnification show ring-like inclusions of GFAP around what appear to be “hollow” centers. Triple staining shows that GFAP is in the innermost part of these inclusions while alpha tubulin surrounds (far right panel).

Figure 4. Golgi is mislocalized in cells with perinuclear GFAP aggregates

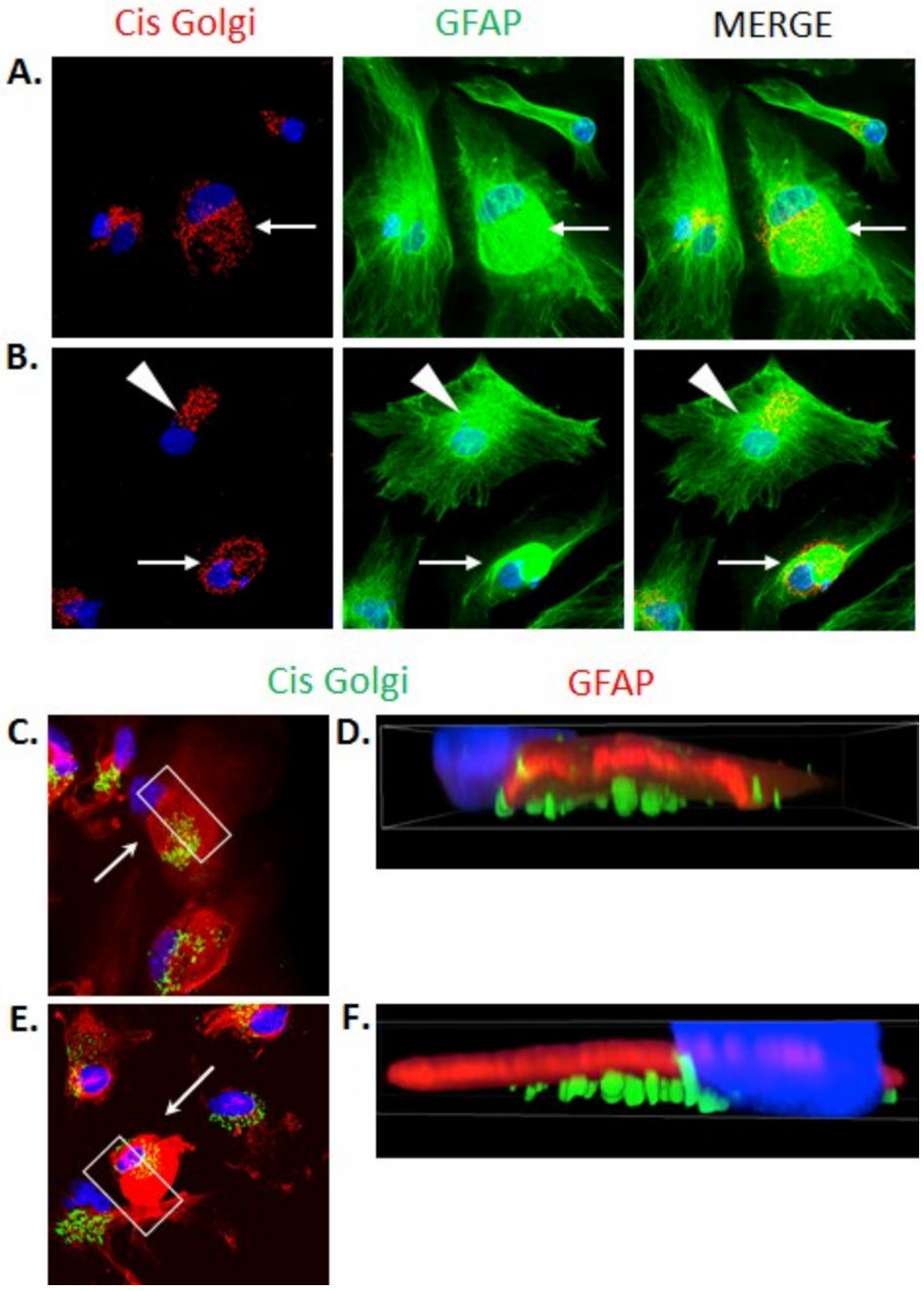

Tg primary mouse astrocytes grown for 2-4 days in vitro after replating from culture flasks were fixed and co-immunostained for GFAP and GM130, a marker for the cis Golgi and DAPI showing nuclei. (A, B) Arrows mark cells with perinuclear inclusions while arrowhead marks normal-appearing cell. Note that the golgi (red) in inclusion-bearing cells appears mislocalized (A, B, arrows, left panel), in comparison to golgi in normal appearing Tg cell (B, left panel arrowheads). (D, F) 3-D reconstruction of cells bisected in position of box in (C, E) respectively. GFAP (red) often appears on top of or associated with cis Golgi (green). Arrows in C, E represent direction from which images were reconstructed.

Figure 5. Increased immunohistochemical expression of BIP in astrocytes of AxD patients

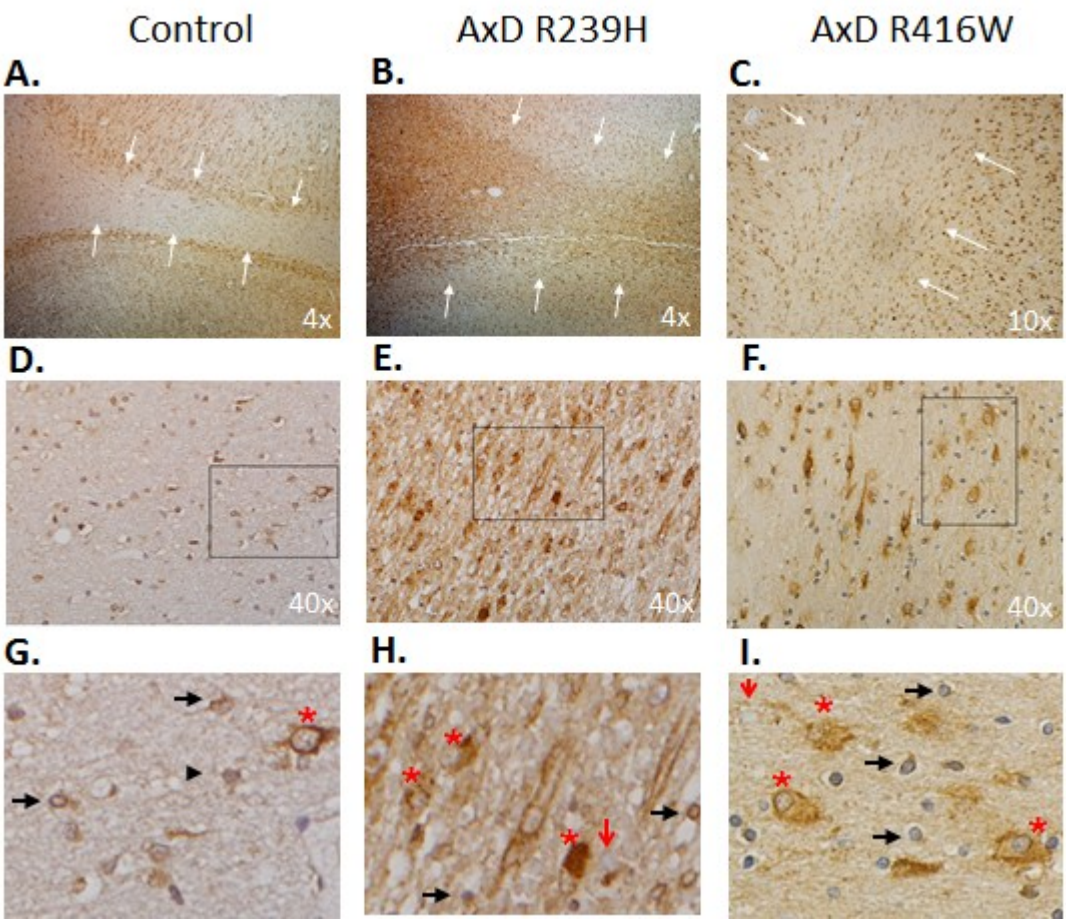

(A-C) Immunohistochemical analysis of BIP expression in subcortical white matter and adjoining cortex at low magnification. (A) Control patient cortical section shows high levels of BIP in neurons of the grey matter which flanks, above and below, the white matter (arrows), that appears lightly immunostained at this low magnification (4x). This is in stark contrast to the heavily stained white matter of an AxD patient with the R239H mutation (arrows) in (B) where the surrounding cortex appears lightly stained in comparison. (C) The white matter from a AxD patient with a R416W mutation (arrows) in (C) has more intense immunoreactivity to BIP than the control patient (A), but less so than the R239H mutation (B).

Heavily stained neurons can be seen in the flanking cortical tissue to the right and the upper left-hand corner. Boxed selections in (D-F) are shown at higher magnifications below. (G-I) High-power magnification of white matter in boxed sections, above. (G) Control patient white matter shows an astrocyte (G, asterisk) with compact BIP in the cell body, around the nucleus. Many oligodendrocytes (black arrows), show BIP immunoreactivity compactly located in cell bodies – staining can sometimes be seen in lacey processes (arrowhead). (H and I) Almost all astrocytes in white matter of AxD patient have granular deposits of BIP in their cell bodies (asterisks, H). Most oligodendrocytes seem to have diminished or no BIP immunostaining, and no lacey processes are visibly immunostained (black arrows, H). Rosenthal fibers are not appreciably stained with BIP. (I) Astrocyte on the lower right contains a large, perinuclear Rosenthal fiber which appears lighter than does the surrounding granular BIP immunostaining (asterisk, I). This is in contrast with the large Rosenthal fiber on the top left which is just barely rimmed by BIP (red arrow). Oligodendrocytes are marked with black arrows, and show remarkably less BIP immunostaining, than do oligodendrocytes in control brain tissue.

Figure 6. Immunofluorescent expression of BIP is increased in Tg/KI mice

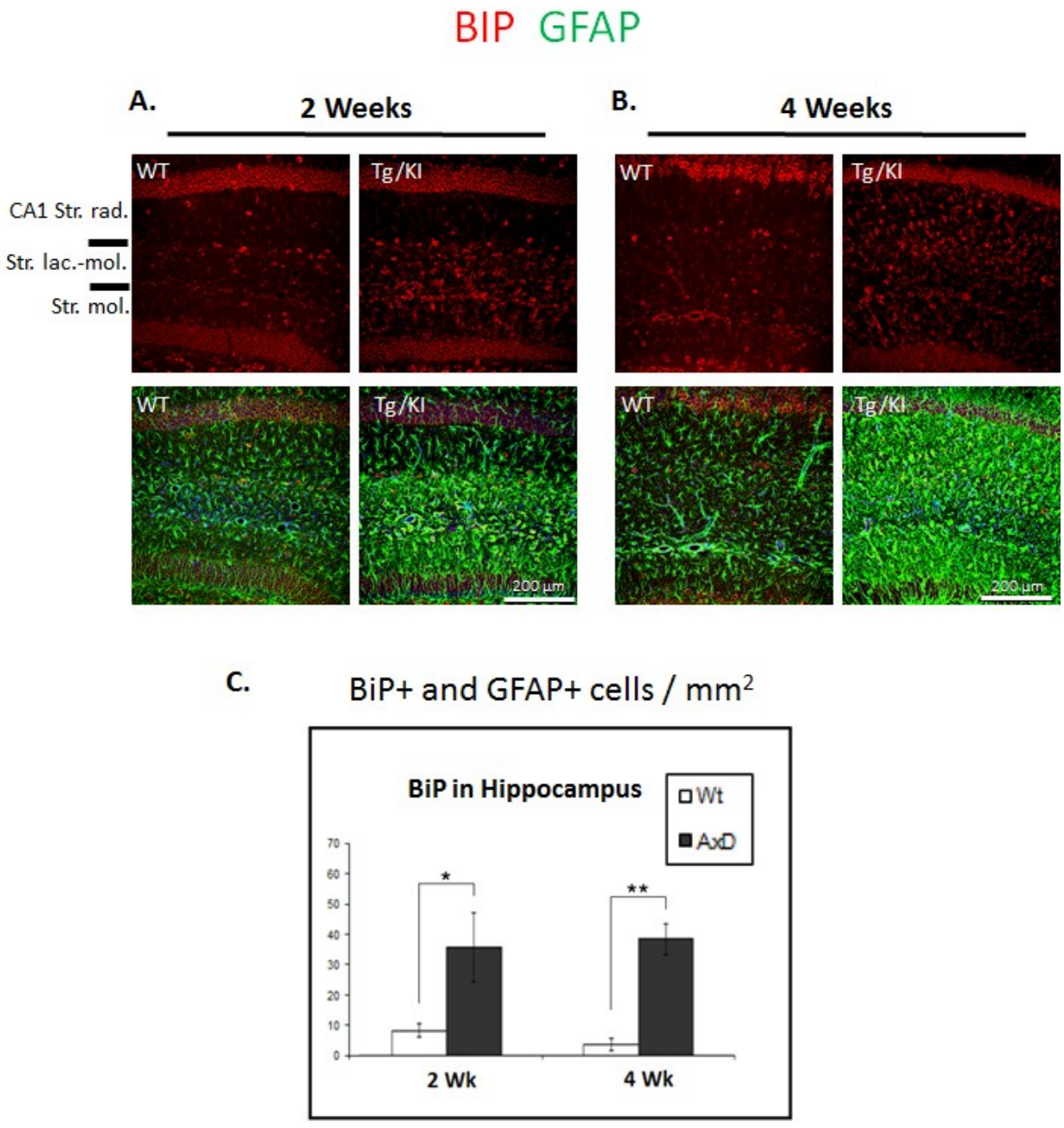

(A-B). Immunofluorescence for BIP was performed in the (A) 2 week (B) and 4 week hippocampus of WT and Tg/KI AxD mouse. Co-immunostaining for GFAP is shown in lower panel. Confocal images of merged stack are shown. (C) Quantitative analysis of BIP+ and GFAP+ cells finds the number of BIP+ astrocytes increased at 2 weeks (*p=0.037) and 4 weeks (**p=0.0085) in Tg/KI total hippocampus. The numbers of labeled cells in a 1-mm^2 area of the indicated hippocampal regions were calculated as described in materials and methods. Data are mean +/- standard error of mean (SEM) of 3 independent experiments. Two way ANOVA with Tukey test; *$p < 0.05$, ***$p < 0.0005$, ****$p < 0.00005$.

.

Figure 7. BIP is associated with GFAP+ astrocytes in hippocampus of Tg/KI mice

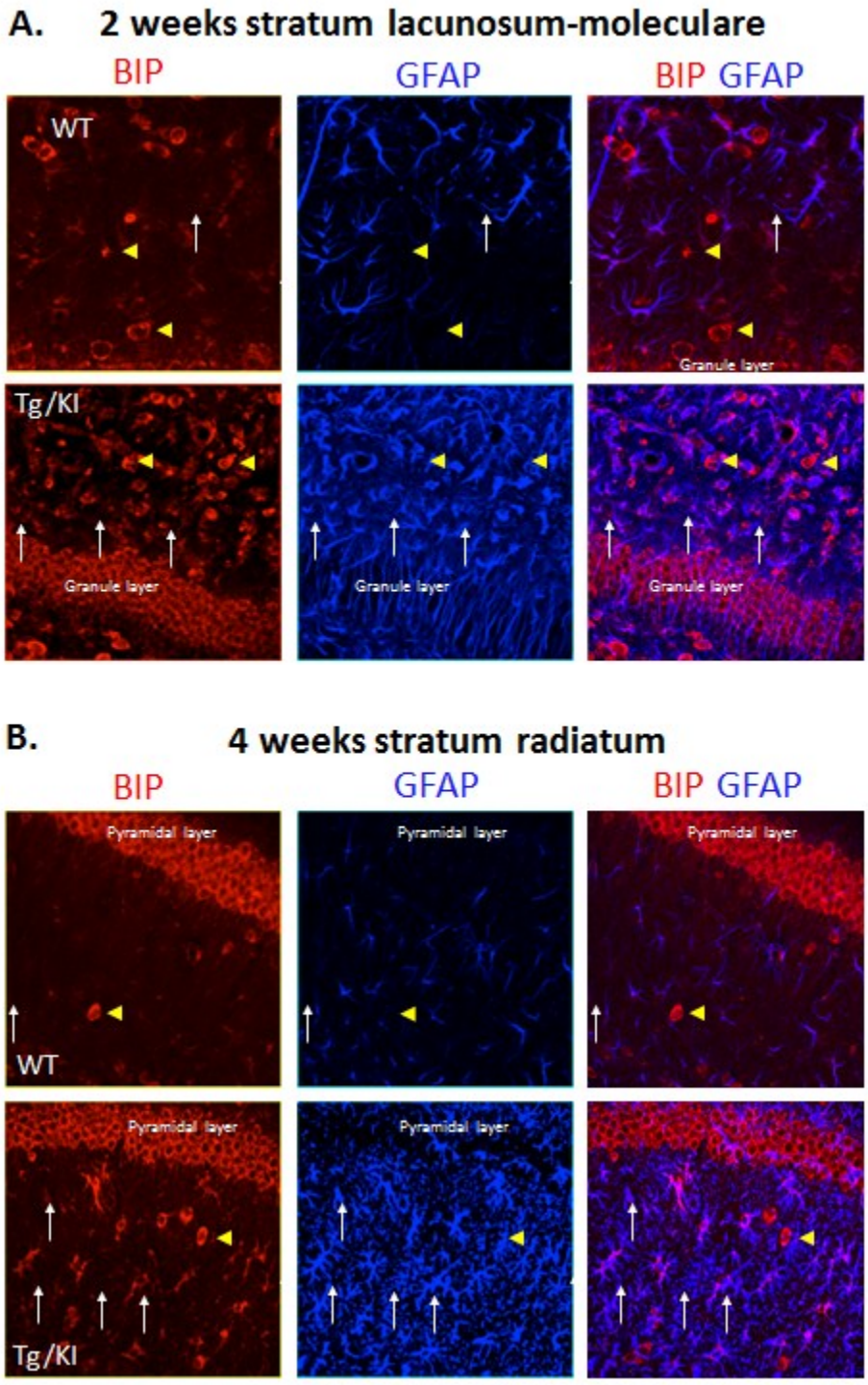

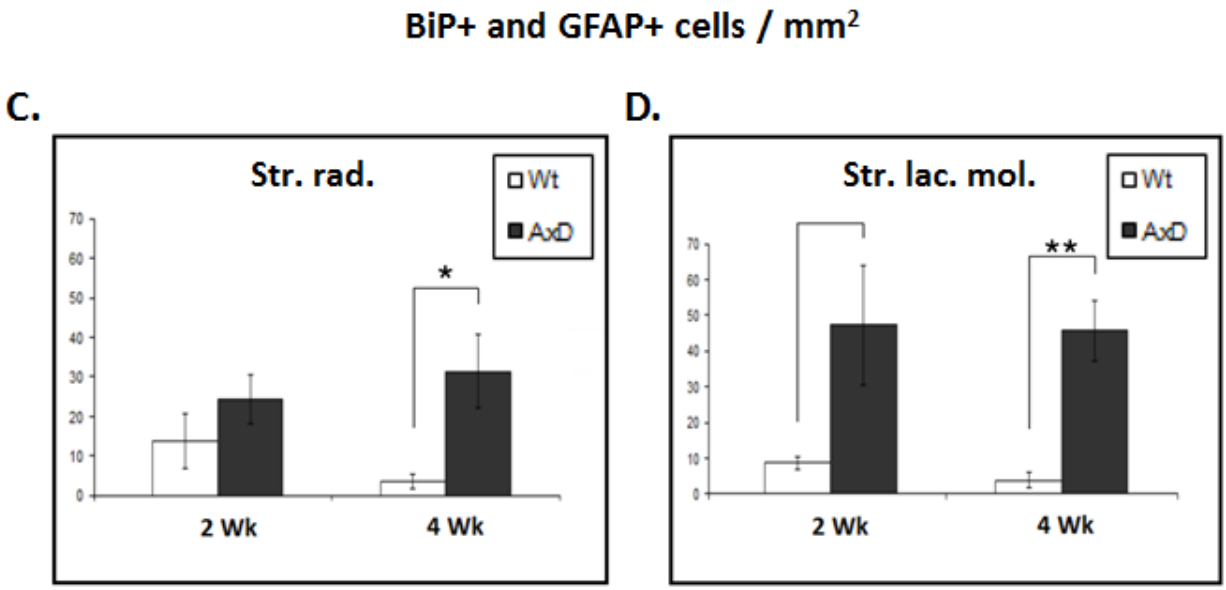

Immunofluorescent expression patterns of BIP in the 2 week (A) and 4 week (B) hippocampus of WT and Tg/KI AxD mouse. (A) In 2 week AxD mouse str. lac.-mol., highest immunoreactivity to BIP in WT (top panel) is in GFAP negative cells (yellow arrowheads), most likely neurons. Astrocytes (white arrows) are lightly immunostained. In Tg/KI animal (bottom panel) many astrocytes show immunostaining for BIP (white arrows), as do GFAP negative cells. (B) 4 week WT animal Str. Rad. (top panel) shows BIP immunostaining in GFAP negative cells (yellow arrowheads), most likely neurons. Astrocytes (white arrows) show light or no immunostaining - less than do 2 week WT astrocyte in (A). In Tg/KI animals (bottom panel) many GFAP positive cells are double immunostained with BIP. Confocal images of merged stack are shown. (C, D) Quantitative analysis of BIP+/GFAP+ cells in the str. rad. (C) confirms a significant increase in BIP+/GFAP+ cells in this at 4 weeks (*p=0.042), but not at 2 weeks while the str. lac.-mol. (D) shows a significant increase at both 2 weeks (*p=0.041) and 4 weeks (**p=0.008). The numbers of labeled cells in a 1-mm^2 area of each of the hippocampal layers were calculated as described in materials and methods. Data are mean +/- standard error of mean (SEM) of 3 independent experiments. Two way ANOVA with Tukey test; *$p < 0.05$, ***$p < 0.0005$, ****$p < 0.00005$.

Figure 8. BIP expression is increased in morphologically aberrant astrocytes in 1 year Tg mice

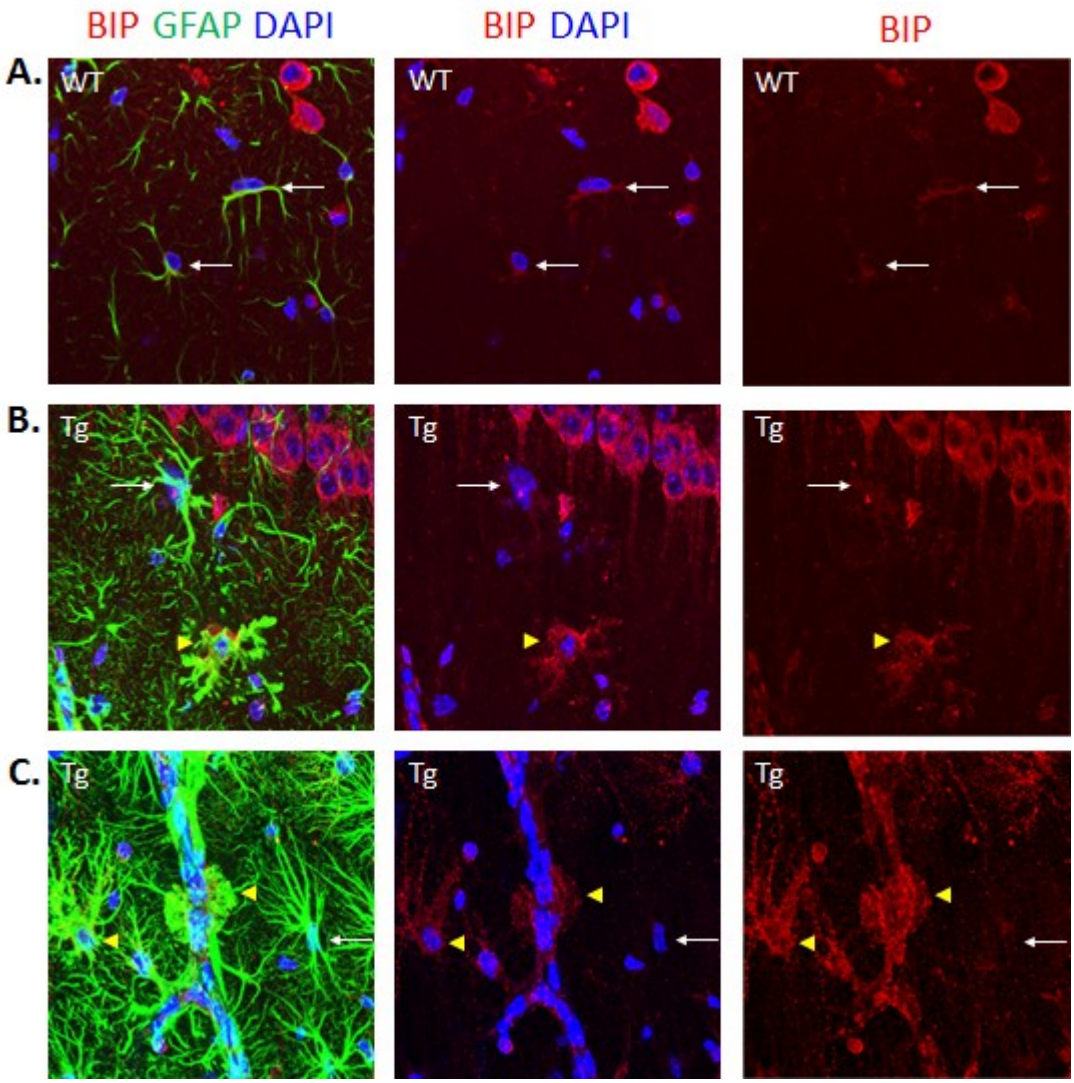

Immunofluorescence for BIP (red), GFAP (green) and DAPI (blue) in the str. rad. of 1 year WT and Tg mice. (A) WT GFAP+ astrocytes (arrows) have compact BIP expression in cell body. (B) Tg shows an astrocyte with aberrant morphology and with what appears to be greatly thickened and retracted processes (yellow arrowhead) while nearby a typical appearing reactive astrocyte has very little BIP expression in comparison (white arrow). (C) High magnification image of a blood vessel in the Tg mouse with GFAP processes surrounding it. Perivascular astrocyte with aberrant GFAP expression (yellow arrow, middle) has large area of reactivity to BIP, while nearby astrocyte (white arrow) appears to have

little or no detectable BIP immunostaining while the astrocyte on the left, with much higher levels of GFAP has greatly elevated BIP (yellow arrowhead, left). Note BIP appears to associate with proximal GFAP processes on this cell in addition to the cell body.

Figure 9. CHOP is co-expressed with BIP in a subset of Tg/KI astrocytes

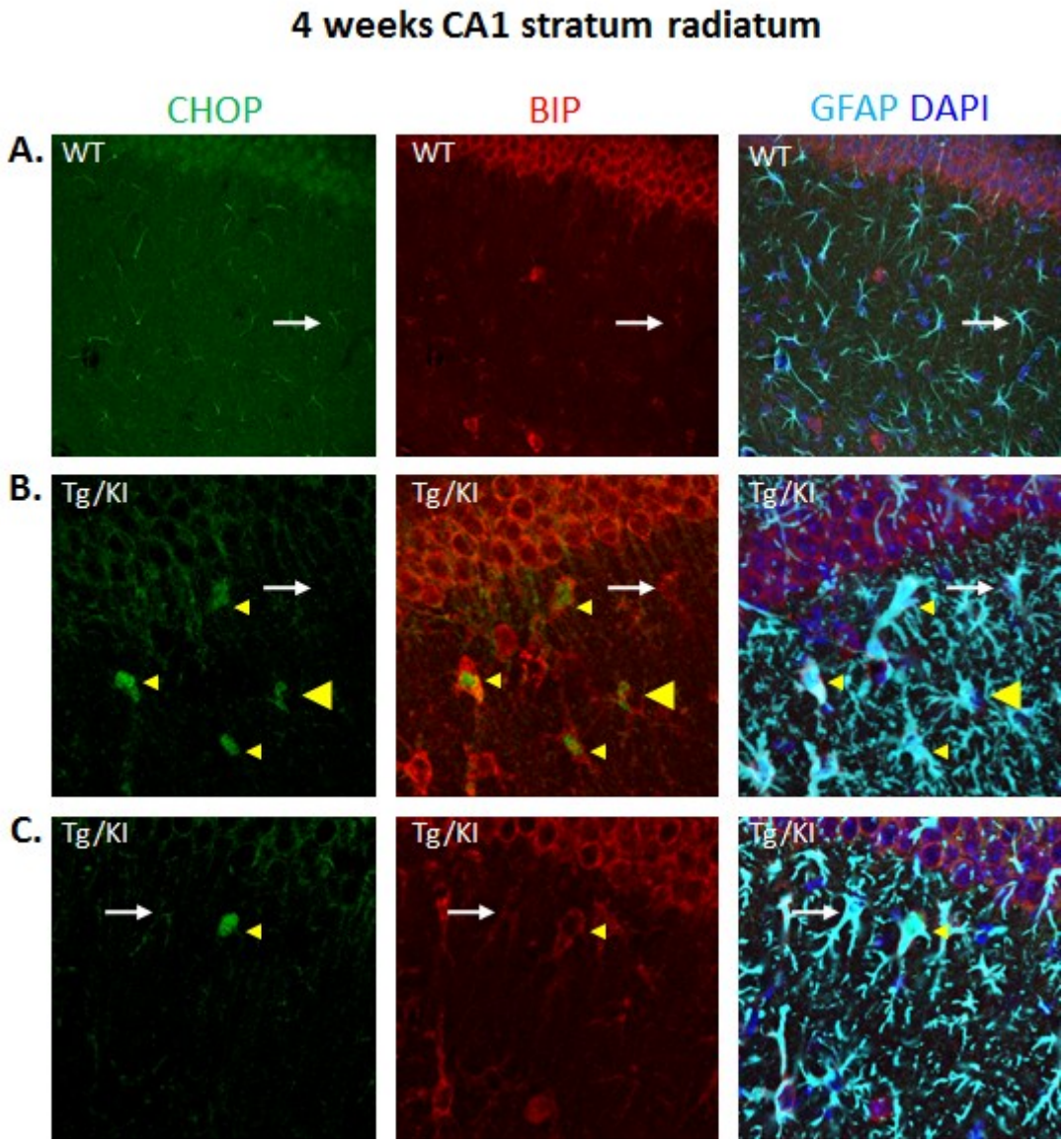

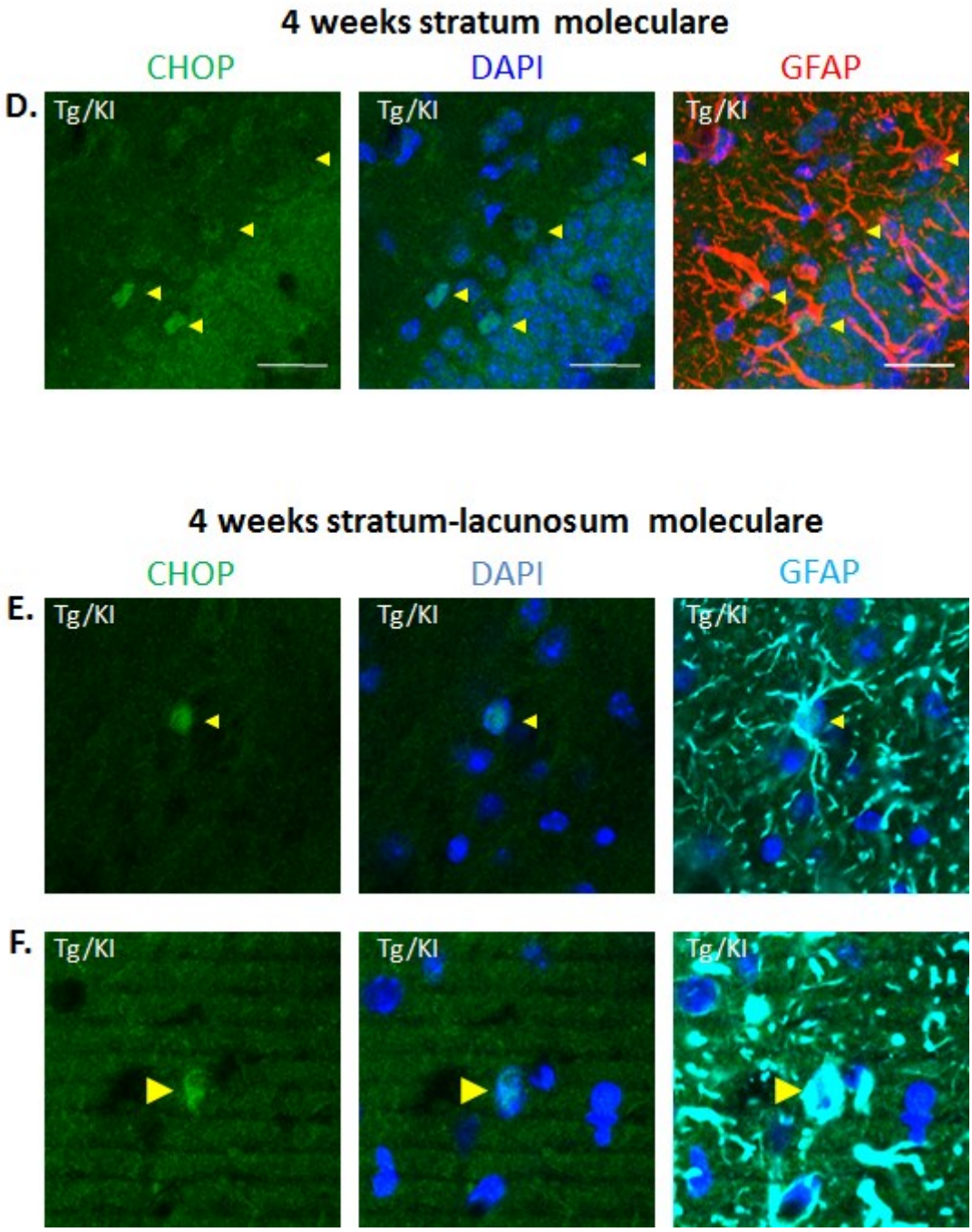

Immunofluorescence for CHOP in the 4 week AxD Tg/KI mouse. CA1 str. rad. (A-C) of WT mouse (A) shows very light immunoreactivity to CHOP in what appears to be GFAP positive processes (white arrows). Astrocytes in Tg/KI animals (B, C) show strong CHOP immunoreactivity in BIP positive and GFAP positive cells (yellow arrowheads). One cell here displays CHOP in the cytoplasm (C, large yellow arrowhead), while other have nuclear expression of CHOP. GFAP positive cells with no reactivity (white

arrows) are far more abundant than these images demonstrate. (D) str. mol. (E, F) str. lac.-mol. Tg/KI GFAP+ cells with CHOP immunoreactivity in the nucleus can be seen (yellow arrowheads). A cell is identified that displays CHOP in the cell body in contrast to most others in the str. lac.-mol. (F, large yellow arrowhead).

Chapter 3

Characterization of CD44, hyaluronan and Ezrin Radixin Moesin proteins in Alexander disease

Introduction

A gene expression study conducted on the olfactory bulb of AxD Tg mice found the mRNA transcript for CD44 was elevated in these mice at both 3 weeks (+ 5 fold) and 4 months (+14 fold) (Hagemann et al., 2005). In the normal human brain CD44 is found in fibrous, sub-pial and sub-ependymal astrocytes, regions where there is higher constitutive expression of GFAP and abundant numbers of Rosenthal fibers in AxD patients. In this chapter, I characterize the expression of CD44 in the brains of AxD patients and mouse models. Second, I explore via immunohistochemistry the expression of its principal ligand, hyaluronan, in the AxD Tg/KI mouse. Finally, I examine the ezrin radixin moesin (ERM) proteins that are associated with the cytoplasmic tail of CD44 in AxD patient tissue and in 1 year old KI mice.

CD44 is a single pass cell surface glycoprotein that was first purified by Underhill and colleagues from white blood cells (Underhill et al., 1985) and was found to be the principal receptor for the extracellular matrix molecule, hyaluronan (Aruffo et al., 1990). CD44 has been found in the mature mammalian CNS localized to the fibrous, sub-pial, sub-ependymal astrocytes (Girgrah et al., 1991; Picker et al., 1989; Quackenbush et al., 1985)and in Muller cells of the retina (Chaitin et al., 1994).

Multiple isoforms of CD44 are generated from a single gene by alternative splicing of 10 (mouse) and 9 (human) non-conserved variant exons which lie between two highly-conserved constant regions (Screaton et al., 1992). The most common isoform, CD44s (for standard), is produced by the excision of all variant exons between the two constant regions, and because it is found on hematopoietic cells is sometimes referred to as CD44H (Peach et al., 1993). This isoform, found expressed in human white matter by Western blot (Girgrah et al., 1991), has a molecular weight of approximately 50kDa, but because of extensive post-translational modifications is usually found to run on SDS gels at between 75-85kDa.

The extracellular region of CD44s, encoded by the first five non-variant axons, is a globular domain and at its far amino terminal end resides a stretch of 90 amino acids called the “link domain” that can bind the extracellular matrix molecule, hyaluronan, and other glycosaminoglycans (Peach et al., 1993; Sherman et al., 1994). The link domain is also found in another glycoprotein, the link protein, which stabilizes the interaction between hyaluronan and aggrecan in the extracellular matrix (Neame and Barry, 1993). Other extracellular matrix proteins – collagen, laminin, fibronectin and osteopontin – can bind to the globular domain of CD44, but their binding sites are not characterized and there appears to be no cellular signaling which is generated by their interaction with CD44 (Borland et al., 1998; as reviewed by Ponta et al., 2003).

Larger splice isoforms of CD44 are generated by insertion of any number of the ten variant domains between the globular domain and the transmembrane domain. The largest among these, CD44v1-10, is expressed by colorectal cancer cells and keratinocytes (as reviewed by Lesley et al., 1993; Ponta et al., 2003; Ponta et al., 1994). In theory, hundreds of splice isoforms of CD44 are possible (van Weering et al., 1993) and several dozen have been detected (Lesley et al., 1993).

CD44 has been found to function as a platform organizer for cell surface proteins and metalloproteases (as reviewed by Ponta et al., 2003) and as a co-receptor for several proteins including Met (Nestl et al., 2001), ERB1 and ERB2 (Yu et al., 2002) and with the Beta1 and Beta2 integrins (Fujisaki et al., 1999; Koopman et al., 1990; Lee et al., 2007b; Vermot-Desroches et al., 1995). Most of these co-receptor interactions are associated with variant isoforms (as reviewed by Ponta et al., 2003).

The c-terminal, cytoplasmic domain of CD44 has sites that bind the phosphorylated ERM (P-ERM) of proteins (Legg and Isacke, 1998; Tsukita et al., 1994; Yonemura et al., 1998), and a separate site for an association with ankyrin (Lokeshwar et al., 1994). Deletion of the ankyrin binding domain of CD44 dramatically reduces its binding to hyaluronan (Lokeshwar et al., 1994) and there are conflicting reports

of the importance of the ERM-binding region to hyaluronan binding (Brown et al., 2005; Legg and Isacke, 1998).

The affinity CD44 has for hyaluronan has been reported to be impacted by many factors: isoform expressed, receptor number and clustering, post-translational modifications; the phosphorylation of CD44 cytoplasmic domain and mitogenic stimuli (as reviewed by Ponta et al., 2003). There are five potential N-linked glycosylation sites on CD44, all of which if mutated abrogate binding (Bartolazzi et al., 1996), however the actual necessity of N-linked or O-linked glycosylation for hyaluronan binding varies between cell type, likely due to influence of the other factors mentioned above (Bartolazzi et al., 1996; Bennett et al., 1995; Katoh et al., 1995; Lokeshwar and Bourguignon, 1991).

CD44-hylauronan interactions in astrocytes have not been well documented. In general, interactions with high molecular weight (HMW) tend to mediate cell migration (Bourguignon et al., 2007; Thomas et al., 1992), pericellular matrix assembly (Knudson et al., 1993), cell aggregation (Green et al., 1988) and the endocytosis and subsequent clearance of hyaluronan in low-pH vesicles (Culty et al., 1990; Miyake et al., 1990; Stamenkovic et al., 1991; Tammi et al., 2001)Membrane-associated metalloproteases are able to cleave the extracellular domain of CD44 close to the transmembrane domain, creating a soluble fragment(Okamoto et al., 1999b). This proteolysis occurs and is regulated by multiple signaling pathways including PKC, cellular calcium influx, members of the Rho family of GTPases and the Ras oncoprotein (Okamoto et al., 1999a). Subsequent to this cleavage, sequential presenilin-1 mediated processing of the transmembrane region (Lammich et al., 2002; Murakami et al., 2003) produces an intracellular domain that travels to the nucleus and acts as a transcription factor for, among other genes, CD44 itself (Okamoto et al., 1999b). Mettaloprotease processing and subsequent intracellular domain generation is preferentially observed on immortalized cancer cells and is thought to contribute to cell motility (Okamoto et al., 1999b).

In development CD44 is expressed on an astrocyte-restricted precursor found in the rat spinal cord (Liu et al., 2004) and the white matter of the mouse cerebellum (Cai et al., 2012). When sorted from embryonic brains and cultured without growth factors, most of these astrocyte restricted precursors cells die, however surviving cell differentiate into GFAP+ astrocyes and under no conditions differentiate into neurons or oligdendorcytes. CD44 is also expressed on neuronal precursor cells (NPCs) derived from brains of the rat and human embryo (Baghbaderani et al., 2011; Rampon et al., 2008).

In pathologies of the CNS, CD44 is found on reactive astrocytes both in white and grey matter. It has been found on astrocytes of patients with Multiple Sclerosis (MS) (Cruz et al., 1986; Girgrah et al., 1991), children with perinatal white matter injury (Buser et al., 2012), and in canine distemper disorder (Alldinger et al., 2000) where astrocytes are a viral target. In rodent models of disease and injury, CD44 has been found in astrocytes in EAE mice (Haegel et al., 1993), EAE rats (Kim et al., 2004) and in SOD1G93A ALS model mice (Matsumoto et al., 2012). The transcript has also been found upregulated in astrocytes at very early timepoints after both middle cerebral artery occlusion and LPS injection (Zamanian et al., 2012).

CD44 is widely expressed in cancer cells and is a marker for cancer stem cells (Visvader and Lindeman, 2008). In rodent CNS gliomas it has been observed to be preferentially expressed on cells located on the invasive front of the tumor and is seen on cells that escape through GFAP positive cells which separate the tumor from the surrounding parenchyma (Wiranowska et al., 2006). Additionally, CD44 is found on astrocytoma cell lines one of which, interestingly, has been demonstrated to bind and internalize myelin basic protein preferentially via a spice variant (Owh et al., 1997).

We found CD44 to be a compelling candidate to explore with respect to AxD pathology for three reasons: first, its elevation at both early and late time periods as determined by microarray (Hagemann et al., 2005); second, the expression pattern of CD44 in the normal brain—astrocytes in the white

matter, sub-pial and subependymal regions—parallels that of normal astrocytes with higher levels of GFAP expression, and of Rosenthal fibers in AxD; and third, its expression in association with demyelinating tissue (Alldinger et al., 2000; Buser et al., 2012; Cruz et al., 1986; Girgrah et al., 1991; Haegel et al., 1993; Kim et al., 2004; Matsumoto et al., 2012). Here I characterize CD44 expression in AxD patient tissue and in that of AxD model mice. Additionally, I characterize the expression of the extracellular matrix molecule hyaluronan, the principal ligand of CD44 (Aruffo et al., 1990). Finally, I characterized ERM proteins, which are able to link CD44 to the actin cytoskeleton. I reveal several novel findings in increased expression of CD44 and ERM proteins in both AxD mice and in patient tissue, and hyaluronan in Tg/KI mice.

Results

AxD patients have increased immunohistochemical expression of CD44

In the normal human brain, CD44 is expressed in fibrous, sup-pial and sub-ependymal astrocytes, areas where normally GFAP is highly expressed and in AxD patients, and where there are abundant Rosenthal fibers and pathological astrocytes. In order to determine if CD44 protein is elevated in expression in patients as is its transcript in AxD Tg mice (Hagemann et al., 2005), we conducted by an immunohistochemical analysis of CD44 expression in two AxD patients and two control patients using a monoclonal antibody that recognizes all isoforms of the protein. We first examined the subcortical white matter and proximal cortex. In the control patient the white matter showed very light, diffuse immunostaining of much of the white matter and was especially strong around blood vessels (Fig 1A, white arrow). Individual astrocytes (Fig 1C, black arrow) and long, thin astrocytic processes could be distinguished, some extending into the adjoining cortex where there was little overall CD44 reactivity (Fig 1C, white arrows). In comparison to control tissue, in the AxD R239H patient subcortical white matter, there was very intense overall immunostaining of the white matter that extended well into the proximal cortex (Fig 1B, D), unlike that of the control patient. Immunostaining was not ascribable to

individual cells or even blood vessels, except for occasional enlarged astrocytes which could be more easily distinguished in the proximal cortex (Fig 1B and D). Immunostaining in AxD patient tissue was also found greatly increased at the pial surface (Fig 1F), in comparison to controls (Fig 1E). We next examined the hippocampus, where protoplasmic astrocytes express high levels of GFAP and where in autopsy tissue of AxD patients, there is extensive loss of CA1 neurons(Tian et al., 2010). In the control patient, there was a thin band of intense CD44 immunoreactivity in the str. lac. mol. (Fig 1G, arrowhead) and diffuse overall immunostaining of the hilus (Fig 1G, "Hilus"), especially around blood vessels, similar to what we observed in the control white matter. In the AxD R416W hippocampus there was intense and greatly increased immunoreactivity to CD44 in the str. lac. mol., CA1 and hilus (Fig 1H, arrowhead, arrows and "Hilus," respectively). When I compared CD44 protein expression by Western blot in three patients versus two controls, differences in CD44 expression levels were not apparent (Fig 1L). This may be due to degradation of tissue stored and freeze-thawed many times over long periods and also to the fact that we attempted to isolate white matter, which is often difficult in type I patients because it is degraded and substantially cavitated.

CD44 is elevated in at 2 and 4 weeks in AxD Tg/KI mouse

We next examined total protein levels and the anatomic expression of CD44 in the Tg/KI mouse hippocampus at 2 and 4 weeks. Immunofluorescent expression of the CD44 in the WT mice was strictly confined to a distinct arc covering the str. lac.-mol. and an immediately adjacent portion of the str.rad. at both 2 (Fig 2A, left) and 4 weeks (Fig 2B, left). At 2 weeks in the Tg/KI mouse, an intensely abnormal expression pattern of CD44 can already be seen (Fig 2A, right). The diffuse overall immunostaining of WT str. lac.-mol. is gone and instead, many focal increases of CD44 immunoreactivity can be detected throughout the str. lac.-mol. and extending into the proximal str. rad. and most of the str. mol. By 4 weeks, CD44 immunoreactivity extends into the entire str. rad. mol. and appears elevated throughout the hippocampal layers we examined. Western blot analysis of CD44 protein expression in the Tg/KI

mouse hippocampus at 2 and 4 weeks confirmed what we had found by immunofluorescence (Fig 2C) and densitometric analysis demonstrated that there was an approximately 2.5-fold increase in CD44 in the Tg/KI hippocampus at 2 weeks (*$p < 0.05$) and a greater than 3 fold increase at 4 weeks (***$p < 0.0005$). Additionally, CD44 levels rose significantly in the Tg/KI hippocampus between 2 weeks and 4 weeks (*$p<0.05$) where there was no significant rise in CD44 in the WT hippocampus between those two timepoints. Data are mean +/- standard error of mean (SEM) of 3 independent experiments. Two way ANOVA with Tukey test; *$p < 0.05$, ***$p < 0.0005$, ****$p < 0.00005$.

Comparison of CD4 and GFAP in all AxD mice

Next I examined CD44 in the hippocampi of Tg/KI mice at 4 weeks along with GFAP expression and compared it to WT, KI and Tg littermates (Fig 3). In line with previous reports (Hagemann et al., 2006; Messing, 1998), many astrocytes in the hippocampi in the Tg and KI animals displayed high levels of GFAP versus WT (Fig 3E and H), although the GFAP+ astrocytes in both were less widely distributed than in the Tg/KI mice (Fig 3K). The Tg/KI mice show very high levels of CD44 at 4 weeks (Fig 3J) and this coincided anatomically with areas of increased GFAP signal (Fig 3K and L). Astrocytes in the KI and Tg mice accumulated CD44 in the str. mol. and str. rad. immediately adjacent to the str. lac.-mol., but to a much lesser extent than in the Tg/KI mice (Fig 3D and G). In the 4 week Tg and KI mice, reactive-like astrocytes were observed mainly in the str. lac.-mol. (Fig 3E and H, arrows), similar to the pattern observed in Tg/KI mice younger than 2 weeks (Sosunov et al., 2013). Thus, both the Tg and KI mice showed pathological changes in expression of GFAP and CD44 similar to, but far less severe, than those in the Tg/KI mice.

Heterogeneous expression of CD44 in Tg/KI mice occurs in GFAP positive astrocytes

While the increased levels of GFAP immunostaining seemed to be coincident with increases seen in CD44 in KI, Tg and Tg/KI mice (Fig 3), we next examined more closely 4 week old WT and Tg/KI mice for co-expression of these two proteins. At low magnification, 4 week old WT animals display a single swath

of intense diffuse CD44 immunoreactivity that covers the entire str. lac.-mol., extending into the str. rad. and this cannot be ascribed to individual cells. At this same magnification in 4 week Tg/KI animals, many individual astrocytes can be seen that display CD44 immunoreactivity around GFAP positive cells (Fig 4B, yellow arrowheads); however, the immunostaining is heterogeneous from astrocyte to astrocyte. Some GFAP+ positive cells next to GFAP+/CD44+ cells show little or no detectable CD44 (Fig 4B, white arrows). We noted especially high signal for CD44 that was very closely associated with GFAP+ processes that was not associated with a nucleus in this merged stack (yellow arrowheads). We looked more closely at CD44 in two week WT animals using higher magnification at the str.lac./str. mol. border and found CD44 signal to be heterogeneous on WT astrocytes also (Fig 4C). Some astrocytes could be observed with diffuse membrane staining (Fig 4C, yellow arrowhead) while others appeared to have no membrane staining (white arrow Fig 4C). In addition to the GFAP+ processes, which appear to be extending from the dentate gyrus is also CD44+, it is likely that the WT expression of CD44 in the str. lac./str. rad. of the hippocampus stems from astrocytes.

Aberrant CD44 immunostaining of astrocytes in 4 week old Tg/KI animal

Astrocytes have many fine, intricate processes, which allow them to make contact with other cells. As a plasma membrane protein, CD44 displays a diffuse and fluffy appearance when observed in the 4 week str. lac.-mol. by high magnification (Fig 4D). This is similar to what I observed on astrocytes in 2 week old WT animals (Fig 4C). When I examined astrocytes at high magnification in the 4 week Tg/KI SLM I see what appears to be a reticulated expression of CD44 on membranes. In the WT, the staining looks granular and fairly homogeneous, while in the Tg/KI it looks less granular and more linear, with a lack of immunostaining in between these short lines. This is similar to the change we observe in other astrocytic membrane proteins, Glast and Glt-1, that we observed in the Tg/KI hippocampus of animals of this age (Sosunov et al., 2013). Thus, it appears that the plasma membrane of astrocytes is remarkably different in the 4 week old Tg/KI animal compared with WT animals.

Hyaluronan accumulates Tg/KI mouse

Because CD44 is the principal receptor for the extracellular matrix molecule hyaluronan (Aruffo et al., 1990), I next examined the distribution of hyaluronan in the hippocampus of the 2 and 4 week Tg/KI mice and WT controls using a biotinylated hyaluronan-binding protein, and subsequently visualized using a fluorescently labeled streptavidin probe. We double stained these sections with an antibody to CD44. The hyaluronan staining in WT animals at both 2 (Fig 5A) and 4 (Fig 5B) weeks of age was strictly limited to the str. rad. and could also be observed above the pyramidal cell layer in the stratum oriens. The str. lac.-mol. and str. mol. have a far lower hyaluronan signal than the str. rad. When I compared CD44 with hyaluronan in these same WT animals and merged the images (Fig 5A and B bottom panel) the degree to which the two occupied separate but adjacent layers in the hippocampus was striking as was the lack of immunoreactivity in the str. mol. (Fig 5B bottom). Thus, the hyaluronan binding protein distribution did not match that of CD44 in the WT hippocampus. In contrast, the hyaluronan staining in the Tg/KI animals was visible throughout the hippocampus at both 2 weeks (Fig 5A) and 4 weeks (Fig 5B) as was the distribution of CD44. The specificity of the biotinylated probe for hyaluronan was demonstrated by treating a 4 week Tg/KI section with bovine testicular hyaluronanidase before immunostaining with the biotinylated hyaluronan-binding protein and streptavidin-labeled fluorescent secondary antibody (Fig 5C). Because AxD disease patients show pathology at the pial surface, I also examined the pial surface of the cortex of 4 week Tg/KI mice and found increased expression of hyaluronan here also (Fig 5D). The immunostain also shows far more GFAP in the upper cortical layers in the Tg/KI mouse. To quantitate hyaluronan expression, optical density measures were taken and found to be significantly increased in the total hippocampus of Tg/KI mice at 4 weeks (*p=0.035) (Fig 5E) and when optical density was quantitated by hippocampal layers, hyaluronan expression was found significantly increased at 4 weeks in Tg/KI animals in the str. mol. (**p=0.007) and str. lac. (*p=0.035) over WT counterparts (Fig 5G).

AxD patient tissue shows increased immunohistochemical staining of P-ERM

Because CD44 can associate with actin and the underlying cytoskeleton through interactions with phosphorylated ERM proteins (P-ERM), I was next interested in examining the expression of ERM proteins in AxD patient tissue. Cortical sections that included underlying white matter of a R239H patient and an age-matched control were examined (Fig 6). First I used an antibody that is reported to recognize the total pool of ERM proteins, both phosphorylated and non-phosphorylated, to examine the white matter and adjacent cortex (Fig 6A and 6B). The AxD patient showed total ERM staining in some astrocytes (Fig 6B, white arrows) and faint localization to Rosenthal fibers. The control patient showed only staining of blood vessels (Fig 6A). Next I used an antibody for P-ERM that recognizes the activated pool of ERM proteins to examine patient tissue. While there was no reactivity to P-ERM antibody in the control cortex or white matter (Fig 6F) and none in AxD cortex (Fig 6G), AxD patient white matter was positive for P-ERM (Fig 6C, D and E). In well-preserved portion of AxD patient white matter, there is an increased overall staining for P-ERM (Fig 6C) and individual astrocytes can be seen with immunoreactivity to P-ERM in their cell bodies (Fig 6C, white arrows). In deeper, more pathological white matter, where there is widespread loss of myelin, immunostaining of astrocytes is dramatic (Fig 6D and E). There are many streaks of relatively straight processes that are immunostained for P-ERM and some can be seen to localize to astrocytes (yellow arrowhead). In addition there are intensely immunostained and unusual clusters of Rosenthal fibers (red arrows).

Glioblastomas have high levels of immunoreactivity to ezrin (Geiger et al., 2000). Accordingly, I immunostained two serial sections of glioblastoma tissue for P-ERM (Fig 6H) and total ERM (Fig 6I) as positive controls, and found the necrotic core (Fig 6H, arrows) to be more reactive to P-ERM than total ERM, demonstrating that increased reactivity shown by AxD tissue to the P-ERM antibody versus total ERM antibody by AxD tissue is most likely a function of difference in affinity of antibodies to antigens and not a function of AxD pathology.

ERM proteins are greatly increased in 1 year old KI mice

Given the increased expression of CD44 in patients and mice, the striking immunostaining of patient tissue with P-ERM and the potential for CD44 and ERM proteins to interact (Legg and Isacke, 1998; Tsukita et al., 1994; Yonemura et al., 1998), I examined several different genotypes of AxD mice for expression of P-ERM. We used an advanced age for Tg and KI mice, reasoning that the pathology may be more severe with aging. In 1 year old WT mice examined at low magnification, I observed a light, diffuse overall immunostaining for P-ERM (Fig 7A). However, in the 1 year old KI (Fig 7B) and 9 month Tg (Fig 7C) there was intense focal immunoreactivity for P-ERM in the str. rad. and the stratum oriens, while the diffuse overall immunostaining observed in WT mice did not seem to be present (Fig 7A and B). In 1 month WT there was almost no detectable P-ERM in contrast to the 1 year WT. Surprisingly, the 1 month old Tg/KI mouse had less immunoreactivity to P-ERM than did both the 1 year KI and Tg mice. There was less P-ERM immunostaining than in the aged Tg and KI mice, but still above that for one month WT, while there was the high immunoreactivity to P-ERM in both KI and Tg animals. I further characterized ERM protein expression with respect to CD44 and GFAP in the 1 year KI mouse. When we co-immunostained for CD44 and P-ERM, CD44 expression was more widespread (Fig 7F) and the two proteins were variably coexpressed on the same cells (Fig 7G). Some cells were found to coexpress CD44 and P-ERM (Fig 7G bottom panel, arrow), while many cells do not (Fig 7G top panel). I next co-immunostained for GFAP and P-ERM and found interestingly that at least some of the abnormal P-ERM immunoreactivity was associated with GFAP positive cells (Fig 7I, J and K, arrows). Notable and surprise was the bizarre pattern of P-ERM expression in relation to GFAP (Fig 7J and K). These immunostains suggested the astrocyte membrane may be retracted. In order to determine if this was true, I next co-immunostained the KI mouse hippocampus with P-ERM and GLT-1, an astroctytic membrane-localized glutamate transporter. I found that cells with abnormally close association between P-ERM and GFAP

did not show alteration in GLT-1 immunostaining. Thus, while P-ERM appears to have lost its association with the membrane, the membrane is intact (Fig 7L).

Total moesin and total ezrin are dramatically increased in 1 year old KI mice and moesin co-localizes with CD44

To try to gain insight on which of the three ERM proteins are aberrantly associated with GFAP positive cells, I further characterized KI mice for total ezrin (Fig 8) and total moesin (Fig 9) expression. Ezrin has been found to be associated with fine astrocytic processes ensheathing synapses (Derouiche and Frotscher, 2001). Given the morphological changes we observed in AxD astrocytes (Chapter 2 Fig 2-4) (Sosunov et al., 2013), I was interested in analyzing immunofluorescent expression of this membrane to cytoskeletal linker protein in the AxD mouse hippocampus. We found ezrin expression increased in the 1 year old KI mouse (Fig 8B, bottom), however if tissue section were not treated with antigen retrieval ezrin expression was difficult to determine (Fig 8A) and therefore we did not determine if there is co-expression of this protein with CD44 (Fig 8A). Co-immunostaining with GFAP revealed some that some ezrin immunoreactivity was closely associated with GFAP+ processes (Fig 8B, bottom), especially in the stratum oriens (Fig 8B, bottom). Moesin immunostaining is also increased in comparison to WT (Fig 9A and B) and moesin and CD44 appear to have a high co -expression with cd44 (Fig 9A).

Discussion

In this chapter, I used immunohistochemistry and Western blot analysis to study the expression and distribution of CD44, along with its ligand hyaluronan, and ERM proteins which are able to link many cell surface receptors, including CD44, to the underlying cytoskeleton. Because the expression of these proteins has never been characterized in AxD patients or model mice, these findings are novel and some are notable. First I discovered that CD44 is increased in expression in the CNS of AxD patient tissue and dramatically increased in the hippocampus of Tg/KI AxD mice. I noted that this expression in the mouse coincided spatially and temporally to increases in the levels of GFAP. Most remarkably I found

widespread increases in the amount of hyaluronan that was recognized by a biotinylated hyaluronan binding protein Finally, I found in patient tissue and AxD 1 year old KI mice increased and unusual expression of Phospho-ERM proteins (PERM). Further characterization of CD44 and ERM proteins determined a high degree of co-immunostaining between cd44 and moesin.

High levels of Hyaluronan immunostaining in Tg/KI mice

I found very high levels of hyaluronan immunostaining in both the 2 week and 4 week Tg/KI mouse. While other AxD model mice and AxD patient tissue has not been stained for hyaluronan, the overwhelming presence at both two weeks and four weeks of age, along with CD44, suggests that this may be a significant finding. Hyaluronan serves as an organizer of the extracellular matrix in cartilage (Knudson, 1993) and from experiments showing neurocan and chondroitin sulfate release after hyaluronanidase treatment, it appears to function similarly in the hippocampus (Forster et al., 2001).

CD44 and hyaluronan also found together in demyelinating disorders

Type I AxD is a leukodystrophy. Infant AxD patients have massive, frontal myelin loss and type II patients often have focal white matter lesions that would suggest myelin damage or loss that was not able to be repaired. The mechanism by which a mutation in GFAP causes the de/dysmyelination in AxD is entirely unknown. We found greatly increased expression of CD44 on astrocytes and a widespread and significant increase in the CD44 ligand hyaluronan in the hippocampus of AxD Tg/KI mice and found CD44 increased in AxD patient tissue (hyaluronan expression was not assayed in patients). CD44 on astrocytes (Alldinger et al., 2000; Back et al., 2005; Buser et al., 2012; Cruz et al., 1986; Girgrah et al., 1991; Haegel et al., 1993; Kim et al., 2004) and, more recently, hyaluronan in the surrounding ECM (Back et al., 2005; Buser et al., 2012; Sloane et al., 2006) have been noted in other diseases and disorders where myelin is lost.

The role for CD44 in astrocytes in conditions of demyelination has not been elucidated. One author hypothesized that the white matter injury itself may be the source of increased CD44 on astrocytes (Alldinger et al., 2000), drawing from a study that a found a 100kDa splice variant of CD44 on an astrocytoma line could preferentially bind and internalize myelin basic protein, which in turn increased the expression of CD44 on these cells (Owh et al., 1997). A T-cell-like role for astrocytes expressing the v6 CD44 isoforms has also been proposed (Haegel et al., 1993), partially due to the fact that primary astrocytes in culture stimulated with cytokines express the same v6 isoform of CD44 as that is expressed by activated T cells.

Post-translational modifications are critical for the functioning of CD44 with respect to binding and uptake of hyaluronan. We found that in human tissue cd44 was expressed at about 80 kDA and this did not appear to vary between patient tissue and control tissue. In mice CD44 this was at a slightly lower molecular weight than in humans – at about 72kDa. In four week animals, two of three experiments showed slightly higher MW for the Tg/KI mice over AxD patient controls (only one shown).

CD44 isoforms

CD44 mRNA can be extensively processed to isoforms larger than CD44s. Treatment of rat primary astrocytes with TNF alpha induces expression of the v6 isoform (Haegel et al., 1993), which migrates more slowly on a Western blot than does CD44s. As mentioned above, CD44 on our Western blot analysis of AxD patient tissue ran at about 80kDA and no larger isoforms were observed. In Tg/KI mouse lysates at both 2 weeks and 4 weeks, the IM7 antibody, which reacts with the epitope of CD44 common to all splice isoforms, also showed no evidence of more slowly migrating bands. However, because these splice isoforms are likely expressed at lower levels, they may not have been detected. Western blot of AxD and control patient tissue showed no difference with respect to CD44 expression. This is contradictory to my immunohistochemistry of CD44, which showed a much higher presence of CD44 in AxD tissue. The IM7 antibody we used requires non-reducing conditions, which may affect the ability to

detect differentially post-translationally modified species of CD44. Collectively, these reasons further support a thorough biochemical analysis of CD44 in both mouse and human tissue, including immunoprecipitation of CD44 to determine if alternates are expressed.

Reactive astrocytes and CD44

The likelihood that increased CD44 is specific to white matter disorders is unlikely. It is widely expressed on reactive astrocytes in a range of CNS diseases and after injury, including as early as one day after LPS induced inflammation and or middle cerebral artery occlusion (Zamanian et al., 2012), suggesting that both the presence of cytokines and conditions of oxidative stress or hypoxia impact its expression.

Along with increased levels of CD44, I also found profound changes in shape to these astrocytes. Because CD44 participates in a diverse number of events related to cell motility, such as the extravasion of leukocytes and migration of cancer cells (as reviewed by Marhaba and Zoller, 2004), and participates in both the retraction and extension of cell processes in migration (Marrero-Diaz et al., 2009), it is possible that the increase in CD44 expression on these astrocytes mediates this shape change through interactions with the underlying ECM.

In the four week old animal I noticed that some of the highest levels of immunoreactivity to CD44 were with GFAP+ processes that could not be traced to a perinuclear cell body within the image (Fig 4B, yellow arrowheads). This suggests these processes were distal from the cell body and possibly extending. I noticed that CD44 was much more closely associated with the GFAP+ processes in these cells than in some other CD44+ cells, suggesting that the plasma membrane may be retracting into a hypertrophied GFAP process or vice versa. CD44 is expressed on cells transformed from an epithelial to a mesenchymal phenotype, where cells re-express stem cell markers (as reviewed by Marhaba and Zoller, 2004). These cells may participate in the transformation of astrocytes to a reactive phenotype. In cultured astrocytes cd44-hyaluronan interactions induce Rac1 signaling and cytoskeleton-mediated

migration, and this may be indicated in these cells by the abundance of hyaluronan (Bourguignon et al., 2007).

It is also possible that the CD44 on these cells is inhibitory to proliferation. A subset of reactive astrocytes in models of injury and disease are able to proliferate (Buffo et al., 2008; Guo et al., 2011; Miyake et al., 1988). CD44-null NPCs hyperproliferate both *in vitro* and in the subgranular zone of older adult mice. It is possible that CD44 serves as an inhibitory molecule to astrocyte proliferation, possibly through interactions with hyaluronan.

In AxD, as in other conditions of reactive gliosis where CD44 is found on astrocytes, we do not know the what role this membrane glycoprotein plays, however its abundant expression on GFAP + astrocytes in the hippocampus of these mice offers an opportunity for biochemical analysis of isoforms expressed, post-translational modifications and through co- immunoprecipitation assays the determination of associated proteins. In other words, AxD mice present an opportunity to potentially elucidate the role of CD44 in reactive astrocytes.

Hyaluronan increase may have inhibitory effects on OPC differentiation and neurogenesis

The high levels of hyaluronan observed in AxD Tg/KI mice could be significant to the pathology of AxD with respect to myelination and deficits in memory and learning observed in the mouse. Hyaluronan or hyaluronic acid (HA), is a very large glycosaminoglycan that consists of highly regular repeats of multiple disaccharide units of glucuronic acid and N-acetylglucosamine (Toole, 2004). It is produced by hyaluronan synthetases, HAS1, HAS2 and HAS3, which are located just under the plasma membrane of cells (Luke and Prehm, 1999). Hyaluronan usually exists as a high molecular weight (250kDa-4,000kDa), and at this high molecular weight has been demonstrated to initiate angiogenesis, motility of cells and cell growth. Hyaluronan has a very short half-life.

The mechanisms of hyaluronan signaling, synthesis, degradation and uptake are much better understood in the periphery than in the CNS. For example, it is known that hyaluronan receptor for endocytosis (HARE) and hyaluronanidases such as the GPI-linked HYAL-2 are involved in uptake and degradation of hyaluronan (Sampson et al., 1992; Weigel and Weigel, 2003). In the CNS, where HARE is not found (Weigel and Weigel, 2003), it is hypothesized but not yet demonstrated that uptake of hyaluronan occurs through CD44-mediated interactions on astrocytes. Thus, the impaired function of astrocytes in AxD could impede this process.

Hyaluronan is highly expressed in the CNS in development and thought to provide a hydrated and otherwise beneficial environment that facilitates growth and migration of developing cells (Bignami and Asher, 1992). As rodents develop, hyaluronan expression at the perinatal period in the CNS declines – about the same time that vimentin decreases, GFAP expression increases and myelination begins (Bignami and Dahl, 1985).

There are a number of "hyaluadherins" other than CD44 that might mediate molecular change, including RHAAM, CDC37, Hbp, IHABP4, TSG-6, LYVE-1, LEC (as reviewed by Girish and Kemparaju, 2007). In addition, other ECM proteins can adhere to hyaluronan such as versican, aggrecan, link protein, brevican, neurocan and fibrinogen (as reviewed by Girish and Kemparaju, 2007). Interactions of hyaluronan with these components of ECM may also have an effect in the Tg/KI hippocampus.

Interestingly, small, potentially more pathological LMW fragments of hyaluronan can be produced by both hyaluronanidases and inflammatory events such reactive oxygen species (Agren et al., 1997; Moseley et al., 1997; Sampson et al., 1992) and these LMW fragments have been shown to participate in signaling and generate a variety of cytokines, including monocyte chemoattractant protein-1 (MCP-1) (McKee et al., 1996), which was found highly upregulated in the Tg mice via microarray (Hagemann et al., 2005) and that I have found increased in AxD Tg/KI mice primary cultures (E. Guilfoyle, E. Hod

unpublished data). The molecular weight determination for hyaluronan in the Tg/KI hippocampus have not yet determined, therefore the effect of excess hyaluronan in the Tg/KI mouse hippocampus is difficult to predict.

The aberrant presence of hyaluronan in AxD mice may have inhibitory effects on oligodendrocyte precursor cell (OPC) proliferation and differentiation. Studies from two separate groups studying hyaluronan in the context of MS and animal demyelination have demonstrated that the presence of hyaluronan is inhibitory to OPC differentiation (Sloane et al., 2010). While one group found HMW hyaluronan preferentially inhibitory to OPCs, Sloane and colleagues, in a more extensive study, found that LMW hyaluronan generated from HMW hyaluronan by hyaluronanidase expression on OPCs inhibitory through interaction with TLR2 expressed by OPCs in MS lesions in conjunction with MyD88 (Sloane et al., 2010). This suggests several avenues of research with respect to the expression of hyaluronan in AxD and its inhibitory effects on OPCs. It may be mechanism for demyelination in AxD or the inhibition of myelin repair.

The increase and aberrant localization of hyaluronan in AxD mice may also have effects on adult neurogenesis. This may explain why older AxD model mice show deficits in memory and learning (Hagemann et al. unpublished results). The presence of hyaluronan in the adult dentate gyrus subgranular zone has been shown to be necessary to maintain NPCs at a quiescent state (Su et al., 2010). CD44 is expressed on neonatally-derived NPCs (Rampon et al., 2008), so it may be through interactions with this receptor that inhibition takes place. CD44-null NPCs hyper-proliferate in vitro and in the subgranular zone of older adult mice, giving rise to elevated numbers of doublecortin mmunoreactive cells in this region. Additionally, CD44-null mice have memory and learning deficits which are consistent with abnormal neurogenesis (Su et al., 2010). It should be noted that the critical

reference with respect to adult neurogenesis and cd44 (Su et al., 2010) was presented as a talk at Society for Neuroscience in 2010 and does not appear to have been subsequently published.

There seem to be several ways possible that the pathology I observed with respect to hyaluronan and CD44 might impact neurogenesis in the hippocampus of older KI or Tg mice. The abnormal presence of hyaluronan in the hippocampus may inhibit differentiation of NPCs. On the other hand, because I have not yet determined the molecular weight of the hyaluronan expressed in the hippocampus, it is possible that it is in a smaller LMW form, possibly due to reactive oxygen species (ROS). In addition, in the dentate gyrus, there is very severe CD44 pathology in, presumably, astrocytes (I did not examine this area closely). The presence of CD44 on astrocytes where they are not normally expressed could interfere with the endogenous hyaluronan in the subgranular zone – either by facilitating uptake or aggregation of the molecule. CD44-hyaluronan interactions with respect to NPCs in the adult hippocampus presents an interesting area for further exploration.

CD44 and vimentin

Recently the hyaluronan binding domain of CD44 has been found able to interact with the head domain of vimentin like GFAP, a type III intermediate filament protein and one found in increased levels in AxD and the Tg/KI mice (Sosunov et al., 2013) as well as in reactive astrocytes in many other disorders. Cell surface vimentin expressed by endothelial cells was demonstrated to bind soluble CD44 and the interaction was suggested to be direct (Pall et al., 2011). While there is no evidence to suggest CD44 is shed by astrocytes in AxD or model mice, vimentin was found secreted by activated macrophages, dependent upon phosphorylation of the protein (Mor-Vaknin et al., 2003), and using mass spectrometric, proteomic approaches, vimentin has also been identified as a protein found in the conditioned media of astrocyte cultures (Greco et al., 2010; Keene et al., 2009). Because we found vimentin to be increased in the Tg/KI mice in the same anatomic region as GFAP, and because vimentin is upregulated in reactive astrocytes, it is worth further investigation to determine if secreted vimentin

may interact with CD44, especially because this interaction may interfere with the uptake of hyaluronan and/or block CD44-hyal signaling

Ezrin, radixin and moesin proteins and AxD

ERM proteins are broad family of proteins know to function in cell polarity, membrane trafficking and cell motility. ERM proteins, in their phosphorylated state, link CD44 and many other plasma membrane proteins, such as ICAMs, to the underlying actin cytoskeleton. Ezrin has been demonstrated to be localized with actin in fine perisynaptic astrocytic processes (Derouiche and Frotscher, 2001), and ERM proteins potentially link GLAST to the underlying cytoskeleton through interactions with NHERF-1 (Lee et al., 2007a).

Unusual P-ERM immunostaining in patients and in 1 year old KI mice

I found two interesting patterns of reactivity for P-ERM. In intact WM of the R239H patient (Fig 6C), I found a striking increase via immunohistochemistry in P-ERM in AxD patient tissue (Fig 6A) and a similar striking change in one year old KI mice (Fig 7D-K), but such dramatic changes in P-ERM staining were not observed in the one month old Tg/KI mouse, suggesting these changes might occur with prolonged accumulation of GFAP and/or astrocyte reactivity. In order to better understand the P-ERM immunoreactivity, I examined tissue from the one year KI mice with antibodies that react to the total pool of ezrin (Fig 8) and moesin (Fig 9). I found a large increase in the expression of both proteins in GFAP positive astrocytes in the 1 year old KI mouse, but the WT mouse showed little immunostaining for either protein (Fig 8B and 9A). When I examined CD44 co-expression with these proteins, moesin appeared to colocalize with CD44 to a greater extent than did ezrin. This may provide an additional clue to CD44 function in the AxD mouse hippocampus.

Ezrin

In human astrocytes, ezrin weakly stains peripheral processes (Geiger et al., 2000). In rat, ezrin in astrocytes has been found by electron microscopy to localize with actin to small processes associated with synapses (Derouiche and Frotscher, 2001). Later studies demonstrated that ezrin and the metabotropic glutamate receptors (mGluRs) 3 and 5 are compartmentalized to these processes and require phosphorylated ezrin for formation and motility and that glutamate and glutamate analogues induced rapid motility of these processes that is mediated by mGluRs 3 and 5 (Lavialle et al., 2011).

There are sparse reports of increased ERM protein expression in reactive astrocytes, however ezrin expression had been documented in association with neuronal death in cerebral HIV infection (Geiger et al., 2006). In this study, reactive astrocytes, as assessed by increased staining of GFAP, were found in all patients, however only in case of encephalopathy was ezrin increased. Additionally in cases where neuronal apoptosis could be detected, ezrin immunoreactivity was highest (Geiger et al., 2006)

Moesin

In human tissue, expression of moesin has been found in both normal and reactive astrocytes, and in both its staining is distinct from that of ezrin in that it resides mainly in the cytoplasm of the cell body and extends into processes (Stemmer-Rachamimov et al., 1997). Our human tissue immunostaining pattern for P-ERM was just this, so it is possible that we are preferentially observing expression of phosphor-moesin here. Moesin has been found to be strongly expressed in human tissue by pyramidal neurons of the hippocampus (Stemmer-Rachamimov et al., 1997), and is also the dominant ERM protein expressed by cultured differentiated hippocampal neurons (Jeon et al., 2002). Moesin is phosphorylated by PKC and Rho A in response to glutamate and has been found important to the formation of new filopodia in dendrites in pre-synaptic active boutons (Kim et al., 2010).

ERM proteins are very similar in structure, but moesin is unique in that has fewer amino acids than do ezrin and radixin so it migrates at a unique length than do ezrin and radixin, which are found at ~80kDa on SDS gels. Moesin, unlike ezrin and radixin, shows a striking resistance to Calcium-mediated proteolysis (Shcherbina et al., 1999). This attribute is thought important to its role as the major ERM protein expressed in lymphocytes and blood cells which have active calcium signaling mechanisms (Shcherbina et al., 1999) and may be the reason it is expressed preferentially on pyramidal neurons. Interestingly, calcium-mediated cleavage of GFAP, via Calpain, generates a species of the protein which migrates at 2-3 kDa less than the intact protein, which migrates at ~50 kDa. Our Western blot analysis of GFAP using a rabbit polyclonal antibody shows a significant band that migrated at this approximate MW in Tg/KI mice, but not at all in WT mice (Fig 1). We also obtained this faster migrating ~ 48kDa band for Tg/KI hippocampus, but not WT using a separate mouse monoclonal antibody.

Also of note regarding ERM proteins, overexpression of moesin and ezrin has been found to disrupt stable microtubule formation involved with vesicle and cytoskeletal trafficking in retroviral infection (Haedicke et al., 2008; Naghavi et al., 2007), and this is interesting with respect to the microtubule disruption I observed in Tg mouse primary astrocytes. We did not examine P-ERM expression with respect to microtubules in culture.

Chapter 3: Figures

Figure 1. CD44 expression in AxD patient tissue by immunohistochemistry and Western blot

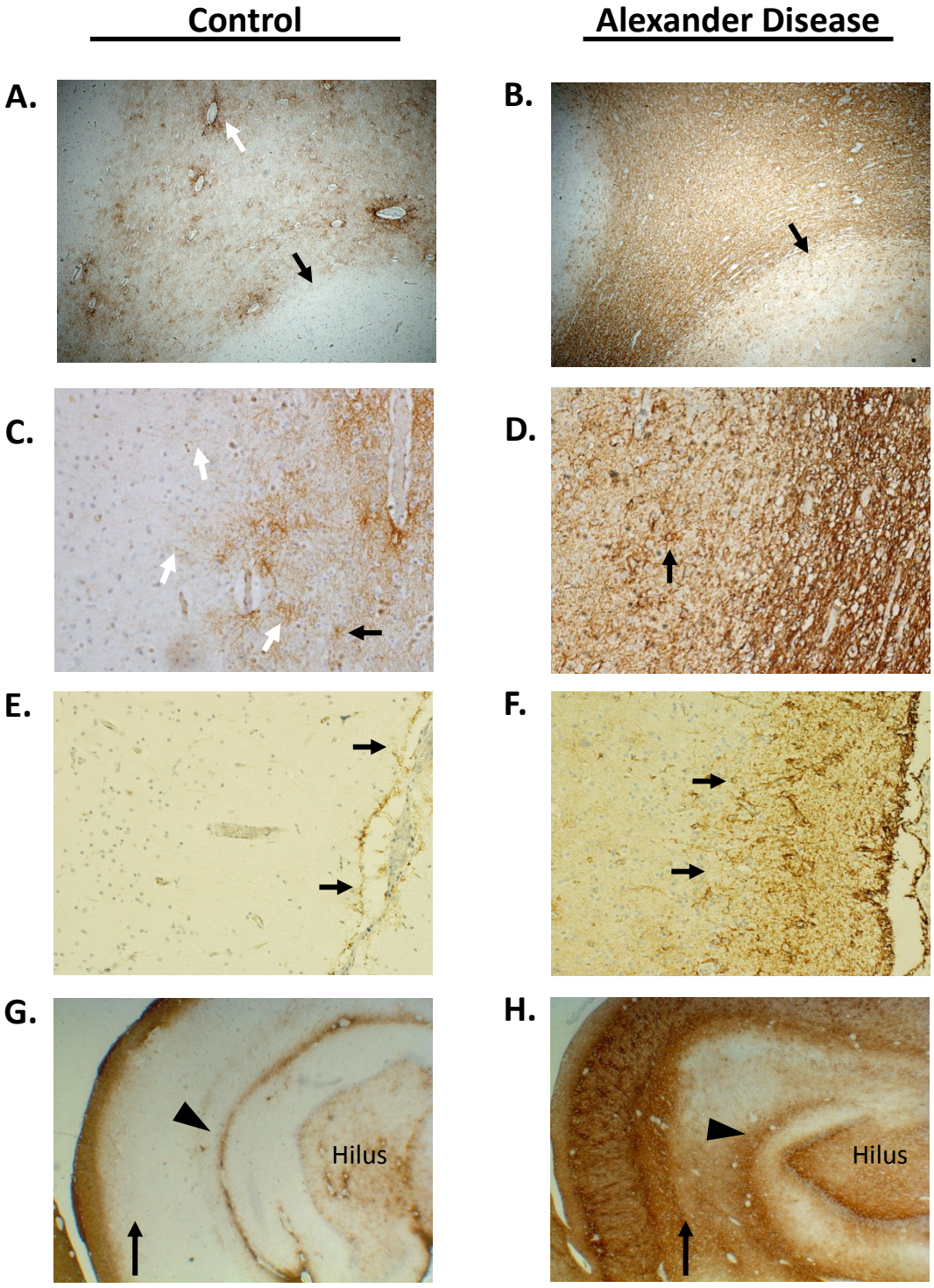

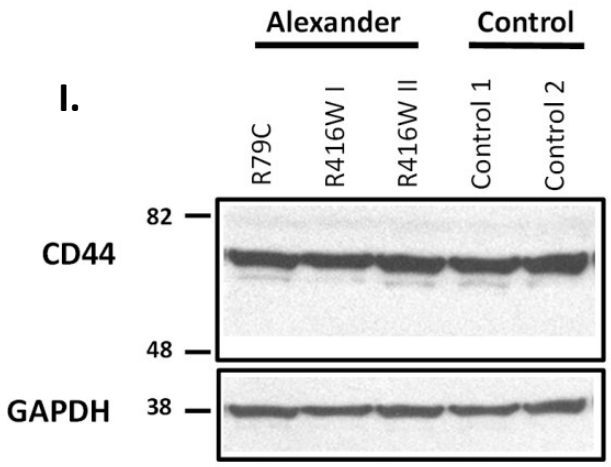

Immunohistochemistry of R239H AxD patient sub-cortical white matter and adjoining cortex (A-D). (A-B) Low magnification of (A) control patient shows diffuse immunostaining throughout the white matter with especially heavy staining around large blood vessels (white arrow) and no visible immunostaining, at this low magnification, of adjoining cortex (black arrow), while (B) AxD patient shows high immunoreactivity to CD44 in white matter and immunostaining also into the adjoining cortex (black arrow). (C-D) Higher magnification images show in (C) control that there is light diffuse immunostaining of much of the white matter. Individual astrocytes can be detected in the white matter (black arrow) and long, linear and thin astrocytic processes extend into the adjoining cortex (white arrows). Thin astrocyte processes cannot be observed in the (D) AxD patient and individual cell that appear to be CD44+ reactive astrocytes can only be observed in the adjoining cortex (black arrow). (E-F) Pial surface of (E) control patient tissue shows light immunostaining only at the pial surface (black arrows), while (F) AxD patient shows heavy immunostaining for CD44 into lower layers of the cortex (black arrows). (G-H) Low magnification of the hippocampus (G-H) shows (G) control patient with a thin band of intense CD44 reactivity in the str. lac. (arrowhead) and diffuse immunostaining of the hilus (as marked). The CA1 can be observed (black arrow) with faint immunostaining in contrast to that of the str. lac. (H) At the left, AxD R416W patient shows greatly increased immunoreactivity to CD44 in the str. lac. (arrowhead) but far more CD44 in the CA1 sector of the str. rad. (black arrow) and hilus. (I) Western

blot analysis of CD44 in two controls and three AxD patients with tissues taken from neocortex and white matter were assessed for expression of CD44 and found to be roughly equal. GAPDH is shown as a loading control. 20ug total protein.

Figure 2. CD44 is increased in hippocampus of AxD Tg/KI mouse at 2 and 4 weeks

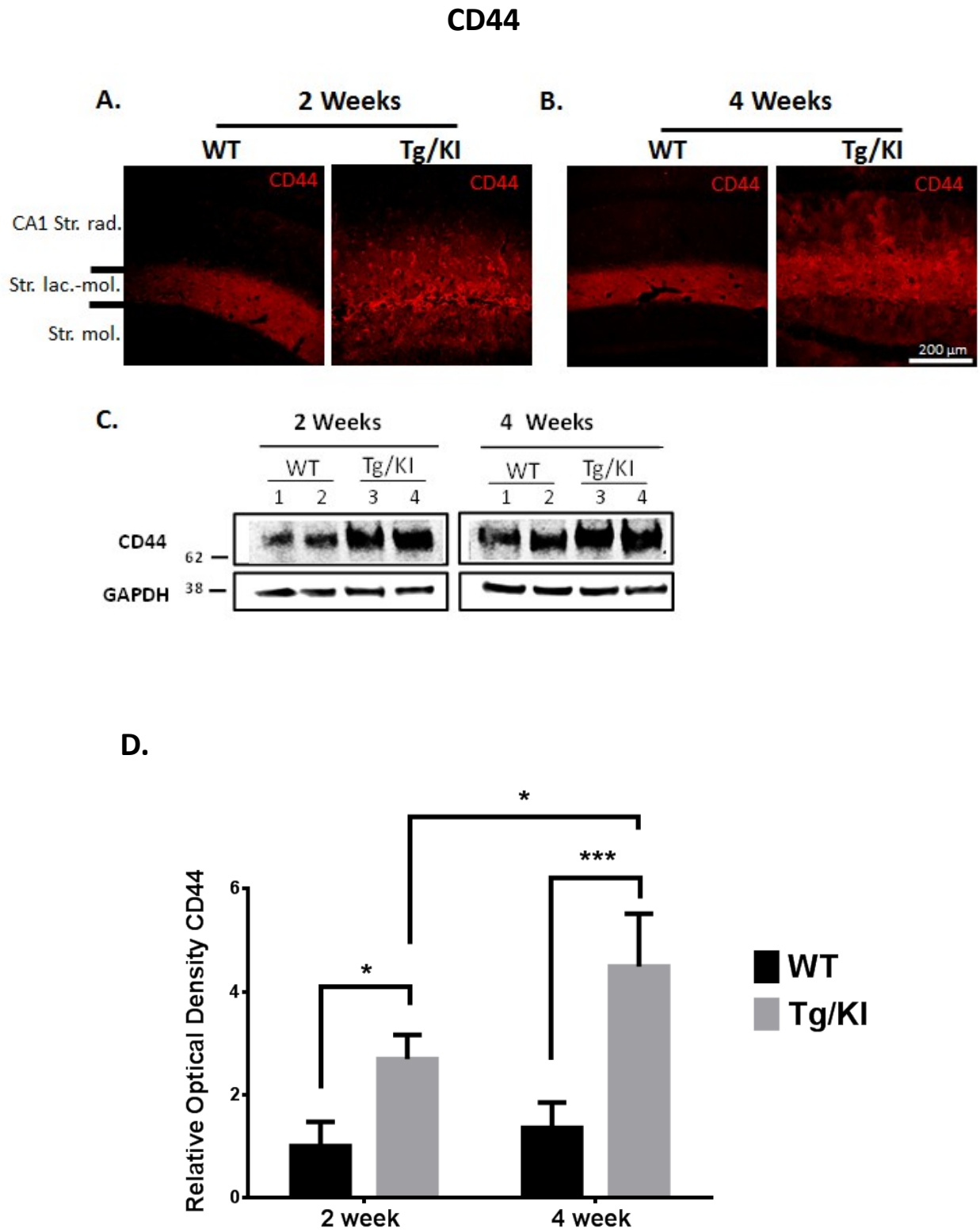

Confocal images of CD44 immunofluorescence in (A) 2 week and (B) 4 week hippocampus of Tg/KI and WT mice. (C) Western blot analysis of CD44 protein in hippocampi of 2 week and 4 week WT and Tg/KI mice. GAPDH is assessed as a loading control. One of three independent experiments are shown. (D) Quantification of optical density of CD44 bands in Western blot shows a significant increase of CD44 expression of Tg/KI mice at 2 weeks (*p=0.025) and 4 weeks of age (**p=0.00037). Data are mean +/- standard error of mean (SEM) of 3 independent experiments. Two way ANOVA with Tukey test; *p < 0.05, ***p < 0.0005, ****p < 0.00005.

Figure 3. Immunohistochemical profile of CD44 and GFAP in hippocampus of all AxD model mice at 4 weeks

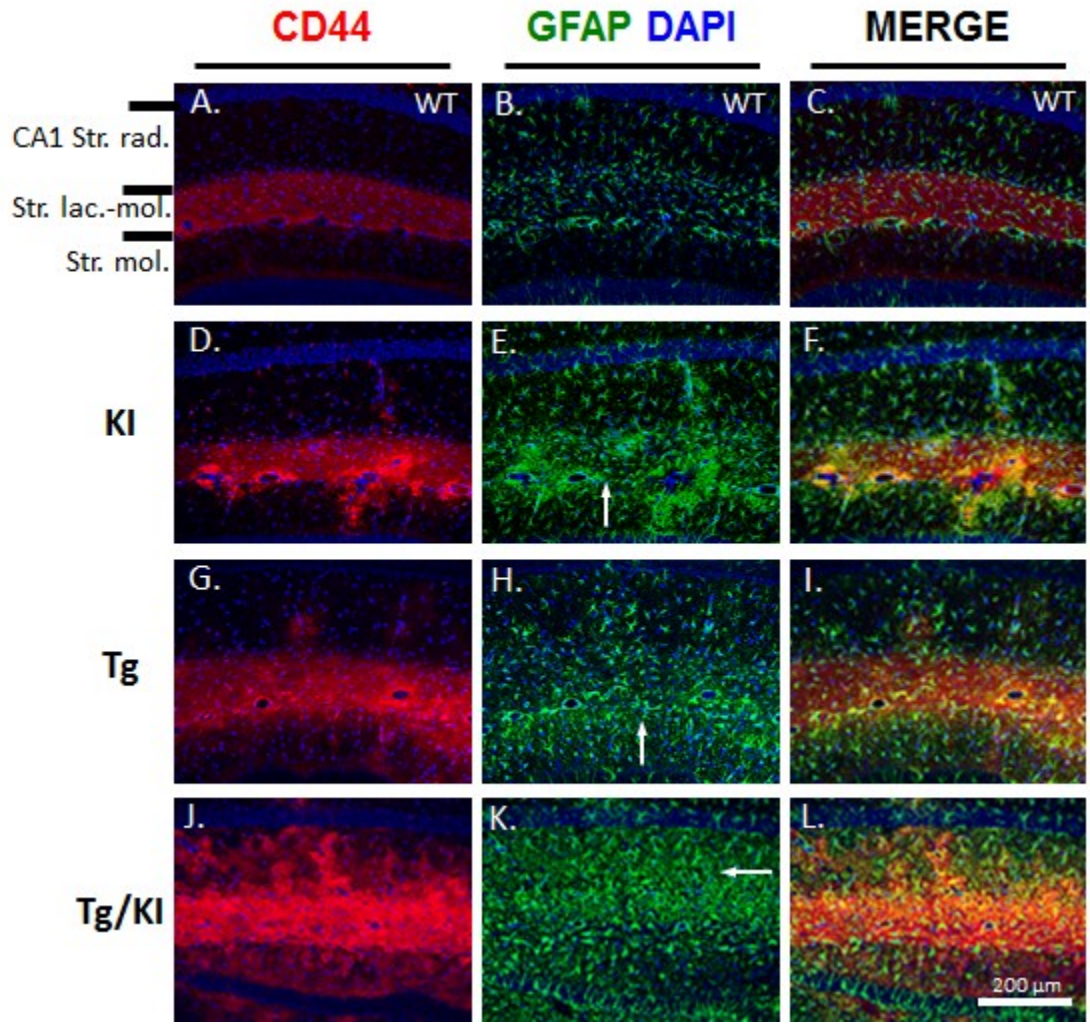

Immunofluorescence for CD44 (red) and GFAP (green) in the 4 week WT, KI, Tg and Tg/KI mice. WT animals (top panels A, B, C) show normal distribution and labeling pattern of CD44 and GFAP in the hippocampus. CD44 in (A) is localized to a distinct arc centering on the str. lac.-mol. and GFAP immunostaining (B) is also higher in in this area where there are abundant blood vessels surrounded by GFAP positive endfeet. Increased immunostaining for both GFAP and CD44 occurs in the KI mouse (panels D, E, F) and merged image (F) shows that these increase are coincident and occur in both the str. lac.-mol. (arrow, E) and the adjoining str. mol. The TG mouse (panels G, H, I) shows similar increases in str. lac.-mol. GFAP (white arrow, H) that coincides with increases with CD44. The most severely affected

of the AxD mice, the Tg/KI, is shown in panels at bottom (J, K, L) where GFAP immunoreactivity (K) is greatly increased beyond the str. lac.-mol. and into the str. rad. (white arrow, K) where CD44 is also greatly increased. Merged stack confocal images.

Figure 4. CD44 is increased heterogeneously by a subset of GFAP positive astrocytes

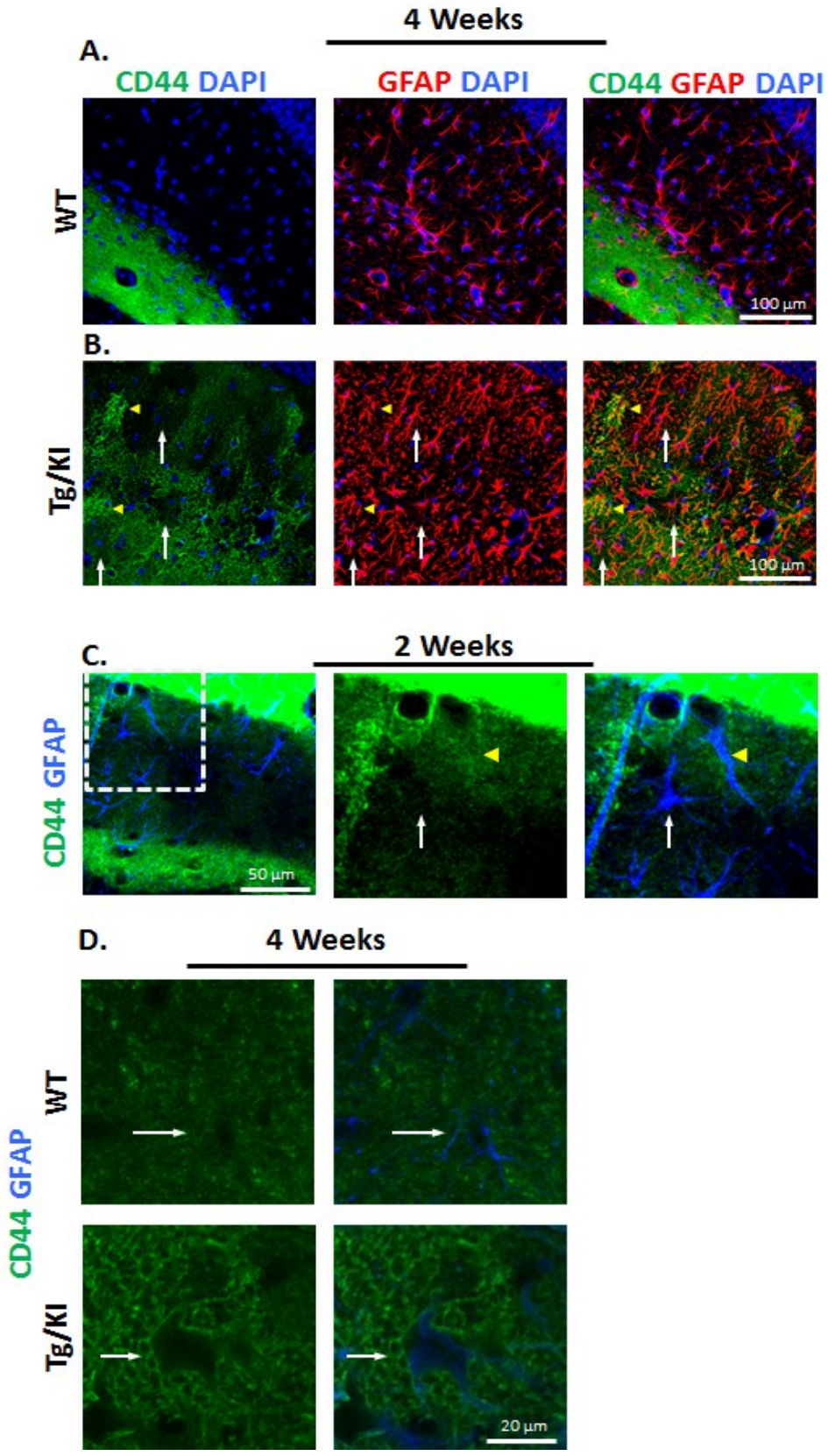

Immunofluorescent expression of CD44 in WT and Tg/KI hippocampus at 4 weeks. (A) WT. CD44 is localized to a distinct diffuse arc of reactivity centering on the str. lac.-mol. Individual cells cannot be detected at this magnification. (B) Individual CD44+ cells can be distinguished in Tg/KI hippocampus where they are associated with enlarged GFAP+ astrocytes. CD44 can be localized to some, but not all, individual astrocytes -- some cells have greater expression while others appear to express far less or none at all (white arrows). (C) Immunofluorescence of artificially enhanced CD44 expression (ImageJ) shows that 2 week WT astrocytes in the str. mol. layer of CD44 appear to express low levels of CD44 that is also heterogeneous. Images at right are higher magnification of boxed selection in images at left. CD44+/GFAP+ astrocyte is seen (yellow arrowhead) while GFAP+ astrocyte without CD44 expression is in the nearby str. mol. (white arrow). Note the long, radial GFAP process that is CD44 positive extending from dentate gyrus. CD44 expression (green) is more diffuse around GFAP positive cells. (D) High magnification single Z-series image of 4 week WT and Tg/KI str. lac.-mol. astrocytes. CD44 reactivity in WT animal (top) appears bushy and diffuse and surrounds a GFAP (blue) positive astrocyte (arrow). In lower panel Tg/KI astrocyte (arrow) has a larger GFAP positive cell body (blue) and thicker proximal processes along with an altered, more linear CD44 immunoreactivity. Single Z-series images.

Figure 5. Hyaluronan is increased in AxD Tg/KI mice at 2 and 4 weeks

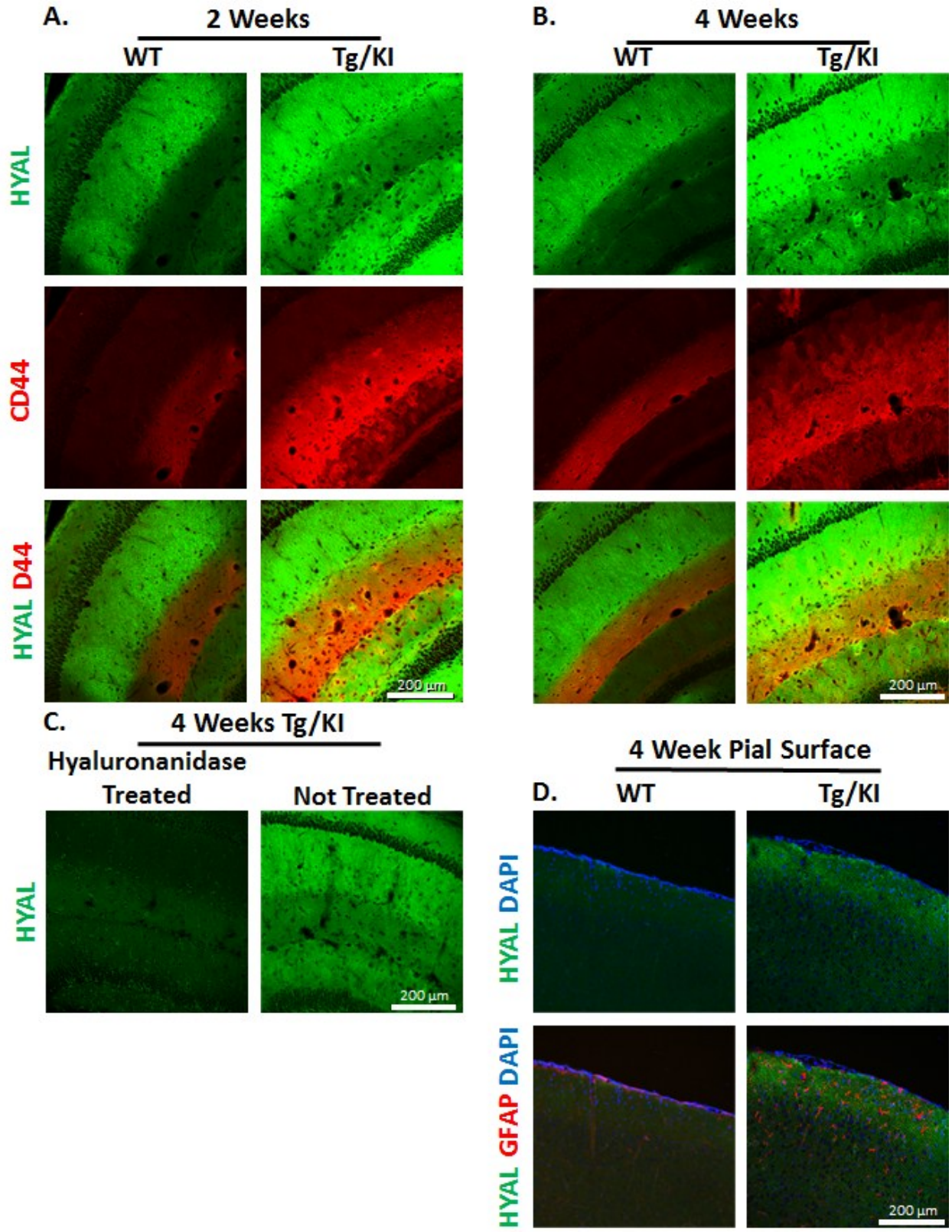

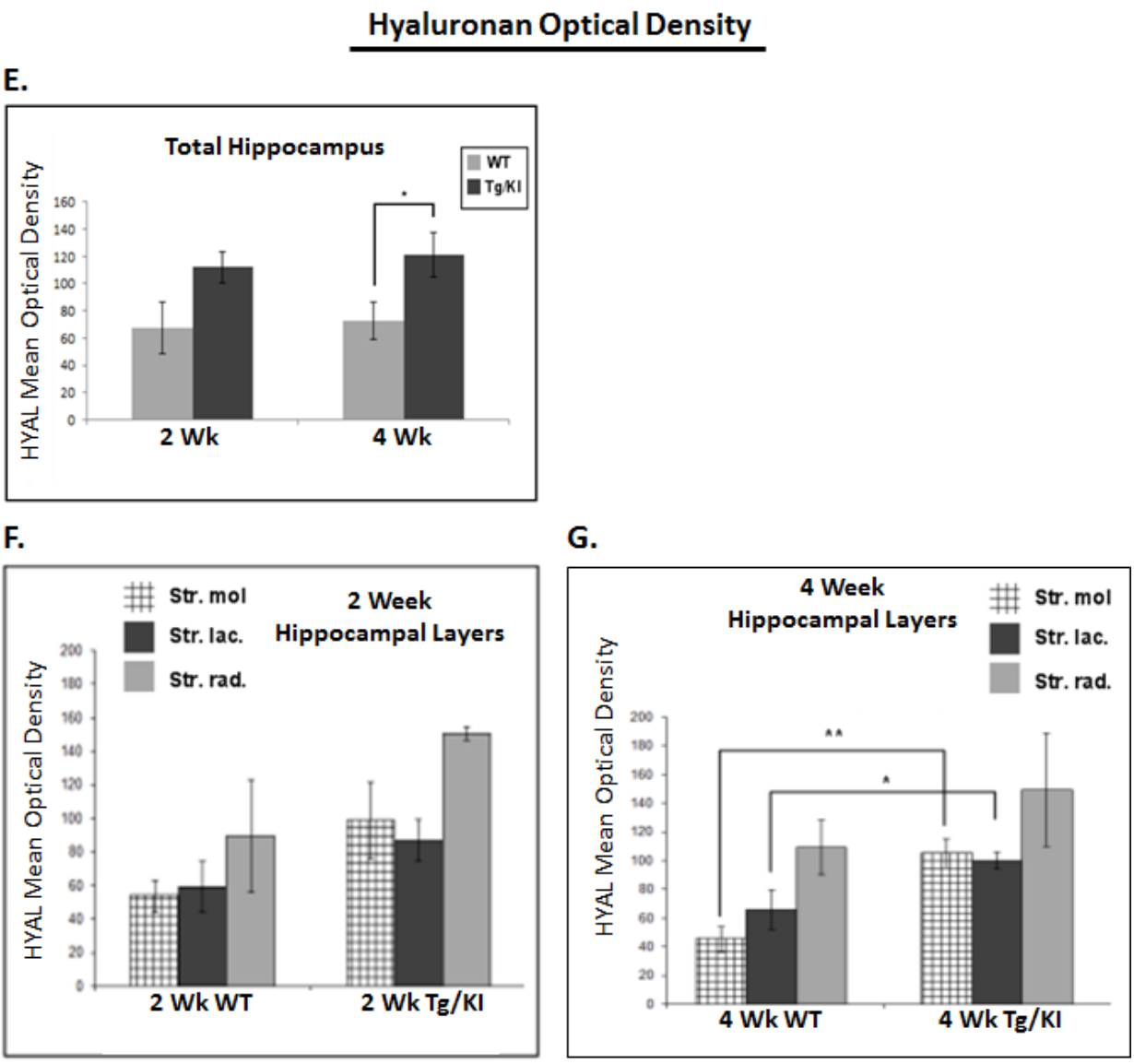

Reactivity to a streptavidin-labeled probe to biotinylated hyaluronan binding protein (HABP) is shown in green. (A,B) Double immunofluorescence for HABP and CD44 (red) in WT and Tg/KI mice at both 2 weeks (A) and 4 weeks (B). Specificity of staining is shown by hyaluronanidase treated and untreated sections from 4 week Tg/KI mice (C). Double immunofluorescence for HABP and GFAP (red) in the cortex and pial surface of 4 week Tg/KI and WT mice shows higher levels of GFAP and increased binding of HABP at the neocortical pial surface of Tg/KI mice. Optical density of overall immunofluorescence in (E) hippocampus (*p=0.035) and of hippocampal layers at (F) 2 weeks and (G) 4 weeks (* p=0.042: **p =.007) (G). Data are mean +/- standard error of mean (SEM) of 3 independent experiments. Two way

ANOVA with Tukey test; *p < 0.05, ***p < 0.0005, ****p < 0.00005. Data are mean +/- standard error of mean (SEM) of 3 independent experiments. Two way ANOVA with Tukey test; *p < 0.05, ***p < 0.0005, ****p < 0.00005.

Figure 6. Immunohistochemical expression of ERM proteins in AxD patient tissue

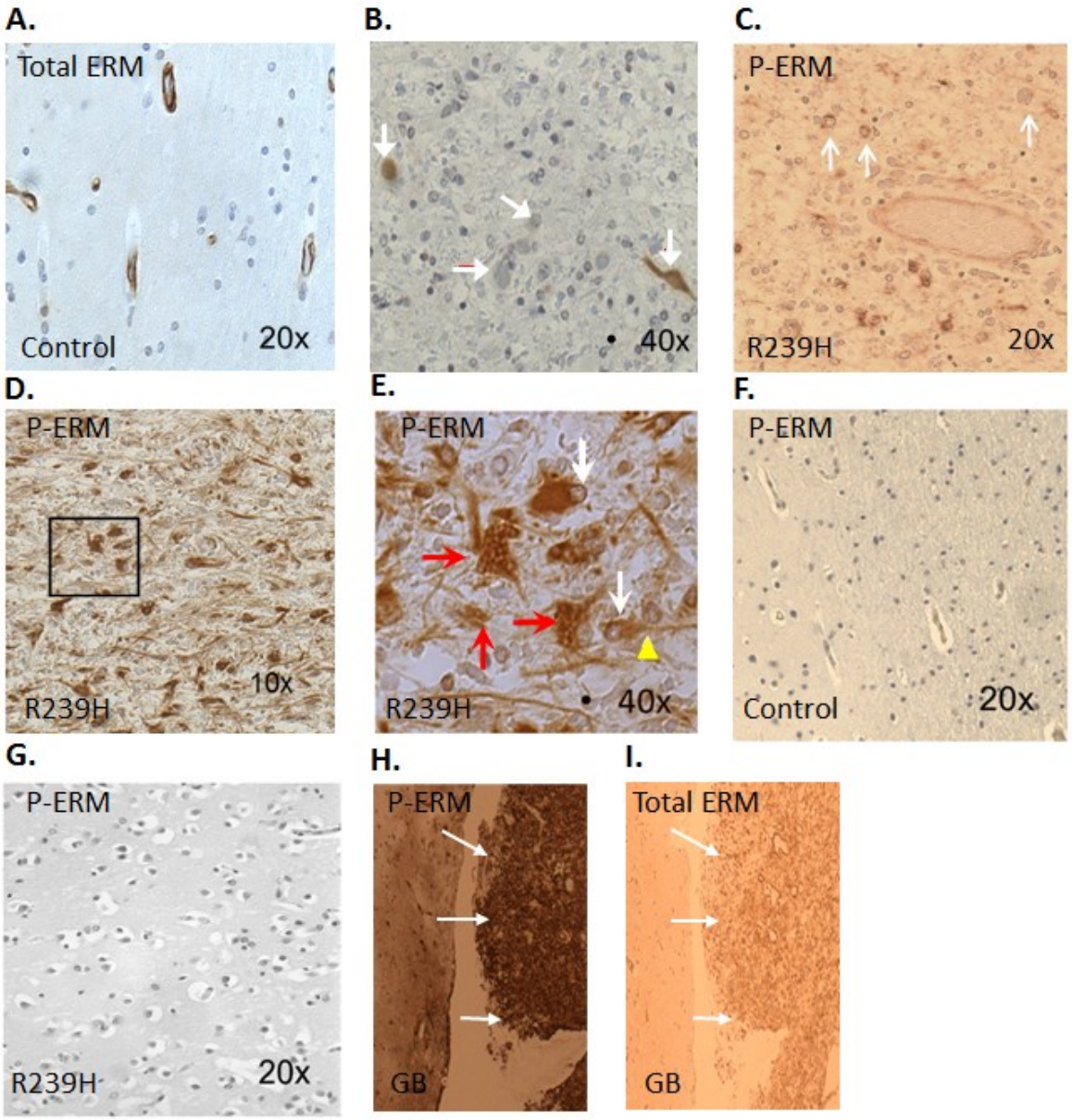

Total-ERM (A-B) in the white matter and adjacent cortex of control (A) and R239H AxD patient.(B). Astrocytes in AxD patient shows accumulation of ERM (white arrows) while control (A) shows reactivity only in blood vessels. P-ERM (C-G) in sub-cortical white matter of AxD R239H patient (Fig C-E), control cortex and white matter border(F) and R239H cortex (G). (C) Less affected white matter of R239H shows astrocytes with P-ERM reactivity in the cell body (arrows, C). Boxed image in (D) is shown at higher magnification in (E) where white arrows mark 2 of many astrocytes whose cell bodies are filled with P-ERM immunoreactivity. Astrocyte marked with white arrow on right shows long straight astrocyte process extending from cell body of the astrocyte (yellow arrowhead). Similar processes appear throughout the white matter. Red arrows point to unusual perinuclear bundles of Rosenthal fibers surrounded by P-ERM reactivity. No immunoreactivity to P-ERM is shown in control white matter and adjacent cortical section (F) or in R239H patient cortex (G). Glioblastoma (H-I) sections are positive controls for P-ERM (H) and Total ERM (I).

Figure 7. Immunofluorescent expression profile of P-ERM in AxD mice

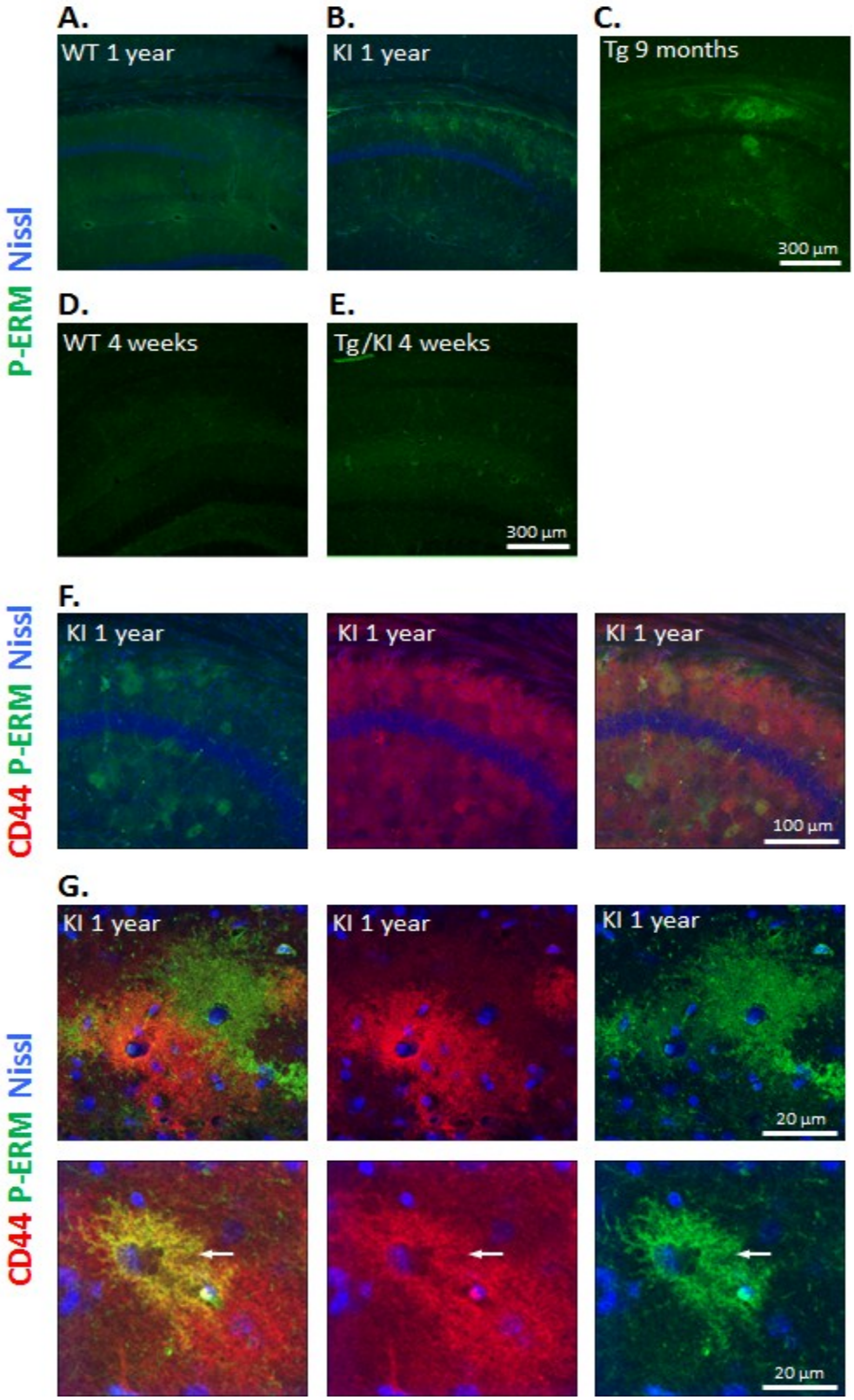

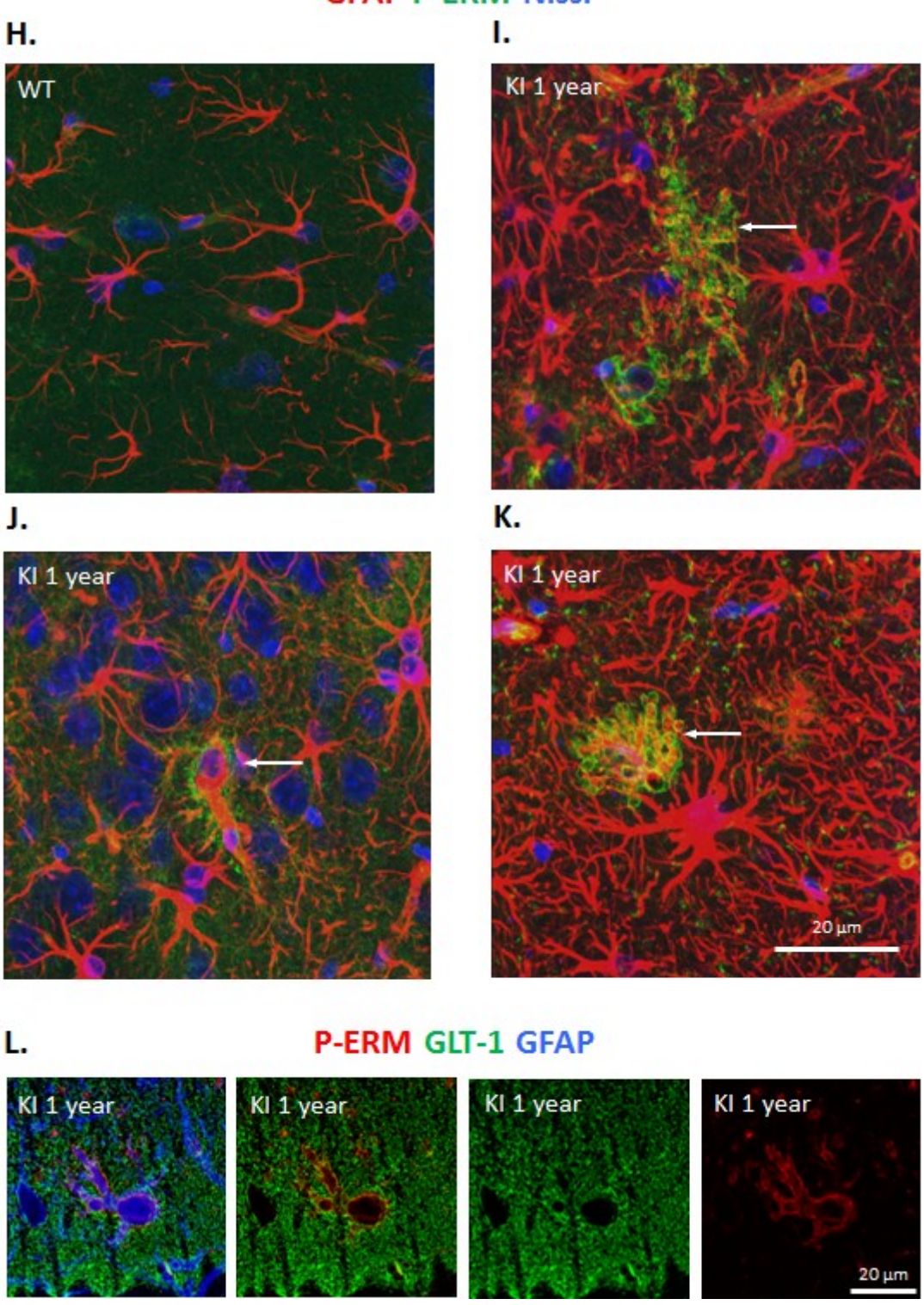
GFAP P-ERM Nissl
H.
WT
I.
KI 1 year
J.
KI 1 year
K.
KI 1 year
20 µm
L.
P-ERM GLT-1 GFAP
KI 1 year
KI 1 year
KI 1 year
KI 1 year
20 µm

P-ERM immunofluorescent expression in (A) 1 year WT, (B) 1 year KI, (C) 9 month Tg, (D) 4 week WT and (E) 4 week Tg/KI. P-ERM expression is increased in the str. rad and stratum oriens of 1 year KI and 1 year Tg mice and to a lesser extent in the 4 week Tg/KI mouse. (F) CD44 and P-ERM co-expression in str. rad and stratum oriens of 1 year KI mice. (G) Higher magnification of CD44 and P-ERM co-expression in str. rad. of 1 year old KI mice shows heterogeneity in co-localization of CD44 and P-ERM. The top panel shows little colocalization between some cells with high reactivity to P-ERM and CD44, while lower panel shows a cell with high coreactivity to antibodies for both proteins. (H-L) Colocalization of P-ERM with GFAP in WT and KI animals demonstrates that aberrant P-ERM expression in KI animals (I-K) is associated with GFAP positive cells (arrows). WT shows little P-ERM expression (H). Co-localization in KI animal of P-ERM, membrane protein GLT-1 and GFAP (L) in a single optical slice demonstrates that while P-ERM expression is aberrant, the astrocyte membrane does not appear to be completely retracted as is P-ERM expression in this cell.

Figure 8. Immunofluorescent expression profile of total ezrin in 1 year old KI mouse

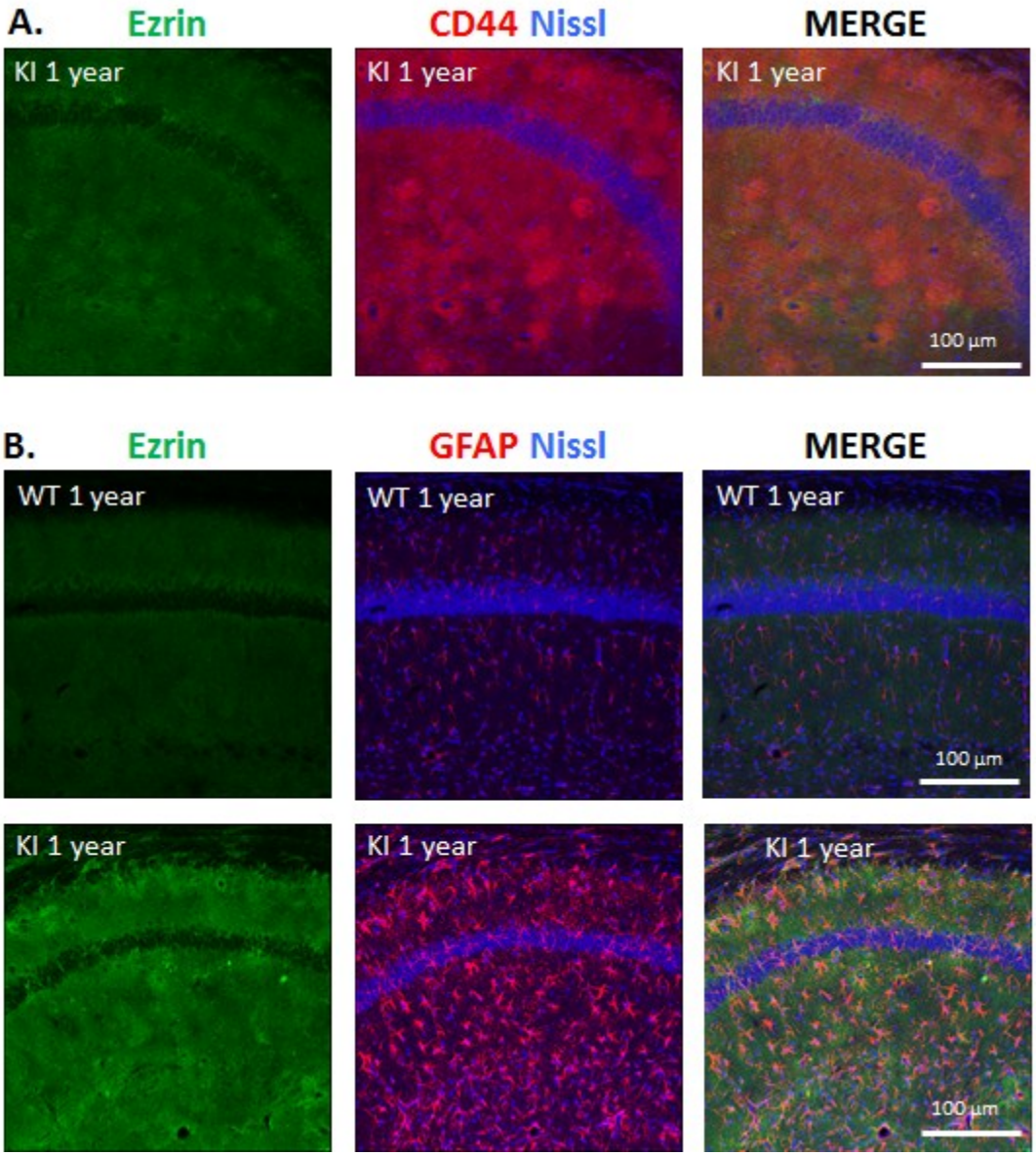

Immunofluorescence of ezrin in 1 year old KI mouse. (A) Co-immunofluorescence of ezrin with CD44 in the 1 year KI mouse demonstrates more overall immunostaining for CD44 than ezrin. Coexpression of proteins is not apparent in cells highly reactive to CD44. (B) Co-immunofluorescence of ezrin with GFAP in 1 year old WT (top panel) and 1 year KI mouse (bottom panel) shows co-expression in some cells of 1 year old KI mouse (right panel). There is little reactivity to ezrin in 1 year WT mice (left-panel).

Figure 9. Immunofluorescent expression profile of total moesin in 1 year old KI mouse

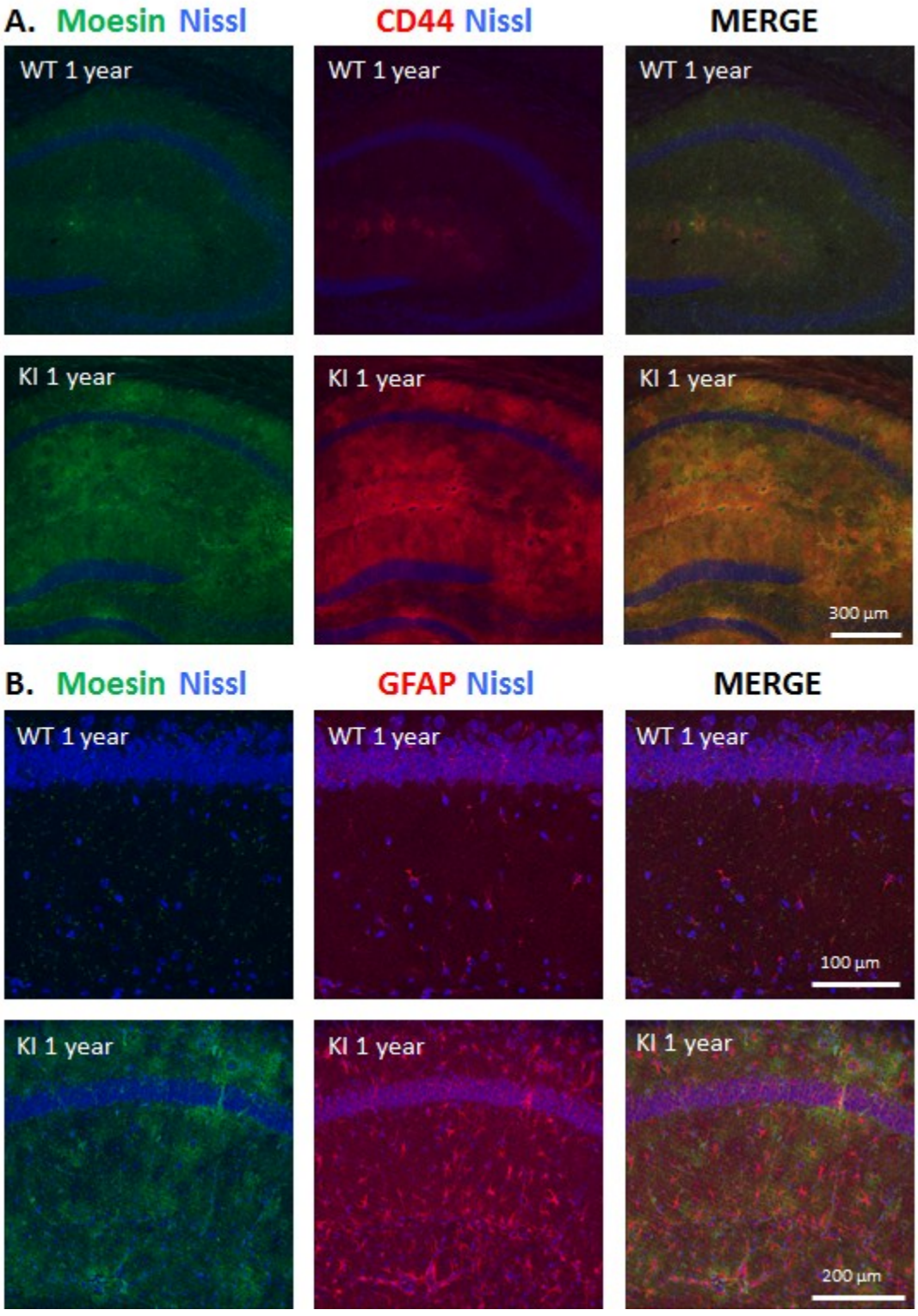

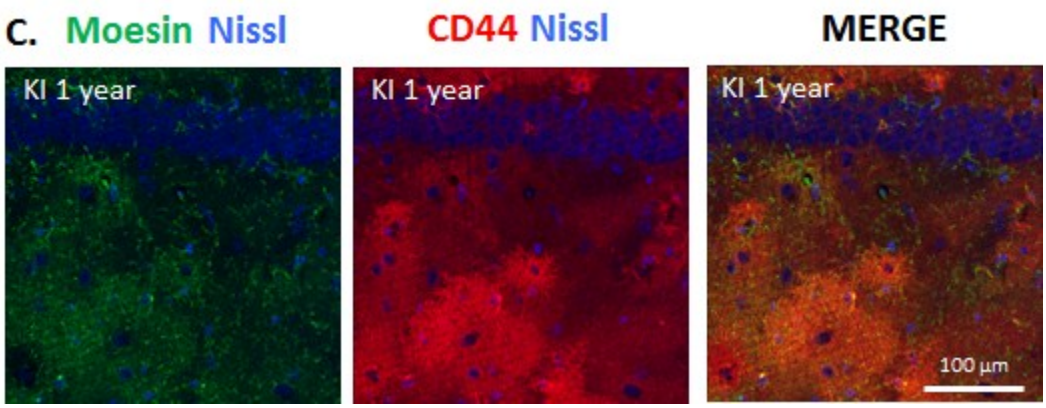

Immunofluorescent expression of moesin in 1 year old WT and KI hippocampus. (A) Co-immunofluorescence of moesin with CD44 and KI mouse is shown. (C) Higher magnification. WT mice show little moesin reactivity. High immunoreactivity to CD44 in KI mouse appears to be coincident in many cells with the expression of moesin. Most cells that are brightly immunostained with CD44 also show some expression of moesin. An exception is noted in higher magnification images in (C) (arrow). Co-immunofluorescence of moesin with GFAP in 1 year old WT and KI mice (B). WT animals shows little expression of moesin, while KI animals show in WT animals while KI animals show a much higher immunoreactivity that, especially in the stratum oriens, coincides with GFAP positive cells.

Chapter 4

A brief histochemical analysis of Iron, ferritin, ceruloplasmin and ferroportin in the Alexander disease CNS

Introduction

Iron, the 23rd element of the Periodic table, is necessary for the growth and survival of almost every organism. This *d*-block transition element can exist in oxidation states ranging from -2 to +6, by participating in electron transfer reactions, but in biological systems these states are limited to the ferrous (Fe2+), ferric (Fe3+) and ferryl (Fe4+) states and in this work I will only discuss Fe2+ and Fe3+. The interconversion of oxidation states allows iron to reversibly bind ligands, through its unoccupied *d* orbitals, and its preferred ligands are oxygen, nitrogen and sulfur. These properties make this metal an essential cofactor and well-suited to participate in generally three types of reactions – oxygen transport and storage, electron transfer and substrate oxidation-reduction (redox) (as reviewed by Beard, 2001). In the CNS, iron participates in the control of many metabolic signaling pathways including respiration, myelination and neurotransmitter synthesis (as reviewed by Beard, 2001; Crichton et al., 2011; Richardson et al., 2010; Todorich et al., 2009). The same properties that allow iron to drive one-electron reactions, also give iron the ability to generate radicals or "free radicals" – any species that has an unoccupied electron orbital and is thus able to exist on its own (as reviewed by Halliwell, 1992). Radicals derived from oxygen are called reactive oxygen species (ROS). These, iron-derived and not, are generated constantly in cells as by-products of normal metabolic processes and are effectively scavenged by a cell's physiological antioxidant defenses (Marks et al., 2009; Valko et al., 2005). Disrupted iron homeostasis can cause excessive ROS which may overpower antioxidant defenses, causing oxidative stress and damage to DNA, lipids and proteins (as reviewed by Valko et al., 2005).

In Chapter 1, I discussed how Fe3+ iron was found by modified Perls' staining to be greatly increased in astrocytes of the olfactory bulb and hippocampus in AxD KI and Tg mice; this was also found true for ferritin by immunostaining (Hagemann et al., 2006; Hagemann et al., 2005; Hagemann et al., 2012). Iron and ferritin are found prevalently in oligodendrocytes in the normal brain (as reviewed by Connor and Menzies, 1996). Microglia accumulate iron and ferritin when iron is released under pathological

circumstances such as cerebral hemorrhage, hypoxia-ischemia and MS (Bishop and Robinson, 2001; LeVine, 1997; Wu et al., 2003). Therefore, iron accumulation in astrocytes in AxD mice is abnormal and suggests that iron metabolism is misregulated in the CNS of AxD mice.

This is interesting with respect to AxD pathogenesis for several reasons. First, because astrocytes express proteins that allow transport of iron into and out of cells and make contact with endothelial cells of the blood vessels, through which the vast majority of iron enters the CNS, it has been hypothesized that astrocytes play a role in the distribution of iron from blood vessels into the brain (Dringen et al., 2007; Jeong and David, 2006). If this is true, then accumulation of iron in astrocytes might suggest that distribution of iron to other cells in the CNS may in some way be impaired.

Second, iron is critical to myelination (as reviewed by Todorich et al., 2009), and in AxD myelination is severely impacted. As reviewed in Chapter 1, type I AxD is a leukodystrophy and children suffer extensive frontal de/dysmyelination while type II patients show areas of focal demyelination suggestive of a defect in the ability of these cells to remyelinate (Prust et al., 2011). Accordingly, the accumulation of iron in AxD astrocytes may represent impaired iron efflux from these cells, resulting in a deficiency in the extracellular supply of iron for use by oligodendrocytes and therefore which might impact myelination and remyelination.

Finally, because iron is a well-known initiator of ROS (as reviewed by Valko et al., 2005), its increase in astrocytes might deplete them of antioxidant defense mechanisms ultimately producing oxidative damage to DNA, as well as lipids and proteins. Transition metal-mediated oxidative stress is hypothesized to play a role in several neurodegenerative diseases including Parkinson's disease, Amyotrophic lateral sclerosis, aceruloplasminemia and Alzheimer disease (as reviewed by Carri et al., 2003; Crichton et al., 2011; Kono, 2012; Rouault and Cooperman, 2006) and, as discussed in Chapter 1, there are multiple indications of oxidative stress or an oxidative stress response in AxD patients

(Castellani et al., 1998; Castellani et al., 1997), AxD model mice and primary cells (Cho and Messing, 2009; Hagemann et al., 2006; Hagemann et al., 2005; Hagemann et al., 2012) and AxD model drosophila (Wang et al., 2011). If there is evidence of iron accumulation in astrocytes of AxD patients, as there is in model mice, it could present a plausible hypothesis about how iron-mediated oxidative stress may exacerbate the proteasomal inhibition known in AxD astrocytes , deplete astrocytes of endogenous antioxidant defenses and activate multiple signaling cascades . This could ultimately impede their ability to maintain a hospitable environment for oligodendrocytes and neurons.

Iron metabolism

Iron metabolism in the periphery

Mammals obtain iron from their diet, and therefore many of the mechanisms of iron uptake from the gut and its subsequent transport to blood serum and use by individual cells have been well characterized. The proton-coupled divalent metal transporter 1 (DMT1) transports Fe2+ iron from the apical membrane of duodenal enterocytes in the intestine into the lumen of these cells after it has first been reduced to Fe2+ by the duodenal cytochrome b reductase (Dcytb) (as reviewed by Wang and Pantopoulos, 2011). Iron not utilized by these cells is either stored in the iron storage protein, ferritin, or exported to the plasma from the basolateral membrane by the iron efflux transporter ferroportin 1 (FPN1) (previously known at DCT1 or Nramp2) (Abboud and Haile, 2000; Donovan et al., 2000; McKie et al., 2000). As iron exits the cell it most likely oxidized by hephaestin, a membrane-bound ferroxidase closely associated with and important for FPN1-mediated Fe2+ exit from cells (Donovan et al., 2000; Kaplan and Kushner, 2000; McKie et al., 2000; Vulpe et al., 1999; Yeh et al., 2009). In the plasma, an excess of high affinity transferrin, mediates Fe3+ transport, but also contributes to the health of the organism by keeping iron bound in a non-reactive state.

The transferrin cycle

Many cells outside of the CNS obtain iron from the transferrin cycle (Fig B) (as reviewed by Wang and Pantopoulos, 2011). Transferrin bound to Fe3+ (holo-transferrin) in the plasma binds with high affinity to the transferrin receptor (TfR1) expressed on the surface of cells. The transferrin and receptor complex is endocytosed in clathrin coated pits and transported to endosomes, which are acidified by a proton pump triggering the release of iron from the transferrin-receptor complex. Fe3+ iron is converted to soluble Fe2+ iron by a ferrireductase such as STEAP3 and transported from the endosome to the cytosol via DMT1, which takes on a second role in some cells in transport of Fe2+ iron from the endosome. Without iron, TfR1 and transferrin dissociate and transferrin is recycled to the plasma while TfR1 remains on the cell surface (as reviewed by Wang and Pantopoulos, 2011).

Brain iron metabolism

While some mechanisms of uptake and delivery of iron in the CNS are similar to that in the periphery, many of the specifics of brain iron metabolism are unique and others have yet to be uncovered. Transferrin-bound iron in the plasma travels into the blood vessels of the brain. Here, the blood brain barrier (BBB) consisting of blood vessel endothelial cells (BVECs) in contact with pericytes and astrocyte endfeet (as reviewed by Moos et al., 2007) prevents plasma, transferrin and many other molecules from freely entering the brain. While all BVECs have both a luminal and abluminal membrane, only BVECs of the blood brain barrier have polarity in their protein expression, induced by the contact of the endfeet of astrocytes with these cells (as reviewed by Abbott et al., 2006). Tfr1 is found on the luminal membrane (as reviewed by Bradbury, 1997; Moos and Morgan, 2000), which is exposed to plasma, while the abluminal membrane of BVECs are covered by astrocyte endfeet, brain interstitial fluid and in some cases neuronal processes (as reviewed by Rouault and Cooperman, 2006). Labeled transferrin receptor is endocytosed by BVECs but very little radiolabeled transferrin or its receptor subsequently

enter the CNS (Gosk et al., 2004; Moos and Morgan, 2001). Apotransferrin is recycled to the blood, while iron is left within endothelial cells.

The mechanism by which iron leaves the endosome and subsequently enters the CNS is uncertain because DMT1, crucial for the transferrin cycle and for endosomal export of iron, is not found in BVECs in the rat, but is instead has been found both by immunohistochemistry and by electron microcopy on astrocytic processes where these cells make contact with BVECs (Wang et al., 2002).

Within the CNS indications are that iron exceeds the binding capacity at of transferrin, so that some of it in a non-transferrin bound form (Moos and Morgan, 1998, 2000). Thought on how non-transferrin bound iron exits endosomes or BVECs and moves within the CNS to cells varies widely and has not yet been demonstrated (Connor, 2002; Moos et al., 2007; Rouault and Cooperman, 2006).

In addition to the iron derived from the vasculature, functional studies using radiolabeled iron injected into hypotransferrinemia mice have demonstrated that a small amount of iron in the CNS is derived from the cerebrospinal fluid (CSF), but that transferrin is not necessary for this uptake, which occurs via the choroid plexus. Transfer of radiolabeled iron emanating from CSF, however, is low and the diffusion rate limited, reaching only the nearest cells (Moos, 1996; Ueda et al., 1993).

Iron levels in the CNS during development

The level of iron taken into the normal brain changes dramatically during development and varies within region and cell type. In the rat cerebellum pons and cortex, iron, transferrin and ferritin levels are higher at birth than at any other time (Roskams and Connor, 1994). These levels decrease until day 17 when ferritin and total iron begin to rise, but transferrin levels remain constant (Roskams and Connor, 1994). The high levels of iron at birth may be explained by iron that reaches the CNS before the BBB is formed. Indeed, in the developing brain, ameboid cells, resembling macrophages, stain with high levels of iron (Connor et al., 1995; LeVine and Goldman, 1988). The midbrain region, which includes the iron-

rich regions such as the globus pallidus, substantia nigra, and red nucleus, has consistently high levels of iron, ferritin and transferrin at all ages (Roskams and Connor, 1994).

Peak Iron influx coincides with the period of myelination

Studies by Connor's group find that Tfr1 levels expressed by endothelial cells also fluctuate during development and are highest at P15 (Gosk et al., 2004; Moos and Morgan, 2001), which coincides with the peak period of myelination in the rodent. Levels of radiolabeled Trf1 antibody (OX26) injected into rats were twice that at 15 days postnatal (P15) than at postnatal day 0 (P0), and this is twice that than in adults (P70) (Moos and Morgan, 2001). On one hand this might suggest that high uptake of iron into endothelial cells coincides with a high need of iron for myelination or because transferrin receptor is upregulated in the brains of rats fed a low iron diet (Chen et al., 1995), but it might also suggest transferrin receptor upregulation at this age is due to the decreases in iron from levels found at birth. Levels of radiolabeled OX26 did not change between iron deficient and sufficient rats at P15 and the authors suggest this may be due to the receptor expression having reached a capacity during this period of myelination (Moos and Morgan, 2001).

Iron in oligodendrocytes and its importance to myelination

Iron is detected by MRI and subcellular fractionation at higher levels in the white matter than it is in grey matter (Curnes et al., 1988; Rajan et al., 1976), and within the white matter oligodendrocytes consistently stain strongest for iron in humans (Connor et al., 1990; Dwork et al., 1988; Morris et al., 1992), rats (Benkovic and Connor, 1993) and mice (LeVine, 1991). Iron is essential to the onset and maintenance of myelin (Connor, 1994; Connor and Menzies, 1996; Todorich et al., 2009), a lipid-rich cellular organelle of oligodendrocytes that enable these cells to ensheath axons providing greatly increased conduction of electrical impulses (Lemke, 1992).

While iron is important to any cell, it is especially so to oligodendrocytes in order to meet the high metabolic demands required to establish and maintain lipid and cholesterol-rich membrane sheaths that can sometimes outweigh their cell bodies by 100 fold (Wiggins et al., 1974). Iron-containing enzymes important to metabolism and biosynthesis such as glucose-6-phosphate dehydrogenase, dioxygenase, succinic dehydrogenase, NADH dehydrogenase and the cytochrome oxidase system are all elevated in oligodendrocytes compared to other cells in the CNS (Cammer, 1984). Additionally HMG-CoA reductase, which catalyzes the NADPH-dependent reduction of HMG-CoA to mevalonate, the first committed reaction and a major regulatory step in cholesterol synthesis, is also enriched in oligodendrocytes (Pleasure et al., 1984).

The labeling of iron and myelin proteins in oligodendrocytes in the developing brain suggests that the appearance of iron immediately precedes genesis of myelin. Perls' labeling of oligodendrocytes in the developing brain find iron-positive patches surrounding blood vessels (Burdo et al., 1999). These same areas around blood vessels are where focalized areas of myelinogenesis occurs during the second post-natal week (as reviewed by Connor and Menzies, 1996).

Iron deficiency causes hypomyelination and impacts OPC proliferation

Chronic severe iron deficiency in rats induced through maternal iron deprivation between gestational day 5 through weaning produces hypomyelination in 25 day old rats (Ortiz et al., 2004; Wu et al., 2008) in the subcortical white matter but not the hippocampus, and these mice also have behavioral impairments in surface righting reflex, negative geotaxis reflex, vibrissae-evoked forelimb placing test and novel object recognition task (Wu et al., 2008). A less severe course of iron deprivation can also negatively impact myelination. Both pre-weaning (postnatal days 4-12 or 4-21) and post-weaning (postnatal days 21-63) iron deprivation in rats causes myelin deficiency in the cerebrum and hindbrain (Beard et al., 2003).

Using this same model of maternal iron deprivation as described above, glial precursor cells in the developing spinal cord and corpus callosum were assessed for proliferation by measuring the number of cells positive for the glial precursor cell marker A2B5 and for BrdU incorporation, which had been injected into the mothers. At embryonic day 17 (E17) there were significantly higher numbers of these cells in the iron deprived pups in all areas of the brain assessed, including the spinal cord and corpus callosum. The same rats were assessed at P7 and P14 for GalC expression, a marker of mature oligodendrocytes (Morath and Mayer-Proschel, 2002). While there were fewer GalC+ cells in the spinal cord, surprisingly, at P7 and P14 there were 3-fold and 1.5-fold more of these cells in the corpus callosum. This result suggests that iron has both a regional and developmental impact on myelination.

In vitro, iron has also been found to impact oligodendrocyte precursor cell (OPC) proliferation. The oligodendrocyte line cell ONL-93 is inhibited from proliferating by both Ferric and Ferrous iron chelators, and the application of excess ferric ammonium citrate (FAC) prevents the inhibition of proliferation by the Fe3+ iron chelator deferoxamine (Hohnholt et al., 2010; Morath and Mayer-Proschel, 2001)

Astrocytes and iron metabolism

Because astrocytes make contact with endothelial cells where iron enters the brain (Brightman and Reese, 1969; Kacem et al., 1998), it has been hypothesized that astrocytes play a role in brain iron uptake. Electron microscopy has confirmed the immunohistochemical expression of DMT1 in astrocytic processes at endfeet where they make contact with BVEC's in the rat brain (Burdo et al., 2001; Wang et al., 2002). However, by immunohistochemistry, transferrin receptor has not been found in these cells in the rodent brain (Giometto et al., 1990; Moos, 1996) or human brain, although transferrin receptor is expressed by primary rat astrocytes in culture (Qian et al., 1999). These results suggest astrocytes in vivo are capable of uptake of Fe2+ via DMT1, but not transferrin-bound iron, however may be induced to do so under conditions of stress.

Conner et al. examined immunohistochemical expression of iron, transferrin and ferritin in the adult brain and found that while the majority of iron, ferritin and transferrin was found in oligodendrocytes in all areas of the brain, a subset of astrocytes were positive for iron, ferritin and transferrin in several subcortical regions examined, including the basal ganglia, striatum, hippocampus and amygdala (Connor et al., 1990). In the aging brain, however transferrin expression was routinely seen in white matter astrocytes, while its expression was unchanged in the grey matter. Transferrin mRNA is expressed in cultured astrocytes (Espinosa de los Monteros et al., 1990), so this expression may be due to gene activation later in life in these cells.

Iron efflux from astrocytes

FPN1, the only known transporter for iron efflux (McKie and Barlow, 2004), has been found in primary rat astrocytes, C6 cells and rat astrocytes in vivo (Burdo et al., 2001; Jeong and David, 2003) and primary astrocytes from the mouse express mRNA for FPN1 (Jeong and David, 2003). FPN1 is stabilized on the cell surface of rat C6 glioma cells by expression of the ferroxidase, ceruloplasmin (Cp) (De Domenico et al., 2007). In the human brain mRNA for Cp has been found localized specifically to a subpopulation of astrocytes surrounding the brain microvasculature and surrounding dopaminergic neurons in the substantia nigra (Klomp and Gitlin, 1996).

Interestingly, FPN1 expression in astrocytes has been found important to remyelination. Knockout of FPN1 specifically in astrocytes, by crossing mice expressing tomoxifen-inducible Cre driven from the GLAST promoter (GLAST::CreERT2) with ferroportin floxed mice ($FPN^{flox/flox}$) for five days in post-weanlings and then administering the focal demyelinating agent lysophosphatidylcholine, was demonstrated to decrease the subsequent remyelination of FPN1 KO mice versus that in controls (Schulz et al., 2012). Immunostaining of the tissue found cells positive for both Olig2 and proliferation marker KI67 were significantly fewer ($p \leq 0.05$) in the astrocytes of FPN1 KO mice.

The labile iron pool, the hydroxyl radical and ROS

In a normal cell, free iron, also known as the chelatable or "labile iron pool," constitutes less than-5% of total iron in a cell. This pool of catalytically active iron exists in both Fe2+ and Fe3+ states (as reviewed by Kakhlon and Cabantchik, 2002; Valko et al., 2005) and available for use in the cell, for example, as a cofactor by cellular enzymes involved in DNA and RNA synthesis, respiration and metabolism. Iron in the labile iron pool is often bound by low molecular weight chelators such as citrate, phosphate, carboxylates and also nucleotides. These can bind iron in a way that at least one of its six coordination sites is available for catalytic activity (as reviewed by Valko et al., 2005).

The properties of transition metals, like iron, that allow them to catalyze electron transfers and make them excellent cofactors but also enable hydroxyl radical generation through the Fenton reaction (Fig A, equation 2). Here Fe2+ in the labile iron pool reacts with hydrogen peroxide to generate Fe3+ and the hydroxyl radical, the most reactive free radical in biological systems (as reviewed by Nappi and Vass, 2002). The reaction of Fe3+ with superoxide produces Fe2+, which is then available for the Fenton reaction. Because superoxide and hydrogen peroxide are both produced liberally as by-products during oxidative metabolism and other cellular processes, any iron in a reactive state, is at risk generating the hydroxyl radical (Dringen et al., 2007; McCord, 2004).

Like iron, copper is another transition metal that can undergo redox cycling and generate the hydroxyl radical and other reactive oxygen species (as reviewed by Valko et al., 2005), however because free copper in a cell is so limited, estimated at only one atom of free copper per normal cell (Rae et al., 1999), iron has been found to be the predominant metal participating in the Fenton reaction when Jurkat cell are challenged with H_20_2 (Barbouti et al., 2001). While this chapter focuses on iron and therefore iron-mediated oxidative stress, is important to note that free copper can cause similar damage, if available.

Damage to molecules by the hydroxyl radical

The hydroxyl radical can damage nucleotides, lipids and proteins. A brief summary of such modifications are below.

DNA. One of the early events to occur after oxidative stress exposure in the human cell is DNA damage (as reviewed by Halliwell, 1992). Hydroxyl radical, but not other oxygen radicals like superoxide, damage DNA when iron or low molecular weight iron chelates bind DNA at phosphates in the backbone or purine or pyrimidine bases. Here, iron can reside at a center for repetitive generation of the hydroxyl radical. Because the hydroxyl radical is extremely diffusion limited, this positions allows it to make DNA modifications (as reviewed by Valko et al., 2005; Welch et al., 2002). Products of this oxidation of DNA include single and double strand breaks, modified bases, DNA-protein cross-links and chemical modification of the sugar moiety (as reviewed by Valko et al., 2005).

Lipids. Lipid oxidation (or peroxidation) occurs when iron-induced oxygen radicals attack polyunsaturated fatty acid residues of membrane and circulating phospholipids, which are enriched in the brain (as reviewed by Valko et al., 2005). The function of membrane-bound organelles such as mitochondria can be compromised and furthermore produce extremely reactive aldehydes, such as malondialdehyde (MDA), acrolein and 4' hydroxynonenal (HNE). These aldehydes are more stable than the hydroxyl radical and can do additional damage to proteins located within the membranes from which they have been generated or travel distances and even escape the cells to do harm (as reviewed by Halliwell, 1992; Uchida, 2003; Valko et al., 2005).

Protein Modifications. Metal catalyzed damage to proteins include introduction of carbonyl groups, oxidative cleavage, loss of histidine residues, bityrosine cross-links, reduction of intramolecular disulfide bridges, and the formation alkyl radicals which can further damage proteins (Lipinski, 2011; Valko et al., 2005).

Antioxidant Defense

Three means of antioxidant defense are known to be employed in cells and organisms to deal with both normal and pathological ROS. First, the prevention of ROS formation occurs through deterrence of electron leakage from reactive metals. Proteins that bind iron in a redox inactive form such as ferritin, transferrin and lactoferrin contribute to this effort. Second, the interception of oxidative damage by scavenging can remove partially reduced oxygen species before they can react with free iron. Antioxidant enzymes such as catalase, superoxide dismutase and glutathione peroxidase are important in this respect. The third mechanism for antioxidant defense in a cell is the repair or swift removal of damaged molecules (as reviewed by Carri et al., 2003; Welch et al., 2002).

Clearance of oxidatively or HNE-modified molecules

Oxidatively modified proteins are often efficiently cleared from the cell. For example, the oxidation of IRP2 by iron drives its ubiquination and subsequent proteasomal degradation (Iwai et al., 1998). Efficient degradation of other oxidatively modified proteins can alternatively occur in a non-proteolytic specific manner (as reviewed by Dalle-Donne et al., 2006) and HNE-modified proteins have been found to be degraded by a ubiquitin and lysosomal-dependant, but proteasomal independent pathway (Marques et al., 2004).

Not all oxidatively or HNE modified proteins are efficiently cleared, however. Hydroxyl radical damage to proteins may also cause protein aggregation. For example, reduction of intramolecular disulfide bridges followed by the exposure of hydrophobic epitopes can have such an effect (as reviewed by Lipinski, 2011). This appears to be the case with beta amyloid (Aβ) which is covalently crosslinked and aggregates when exposed to HNE in cell free systems (Siegel et al., 2007).

GSH and removal of damaged lipids

GSH has been found important to the prevention of HNE-modified damage by first acting to reduce lipid hydroperoxides before they react with redox metals to produce very destructive epoxides and aldehydes, one of which is HNE, and second through detoxification of lipids by its conjugation to lipid adducts, catalyzed by glutathione S-transferases (Malone and Hernandez, 2007). GSH conjugated to lipid adducts are subsequently removed from the cell.

Summary

Given the potentially damaging effects of iron-induced ROS, I undertook the work in this chapter to determine if there is evidence that iron is misregulated in astrocytes of AxD patients, as has been found in AxD model mice (Hagemann et al., 2006; Hagemann et al., 2005; Hagemann et al., 2012). I conducted a histochemical analysis of two infant onset, type 1 AxD patients and a control patient using a modified Perls' iron stain for Fe3+ iron and antibodies to ferritin, ferroportin and ceruloplasmin. I focused on regions of the subcortical white matter where GFAP expression in astrocytes is normally high and in AxD where there is an abundant presence of Rosenthal fibers and extensive demyelination. In addition I sometimes examined the pial surface, where there also abundant Rosenthal fibers, and the brain stem where there is considerable pathology, especially in adult patients. I detected abnormal accumulation of iron and ferritin in astrocytes. Iron was detected in Rosenthal fibers accumulated in the cell bodies of astrocytes in the brain stem. Ferritin, ferroportin and ceruloplasmin were found greatly increased in astrocyte cell bodies. These results suggest that iron is misregulated in astrocytes in AxD patients. At the conclusion of this chapter, I propose a model for the pathological exacerbation of AxD by iron.

Results

Fe3+ Iron accumulates in Rosenthal fibers and astrocytes in AxD patient tissue

Fe3+ iron has been found greatly increased in AxD mouse astrocytes (Hagemann et al., 2006; Hagemann et al., 2005; Hagemann et al., 2012). In order to determine if similar increases in iron occur in AxD

patients, I used a modified DAB-enhanced Perls' stain (Nguyen-Legros et al., 1980a) on 5μm-thick deparaffinized sections to visualize Fe3+ iron in two infant onset, type I AxD patients, one with the R239H mutation and another with the R416W mutation, age 10 and 7, and compared these to tissue from an infant, aged 22 months. In the R239H and control patients we first examined sections of the cortex which also contained subcortical white matter, areas where there are abundant Rosenthal fibers (Fig 1A and B). In the R239H AxD patient, positive iron staining in Rosenthal fibers in the white matter was apparent even at low magnification (Fig 1B, left of open arrowheads), while at low magnification in control, there was little positive immunostaining except in blood vessels (Fig 1A). Higher magnification images in control tissue revealed positive iron staining in cells with small nuclei, resembling oligodendrocytes (Fig 1C, arrows), in addition to blood vessels (open arrowhead). This agrees with published reports of iron localization in white matter in oligodendrocytes (Connor et al., 1990; Dwork et al., 1988; Morris et al., 1992). At higher magnification in the R239H patient white matter Rosenthal fibers were clearly distinguishable (Fig 1D, arrowheads) and many were located around blood vessels (Fig 1D, BV). This characteristic feature of Rosenthal fiber-staining can be observed in a hematoxylin and eosin stain of a similar white matter section from the same patient where Rosenthal fibers, stained bright pink, are of similar shape and location around blood vessels (Fig 1E).

In AxD patients, the pial surface of the cortex consistently shows abundant Rosenthal fibers. We were interested to see if these too contain Fe3+ iron, so next examined the pial surface of the AxD R239H patient and the control patient. Similar to what we saw in the white matter, we found iron staining apparent in the abundant Rosenthal fibers at the pial surface of the R239H patient, even at low magnification (Fig 1G, arrowheads), but none at the pial surface or adjoining cortex in the control patient (Fig 1F, arrowheads). Higher power magnification of the pial surface of this patient revealed iron positive Rosenthal fibers at both the pial surface and in the adjacent cortex including many surrounding a blood vessel (Fig 1H, arrowheads). We noticed no Fe3+ oligodendrocytes in the AxD tissue, however

given many Rosenthal fibers are roughly the size and shape of oligodendrocyte nuclei, we can make no conclusions about the presence or absence of Fe3+ iron in AxD patient oligodendrocytes without counterstaining for oligodendrocyte markers.

The brain stem is an area where in AxD there is atrophy and focal demyelination in some adult, type II cases, and deficits such as speech and swallowing difficulties in some type I AxD patients can be traced to this area. I examined brain stem sections from the R416W patient for Fe3+ iron and found intense iron staining throughout this tissue and astrocytes were apparently positively stained (Fig 1I,l blue arrowheads figure 1I). At higher magnification we could localize some of the iron staining to completely filled cell bodies and proximal processes of cells that appeared to be astrocytes (Fig 1J, blue arrowheads). AxD patient sections incubated in a control solution without potassium ferrocyanide showed no positive staining for iron (data not shown).

Ferritin is increased in AxD patient tissue

Most cells store excess iron in ferritin. In this way the transition metal accumulates in a non-reactive, biochemically inert form and is kept as a reserve for cellular iron needs (as reviewed by Harrison and Arosio, 1996). In the normal adult human brain, ferritin is occasionally found in astrocytes in the striatum, hippocampus, and amygdala (Connor et al., 1990). Because iron in a cell can trigger translational activation of ferritin through IRP1 and IRP2 (as reviewed by Arosio and Levi, 2002), we sought to determine if ferritin was detectable in AxD astrocytes. Ferritin is composed of 24 subunits of H ferritin and L ferritin, expressed by separate genes and which are expressed at varying ratios based upon cell type and tissue (as reviewed by Harrison and Arosio, 1996). In order to detect either of these, we used an antibody that recognizes both of these ferritins in our DAB-enhanced immunohistochemistry of R239H AxD patient and control white matter, where we had previously found iron positive Rosenthal fibers. In the control tissue we found light, diffuse perinuclear ferritin immunostaining of cells resembling oligodendrocytes (Fig 2A, black arrows). Several other cells had detectable ferritin

immunostaining, but were difficult to identify without double immunostaining with cell markers. In the AxD R239H patient we found ferritin to be greatly increased throughout the white matter. Large nuclei of reactive astrocytes can be seen (Fig 2B, blue arrowheads) and are surrounded by both light and more prominent immunostaining for ferritin in their cell bodies. Many Rosenthal fibers, stained light blue with a hematoxylin counterstain, can be observed. Some are surrounded by intense positive immunostaining for ferritin (Fig 2B, black arrowheads), which indicates that ferritin is in the processes of astrocytes that contain Rosenthal fibers. Cells with small, round nuclei, representing oligodendrocytes also appear to stain positive for ferritin (Fig 2B, black arrows), as they had in control tissue.

Ferritin is expressed by astrocytes in AxD mouse hippocampus

Given the high Fe3+ iron and ferritin in patients, and that high Fe3+ iron that had been observed in mice, we next examined the one year old KI R236H mouse using immunofluorescence for ferritin and GFAP, in order to identify astrocytes. In the wild type mouse, few cells were positive for ferritin, however we did find occasional cells resembling oligodendrocytes (Fig 3A, arrow). Additionally there was a light punctate reactivity to ferritin in what appeared to be a white matter tract in the stratum oriens (Fig 3A). Examining the KI mouse stratum oriens, we found increased immunoreactivity to ferritin, all of which appeared to be stemming from GFAP+ astrocytes (Fig 3B, white arrows) and none from oligodendrocytes. The immunoreactivity appeared to fill most of the astrocytes, including fine processes not positive for GFAP. Additionally, in AxD model mice we often saw punctate immunoreactivity to GFAP that does not appear to be contiguous with a cell process (Sosunov et al., 2013), perhaps resembling Rosenthal fibers or representing small astrocyte processes. In the KI mouse we observed these focal areas of GFAP immunoreactivity and some were positive for ferritin (Fig 3B, small blue arrows). In the time since conducting these experiments, Hagemann, Messing et al. have published data demonstrating ferritin immunostaining in astrocytes of KI mice (Hagemann et al., 2012), supporting our findings here.

Ceruloplasmin and Ferroportin are increased in AxD patient tissue

While Fe3+ iron and ferritin are sometimes observed in some astrocytes of adults, which increases with aging, particularly in the striatum (Connor et al., 1990), detection of iron and ferritin in subcortical astrocytes is not common, especially on the scale that we observed here. In normal white matter, oligodendrocytes are the cells that predominantly stain positive for iron and ferritin in the human brain (Connor et al., 1990; Dwork et al., 1988; Morris et al., 1992). Though it is rare, the best -known condition that causes abnormal iron accumulation in astrocytes (Kaneko et al., 2002b; Oide et al., 2006) and the liver is aceruloplasminemia (Acp), a rare autosomal recessive disease caused by mutations in the ferroxidase ceruloplasmin (Cp) (Harris et al., 1995; Morita et al., 1995). Interestingly, astrocytes show large iron-positive protein accumulations in astrocyte endfeet in this disorder (Kaneko et al., 2002b; Oide et al., 2006). Cp safely oxidizes Fe2+to Fe3+, coupling this to the controlled reduction of oxygen to water (as reviewed by Vassiliev et al., 2005). Two isoforms of Cp are found in primary astrocytes from rodents. Secreted Cp has been found in mouse astrocytes (Klomp et al., 1996) while rats express both secreted (Zahs et al., 1993) and an alternately spliced glycophosphatidylinositol (GPI)- bound form (Patel and David, 1997). The ferroxidase activity of Cp has been found necessary to maintain the cell surface stability of FPN1 which is recognized by a ubiquitin ligase while bound by Fe2+i (De Domenico et al., 2007). FPN1 is an iron efflux protein which possesses a unique protein sequence and shares no homology with other transporters, so is thought to be the sole means by which iron can be transported from cells (McKie and Barlow, 2004). Because FPN1 cell surface expression has been linked with the ferroxidase activity of ceruloplasmin, it has been hypothesized that iron accumulation in the brain in Acp stems from a lack of iron efflux from astrocytes (De Domenico et al., 2007; Jeong and David, 2003).

Given that iron accumulation in astrocytes has been found in both AxD and Acp, we sought to determine the immunohistological expression of FPN1 and Cp in AxD and control tissue. We first examined the deep, subcortical white matter, an area of intense Rosenthal fibers and diminished myelination in many

patients, with an antibody for FPN1 and found in the control patient many cells including astrocytes (Fig 1A, blue arrowheads) and oligodendrocytes (Fib 4B, black arrows) were positive. In the AxD R416W patient the immunostaining for FPN1 in astrocytes was striking. All astrocytes appeared to be positive for FPN1 and many had large accumulations of the protein in the cell body cytoplasm (Figure 4B, blue arrowheads). Furthermore while there was a diffuse background staining of the parenchyma, astrocytes appeared to be the primary cells expressing the protein. Oligodendrocytes could be observed, but some did not appear to express FPN1 (Fig 4B, black arrows). Ferroportin can also be seen accumulated in the cell body of binucleated astrocytes (Fig 4B, *). Expression of FPN1 in the deep white matter of the R239H patient, which appeared to be extensively demyelinated, showed intense FPN1 reactivity. Many light blue hematoxylin stained Rosenthal fibers can be seen and the majority are strongly rimmed in positive immunostaining for FPN1 (Fig 4C, black arrowheads) indicating that there is FPN1 reactivity in astrocyte cell bodies and processes which contain Rosenthal fibers. Individual cells were difficult to identify, but a heavily immunostained astrocyte can be seen (Fig 4C, blue arrowhead).

We next looked at the expression of Cp in the AxD R416W and control patients' deep white matter using an antibody that should recognize both secreted and GPI-linked forms of this protein. In the control tissue there many cells positively immunostaining for Cp that were difficult to identify without double immunostaining for cell markers. In the AxD R416 patient we found greatly increased reactivity to the ceruloplasmin antibody throughout the parenchyma, some of which was difficult to ascribe to individual cells. In this patient we also observed intense accumulations of ceruloplasmin in clusters of binucleated and multinucleated astrocytes (Fig 4E, white arrowheads).

Discussion

In this chapter I present a brief but novel immunohistochemical study of Fe3+, ferritin and Cp and FPN1 in the CNS of AxD patients. I show evidence that there is an accumulation of iron and ferritin in

astrocytes of children with type I AxD. Additionally, I present evidence that there is ferroportin accumulation in the cell bodies of astrocytes of two AxD patients and an overall increase in immunostaining with an antibody for Cp in a single AxD patient. These results expand the findings of Hagemann and colleagues who found an accumulation of iron in astrocytes in Tg and KI AxD mice (Hagemann et al., 2006; Hagemann et al., 2005; Hagemann et al., 2012). I also confirm their observation that there is an increase in ferritin immunofluorescence in astrocytes in KI animals (Hagemann et al., 2012). I note striking similarities between Rosenthal fibers and protein inclusions in Acp and suggest that the unusual and high levels of iron and ferritin we have found in AxD patient tissue may, as in other disorders, serve as a source for oxygen radical generation. At the conclusion of this chapter, I propose a model for the pathological exacerbation of AxD by iron.

Rosenthal Fibers and astrocytes contain Fe3+

Despite a wide range of disease courses and neuropathological findings that are observed in AxD (Prust et al., 2011), Rosenthal fibers are found universally. I found discrete deposits of Fe3+ that coincided in shape and location to Rosenthal fibers in white matter of the R239H patient (Fig 1B, D and H). In contrast, when I examined this same patient and type of tissue for the iron storage protein ferritin, I was surprised to find large amounts of this protein dispersed throughout the tissue in varying intensity and located in what appeared to be astrocytes (Fig 2B). Ferritin staining was not within Rosenthal fibers, but instead around them, sometimes very strongly rimming the edges.

These findings might be interpreted by comparison to previous studies of Perls' staining of the liver, which is high in iron and ferritin content. In liver, dispersed soluble ferritin gives only a faint background staining by Perls' method, whereas hemosiderin, a product of iron overload produced when a cell's capacity to synthesize ferritin is exceeded, is prominently Fe3+ stained (as reviewed by Harrison and Arosio, 1996). Considering my obesrvations of the R239H subcortical white matter in light of these studies, several things are suggested. First, iron contained within ferritin is most likely accumulated

throughout most of astrocytes, though is unable to be detected by Perls' staining due to limitations in this technique (as reviewed by Todorich et al., 2009). Second, I cannot be certain that Rosenthal fibers do not contain ferritin because immunohistological determination of protein content within Rosenthal fibers is difficult to assess through standard light microscopy, due to difficulty of penetrating these extremely dense structures with antibodies. However, because the Perls' staining was strong, it is likely that the iron that is seen in Rosenthal fibers is most likely precipitated out of ferritin or otherwise pathologically accumulated. Finally because the iron in Rosenthal fibers is unlikely to be normally bound by ferritin, it may be available for reactions that produce damaging oxygen radicals.

In contrast to the discrete Fe3+ positive Rosenthal fibers in the R239H patients, there is strong staining of whole astrocyte cell bodies in the brain stem of the R416W patient. This suggests massive accumulation of Fe3+ iron in these cells. Although I did not immunostain this section with antibodies for ferritin, it is possible that this high amount of iron might overwhelm cellular ferritin.

These two patterns of Fe3+ iron localization in cells, discretely in Rosenthal fibers in the white matter of one patient, and vividly in the cell bodies of astrocytes in another, are quite different. While it is likely there are differences in the endogenous amounts of iron found in the subcortical white matter and the brain stem it is also possible that this disparity may arise from differences in what may be protoplasmic astrocytes in the brain stem and fibrous astrocytes in the white matter and inherent differences in iron transport and regulatory mechanisms between these cell types and regions of the brain.

The iron storage disorder Aceruloplasminemia and AxD share similarities

Iron in astrocytes, as observed in these children with AxD, is not common. Two noted instances where iron is observed in astrocytes is in the adult, and especially, aging hippocampus and striatum (Connor et al., 1990; Schipper et al., 1998) and in the cerebral cortex and basal ganglia in aceruloplasminemia (Acp). Acp is caused by mutations in the gene encoding Cp (Harris et al., 1995; Morita et al., 1995). Because

the ferroxidase activity of Cp has been found necessary to maintain the cell surface stability of the iron export transporter FPN1 (De Domenico et al., 2007), the iron accumulation in astrocytes in Acp is hypothesized to originate from impaired iron efflux from these cells. Acp onset is usually in middle age and CNS disturbances of ataxia, involuntary movement, parkinsonism and cognitive dysfunction are thought to reflect sites of iron deposition in the basal ganglia and cerebral cortex (Miyajima et al., 2003).

The similarities between Rosenthal fibers and the protein inclusions in Acp are notable. Similar to Rosenthal fibers, Acp patients bear Fe3+ iron containing, membraneless, proteinaceous, electron dense inclusions in astrocytes, many at perivascular endfeet (Oide et al., 2006). These have been noted be similar to "grumose foamy bodies" (GSFBs) found in other disorders (Arai, 1995). Both Rosenthal fibers and the GSFB-like inclusions in Acp immunostain for ubiquitin, HNE and GFAP (Kaneko et al., 2002b; Oide et al., 2006). Like in AxD, by electron microscopy (see Chapter 1, Fig 3B), GFAP filaments can be seen ringing these inclusions (Kaneko et al., 2002b). GSFBs in other disorders have HSP27 and alpha B-crystallin, although these are not reported in Acp. In contrast to Rosenthal fibers, GSFBs in Acp can become much larger than the average Rosenthal fiber, and are only mildly eosinophilic. Notably, whereas Rosenthal fibers do not generally immunostain positive for even GFAP, except around their periphery, because they are so dense, GSFBs immunostain positive for ferritin, and for GFAP, possibly because they are more diffuse in their electron density so antibodies are able to penetrate the surface, which is not generally the case in AxD.

Abnormal and multi-nucleated astrocytes in AxD are well-documented (for example see Fig 4B asterisk, 4C arrowheads); similarly, some of these same striking features can be observed in nuclei in astrocytes in the basal ganglia and cerebral cortex in Acp patients in cells that also stain positive for Fe3+ (Oide et al., 2006). Finally, I find similar the two patterns of Fe3+ iron localization that are observed in AxD tissue. Both GSFBs and Rosenthal fibers appear to stain positive for Fe3+ while the rest of the astrocyte

process normally does not, however in other astrocytes Fe3+ appears to fill much of the cell body (Fig 1I, J) (Oide et al., 2006).

Clinical and pathologic studies of Acp patients suggest that iron-mediated oxygen radical damage through increased lipid peroxidation and mitochondrial dysfunction are likely primary causes of the clinical manifestation of this neurological disorder (as reviewed by Kono, 2012). The similarities to AxD patients with respect to iron accumulation in astrocytes, nuclear abnormalities and protein inclusions that contain iron, HNE, ubiquitin and GFAP suggest that iron found in AxD astrocytes might inflict similar oxidative damage

GFAP is oxidatively modified in Acp

Carbonylation is thought the most frequent oxidative modification to proteins (England and Cotter, 2005), and is can occur in four ways: (1) oxidative cleavage of protein backbone, (2) direct oxidation of leucine, arginine or histidine , (3) reactive aldehyde-generated (HNE), and (4) glycation or glycation product reaction with lysine residues (as reviewed by Curtis et al., 2012). An assay that detects such modified proteins can be used to isolate these and separate them on a gel for protein determination. This type of experiment demonstrated that GFAP is one of the largest groups of such oxidatively modified proteins in the cerebral cortex of an Acp patient (Kaneko et al., 2002a). A portion of carbonylated GFAP was found at about 40kDa, and therefore may be oxidatively cleaved by this process (Kaneko et al., 2002a), though Kaneko et al. do not rule out proteolytic cleavage of GFAP into smaller peptides. This suggests several important things: first, that normal human GFAP is subject to iron-mediated oxidative damage; second, that GFAP accumulates in Acp; and finally, that iron accumulation in astrocytes in AxD may mediate carbonylation of normal human GFAP and extensively modify it.

The degradation of some oxidatively modified proteins is mediated by proteasomal inhibition

The degradation of carbonylated proteins is thought to occur in a non-proteolytic specific manner (as reviewed by Dalle-Donne et al., 2006). However, several carbonylated proteins have been identified that are susceptible to accumulation after proteasomal inhibition. A carbonyl assay identified seven proteins that were preferentially resistant to degradation by the proteasome after iron treatment of RD4 cells (Drake et al., 2002). These include the heat shock protein HSP27, Cu/Zn SOD and ER chaperone calreticulin (Drake et al., 2002). Though a number of studies have suggested carbonylated proteins are efficiently degraded (Drake et al., 2002; Dukan et al., 2000; Grune et al., 2004; Grune et al., 2003; Huang et al., 1995; Levine et al., 1981), others suggest that aggregation of these proteins is prevalent (Maisonneuve et al., 2008). A review on the topic suggests aggregation of carbonylated proteins occurs as they become more heavily carbonylated and that these will inhibit the proteasome (Dalle-Donne et al., 2006).

Rises in iron meets proteasomal inhibition --Implications for AxD

By extrapolation, these results suggest that existing proteasomal inhibition in AxD by mGFAP and excess GFAP would inhibit degradation of a subset of oxidatively modified proteins that are degraded through the proteasome, should levels of free iron in an astrocyte transiently rise. Additionally, the presence of proteins such as the superoxide scavenger, Cu/SOD, the heat shock protein, HSP27 and the ER chaperone, calreticulin in this pool of oxidatively modified proteins, makes apparent the impact that ROS might have on lost protein function. For example, in the case of Cu/SOD its loss of function could allow an increase in oxidative stress, due to lost scavenging of superoxide radical. Additionally, the presence of Cu/SOD in the cytosol after having been oxidatively modified would make it additionally vulnerable to further modification by radicals which may expose hydrophobic residues and promote aggregation and/or allow for the release of copper. In the case of aggregation, these proteins might further inhibit the proteasome or through aggregation, contribute to cell toxicity. The release of copper,

on the other hand, would further the oxidative stress already presents in the cell. In AxD, existing proteasomal inhibition, compounded by what might be transient rises in iron, could create feed-forward mechanisms of oxidative stress and proteasomal inhibition.

Iron expression in AxD mice is downstream of Nrf2 signaling in astrocyte

I find iron and ferritin accumulated in pathological manner in AxD patient astrocytes, however it is not known how or when this occurs in the disease process. Experiments with AxD KI and Tg mice suggest that iron accumulation is downstream of an oxidative stress response driven by Nrf2. AxD Tg and KI mice accumulate iron and ferritin astrocytes (Hagemann et al., 2006; Hagemann et al., 2005; Hagemann et al., 2012). They also show a robust oxidative stress response, including expression of genes driven from the ARE promoter (Hagemann et al., 2006; Hagemann et al., 2005), which includes many Nrf2 regulated genes, including H-ferritin and L-ferritin. When Nrf2 null mice are crossed with AxD KI mice or Tg mouse to create a Nrf2 null-Tg or Nrf2 null KI, much of the iron detectable by modified Perls' staining is eliminated (Hagemann et al., 2012). Additionally and surprisingly, these mice suffer no ill effect from Nrf2 elimination. The ameliorated iron accumulation in the Nrf2-null AxD mouse crosses are a strong case for iron expression being downstream of an activated antioxidant response in these mice.

Possible Initiators of iron accumulation

Given that the AxD mice show iron accumulation downstream of Nrf2 activation, determining the source of the iron in AxD patients is critical to understanding the mechanisms of this disease and for developing therapeutic treatments. Here I discuss ways in which iron might increase in astrocytes, aside from defects in influx or efflux mechanisms, as is suspected in Acp.

Initiators of iron may be factors that impact iron regulatory proteins directly to increase the free iron pool, such as nitric oxide, superoxide or those that work through indirect mechanisms, such as proteasomal inhibition, depletion of GSH or signaling through HIFs/ HO-1. Finally it is conceivable that

associations of between GFAP and menin1 may impact the increase in iron. I briefly summarize each of these below.

Proteasomal inhibition

Proteasome inhibition has been found a factor in AxD (Chen et al., 2007; Cho and Messing, 2009; Tang et al., 2010; Tang et al., 2006) The degradation of iron regulatory protein2, (IRP2) is known to occur through the proteasome (Iwai et al., 1998). Experiments which used the proteasome inhibitor lactacystin on the dopaminergic neuronal cell line MES23.5 found an early increase in the labile iron pool and accompanying cell death after treatment (Li et al., 2012). Lactacystin treatment also increased IRP2 protein, but not IRP1, which is not degraded by the proteasome. The levels of DMT1, Transferrin Receptor, FPN1 and H-Ferritin were analyzed by Western blot, but only DMT1 and TfR1 were increased in the same early time period. Knocking down DMT1, as well as applying chemical inhibitors to DMT1, had little effect on the iron increase, but antibodies to Tfr1 did have this effect. Finally, shRNAi of IRP2 attenuated the changes seen in Tfr1 and H-ferritin and cell death relative to its ability to decrease expression of IRP2. The authors did report results of shRNAi on total iron levels. These results suggest that a plausible origin for increase of iron I see in AxD patient astrocytes originates from IRP2-mediated upregulation of genes involved in influx of iron into cells via proteasomal inhibition.

Superoxide

Because superoxide can increase iron in a cell, cellular stresses or events that might increase this oxygen radical or inhibit the function of SOD have the potential to increase iron. While superoxide is not as reactive as the hydroxyl radical, it can increase the labile iron pool in two ways (Liochev and Fridovich, 1994). First, it can release iron stored in ferritin, adding to the labile iron pool and therefore making it immediately available for the Fenton reaction (Biemond et al., 1984; Liochev and Fridovich, 1994). Second, hydroxide also releases iron from the iron-sulfur cluster of aconitase inactivating it (Liochev and

Fridovich, 1994). As with ferritin, this produces an immediate increase in the labile iron pool, but additionally, the inactivation of aconitase, through a conformational change, converts this protein to IRP 1, which binds iron regulated elements (IREs) on a group of mRNAs, many of which are involved in iron metabolism (as reviewed by Tong and Rouault, 2007). For example, mRNA for FPN1 and L-ferritin and H-ferritin both contain an IRE on their 5' UTR to which IRP1 binds, inhibiting translation. The opposite effect is elicited by IRP1 interaction with the IRE(s) on the 3' UTRs of mRNA transcripts for DMT1 and transferrin receptor (see Figure C) (as reviewed byRouault, 2006). Therefore, the generation of the superoxide radical can cause an increase in the labile iron pool.

Nitric oxide

Nitric oxide promotes constitutive activation of IRP1, by modifying its iron-sulfur cluster (Soum and Drapier, 2003). Both ROS and reactive nitrogen species (RNS) have been reported to bind IRP1, resulting in constitutively increased IRP1 binding that may result in reduced FPN1 and ferritin. It also results in increased TfR1 protein and DMT1 levels and thus increases the cellular labile iron pool. In cell culture IL-1beta treatment of primary human astrocytes increases the expression of inducible nitric oxide synthetase (Jana et al., 2005), and therefore injury or inflammatory conditions produced by bacterial or viral infection where this cytokine may be released could trigger an influx of iron into astrocytes. Under normal circumstances this might be tolerated while the cell adapts and recover. However AxD astrocytes, under the stress of proteasomal inhibition might both inhibit the proteolytic processing of the increased pool of oxidatively modified proteins, and additionally suffer additional proteasomal inhibition from this pool.

Heme Oyxgenase 1 (HO-1)

Iron accumulation in the mitochondria of aging astrocytes occurs as a by-product of HO-1-mediated degradation of heme, which is caused by oxidative challenge of astrocytes (Schipper, 2004). Increases in

HO-1 occur as a result of the hypoxia inducible factor 1, under hypoxic conditions or other conditions of oxidative stress. With respect to our results, it is unclear if there is iron accumulation in the mitochondria of AxD astrocytes.

GSH-depletion

In dopaminergic N27 cells, inhibiting GSH by using buthionine sulfoxamine (BSO), an inhibitor of γ-glutamyl-cysteine ligase (GCL), the rate-limiting factor in *de novo* glutathione synthesis, increased the labile iron pool. Interestingly, this increase was found independent of either IRP1/IRP2 or hypoxia inducible factor (HIF) induction, but was found dependent on H_2O_2 and protein synthesis (Kaur et al., 2009). GSH is a major cellular antioxidant and has many roles in cellular homeostasis (Arrigo, 1999; Cotgreave and Gerdes, 1998; Dringen et al., 2000). It could be depleted through conditions of intense oxidative stress of many sources. Additionally because it detoxifies HNE through its conjugation to modified lipids, its depletion could also occur after/during lipid peroxidation (as reviewed by Valko et al., 2005). GSH is also important to provide reducing power in the cell, so is under especially high demand when a cell is uses glycolysis instead of aerobic respiration. Any factors that might singly or together increase the demand for GSH might act to increase iron.

GFAP – Menin interactions may impact iron status of cells

GFAP interacts with a number of non-structural proteins, one is a protein known as menin which is encoded by the tumor suppressor gene, multiple endocrine neoplasia type 1 (MEN1) (as reviewed by Wu and Hua, 2011). By GST pull-down analysis and co-immunoprecipitation experiments, Menin was found to associate with intermediate filaments GFAP and vimentin in glioma cells (Lopez-Egido et al., 2002). The head domain of these proteins was found essential to the interaction, and immunofluorescence studies showed endogenous menin to aggregate with GFAP and vimentin when the IF network was disrupted with overexpression of tail-less GFAP (Lopez-Egido et al., 2002). GFAP and

vimentin are hypothesized to sequester menin at the S and early G2 phases of the cell cycle (Lopez-Egido et al., 2002).

As a tumor suppressor, Menin represses cell proliferation and cell cycle in multiple ways and also interacts with transcription factors, such as, NF-κB, PPARγ and VDR, to induce or suppress gene transcription (as reviewed by Wu and Hua, 2011). Menin also suppresses the activity of the AP-1 transcription factor JunD (Naito et al., 2005), known to interact with the *cis* antioxidant response elements (ARE) on 5' untranslated regions of genes involved with antioxidant response. Because menin has the potential to affect such a wide range of transcription factors, it is possible that modification of its normal activity, through aberrant interactions with these two intermediate filaments might influence gene transcription that could affect iron. In any case, if GFAP/Vimentin are impacting Menin's normal transcriptional interactions these might increase as these intermediate filaments become more numerous or more altered.

Iron begets iron – positive feedback

In addition to generating the hydroxyl radical through the Fenton reaction, Fe2+ can react with molecular oxygen in the Earth's ubiquitously aerobic environment to produce Fe3+ and superoxide (Fig A, equation 4) (as reviewed by Valko et al., 2005). Superoxide can immediately increase the labile by extracting iron from ferritin and from the iron-sulfur cluster of aconitase, however this second action, through activation of IRP1, can additionally impact the translation of iron regulatory proteins in a way that increases overall free iron in a cell, despite its iron status. (See Superoxide, above for mechanism.)

Activation of signaling pathways by iron

The transcription factors NFkB, AP-1 and p53 are all sensitive to redox active metals, however the most significant and sensitive to activation are the NFkB and mitogen-activated protein (MAP) kinase/AP-1 (as reviewed by Valko et al., 2005). NFkB primarily mediates the inflammatory response, while the AP-1 is

involved in cell growth and differentiation. The p53 transcription factor serves as a guardian of a critical cell-cycle checkpoint and inactivation of p53 allows the uncontrolled cell divisions that occur in human cancer (as reviewed by Meplan et al., 2000). Notably, because GFAP has both AP-1 and NFkB elements on its promoter (Pennypacker et al., 1994; Rossi et al., 2005), an increase in iron-mediated ROS may increase GFAP, contributing to a feed-forward activation of the disease progression.

Of note is that HNE activates an antioxidant response. Treatment of optic nerve head astrocytes with HNE induces the expression of Nrf2, which induces the expression of antioxidant response genes, including glutathione S-transferases (Malone and Hernandez, 2007). This enzyme catalyzes the conjugation of GSH to lipid adducts, thereby detoxifying them (Di Ilio et al., 1986).

Iron and oxidative stress in other neurodegenerative disorders

With the addition of iron as a component of Rosenthal fibers, there are similarities not only between these protein inclusions and those in Acp, but I also add what may be an important component to list of similarities between Rosenthal fibers and the extracellular plaques of Alzheimer disease and Lewey bodies of Parkinson's disease. Fe3+ iron joins, HNE, the heat shock proteins HSP27 and alpha B-crystallin and ubiquitin as components of membraneless protein inclusions (Castellani et al., 1998; Castellani et al., 2000; Head et al., 1993; Hirsch et al., 1991; LeVine, 1997; Renkawek et al., 1993; Sayre et al., 1997; Shinohara et al., 1993; Tomokane et al., 1991; Yoritaka et al., 1996). Because iron-mediated oxidation reactions have been implicated in the pathogenesis of these other disorders, it is imperative that we begin to widen our view and learn not only from Acp (as discussed above), but from the extensive research that has been conducted over many years on Alzheimer disease and Parkinson's disease and consider iron as a potential damaging factor in AxD.

Iron potentiates AxD pathology – A Model

We found aberrantly high levels of iron in astrocytes of two AxD type I patients. Though I have no direct evidence, I propose that iron-induced oxidative stress contributes to the accumulation of GFAP and proteasomal inhibition in AxD. Though I feel iron is important to the formation of protein aggregates/Rosenthal fibers in AxD, we have left this out of the model for the sake of simplicity – protein aggregates/Rosenthal fibers may be implied by "proteasomal inhibition."

I propose the following simplified model for the potentiation of AxD pathology by iron-induced ROS in astrocytes (Figure 5): First, as demonstrated by work in our lab, and supported by work in others, mutations in GFAP and accumulation of GFAP inhibit the proteasome (Chen et al., 2011; Cho and Messing, 2009; Tang et al., 2010; Tang et al., 2006), which initiates the JNK/p38 stress pathway, thereby activating AP-1 transcription factors that can increase GFAP and in doing so, generate a positive feedback loop (Tang et al., 2006). An increase in the labile iron pool may occur as a result of proteasomal inhibition (Li et al., 2012) and/or may additionally increase through other means such as GSH depletion, oxidative or nitrosative stressors, or the interaction of GFAP with menin (Lopez-Egido et al., 2002). Next, free iron produces ROS through the Fenton reaction. Fourth, ROS damages biomolecules such as DNA, lipids and proteins and the lipid peroxidation product HNE additionally may damage proteins. Finally three positive feedback loops are enacted by ROS: (1) excessively oxidatively modified proteins can exacerbate proteasomal inhibition, (2) iron-mediated ROS activates the transcription factors, NFkB and AP-1, which can additionally increase GFAP (Brambilla et al., 2005; Pennypacker et al., 1994), and subsequently inhibit the proteasome, and (3) hydroxide radical releases iron from proteins and activates IRP1, additionally increasing free iron pool.

Conclusion

In this chapter I contribute to the increasing body of work which suggests there is oxidative stress involved in the pathological manifestations of AxD. My histological examination of the CNS of two AxD

patients found Fe3+ iron and ferritin accumulated in astrocytes, where normally this occurs in oligodendrocytes. This furthers work from the Messing lab that found Fe3+ and ferritin increased in astrocytes in AxD KI and Tg mice (Hagemann et al., 2006; Hagemann et al., 2005; Hagemann et al., 2012). Additionally, I found FPN1 and CP abundantly localized in cell bodies of astrocytes in patient tissue.

In this chapter I note that iron accumulation in AxD patient astrocytes is comparable to that found in astrocytes in Acp. Protein inclusions in these cells are strikingly similar. Because the clinical manifestations of Acp are thought to stem from iron-mediated oxygen radical damage (as reviewed by Kono, 2012), I propose that the iron accumulation in AxD patients is likely to cause oxygen radical generation and contribute to the clinical manifestations of AxD.

Chapter 4 Figures

Figure A. Iron and Free Radicals

Equation 1

$Fe^{3+} + O_2\bullet^- \leftrightarrow Fe2+ + O_2$

Ferric iron + superoxide ↔ Ferrous iron + Molecular oxygen

Equation 2 - Fenton Reaction

$H_2O_2 + Fe^{2+} \rightarrow Fe^{3+} + \bullet OH + OH^{--}$

Hydrogen peroxide + ferrous iron → Ferric iron + hydroxyl radical + hydroxide

Equation 3

The above steps (1 and 2) combined are called Haber-Weiss reaction:

$O_2\bullet^- + H_2O_2 \leftrightarrow O_2 + \bullet OH + OH^-$

Superoxide + hydrogen peroxide ↔ Molecular oxygen + hydroxyl radical + hydroxide

Equation 4

$Fe^{2+} + O_2 \rightarrow Fe^{3+} + O_2\bullet^-$

Ferric iron + molecular oxygen → Ferrous iron + superoxide

(Valko et al. Curr. Med. Chem. 2005; 12:1161-208)

Figure B. Transferrin Cycle

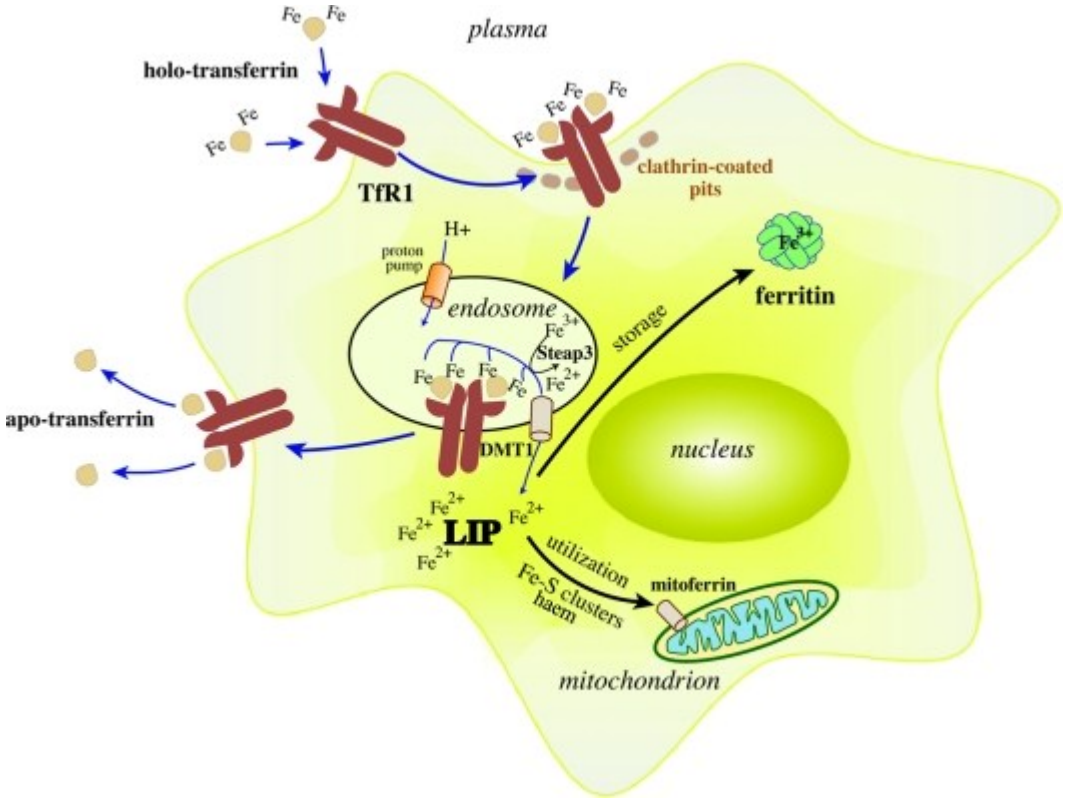

Developing erythroid cells, as well as most other cell types, acquire iron from plasma Tf. Iron-loaded holo-Tf binds with high affinity to TfR1 on the surface of cells, and the complex undergoes endocytosis via clathrin-coated pits. A proton pump promotes acidification of the endosome to pH 5.5, triggering the release of Fe3+ from Tf that remains bound to TfR1. The ferrireductase STEAP3 reduces Fe3+ to Fe2+, which is transported across the endosomal membrane by DMT1 to the cytosol or, possibly, directly to mitochondria in erythroid cells. Following the release of iron, the affinity of Tf to TfR1 drops ~500-fold, resulting in its dissociation. In the final step of the cycle, apo-Tf is secreted into the bloodstream to recapture Fe3+. (Wang, 2001 Biochm. J).

Figure C. IRP1 and IRP2 bind iron responsive elements

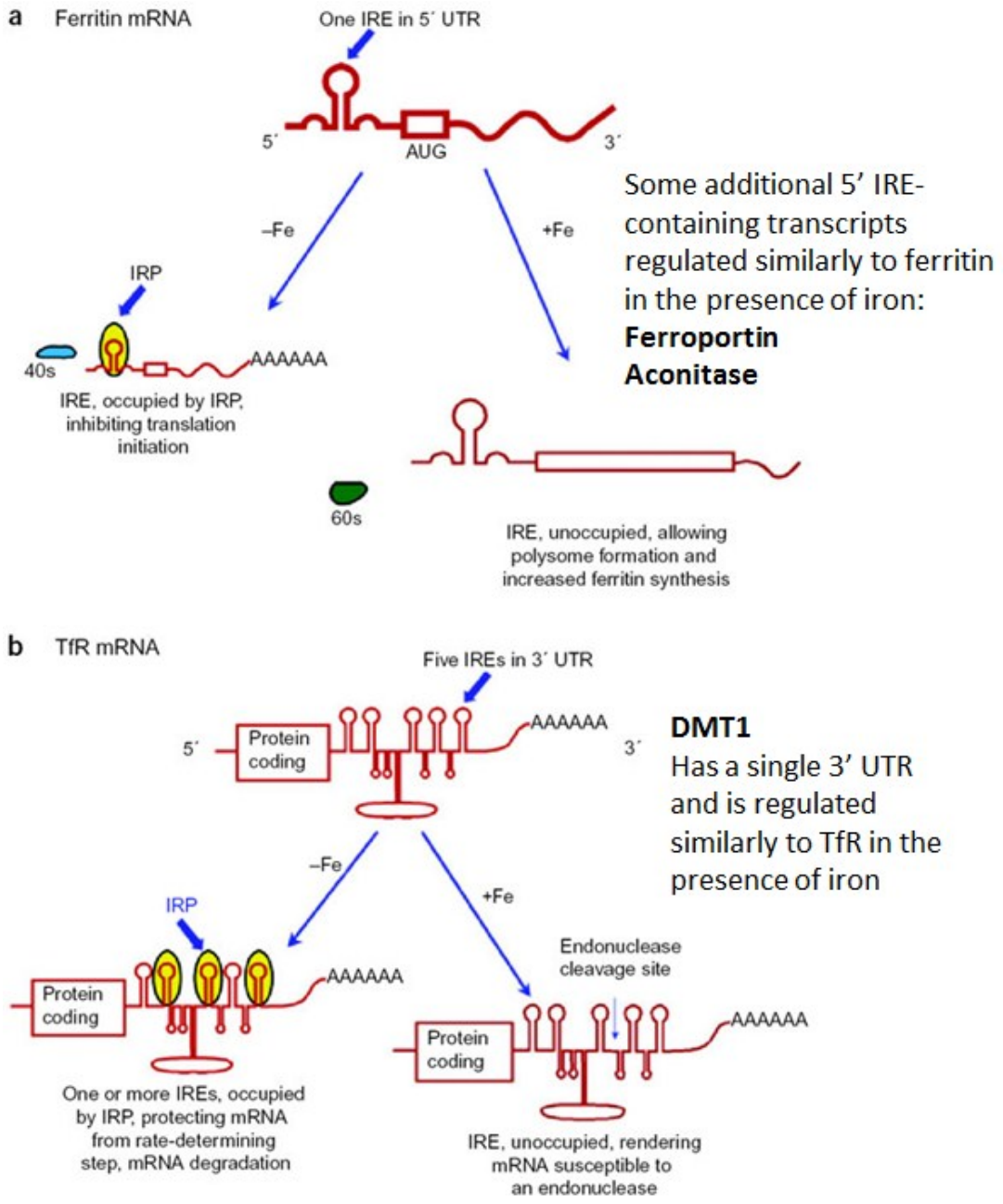

Regulation of ferritin (a) and transferrin (b) mRNAs by high (+Fe) and low (-Fe) iron availability. Under +Fe conditions iron regulatory proteins (IRPs) are unavailable to bind the iron response element (IRE) either due to conformational change (IRP1) or oxidative modification and degradation (IRP2). This increases ferritin synthesis and inhibits TfR synthesis. (Adapted from Rouault, 2006 . Nat. Chem.Biol)

Figure 1. Immunohistochemical profile of $Fe3^{+}$ in AxD patient autopsy tissue

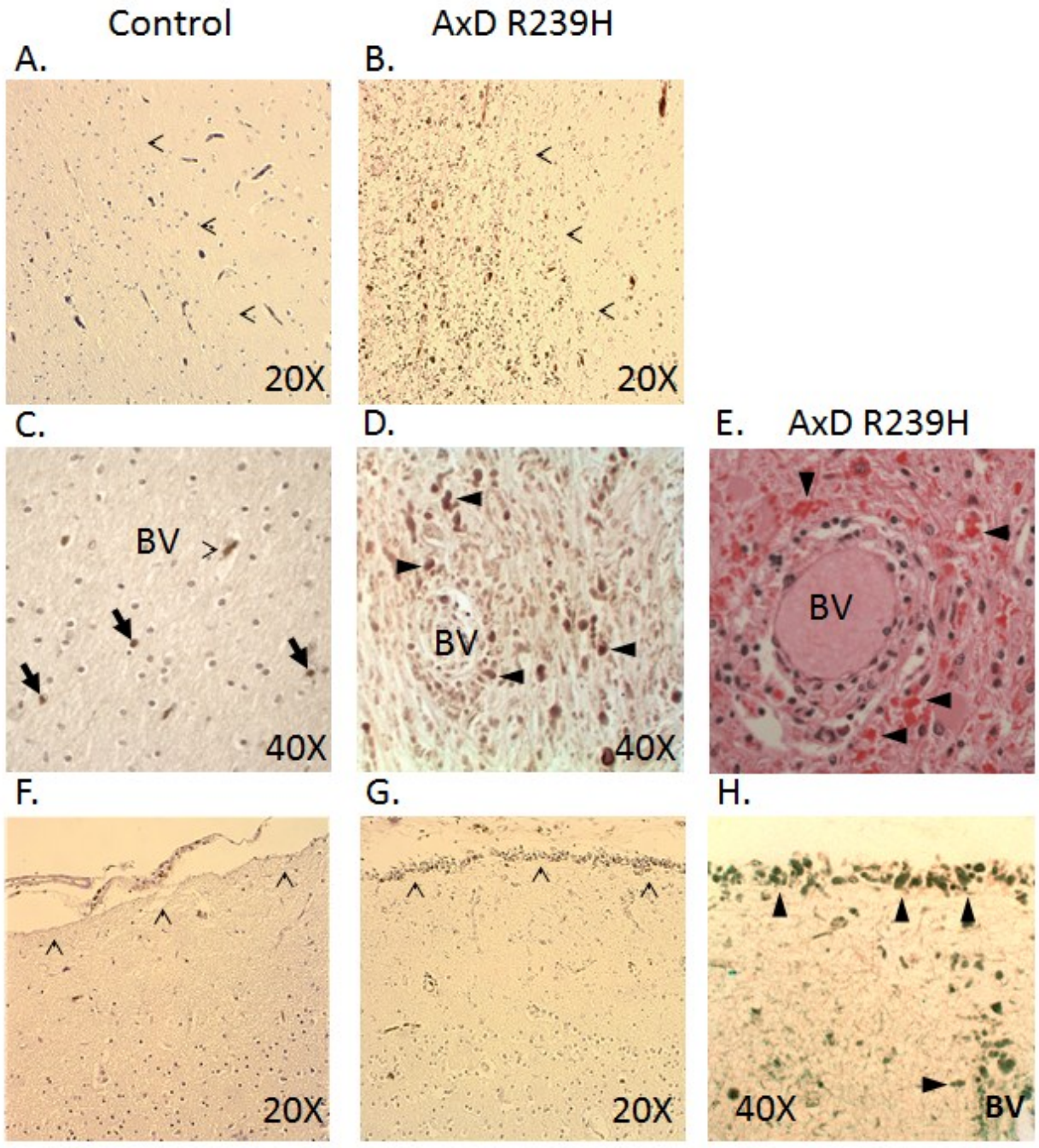

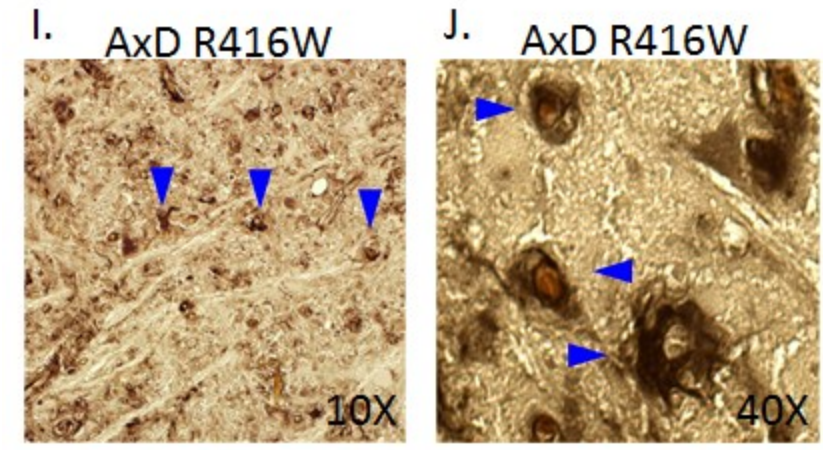

(A and B) Subcortical white matter (left of arrowheads) and adjacent cortex (right of arrowheads) of control (A) and AxD R239H (B) patient. Note in (B) the abundance of positively stained, globular Rosenthal fibers in white matter. The subcortical white matter is examined at higher magnification in control (C) and R239H (D-E) patient tissue. In control patient (C), iron staining appears in cells with small nuclei, characteristic of oligodendrocytes (black arrows) and also in blood vessels (BV). R239H AxD patient (D) shows positive staining for Fe3+ iron in Rosenthal fibers around a blood vessel (BV) and throughout the white matter. Rosenthal fibers (arrow heads) are seen staining strongly for eosin (bright pink) in hematoxylin and eosin stain of AxD R239H patient (E). Pial surface (open arrowheads) is examined (F and G). AxD R239H patient shows abundant Rosenthal fibers positively stained for Fe3+ iron lining the pial surface (G) and these can be seen in more detail (arrowheads) at higher magnification (H). Note Rosenthal fibers surrounding a nearby blood vessel (BV). In the brainstem of a AxD R416W patient there is intense Fe3+ iron staining as seen at low magnification(I), though even here Fe3+ positive astrocytes can be detected (I, blue arrowheads). At higher magnification, astrocytes in the brainstem can be seen filled with Fe3+ iron (J, blue arrowheads).

Figure 2. Ferritin accumulates in astrocytes of R239H AxD Patient

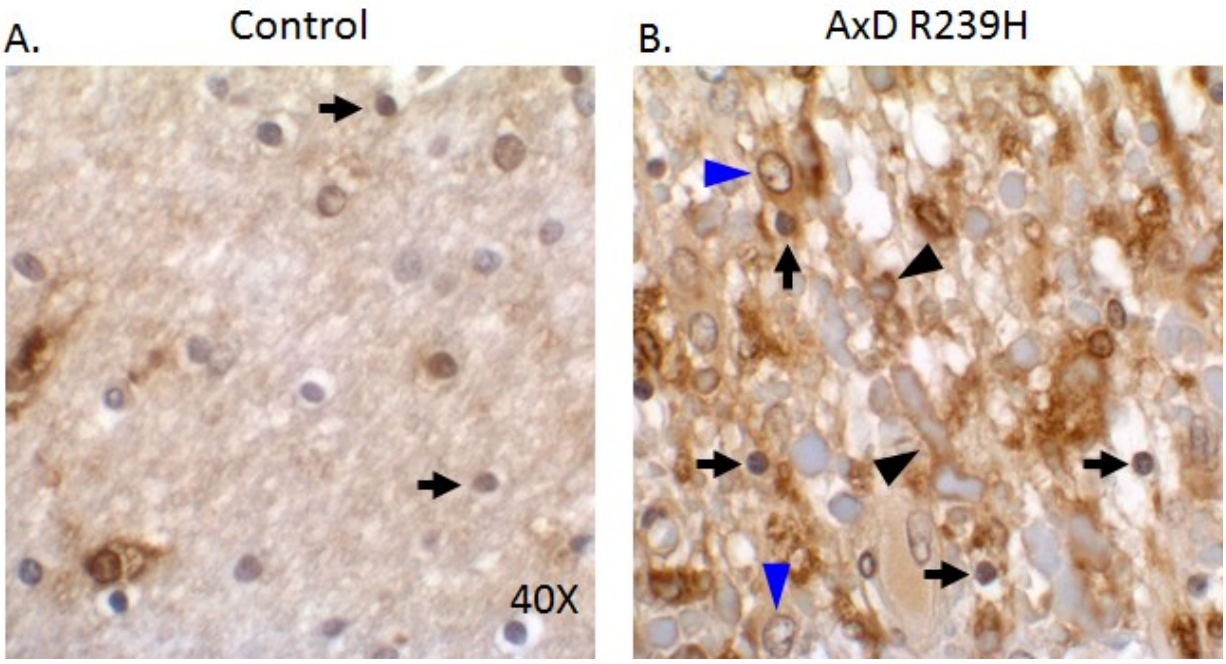

In control patient (A), an antibody with reactivity to both H and L ferritin stains oligodendrocytes (black arrows) and blood vessels. In AxD R23(H patient (B), ferritin staining is principally in astrocyte cell bodies (blue arrows) and can be seen in close association with the periphery of Rosenthal fibers (black arrowheads), which indicates ferritin is within astrocyte processes which contain these cytoplasmic inclusions. Ferritin can also be observed in small cells resembling oligodendrocytes (black arrows).

Figure 3. Ferritin immunostaining in one year old mouse

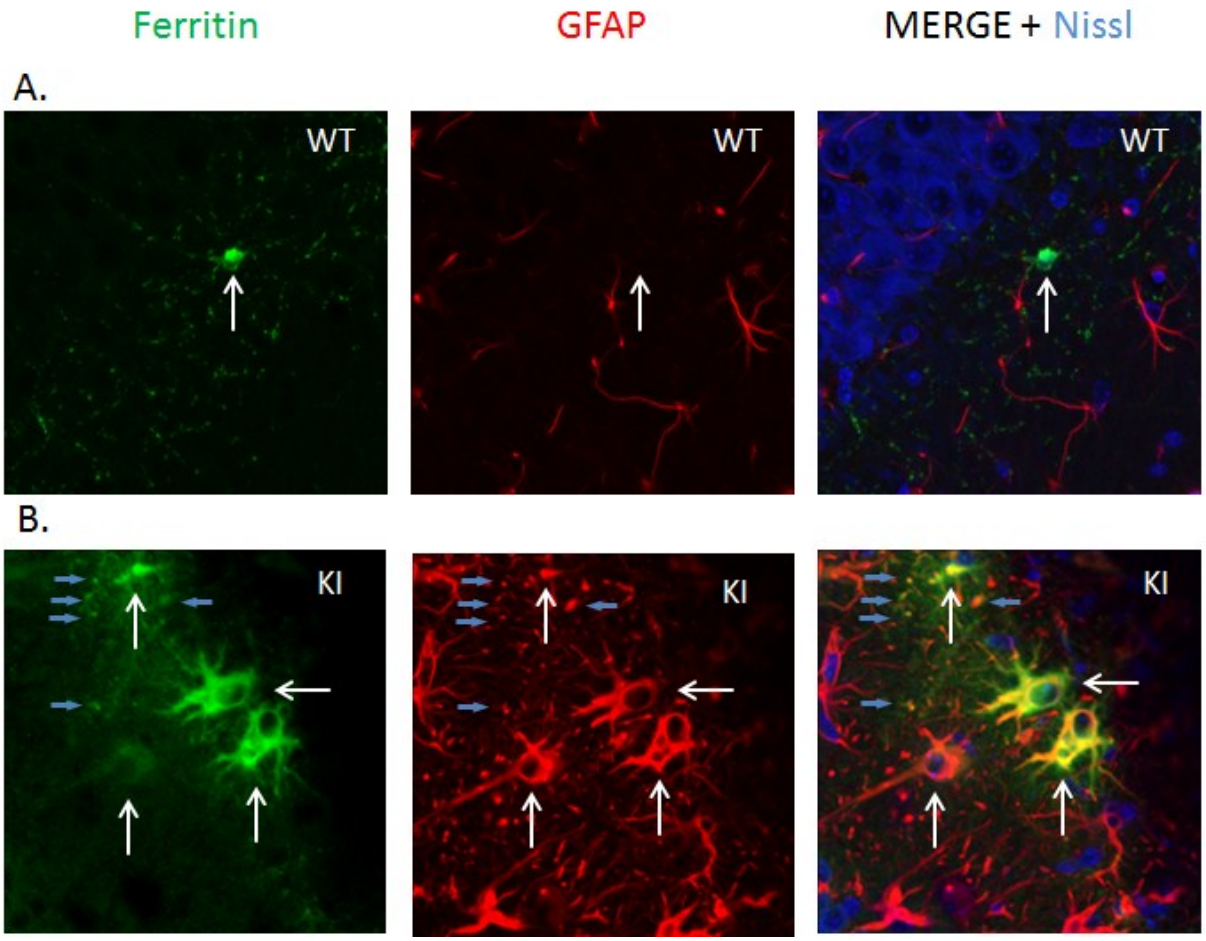

Immunofluorescence for GFAP (red) and Ferritin (green) in Str. oriens in hippocampus of wild type (WT) (A) and R236H KI *GFAP* (B) mouse. (A) WT shows immunostaining in what is likely an oligodendrocyte cell body (white arrow). (B) AxD mouse, in contrast, displays ferritin immunostaining in much of the cell body and distal fine processes in several GFAP+ astrocytes (white arrows). Some focal areas of GFAP immunoreactivity are also positive for ferritin (small blue arrows).

Figure 4. Ferroportin and ceruloplasmin immunohistochemistry in AxD patient tissue

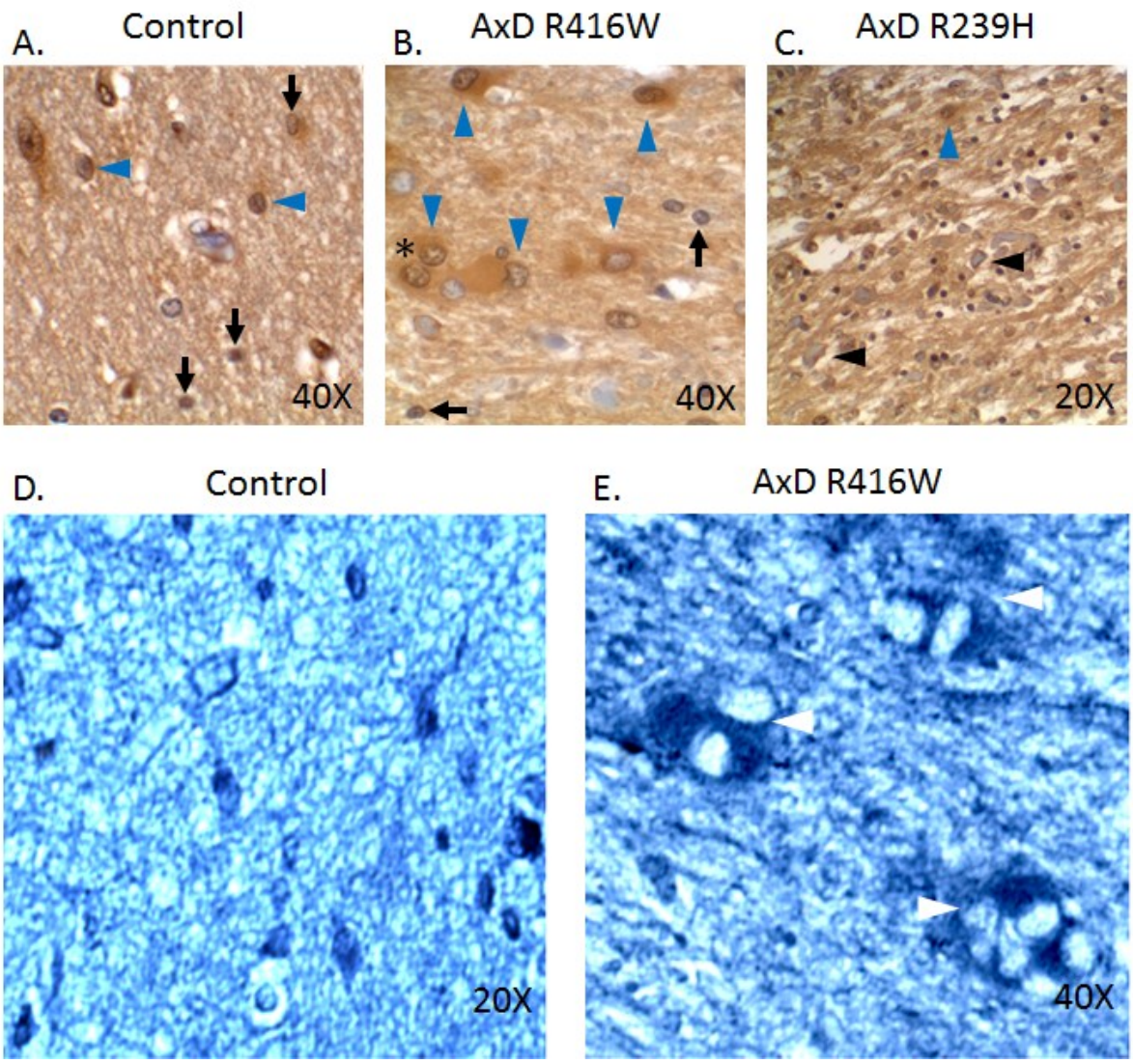

In control tissue (A), oligodendrocytes (black arrows) and astrocytes (blue arrowhead) cell bodies are positive for the iron transporter FPN1. In R416W AxD tissue (B), however there is intense accumulation of FPN1 in cell bodies of many astrocytes (B, blue arrow heads) some binucleated (B, *). Cells resembling oligodendrocytes in AxD R416W appear to express less ferroportin than do control (B, black arrows). In AxD R236H tissue (C) a high overall immunostain for ferritin is seen in greatly degraded tissue. Several Rosenthal fibers stain for FPN1 (black arrowheads), indicating the FPN1 immunoreactivity is in an

astrocyte process. Few cells can be clearly distinguished, but an astrocyte can be seen (C, blue arrowhead). In control tissue (D), Ceruloplasmin (Cp) is seen in or around many different types of cells that are difficult to identify without counter staining. In R416W patient (E), Cp accumulates in the cell bodies of multinucleated astrocytes (white arrows).

Figure 5. Iron in astrocytes may potentiate AxD pathology – a model

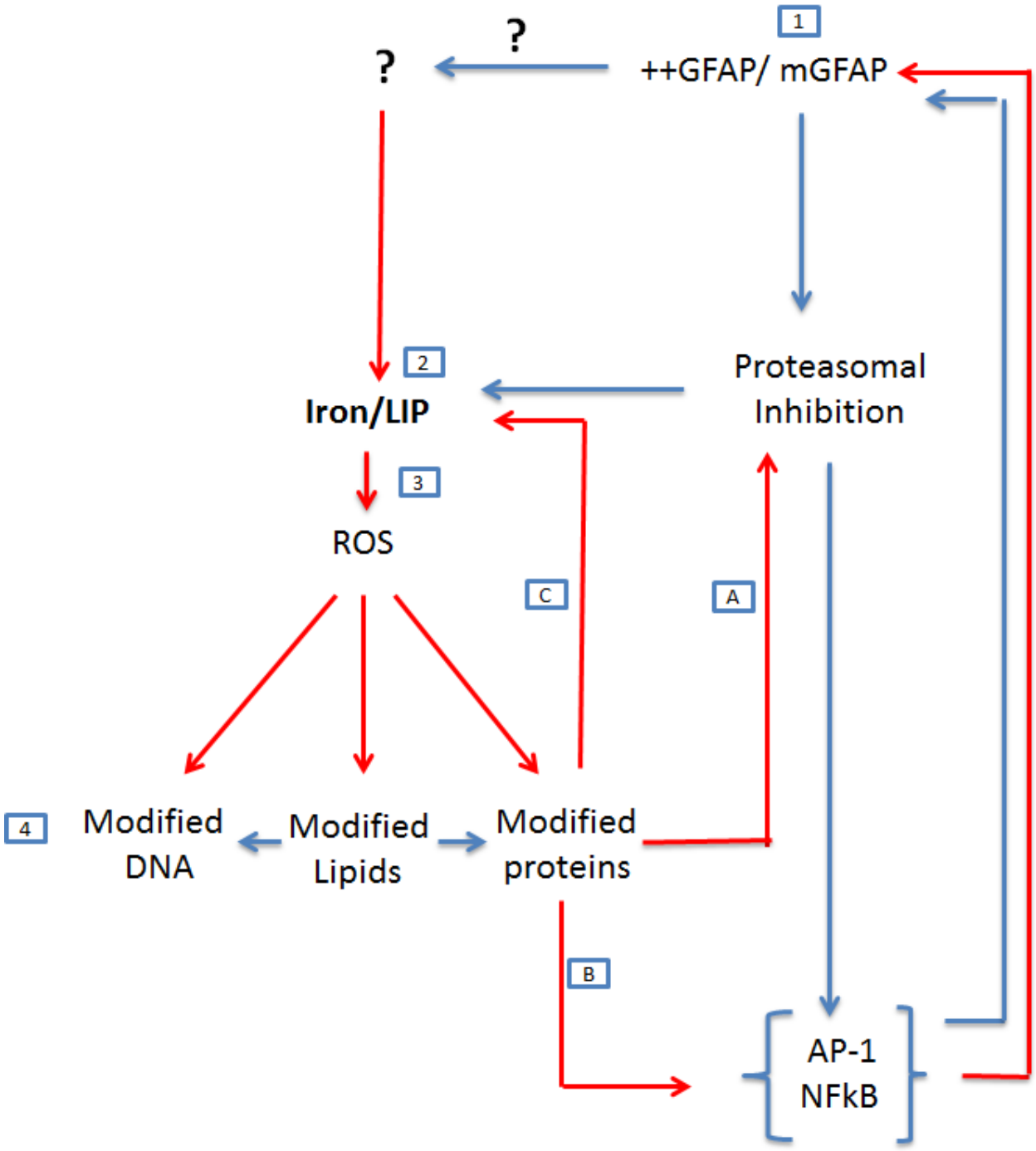

(1) Mutations in GFAP and accumulation of GFAP inhibit the proteasome, proteasomal inhibition activates the JNK/p38 stress pathway, thereby activating AP-1 transcription factors, which can increase GFAP transcription generating a positive feedback loop. This primary destructive mechanism is potentiated by the (2) increase of iron into the labile iron pool, which might occur primarily through proteasomal inhibition and/or which might additionally occur through other means such as GSH depletion, oxidative or nitrosative stress, or the interaction of GFAP with menin. (3) Iron through the Fenton reaction produces ROS. (4) ROS damages biomolecules such as DNA, lipids and proteins, and the lipid peroxidation product, HNE, additionally damages proteins. Finally three potentially destructive positive feedback loops are enacted by ROS: (A) excessively oxidatively modified proteins exacerbate proteasome inhibition, (B) iron-mediated ROS activates NFkB and AP-1 transcription factors, which increase GFAP transcription, further inhibiting the proteasome, and (C) ROS releases iron from proteins and also can directly activate iron regulatory proteins, thereby increasing the labile iron pool.

Chapter 5

Conclusion

In this thesis work I have conducted a largely immunohistological investigation of AxD patient autopsy tissue and that from model mice, focusing on factors that might provide insight into the pathological manifestations of AxD, with particular attention to those factors which might contribute to the de/dysmyelination in type I patients. In this thesis I report several novel findings in AxD patients and in Tg/KI model mice. In this final chapter, I will briefly summarize the findings and salient discussion points from each of the three data chapters. I additionally discuss relevant points with respect to Chapter 4 and oxidative stress. Finally, I briefly suggest future directions that arise from my findings.

AxD astrocytes are morphologically and ER stressed

Previous AxD research has demonstrated that astrocytes in AxD are under many forms of stress, including proteasomal inhibition imparted by mutant and excess GFAP (Chen et al., 2011; Cho and Messing, 2009; Tang et al., 2010; Tang et al., 2006). In Chapter 2, I explored other forms of stress that may affect an astrocyte's ability to function. In the hippocampus of the Tg/KI I found that profound morphological changes accompany large increases in GFAP expression in astrocytes (Chapter 1, Fig 1). These astrocytes have hypertrophied processes and some appear greatly retracted or "collapsed," especially in the str. lac.-mol. (Chapter 1, Fig 2A and B). Many have binucleated or otherwise abnormal nuclei (Chapter 2, Fig 2B).

I gained additional insight on these the morphological changes observed *in vivo* by studying primary astrocytes from AxD Tg mice. I found that in some astrocytes the expression of the hGFAP transgene has greatly impacted the localization of GFAP+ filaments. Large perinuclear rings of GFAP immunostaining can be observed (Chapter 2, Fig 3D). These GFAP inclusions are surrounded by alpha tubulin, indicating that both the intermediate filament and microtubule networks are misplaced (Chapter 2, Fig 3). In these same cells I also find that the Golgi apparatus appears disrupted (Chapter 2, Fig 4).

Finally, I examined endoplasm reticulum (ER) stress and the unfolded protein response in AxD. I report the novel finding in that there is greatly increased expression of the ER chaperone BIP/Grp78 in astrocytes in patient tissue (Chapter 2, Fig 5). I confirm this elevation of BIP expression in astrocytes in the Tg/KI mouse and found it coincides temporally and spatially with aberrant appearing astrocytes (Chapter 2, Fig 6 and 7). In addition to BIP, I found another marker for the unfolded protein response, CHOP, in a subset of astrocytes in the Tg/KI mice (Chapter 2, Fig 7).

CD44, Hyaluronan and P-ERM are Increased in AxD

In Chapter 3 I first explored levels of CD44, a protein normally found in fibrous astrocytes of the white matter and therefore presenting a possible relevance to myelin and myelination. Hagemann and colleagues had reported in results of a microarray analysis of the Tg mouse olfactory bulb that CD44 mRNA was increased +5.0 fold at 3 weeks and +14.0 fold at 4 months. I furthered this work, finding immunohistochemical staining of CD44 greatly increased in the CNS of AxD patient tissue (Chapter 3, Fig 1) and dramatically increased in the hippocampus of Tg/KI AxD mice by both western blot and immunofluorescence (Chapter 3, Fig 2). I noted that CD44 expression in the mouse coincided spatially and temporally to increases in the levels of GFAP.

CD44 is a receptor for the extracellular matrix molecule hyaluronan. I found remarkable increases in the amount of hyaluronan that was recognized by a biotinylated hyaluronan binding protein in the Tg/KI mouse. I note this finding may be particularly important in the pathogenesis of AxD because it has been found to be inhibitory to oligodendrocyte precursor cell differentiation (Back et al., 2005; Sloane et al., 2010).

Ezrin, radixin and moesin (ERM) proteins link CD44 and other cell surface proteins to the cytoskeleton. I report novel findings with respect to unusual expression of P-ERM in astrocytes in AxD patient tissue

(Chapter 3, Fig 6D and E) and the 1 year old KI mice (Chapter 3, Fig I-K), though this did not necessarily coincide with expression of CD44 (Chapter 3, Fig 7G).

Iron is a component of Rosenthal fibers and is found in astrocytes of AxD patients

In Chapter 4 I explored iron (Fe3+) and several related proteins in two AxD type I patients and one control patient. The Messing lab found immunohistochemical expression of iron and ferritin increased in astrocytes in AxD KI and Tg mice (Hagemann et al., 2006; Hagemann et al., 2005; Hagemann et al., 2012). I further explored this essential transition metal in AxD patient autopsy tissue due to its importance to oligodendrocytes and myelination (as reviewed by Todorich et al., 2009) and because of its potential to generate destructive ROS (as reviewed byValko et al., 2005). By enhanced Perls' stain we found Fe3+ in Rosenthal fibers in the white matter of one AxD patient (Chapter 4, Fig 1B, D and H) and in the brain stem of another AxD patient, found Fe3+ staining completely filling astrocyte cell bodies (Chapter 4, Fig 1I and J). In the control patient white matter, Fe3+ was only found in oligodendrocytes and blood vessels (Chapter 4, Fig 1A and C). Using tissue from the same patient and brain region where I found Fe3+ in Rosenthal fibers, I found dramatic increases in the iron storage protein ferritin throughout the cell bodies of astrocytes, but this antibody did not react to Rosenthal fiber cores (Chapter 4, Fig 2B). I note that the literature reports pathological accumulation of iron in astrocytes in the neurodegenerative disorder aceruloplasminemia (Kaneko et al., 2002b; Oide et al., 2006), caused by a loss-of-function mutations in the ferroxidase ceruloplasmin. I note the striking similarities between Rosenthal fibers and the protein inclusions in that disease which are also located in perivascular endfeet of astrocytes, some of which contain abnormal nuclei, similar to those in AxD patients (Oide et al., 2006). In both aceruloplasminemia and AxD, membraneless, electron dense protein inclusions contain Fe3+, the lipid peroxidation product HNE, and GFAP (Castellani et al., 1998; Kaneko et al., 2002b; Oide et al., 2006). The literature suggests iron-mediated oxygen radical damage plays a central role in the neurodegeneration of the disease (as reviewed by Kono, 2012).

Iron-mediated oxidative stress may be an important contributor to the pathological manifestations of AxD

Knowing these things about aceruloplasminemia, and greatly supported by research in AxD which suggests oxidative stress may play a role in its pathology (Castellani et al., 1998; Cho and Messing, 2009; Hagemann et al., 2006; Hagemann et al., 2005; Castellani, 1997), especially that which suggests this is an early event (Hagemann et al., 2005, Wang et al., 2011), I suggest that iron-mediated oxidative stress in astrocytes plays a significant role in AxD pathogenesis. In Chapter 4, I described ways that proteasomal inhibition may interfere with degradation of oxidatively modified proteins and that oxidatively modified proteins may exacerbate proteasomal inhibition. Finally, I describe three potential positive feedback loops that may be enacted by ROS: (1) excessively oxidatively modified proteins exacerbate proteasomal inhibition, (2) iron-mediated ROS activates NFkB and AP-1 transcription factors increase GFAP levels that inhibit the proteasome and (3) ROS releases iron from proteins and activates iron regulatory proteins, thereby increasing the labile iron pool.

To my knowledge, oxidative stress was first proposed as to be a factor in AxD by Rudy Castellani in 1997, before there was evidence that mutations in GFAP were the basis of most AxD cases. Castellani and his colleagues found advanced glycation end products (AGEs) in Rosenthal fibers (Castellani et al., 1997). Castellani compared Rosenthal fibers to Lewy bodies in Parkinson disease and extracellular plaques in Alzheimer disease because they both contain HNE, AGEs, and the heat shock proteins alpha B-crystallin and HSP27 (Castellani et al., 1998). Castellani points out that alpha B-crystallin is major component of Rosenthal fibers (Goldman and Corbin, 1988; Iwaki et al., 1989) and has a high lysine content, making it susceptible to AGE and HNE modifications. He suggests that these post-translational modifications to proteins, coupled with oxidative stress, may be the common element in inclusion formation between Rosenthal fibers, Lewey bodies and plaques. In this work I add iron to the list of commonalities between Rosenthal fibers and these inclusions (Chapter 4, Fig 1B, D, G, H) (Castellani et al., 1998; Castellani et al.,

2000; Head et al., 1993; Hirsch et al., 1991; LeVine, 1997; Renkawek et al., 1993; Sayre et al., 1997; Shinohara et al., 1993; Tomokane et al., 1991; Yoritaka et al., 1996). The findings I present in Chapter 4 support Castellani's suggestion that oxidative stress and post-translational modifications play a role in in Rosenthal fiber formation (Castellani et al., 1997). However, as is thought to occur in other neurodegenerative diseases (Halliwell, 2006), I suggest proteasomal inhibition caused by mutations in GFAP or excess GFAP play a causative role in the accumulation of these post-translationally modified proteins.

Future Directions

Iron

Iron accumulation in astrocytes – is it a universal feature of AxD?

The most potentially important finding of the work I have presented in my thesis is the determination of Fe3+ in Rosenthal fibers and the pathological accumulation of iron and ferritin in astrocytes of AxD patients. If this iron accumulation in astrocytes is found a universal feature in all patients, than it positions iron-generated oxidative stress within astrocytes and suggests many pathological consequences for astrocytes and the cells surrounding them. Critically, antioxidant and chelation therapies may be plausible treatments where none currently exist. Less optimistically, the iron in AxD astrocyte that we found might represent an end stage and untreatable event or and furthermore offer little insight on early disease mechanisms.

In any case, an extremely important future direction for AxD research is to conduct a wide(r)-scaled histochemical characterization of Fe3+ and ferritin in, at minimum, both infant/type I and adult/type II patients, and age matched controls.

If this analysis is conducted it would be important to obtain sections from common or similar brain region from each patient analyzed, if available. Based on the results of my initial experiments presented

in Chapter 4, I would suggest at minimum looking at three sections. First, I would examine a cortical section that includes subcortical WM. This will be important to assess iron in astrocytes and RFs in this severely affected region in type I patients. Additionally, results from the experiments presented here suggest this is a fruitful location with respect to iron pathology. Second, and along these same lines, I would use sections from the brain stem, because this is a region that shows pathology by MRI, especially in the adult (Prust et al., 2011) and children have clinical presentations such as swallowing disorders that originate from damage to this region. Further, in AxD there have been reports of lymphocyte invasion in the brain stem (Rankin et al., 1977; Russo et al., 1976; Soffer and Horoupian, 1979; Towfighi et al., 1983). It is possible that the massive accumulation of iron we saw in the R416W patient may have stemmed from an event separate from mutations in GFAP. In any case, analyzing a wider sample of patient brain stem tissue will help us understand this unusual accumulation of iron. A third section I would recommend is one from the substantia nigra or another high iron area in order to understand what occurs to AxD astrocytes in a setting where there is "normally" high levels of iron. One report suggests that iron in the substantia nigra increases 10-fold between the first year of life and the age of 40 (Zecca et al., 2001).

What will the result of this experiment yield?

The results of this study will tell us if iron accumulation in astrocytes is a universal feature of AxD. If this is the case it suggests one of two things. First, that pathological accumulation of GFAP mediates subsequent iron accumulation, perhaps through the effects of proteasomal inhibition on IRP2 (Li et al., 2012). This conclusion may be supported by the iron accumulation in astrocytes that is observed in both the AxD Tg and KI mice, presumably in the absence of a genetic or environmental trigger. Second, if iron accumulation is identified as a common pathological feature of all AxD patients, it could also suggest that an iron trigger may be necessary for the phenotypic expression of AxD.

If iron accumulation in astrocytes is not a feature of all astrocytes and Rosenthal fibers in AxD, then it suggests that GFAP accumulation alone is not sufficient to cause an accumulation of iron in AxD astrocytes. Based upon the composition of the groups of patients that do and do not have iron astrocytic accumulation it might suggest several features of iron accumulation. For example, if all infant onset patients have iron accumulation but adult patients do not it suggests that iron is either a result of the severe infant onset phenotype or perhaps that iron is the trigger driving such a phenotype.

Iron triggering factors

Questions have been raised regarding the sufficiency of GFAP mutations alone to bring about the phenotypic expression of AxD. A central argument towards this end is the presence of individuals who carry mutations in GFAP, yet are asymptomatic and who have been identified in studies of three familial AxD cases (Messing et al., 2012b). If environmental or genetic triggers do play a role in the development of AxD, iron could be such a candidate. Identifying potential genetic or environmental triggering factors or those that predispose individuals to a more severe phenotype may give us insight on disease pathogenesis and suggest preventive or therapeutic strategies.

Potential genetic triggering factors might include those that impact iron status. For example, relatively common occurring mutations on genes that encode hemochromatosis (Hfe), transferrin and ceruloplasmin are known. These mutations often leave individuals asymptomatic (Bulaj et al., 2000; Phatak et al., 2002), however they might trigger an AxD phenotype. Pre-existing iron pathology has long been suggested to be a contributing factor to Alzheimer disease (Goodman, 1953) and a recent studies of 160 Alzheimer disease patients and 79 healthy elderly controls analyzed which several common point in genes encoding Hfe and transferrin in relation to developing Alzheimer disease and it was determined that mutations in Hfe along with associated liver iron abnormalities increased the probability of developing this disorder (Giambattistelli et al., 2012). Genotyping DNA from AxD patients for such

common mutations could be likewise fruitful in this respect. Environmental factors such as head injuries, hypoxia ischemia, and infection have been suspected of playing a triggering role in AxD due to their ability to increase GFAP in astrocytes; however, if we consider iron as a triggering factor, we might look with a different perspective at these same events.

Therapeutics and Diagnostics

If iron is determined to be a factor in AxD it presents, not only the treatment potential, in the form antioxidants and chelation therapies, it also presents an opportunity to use several MRI techniques in diagnosis and potentially, research. This could yield valuable information about the progression of the disease (Bartzokis and Tishler, 2000; Schenck and Zimmerman, 2004).

Iron Challenge of Mice – can we induce AxD pathology?

Another future direction that may stem from this work, and might be further suggested by work described above is iron challenging AxD KI and Tg mice. As mentioned above, if iron pathology in astrocytes is determined to be common to all AxD patients, it might suggest that iron is downstream from GFAP accumulation. This is supported by data from the Tg and KI mice, that both show iron in astrocytes, yet don't have spontaneous seizures and do not de/dysmyelinate despite carrying the GFAP mutation associated with the most severe AxD phenotype in patients(Hagemann et al., 2006; Hagemann et al., 2005; Hagemann et al., 2012). While there are manifold reasons that might contribute to the lack of pathology in mice, this work might suggest that species differences in the ability of mice to favorable store iron in a non-reactive form might allow them to remain asymptomatic. In order to test these questions I propose iron challenging mice in an effort to bring about AxD pathology. Two ways this hypothesis might be tested are to first iron challenge the Tg and the KI mice with an excessively high-iron diet and/or iron injections at a level that is just tolerated by WT mice. Second, by crossing the KI or the Tg mouse with the H-Ferritin+/- mouse (Thompson et al., 2003). While the H-ferritin null mouse is embryotic lethal this mouse develops normally but shows half the normal H-Ferritin of WT mice.

Additionally, this mouse shows signs of oxidative stress. The increase in iron in AxD mice, coupled with the decrease in ferritin of these H-Ferritin heterozygous mice, may be sufficient to induce AxD pathology. Other null and heterozygous mice, such as the LCN -/- mouse, might also be crossed with AxD mice to determine effects on decreases in iron regulatory proteins and accumulation of GFAP.

Chapter 6

Materials and Methods

Mice

The mouse lines have been previous described: (1) a transgenic line (Tg 73-7) in which the normal human *GFAP* is expressed in several copies (Messing et al., 1998); (2) a knock-in line (KI – K146B) in which one of the *GFAP* genes bears an R236H mutation (the mouse homologue of one of the most common human mutation sites) (Hagemann et al., 2006); and (3) a mouse that contains both several copies of the human *GFAP* and the mutated mouse *GFAP*, derived from the mating Tg 73-7 and KI R236H mice (Hagemann et al., 2006). The Tg line was initially generated in an FVB background, but the mice were crossed into a B6 background over 5 generations before they were used for these experiments. The KI line was initially generated in mice with a B6 background. All animal use was performed under the guidelines of the Columbia University Institutional Animal Care and Use Committee.

Human Tissue

Tissue was obtained postmortem from cerebral hemispheric white matter of control subjects or AxD patients and stored at -80 C. For immunohistochemistry the tissue was fixed in formalin then embedded in paraffin. Immunostaining and Western blot analyses were carried out with fixed and frozen (respectively) CNS tissues from Alexander patients with R79C, R239H and two patients with R416W mutations. All AxD cases were diagnosed based on histopathological examination and confirmed by the molecular genetic analysis for GFAP mutation. All were children who manifested the disease as infants and expired within the first decade (10 years, 29 months, and 7 years). All showed typical type I pathology for AxD, including severe leukodystrophy and numerous Rosenthal fibers. All post-mortem intervals were less than 10 hours. Control patient frozen central nervous system tissue for Western blot analysis were from two children, one with no neurological disease, 20 months of age, 18 hour postmortem interval and the other with Werdnig-Hoffman disease (non-AxD, non-leukodystrophy neurological disease without Rosenthal fibers), 22 months, 6 hr postmortem interval. Control patients

for immunohistochemistry were an 8 month old male with congenital heart disease and the above mentioned Werdnig-Hoffman disease patient.

Histology and immunohistochemistry

Mice were anesthetized with ketamine-xylazine before intracardiac perfusion with 4% paraformaldehyde in PBS. Brains were removed and kept in the fixative for 12 - 16 h (4^0 C). 40 μm coronal sections were prepared with a vibratome (Leica VT1000S) and stored in cryoprotectant solution at -20^0 C before usage.

Primary antibodies were used against: glial fibrillary acidic protein (GFAP): monoclonal (1:1000, G3893, Sigma-Aldrich, St. Louis, MO), rabbit polyclonal (1:1000, Z 0334, Dako, Carpinteria, CA), and chicken polyclonal (1:500, PCK-591P, Covance, Berkeley, CA); Ferritin: Rabbit polyclonal (1:400, Sigma-Aldrich, St. Louis, Mo.); Ferroportin (MTPI): Rabbit polyclonal (1:75 48 hours, Alpha Diagnostics) ; Ceruloplasmin: sheep polyclome (1:750); CD44: rat monoclonal (1:150, # 14-0441, eBioscience, Inc. SanDiego, CA) or a mouse monoclonal (1:500, #M7082, clone 1485, DAKO, on human sections performed by the Departmental Immunocytochemistry laboratory); BIP: goat polyclonal (1:100 Santa Cruz); CHOP: rabbit (1:100 Abcam); biotinylated hyaluronan binding protein (1:100 Novus); filamentous actin: rhodamine-conjugated Phalloidin (1:40 with secondary antibodies). Phospho-Ezrin, Radixin, Moesin (P-ERM) rabbit polyclonal (1:400, #3149, Cell Signaling Technologies); Total Ezrin, Radixin, Moesin (P-ERM) rabbit polyclonal (1:400, #3142, Cell Signaling Technologies); Moesin, rabbit polyclonal (1:400, #3150, Cell Signaling Technologies); Radixin, rabbit polyclonal (1:400, #2636, Cell Signaling Technologies). Generous gifts of Y 1/2 (1:200 Millipore) and rabbit GM-130 (1:200 BD) antibodies were provided by Dr. Richard Vallee (Columbia University) and goat anti-BIP/Grp78 (1:150, Santa Cruz) by Dr. Phyllis Faust (Columbia University). Secondary antibodies included: anti-mouse Alexa Fluor 488, 594, and 633; anti-chicken Alexa Fluor 488, 594, 633; anti-rabbit Alexa Fluor 594; all from goat or donkey (1:300 or 1:600).

Double and triple-immunofluorescence: After blocking with 10% normal goat (or donkey) serum (30 min, at room temperature (RT)), free-floating sections were incubated in a mixture of primary antibodies raised in different species for overnight (4^0 C). For visualization, Alexa Fluor -conjugated secondary antibodies were applied for 1 h at RT. Fluorescent Nissl reagent (NeuroTrace 640/660 deep-red, 1:150, Molecular Probes) was used (30 min, RT) for visualization of general histological structure in double immunostaining. DAPI (Vector Lab) was used with triple immunostaining. Blocking serum, primary, secondary antibodies, and fluorescent Nissl reagent were applied in 0.2 % Triton X-100 in PBS. Sections for fluorescent microscopy were mounted on slides in Vectashield (Vector Lab). To control the specificity of immunostaining, primary antibodies were omitted and substituted with appropriate normal serum. Slides were viewed using a Nikon A1R MP confocal microscope. 3D reconstructions were generated from stacks of images with confocal microscope software NIS-Elements. Image analysis was performed with the ImageJ 1.32 (NIH, USA).

Hyaluronidase from bovine testes (Sigma) was prepared in 20 mM sodium phosphate buffer pH 7.0, with 77 mM NaCl, and .1 mg/ml BSA. Tissue slices were treated with 100 □M hyaluronidase for 3 hours at 37C. Tissue was then rinsed, blocked in BSA and stained 1:100 with biotinylated hyaluronan binding protein (Novus). A fluorescent probe conjugated to streptavidin was used to visualize hyaluronan.

Human sections, 5µm thick, followed the immunostaining protocol described above with the addition of antigen retrieval before blocking. After deparaffinization of sections the tissues were antigen retrieved with 0.6% Sodium Citrate buffer pH 6.0 for 30 minutes in a rice cooker, allowed to return to room temperature then rinsed and placed in a solution of 0.3% H202 for 10 minutes followed by rinsing. Secondaries were species-specific biotinylated antibodies (Vector Laboratories, Burlingame CA). The avidin-biotin immunoperoxidase method with 3,3'-diaminobenzidine tetrahydrochloride was used to

visualize bound primaries. Control sections, immunostained by the procedure, but with the omission of primary antibodies.

Modified Perls' Stain for Fe3+ iron: After sections (5.0 μm) were deparaffinized in xylene and rehydrated in graded ethanol, sections were then immersed in a solution of 0.03% H2O2 for 30 min., then incubated in 2% potassium ferrocyanide in aqueous hydrochloric acid (2%) for 24 hrs. and subsequently incubated in 0.75mg/ml 3,3'-diaminobenzidine for 5-10 min (modified from Nguyen-Legros et al., 1980b).

BIP/GFAP Positive Cell Counts in Hippocampus

Confocal (Nikon specifications) stack images of double immunostained hippocampal sections for BIP and GFAP (counterstained with Nissl) were used to determine the total number of BIP positive cells that were also GFAP positive in the str. lac. and str. rad. of the CA1 subfields in 5 representative non-consecutive sections throughout the dorsal hippocampus. BIP positive and GFAP positive cells were intensely labeled, which made them easy to identify with equal chance of being counted and only cells with clearly outlined nuclei (stained with Nissl or DAPI) were taken into consideration. The number of BiIP positive and GFAP positive cells was determined blindly by a single observer; therefore, counting bias was kept to a minimum.

CD44 and Hyaluronan Binding Protein Optical Density (OD) Measurement

Double immunostained hippocampal slices for CD44 and HBP (counterstained with Nissl or DAPI) were imaged using confocal scanning microscopy (Nikon) at constant settings, recording layers at every 0.5 μm (1024 x 1024 pixel resolution, observed area 644 x 644 μm) and parallel confocal planes were superimposed. Using computer-assisted imaging analysis (Image J 1.32j, NIH, USA), I analyzed the expression and density of CD44 and HBP labeling respectively at 2 and 4 weeks of age in both Tg/KI and WT mice by measuring their optical density (OD) as described previously . Briefly, the staining was

observed throughout the thickness of the section (40 µm). No differences were observed in CD44 and HBP immunoreactivity respectively throughout the thickness of the section in Tg/KI and WT animals; hence the changes in OD were used as measure of increased CD44 and HBP expression. The OD was calculated from a relative scale of intensity ranging from 0 to 255, with readout of 0 corresponding to the area with very low CD44 or HBP expression and 255 corresponding to the densest area of labeling. The calibration density was kept constant for measuring all sections to avoid experimental variances. CD44 and HBP densities of the str. mol., str. lac. and str. rad. were measured independently and a single measurement was obtained from every sub-region in each hemisphere. Measurements of mean density were taken and averaged from each of the three hippocampal layers, as well as the total hippocampus, in both the left and the right hemisphere of each slice. The results are shown as CD44 or HBP optical density (IOD/pixel).

Western blots

The hippocampus was dissected from mice and tissue was either frozen on dry ice and then stored at -80C until use or lysed directly in ice-cold buffer (Invitrogen product # fnn0011) to which a 10% SDS stock had been added to make a 2% SDS solution. Lysis buffer was supplemented with protease inhibitor cocktail tablets and phosphatase inhibitors (HALT, Thermo). Tissue was digested for 45 minutes on ice with regular mechanical disruption with a large-orifice pipette tip, sonicated twice for 3 seconds and spun at 14,000 RPM for 10 minutes. Protein determination of the supernatant was determined with Pierce 660nm reagent (Thermo) supplemented with Ionic compatibility reagent (Thermo) as per manufacturer's instructions. Equal amounts of protein were added to loading buffer and, where noted, reducing agent as per manufacturer's instructions (Invitrogen). The proteins were subjected to SDS-PAGE using NuPage 4-12% Tris-Bis gels and transferred to nitrocellulose membranes. The transfer membrane was blocked with 5% skimmed milk in TBS (50 mM Tris-HCl, pH 7.5, 150 mM NaCl) for one hour at room temperature and then incubated overnight at 4^{o}C in 5% skim milk in 0.1% Tween 20 in TBS

(TBS-T buffer) the following primary antibodies used rat anti-CD44 (IM7) for mouse 1:4000 anti-rabbit GFAP anti-GAPDH (1:3000 Millipore) Blots were then washed 3x in TBST and then incubated in blocking solution with, for patient tissue westerns, horseradish-peroxidase conjugated rabbit or mouse secondary (1:1000) Pierce Biotechnology, Rockford, IL) using SuperSignal West Dura Extended Duration substrate (Pierce) or Licor fluorescent probes for mouse tissue and cell culture.

Cell culture media: Unless otherwise stated, all media reagents were purchased from Sigma (St. Louis, MO). DMEM (Invitrogen, Carlsbad, CA) was supplemented with 10% FBS (Invitrogen, Carlsbad, CA), and 100 μg/ml penicillin/streptomycin (Invitrogen).

Cell Culture: Mixed glia cultures were generated in a modified method of McCarthy and De Vellis (McCarthy and de Vellis, 1980). The forebrains of P0- P2 mouse pups were removed, stripped of meninges, and mechanically and enzymatically dissected in a modification of a procedure described elsewhere (Gensert and Goldman, 2001). Briefly, tissue was shredded using forceps and digested in a solution containing 0.125% trypsin (Invitrogen), 20U/ml papain (Roche Applied Science, Indianapolis, IN), and 285U/ml DNAse (Sigma, St. Louis, MO) at 37^{o}C for 30 min. in an incubator (0.5% CO_2). Undigested tissue was transferred to a falcon tube with 5 ml. of culture media and triturated with a 5 ml pipet. The single cell suspension was centrifuged at 800rpm for 10 minutes and the cell pellet resuspended in cell culture media and plated at one brain per 25cm^2 flask. Media were changed every 2-3 days. When cells had reached 80% confluence in 7-10 days, cells were shaken at 160 RPM for 18 hours followed by and one hour at 190 RPM and then treated for 1-4 hours with 50 μm leucine methyl ester to selectively kill microglia and rinsed twice with DMEM warmed to 37 deg. Cells were allowed to recover overnight in media before sub-plating for immunostaining on coverslips in 24 well plates. Briefly, media was aspirated, 3ml of 0.03% Trypsin was added and cells were incubated at 36^{o}C for 2-5 min. When cells had lifted, trypsin was neutralized with an equal amount of 10% horse serum in DMEM and

cells suspended in solution were then collected, and centrifuged at 1000xg for 10 min and replated at a density of $4x10^4$ cells/cm^2. All animal experiments were performed under the guidelines of the Columbia University Institutional Animal Care and Use Committee.

Immunofluorescence Staining of Primary Astrocytes: Cultured cells grown on in 24 well dishes on coverslips were rinsed twice with PBS and fixed in a 4% paraformaldehyde (PFA) solution or with ice-cold methanol for 7 minutes for 20 min at RT stored in PBS at 4°C until use. Cells were blocked with 10% donkey serum (Sigma) with 0.3% Triton-X 100 (Sigma) for one hour at room temperature and all primary antibodies (see above) were applied overnight at 4°C, followed by washes in PBS (15min x 2) and secondary antibodies at one hour at room temperature in the dark

Statistical Analysis

Data are expressed as mean ± SEM. Two-way ANOVA for multiple groups, with Tukey test, and Pearson correlation coefficient were used as appropriate. $p < 0.05$ was considered significant. Quantification was performed using Image J (NIH) and statistics were performed in GraphPad.

References

Abbott, N.J., Ronnback, L., and Hansson, E. (2006). Astrocyte-endothelial interactions at the blood-brain barrier. Nature reviews Neuroscience *7*, 41-53.

Abboud, S., and Haile, D.J. (2000). A novel mammalian iron-regulated protein involved in intracellular iron metabolism. The Journal of biological chemistry *275*, 19906-19912.

Adams, G.A., and Rose, J.K. (1985). Incorporation of a charged amino acid into the membrane-spanning domain blocks cell surface transport but not membrane anchoring of a viral glycoprotein. Molecular and cellular biology *5*, 1442-1448.

Agren, U.M., Tammi, R.H., and Tammi, M.I. (1997). Reactive oxygen species contribute to epidermal hyaluronan catabolism in human skin organ culture. Free radical biology & medicine *23*, 996-1001.

Ainger, K., Avossa, D., Morgan, F., Hill, S.J., Barry, C., Barbarese, E., and Carson, J.H. (1993). Transport and localization of exogenous myelin basic protein mRNA microinjected into oligodendrocytes. The Journal of cell biology *123*, 431-441.

Alexander, W.S. (1949). Progressive fibrinoid degeneration of fibrillary astrocytes associated with mental retardation in a hydrocephalic infant. Brain : a journal of neurology *72*, 373-381, 373 pl.

Alldinger, S., Fonfara, S., Kremmer, E., and Baumgartner, W. (2000). Up-regulation of the hyaluronate receptor CD44 in canine distemper demyelinated plaques. Acta neuropathologica *99*, 138-146.

Anderova, M., Kubinova, S., Mazel, T., Chvatal, A., Eliasson, C., Pekny, M., and Sykova, E. (2001). Effect of elevated K(+), hypotonic stress, and cortical spreading depression on astrocyte swelling in GFAP-deficient mice. Glia *35*, 189-203.

Arai, N. (1995). Grumose or foamy spheroid bodies involving astrocytes in the human brain. Neuropathology and applied neurobiology *21*, 238-245.

Arosio, P., and Levi, S. (2002). Ferritin, iron homeostasis, and oxidative damage. Free radical biology & medicine *33*, 457-463.

Arrigo, A.P. (1999). Gene expression and the thiol redox state. Free radical biology & medicine *27*, 936-944.

Aruffo, A., Stamenkovic, I., Melnick, M., Underhill, C.B., and Seed, B. (1990). CD44 is the principal cell surface receptor for hyaluronate. Cell *61*, 1303-1313.

Back, S.A., Tuohy, T.M., Chen, H., Wallingford, N., Craig, A., Struve, J., Luo, N.L., Banine, F., Liu, Y., Chang, A.*, et al.* (2005). Hyaluronan accumulates in demyelinated lesions and inhibits oligodendrocyte progenitor maturation. Nature medicine *11*, 966-972.

Baghbaderani, B.A., Behie, L.A., Mukhida, K., Hong, M., and Mendez, I. (2011). New bioengineering insights into human neural precursor cell expansion in culture. Biotechnology progress *27*, 776-787.

Barbouti, A., Doulias, P.T., Zhu, B.Z., Frei, B., and Galaris, D. (2001). Intracellular iron, but not copper, plays a critical role in hydrogen peroxide-induced DNA damage. Free radical biology & medicine *31*, 490-498.

Barkovich, A.J., and Messing, A. (2006). Alexander disease: not just a leukodystrophy anymore. Neurology *66*, 468-469.

Bartolazzi, A., Nocks, A., Aruffo, A., Spring, F., and Stamenkovic, I. (1996). Glycosylation of CD44 is implicated in CD44-mediated cell adhesion to hyaluronan. The Journal of cell biology *132*, 1199-1208.

Bartzokis, G., and Tishler, T.A. (2000). MRI evaluation of basal ganglia ferritin iron and neurotoxicity in Alzheimer's and Huntingon's disease. Cellular and molecular biology *46*, 821-833.

Baumann, N., and Pham-Dinh, D. (2001). Biology of oligodendrocyte and myelin in the mammalian central nervous system. Physiological reviews *81*, 871-927.

Beard, J.L. (2001). Iron biology in immune function, muscle metabolism and neuronal functioning. The Journal of nutrition *131*, 568S-579S; discussion 580S.

Beard, J.L., Wiesinger, J.A., and Connor, J.R. (2003). Pre- and postweaning iron deficiency alters myelination in Sprague-Dawley rats. Developmental neuroscience *25*, 308-315.

Becker, L., and Teixeira, F. (1988). Alexander's disease. In The Biochemical Pathology of Astrocytes, M. Norenberg, L. Hertz, and A. Shousboe, eds. (Allen R Liss Inc), pp. 179-190.

Benavides, A., Pastor, D., Santos, P., Tranque, P., and Calvo, S. (2005). CHOP plays a pivotal role in the astrocyte death induced by oxygen and glucose deprivation. Glia *52*, 261-275.

Benkovic, S.A., and Connor, J.R. (1993). Ferritin, transferrin, and iron in selected regions of the adult and aged rat brain. The Journal of comparative neurology *338*, 97-113.

Bennett, K.L., Modrell, B., Greenfield, B., Bartolazzi, A., Stamenkovic, I., Peach, R., Jackson, D.G., Spring, F., and Aruffo, A. (1995). Regulation of CD44 binding to hyaluronan by glycosylation of variably spliced exons. The Journal of cell biology *131*, 1623-1633.

Biemond, P., van Eijk, H.G., Swaak, A.J., and Koster, J.F. (1984). Iron mobilization from ferritin by superoxide derived from stimulated polymorphonuclear leukocytes. Possible mechanism in inflammation diseases. The Journal of clinical investigation *73*, 1576-1579.

Bignami, A., and Asher, R. (1992). Some observations on the localization of hyaluronic acid in adult, newborn and embryonal rat brain. International journal of developmental neuroscience : the official journal of the International Society for Developmental Neuroscience *10*, 45-57.

Bignami, A., and Dahl, D. (1985). Glial filaments in brain differentiation and the transient expression of neurofilaments in Purkinje cell development. Annals of the New York Academy of Sciences *455*, 563-574.

Bishop, G.M., and Robinson, S.R. (2001). Quantitative analysis of cell death and ferritin expression in response to cortical iron: implications for hypoxia-ischemia and stroke. Brain research *907*, 175-187.

Bongcam-Rudloff, E., Nister, M., Betsholtz, C., Wang, J.L., Stenman, G., Huebner, K., Croce, C.M., and Westermark, B. (1991). Human glial fibrillary acidic protein: complementary DNA cloning, chromosome localization, and messenger RNA expression in human glioma cell lines of various phenotypes. Cancer research *51*, 1553-1560.

Borland, G., Ross, J.A., and Guy, K. (1998). Forms and functions of CD44. Immunology *93*, 139-148.

Borrett, D., and Becker, L.E. (1985). Alexander's disease. A disease of astrocytes. Brain : a journal of neurology *108 (Pt 2)*, 367-385.

Bourguignon, L.Y., Gilad, E., Peyrollier, K., Brightman, A., and Swanson, R.A. (2007). Hyaluronan-CD44 interaction stimulates Rac1 signaling and PKN gamma kinase activation leading to cytoskeleton function and cell migration in astrocytes. Journal of neurochemistry *101*, 1002-1017.

Bradbury, M.W. (1997). Transport of iron in the blood-brain-cerebrospinal fluid system. Journal of neurochemistry *69*, 443-454.

Brambilla, R., Bracchi-Ricard, V., Hu, W.H., Frydel, B., Bramwell, A., Karmally, S., Green, E.J., and Bethea, J.R. (2005). Inhibition of astroglial nuclear factor kappaB reduces inflammation and improves functional recovery after spinal cord injury. The Journal of experimental medicine *202*, 145-156.

Brenner, M. (1994). Structure and transcriptional regulation of the GFAP gene. Brain pathology *4*, 245-257.

Brenner, M., Goldman, J.E., Quinlan, R., and Messing, A. (2008). Alexander Disease: A Genetic Disorder. In Astrocytes in Pathophysiology of the Nervous System, V. Parpura, and P.G. Haydon, eds. (Springer Science and Business Media).

Brenner, M., Johnson, A.B., Boespflug-Tanguy, O., Rodriguez, D., Goldman, J.E., and Messing, A. (2001). Mutations in GFAP, encoding glial fibrillary acidic protein, are associated with Alexander disease. Nature genetics *27*, 117-120.

Brenner, M., Lampel, K., Nakatani, Y., Mill, J., Banner, C., Mearow, K., Dohadwala, M., Lipsky, R., and Freese, E. (1990). Characterization of human cDNA and genomic clones for glial fibrillary acidic protein. Brain research Molecular brain research *7*, 277-286.

Brightman, M.W., and Reese, T.S. (1969). Junctions between intimately apposed cell membranes in the vertebrate brain. The Journal of cell biology *40*, 648-677.

Brown, K.L., Birkenhead, D., Lai, J.C., Li, L., Li, R., and Johnson, P. (2005). Regulation of hyaluronan binding by F-actin and colocalization of CD44 and phosphorylated ezrin/radixin/moesin (ERM) proteins in myeloid cells. Experimental cell research *303*, 400-414.

Buffo, A., Rite, I., Tripathi, P., Lepier, A., Colak, D., Horn, A.P., Mori, T., and Gotz, M. (2008). Origin and progeny of reactive gliosis: A source of multipotent cells in the injured brain. Proceedings of the National Academy of Sciences of the United States of America *105*, 3581-3586.

Buffo, A., Rolando, C., and Ceruti, S. (2010). Astrocytes in the damaged brain: molecular and cellular insights into their reactive response and healing potential. Biochemical pharmacology *79*, 77-89.

Bulaj, Z.J., Phillips, J.D., Ajioka, R.S., Franklin, M.R., Griffen, L.M., Guinee, D.J., Edwards, C.Q., and Kushner, J.P. (2000). Hemochromatosis genes and other factors contributing to the pathogenesis of porphyria cutanea tarda. Blood *95*, 1565-1571.

Buniatian, G., Gebhardt, R., Schrenk, D., and Hamprecht, B. (1996a). Colocalization of three types of intermediate filament proteins in perisinusoidal stellate cells: glial fibrillary acidic protein as a new cellular marker. European journal of cell biology *70*, 23-32.

Buniatian, G., Hamprecht, B., and Gebhardt, R. (1996b). Glial fibrillary acidic protein as a marker of perisinusoidal stellate cells that can distinguish between the normal and myofibroblast-like phenotypes. Biology of the cell / under the auspices of the European Cell Biology Organization *87*, 65-73.

Burdo, J.R., Martin, J., Menzies, S.L., Dolan, K.G., Romano, M.A., Fletcher, R.J., Garrick, M.D., Garrick, L.M., and Connor, J.R. (1999). Cellular distribution of iron in the brain of the Belgrade rat. Neuroscience *93*, 1189-1196.

Burdo, J.R., Menzies, S.L., Simpson, I.A., Garrick, L.M., Garrick, M.D., Dolan, K.G., Haile, D.J., Beard, J.L., and Connor, J.R. (2001). Distribution of divalent metal transporter 1 and metal transport protein 1 in the normal and Belgrade rat. Journal of neuroscience research *66*, 1198-1207.

Buser, J.R., Maire, J., Riddle, A., Gong, X., Nguyen, T., Nelson, K., Luo, N.L., Ren, J., Struve, J., Sherman, L.S*., et al.* (2012). Arrested preoligodendrocyte maturation contributes to myelination failure in premature infants. Annals of neurology *71*, 93-109.

Bush, T.G., Puvanachandra, N., Horner, C.H., Polito, A., Ostenfeld, T., Svendsen, C.N., Mucke, L., Johnson, M.H., and Sofroniew, M.V. (1999). Leukocyte infiltration, neuronal degeneration, and neurite outgrowth after ablation of scar-forming, reactive astrocytes in adult transgenic mice. Neuron *23*, 297-308.

Bushong, E.A., Martone, M.E., and Ellisman, M.H. (2004). Maturation of astrocyte morphology and the establishment of astrocyte domains during postnatal hippocampal development. International journal of developmental neuroscience : the official journal of the International Society for Developmental Neuroscience *22*, 73-86.

Caceres-Marzal, C., Vaquerizo, J., Galan, E., and Fernandez, S. (2006). Early mitochondrial dysfunction in an infant with Alexander disease. Pediatric neurology *35*, 293-296.

Cai, N., Kurachi, M., Shibasaki, K., Okano-Uchida, T., and Ishizaki, Y. (2012). CD44-positive cells are candidates for astrocyte precursor cells in developing mouse cerebellum. Cerebellum *11*, 181-193.

Calfon, M., Zeng, H., Urano, F., Till, J.H., Hubbard, S.R., Harding, H.P., Clark, S.G., and Ron, D. (2002). IRE1 couples endoplasmic reticulum load to secretory capacity by processing the XBP-1 mRNA. Nature *415*, 92-96.

Cammer, W. (1984). Oligodendrocytes associated enzymes. In Oligodendroglia, W. Norton, ed. (Plenum Press), pp. 199-232.

Carri, M.T., Ferri, A., Cozzolino, M., Calabrese, L., and Rotilio, G. (2003). Neurodegeneration in amyotrophic lateral sclerosis: the role of oxidative stress and altered homeostasis of metals. Brain research bulletin *61*, 365-374.

Castellani, R.J., Perry, G., Harris, P.L., Cohen, M.L., Sayre, L.M., Salomon, R.G., and Smith, M.A. (1998). Advanced lipid peroxidation end-products in Alexander's disease. Brain research *787*, 15-18.

Castellani, R.J., Perry, G., Harris, P.L., Monnier, V.M., Cohen, M.L., and Smith, M.A. (1997). Advanced glycation modification of Rosenthal fibers in patients with Alexander disease. Neuroscience letters *231*, 79-82.

Castellani, R.J., Siedlak, S.L., Perry, G., and Smith, M.A. (2000). Sequestration of iron by Lewy bodies in Parkinson's disease. Acta neuropathologica *100*, 111-114.

Chaitin, M.H., Wortham, H.S., and Brun-Zinkernagel, A.M. (1994). Immunocytochemical localization of CD44 in the mouse retina. Experimental eye research *58*, 359-365.

Chan, K., and Kan, Y.W. (1999). Nrf2 is essential for protection against acute pulmonary injury in mice. Proceedings of the National Academy of Sciences of the United States of America *96*, 12731-12736.

Chen, J., Rinaldo, L., Lim, S.J., Young, H., Messing, R.O., and Choi, D.S. (2007). The type 1 equilibrative nucleoside transporter regulates anxiety-like behavior in mice. Genes, brain, and behavior *6*, 776-783.

Chen, Q., Connor, J.R., and Beard, J.L. (1995). Brain iron, transferrin and ferritin concentrations are altered in developing iron-deficient rats. The Journal of nutrition *125*, 1529-1535.

Chen, Y.S., Lim, S.C., Chen, M.H., Quinlan, R.A., and Perng, M.D. (2011). Alexander disease causing mutations in the C-terminal domain of GFAP are deleterious both to assembly and network formation with the potential to both activate caspase 3 and decrease cell viability. Experimental cell research *317*, 2252-2266.

Chia, W.J., Dawe, G.S., and Ong, W.Y. (2011). Expression and localization of the iron-siderophore binding protein lipocalin 2 in the normal rat brain and after kainate-induced excitotoxicity. Neurochemistry international *59*, 591-599.

Chihara, K., Saito, A., Murakami, T., Hino, S., Aoki, Y., Sekiya, H., Aikawa, Y., Wanaka, A., and Imaizumi, K. (2009). Increased vulnerability of hippocampal pyramidal neurons to the toxicity of kainic acid in OASIS-deficient mice. Journal of neurochemistry *110*, 956-965.

Cho, W., and Messing, A. (2009). Properties of astrocytes cultured from GFAP over-expressing and GFAP mutant mice. Experimental cell research *315*, 1260-1272.

Chou, Y.H., Bischoff, J.R., Beach, D., and Goldman, R.D. (1990). Intermediate filament reorganization during mitosis is mediated by p34cdc2 phosphorylation of vimentin. Cell *62*, 1063-1071.

Condorelli, D.F., Nicoletti, V.G., Dell'Albani, P., Barresi, V., Caruso, A., Conticello, S.G., Belluardo, N., and Giuffrida Stella, A.M. (1999). GFAPbeta mRNA expression in the normal rat brain and after neuronal injury. Neurochemical research *24*, 709-714.

Connor, J.R. (1994). Iron acquisition and expression of iron regulatory proteins in the developing brain: manipulation by ethanol exposure, iron deprivation and cellular dysfunction. Developmental neuroscience *16*, 233-247.

Connor, J.R. (2002). Mechanism of Iron Transport in the Brain (New York: Marcel Dekker).

Connor, J.R., and Menzies, S.L. (1996). Relationship of iron to oligodendrocytes and myelination. Glia *17*, 83-93.

Connor, J.R., Menzies, S.L., St Martin, S.M., and Mufson, E.J. (1990). Cellular distribution of transferrin, ferritin, and iron in normal and aged human brains. Journal of neuroscience research *27*, 595-611.

Connor, J.R., Pavlick, G., Karli, D., Menzies, S.L., and Palmer, C. (1995). A histochemical study of iron-positive cells in the developing rat brain. The Journal of comparative neurology *355*, 111-123.

Cotgreave, I.A., and Gerdes, R.G. (1998). Recent trends in glutathione biochemistry--glutathione-protein interactions: a molecular link between oxidative stress and cell proliferation? Biochemical and biophysical research communications *242*, 1-9.

Crichton, R.R., Dexter, D.T., and Ward, R.J. (2011). Brain iron metabolism and its perturbation in neurological diseases. Journal of neural transmission *118*, 301-314.

Crome, L. (1952). Encephalopathy following infantile gastro-enteritis. Archives of disease in childhood *27*, 468-472.

Crome, L. (1953). Megalencephaly associated with hyaline pan-neuropathy. Brain : a journal of neurology *76*, 215-228.

Cruz, T.F., Quackenbush, E.J., Letarte, M., and Moscarello, M.A. (1986). Elevated levels of a glycoprotein antigen (P-80) in gray and white matter of brain from victims of multiple sclerosis. Neurochemical research *11*, 877-889.

Cullinan, S.B., and Diehl, J.A. (2006). Coordination of ER and oxidative stress signaling: the PERK/Nrf2 signaling pathway. The international journal of biochemistry & cell biology *38*, 317-332.

Culty, M., Miyake, K., Kincade, P.W., Sikorski, E., Butcher, E.C., and Underhill, C. (1990). The hyaluronate receptor is a member of the CD44 (H-CAM) family of cell surface glycoproteins. The Journal of cell biology *111*, 2765-2774.

Curnes, J.T., Burger, P.C., Djang, W.T., and Boyko, O.B. (1988). MR imaging of compact white matter pathways. AJNR American journal of neuroradiology *9*, 1061-1068.

Curtis, J.M., Hahn, W.S., Long, E.K., Burrill, J.S., Arriaga, E.A., and Bernlohr, D.A. (2012). Protein carbonylation and metabolic control systems. Trends in endocrinology and metabolism: TEM *23*, 399-406.

Dalle-Donne, I., Aldini, G., Carini, M., Colombo, R., Rossi, R., and Milzani, A. (2006). Protein carbonylation, cellular dysfunction, and disease progression. Journal of cellular and molecular medicine *10*, 389-406.

De Domenico, I., Ward, D.M., di Patti, M.C., Jeong, S.Y., David, S., Musci, G., and Kaplan, J. (2007). Ferroxidase activity is required for the stability of cell surface ferroportin in cells expressing GPI-ceruloplasmin. The EMBO journal *26*, 2823-2831.

Derouiche, A., and Frotscher, M. (2001). Peripheral astrocyte processes: monitoring by selective immunostaining for the actin-binding ERM proteins. Glia *36*, 330-341.

Di Ilio, C., Sacchetta, P., Lo Bello, M., Caccuri, A.M., and Federici, G. (1986). Selenium independent glutathione peroxidase activity associated with cationic forms of glutathione transferase in human heart. Journal of molecular and cellular cardiology *18*, 983-991.

Dinda, A.K., Sarkar, C., and Roy, S. (1990). Rosenthal fibres: an immunohistochemical, ultrastructural and immunoelectron microscopic study. Acta neuropathologica *79*, 456-460.

Doetsch, F., Caille, I., Lim, D.A., Garcia-Verdugo, J.M., and Alvarez-Buylla, A. (1999). Subventricular zone astrocytes are neural stem cells in the adult mammalian brain. Cell *97*, 703-716.

Donovan, A., Brownlie, A., Zhou, Y., Shepard, J., Pratt, S.J., Moynihan, J., Paw, B.H., Drejer, A., Barut, B., Zapata, A.*, et al.* (2000). Positional cloning of zebrafish ferroportin1 identifies a conserved vertebrate iron exporter. Nature *403*, 776-781.

Drake, S.K., Bourdon, E., Wehr, N.B., Levine, R.L., Backlund, P.S., Yergey, A.L., and Rouault, T.A. (2002). Numerous proteins in Mammalian cells are prone to iron-dependent oxidation and proteasomal degradation. Developmental neuroscience *24*, 114-124.

Dringen, R., Bishop, G.M., Koeppe, M., Dang, T.N., and Robinson, S.R. (2007). The pivotal role of astrocytes in the metabolism of iron in the brain. Neurochemical research *32*, 1884-1890.

Dringen, R., Gutterer, J.M., and Hirrlinger, J. (2000). Glutathione metabolism in brain metabolic interaction between astrocytes and neurons in the defense against reactive oxygen species. European journal of biochemistry / FEBS *267*, 4912-4916.

Duckett, S., Schwartzman, R.J., Osterholm, J., Rorke, L.B., Friedman, D., and McLellan, T.L. (1992). Biopsy diagnosis of familial Alexander's disease. Pediatric neurosurgery *18*, 134-138.

Dukan, S., Farewell, A., Ballesteros, M., Taddei, F., Radman, M., and Nystrom, T. (2000). Protein oxidation in response to increased transcriptional or translational errors. Proceedings of the National Academy of Sciences of the United States of America *97*, 5746-5749.

Dwork, A.J., Schon, E.A., and Herbert, J. (1988). Nonidentical distribution of transferrin and ferric iron in human brain. Neuroscience *27*, 333-345.

Eddleston, M., and Mucke, L. (1993). Molecular profile of reactive astrocytes--implications for their role in neurologic disease. Neuroscience *54*, 15-36.

Eng, L.F. (1985). Glial fibrillary acidic protein (GFAP): the major protein of glial intermediate filaments in differentiated astrocytes. Journal of neuroimmunology *8*, 203-214.

Eng, L.F., Lee, Y.L., Kwan, H., Brenner, M., and Messing, A. (1998). Astrocytes cultured from transgenic mice carrying the added human glial fibrillary acidic protein gene contain Rosenthal fibers. Journal of neuroscience research *53*, 353-360.

Eng, L.F., Vanderhaeghen, J.J., Bignami, A., and Gerstl, B. (1971). An acidic protein isolated from fibrous astrocytes. Brain research *28*, 351-354.

England, K., and Cotter, T.G. (2005). Direct oxidative modifications of signalling proteins in mammalian cells and their effects on apoptosis. Redox report : communications in free radical research *10*, 237-245.

Espinosa de los Monteros, A., Kumar, S., Scully, S., Cole, R., and de Vellis, J. (1990). Transferrin gene expression and secretion by rat brain cells in vitro. Journal of neuroscience research *25*, 576-580.

Faulkner, J.R., Herrmann, J.E., Woo, M.J., Tansey, K.E., Doan, N.B., and Sofroniew, M.V. (2004). Reactive astrocytes protect tissue and preserve function after spinal cord injury. The Journal of neuroscience : the official journal of the Society for Neuroscience *24*, 2143-2155.

Fawcett, J.W., and Asher, R.A. (1999). The glial scar and central nervous system repair. Brain research bulletin *49*, 377-391.

Fewell, S.W., Travers, K.J., Weissman, J.S., and Brodsky, J.L. (2001). The action of molecular chaperones in the early secretory pathway. Annual review of genetics *35*, 149-191.

Foisner, R., Traub, P., and Wiche, G. (1991). Protein kinase A- and protein kinase C-regulated interaction of plectin with lamin B and vimentin. Proceedings of the National Academy of Sciences of the United States of America *88*, 3812-3816.

Forster, E., Zhao, S., and Frotscher, M. (2001). Hyaluronan-associated adhesive cues control fiber segregation in the hippocampus. Development *128*, 3029-3039.

Friede, R.L. (1964). Alexander's Disease. Archives of neurology *11*, 414-422.

Fujisaki, T., Tanaka, Y., Fujii, K., Mine, S., Saito, K., Yamada, S., Yamashita, U., Irimura, T., and Eto, S. (1999). CD44 stimulation induces integrin-mediated adhesion of colon cancer cell lines to endothelial cells by up-regulation of integrins and c-Met and activation of integrins. Cancer research *59*, 4427-4434.

Geiger, K.D., Stoldt, P., Schlote, W., and Derouiche, A. (2000). Ezrin immunoreactivity is associated with increasing malignancy of astrocytic tumors but is absent in oligodendrogliomas. The American journal of pathology *157*, 1785-1793.

Geiger, K.D., Stoldt, P., Schlote, W., and Derouiche, A. (2006). Ezrin immunoreactivity reveals specific astrocyte activation in cerebral HIV. Journal of neuropathology and experimental neurology *65*, 87-96.

Geisler, N., and Weber, K. (1982). The amino acid sequence of chicken muscle desmin provides a common structural model for intermediate filament proteins. The EMBO journal *1*, 1649-1656.

Gensert, J.M., and Goldman, J.E. (2001). Heterogeneity of cycling glial progenitors in the adult mammalian cortex and white matter. Journal of neurobiology *48*, 75-86.

Gesase, A.P., and Kiyama, H. (2007). Peripheral nerve injury induced expression of mRNA for serine protease inhibitor 3 in the rat facial and hypoglossal nuclei but not in the spinal cord. Italian journal of anatomy and embryology = Archivio italiano di anatomia ed embriologia *112*, 157-168.

Gething, M.J., McCammon, K., and Sambrook, J. (1986). Expression of wild-type and mutant forms of influenza hemagglutinin: the role of folding in intracellular transport. Cell *46*, 939-950.

Giambattistelli, F., Bucossi, S., Salustri, C., Panetta, V., Mariani, S., Siotto, M., Ventriglia, M., Vernieri, F., Dell'acqua, M.L., Cassetta, E.*, et al.* (2012). Effects of hemochromatosis and transferrin gene mutations on iron dyshomeostasis, liver dysfunction and on the risk of Alzheimer's disease. Neurobiology of aging *33*, 1633-1641.

Giometto, B., Bozza, F., Argentiero, V., Gallo, P., Pagni, S., Piccinno, M.G., and Tavolato, B. (1990). Transferrin receptors in rat central nervous system. An immunocytochemical study. Journal of the neurological sciences *98*, 81-90.

Girgrah, N., Letarte, M., Becker, L.E., Cruz, T.F., Theriault, E., and Moscarello, M.A. (1991). Localization of the CD44 glycoprotein to fibrous astrocytes in normal white matter and to reactive astrocytes in active lesions in multiple sclerosis. Journal of neuropathology and experimental neurology *50*, 779-792.

Girish, K.S., and Kemparaju, K. (2007). The magic glue hyaluronan and its eraser hyaluronidase: a biological overview. Life Sci *80*, 1921-1943.

Goetz, D.H., Holmes, M.A., Borregaard, N., Bluhm, M.E., Raymond, K.N., and Strong, R.K. (2002). The neutrophil lipocalin NGAL is a bacteriostatic agent that interferes with siderophore-mediated iron acquisition. Molecular cell *10*, 1033-1043.

Goldbaum, O., Vollmer, G., and Richter-Landsberg, C. (2006). Proteasome inhibition by MG-132 induces apoptotic cell death and mitochondrial dysfunction in cultured rat brain oligodendrocytes but not in astrocytes. Glia *53*, 891-901.

Goldman, J.E., and Corbin, E. (1988). Isolation of a major protein component of Rosenthal fibers. The American journal of pathology *130*, 569-578.

Goldman, J.E., and Corbin, E. (1991). Rosenthal fibers contain ubiquitinated alpha B-crystallin. The American journal of pathology *139*, 933-938.

Gomi, H., Yokoyama, T., Fujimoto, K., Ikeda, T., Katoh, A., Itoh, T., and Itohara, S. (1995). Mice devoid of the glial fibrillary acidic protein develop normally and are susceptible to scrapie prions. Neuron *14*, 29-41.

Goodman, L. (1953). Alzheimer's disease; a clinico-pathologic analysis of twenty-three cases with a theory on pathogenesis. The Journal of nervous and mental disease *118*, 97-130.

Gorospe, J.R., and Maletkovic, J. (2006). Alexander disease and megalencephalic leukoencephalopathy with subcortical cysts: leukodystrophies arising from astrocyte dysfunction. Mental retardation and developmental disabilities research reviews *12*, 113-122.

Gorospe, J.R., Naidu, S., Johnson, A.B., Puri, V., Raymond, G.V., Jenkins, S.D., Pedersen, R.C., Lewis, D., Knowles, P., Fernandez, R.*, et al.* (2002). Molecular findings in symptomatic and pre-symptomatic Alexander disease patients. Neurology *58*, 1494-1500.

Gosk, S., Vermehren, C., Storm, G., and Moos, T. (2004). Targeting anti-transferrin receptor antibody (OX26) and OX26-conjugated liposomes to brain capillary endothelial cells using in situ perfusion. Journal of cerebral blood flow and metabolism : official journal of the International Society of Cerebral Blood Flow and Metabolism *24*, 1193-1204.

Greco, T.M., Seeholzer, S.H., Mak, A., Spruce, L., and Ischiropoulos, H. (2010). Quantitative mass spectrometry-based proteomics reveals the dynamic range of primary mouse astrocyte protein secretion. Journal of proteome research *9*, 2764-2774.

Green, S.J., Tarone, G., and Underhill, C.B. (1988). Aggregation of macrophages and fibroblasts is inhibited by a monoclonal antibody to the hyaluronate receptor. Experimental cell research *178*, 224-232.

Griot, C., Vandevelde, M., Richard, A., Peterhans, E., and Stocker, R. (1990). Selective degeneration of oligodendrocytes mediated by reactive oxygen species. Free radical research communications *11*, 181-193.

Grune, T., Jung, T., Merker, K., and Davies, K.J. (2004). Decreased proteolysis caused by protein aggregates, inclusion bodies, plaques, lipofuscin, ceroid, and 'aggresomes' during oxidative stress, aging, and disease. The international journal of biochemistry & cell biology *36*, 2519-2530.

Grune, T., Merker, K., Sandig, G., and Davies, K.J. (2003). Selective degradation of oxidatively modified protein substrates by the proteasome. Biochemical and biophysical research communications *305*, 709-718.

Gullotta, F., and Kuchelmeister, K. (1986). [GFAP in brain tumors]. Verhandlungen der Deutschen Gesellschaft fur Pathologie *70*, 380-381.

Guo, F., Maeda, Y., Ma, J., Delgado, M., Sohn, J., Miers, L., Ko, E.M., Bannerman, P., Xu, J., Wang, Y.*, et al.* (2011). Macroglial plasticity and the origins of reactive astroglia in experimental autoimmune encephalomyelitis. The Journal of neuroscience : the official journal of the Society for Neuroscience *31*, 11914-11928.

Haedicke, J., de Los Santos, K., Goff, S.P., and Naghavi, M.H. (2008). The Ezrin-radixin-moesin family member ezrin regulates stable microtubule formation and retroviral infection. Journal of virology *82*, 4665-4670.

Haegel, H., Tolg, C., Hofmann, M., and Ceredig, R. (1993). Activated mouse astrocytes and T cells express similar CD44 variants. Role of CD44 in astrocyte/T cell binding. The Journal of cell biology *122*, 1067-1077.

Hagemann, T.L., Boelens, W.C., Wawrousek, E.F., and Messing, A. (2009). Suppression of GFAP toxicity by alphaB-crystallin in mouse models of Alexander disease. Human molecular genetics *18*, 1190-1199.

Hagemann, T.L., Connor, J.X., and Messing, A. (2006). Alexander disease-associated glial fibrillary acidic protein mutations in mice induce Rosenthal fiber formation and a white matter stress response. The Journal of neuroscience : the official journal of the Society for Neuroscience *26*, 11162-11173.

Hagemann, T.L., Gaeta, S.A., Smith, M.A., Johnson, D.A., Johnson, J.A., and Messing, A. (2005). Gene expression analysis in mice with elevated glial fibrillary acidic protein and Rosenthal fibers reveals a stress response followed by glial activation and neuronal dysfunction. Human molecular genetics *14*, 2443-2458.

Hagemann, T.L., Jobe, E.M., and Messing, A. (2012). Genetic ablation of Nrf2/antioxidant response pathway in Alexander disease mice reduces hippocampal gliosis but does not impact survival. PloS one *7*, e37304.

Hagiwara, N., Imada, S., and Sueoka, N. (1993). Cell-type specific segregation of transcriptional expression of glial genes in the rat peripheral neurotumor RT4 cell lines. Journal of neuroscience research *36*, 646-656.

Halliwell, B. (1992). Reactive oxygen species and the central nervous system. Journal of neurochemistry *59*, 1609-1623.

Halliwell, B. (2006). Proteasomal dysfunction: a common feature of neurodegenerative diseases? Implications for the environmental origins of neurodegeneration. Antioxidants & redox signaling *8*, 2007-2019.

Hammond, C., and Helenius, A. (1995). Quality control in the secretory pathway. Current opinion in cell biology *7*, 523-529.

Harding, H.P., Zhang, Y., Khersonsky, S., Marciniak, S., Scheuner, D., Kaufman, R.J., Javitt, N., Chang, Y.T., and Ron, D. (2005). Bioactive small molecules reveal antagonism between the integrated stress response and sterol-regulated gene expression. Cell metabolism *2*, 361-371.

Harris, Z.L., Takahashi, Y., Miyajima, H., Serizawa, M., MacGillivray, R.T., and Gitlin, J.D. (1995). Aceruloplasminemia: molecular characterization of this disorder of iron metabolism. Proceedings of the National Academy of Sciences of the United States of America *92*, 2539-2543.

Harrison, P.M., and Arosio, P. (1996). The ferritins: molecular properties, iron storage function and cellular regulation. Biochimica et biophysica acta *1275*, 161-203.

Hayes, J.D., and McMahon, M. (2001). Molecular basis for the contribution of the antioxidant responsive element to cancer chemoprevention. Cancer letters *174*, 103-113.

Head, M.W., Corbin, E., and Goldman, J.E. (1993). Overexpression and abnormal modification of the stress proteins alpha B-crystallin and HSP27 in Alexander disease. The American journal of pathology *143*, 1743-1753.

Hehnly, H., Xu, W., Chen, J.L., and Stamnes, M. (2010). Cdc42 regulates microtubule-dependent Golgi positioning. Traffic *11*, 1067-1078.

Herndon, R.M. (1999). Is Alexander's disease a nosologic entity or a common pathologic pattern of diverse etiology? Journal of child neurology *14*, 275-276.

Herndon, R.M., Rubinstein, L.J., Freeman, J.M., and Mathieson, G. (1970). Light and electron microscopic observations on Rosenthal fibers in Alexander's disease and in multiple sclerosis. Journal of neuropathology and experimental neurology *29*, 524-551.

Hess, D.C., Fischer, A.Q., Yaghmai, F., Figueroa, R., and Akamatsu, Y. (1990). Comparative neuroimaging with pathologic correlates in Alexander's disease. Journal of child neurology *5*, 248-252.

Hirsch, E.C., Brandel, J.P., Galle, P., Javoy-Agid, F., and Agid, Y. (1991). Iron and aluminum increase in the substantia nigra of patients with Parkinson's disease: an X-ray microanalysis. Journal of neurochemistry *56*, 446-451.

Hohnholt, M., Geppert, M., and Dringen, R. (2010). Effects of iron chelators, iron salts, and iron oxide nanoparticles on the proliferation and the iron content of oligodendroglial OLN-93 cells. Neurochemical research *35*, 1259-1268.

Hol, E.M., Roelofs, R.F., Moraal, E., Sonnemans, M.A., Sluijs, J.A., Proper, E.A., de Graan, P.N., Fischer, D.F., and van Leeuwen, F.W. (2003). Neuronal expression of GFAP in patients with Alzheimer pathology and identification of novel GFAP splice forms. Mol Psychiatry *8*, 786-796.

Huang, L.L., Shang, F., Nowell, T.R., Jr., and Taylor, A. (1995). Degradation of differentially oxidized alpha-crystallins in bovine lens epithelial cells. Experimental eye research *61*, 45-54.

Husain, J., and Juurlink, B.H. (1995). Oligodendroglial precursor cell susceptibility to hypoxia is related to poor ability to cope with reactive oxygen species. Brain research *698*, 86-94.

Isaacs, A., Baker, M., Wavrant-De Vrieze, F., and Hutton, M. (1998). Determination of the gene structure of human GFAP and absence of coding region mutations associated with frontotemporal dementia with parkinsonism linked to chromosome 17. Genomics *51*, 152-154.

Itoh, K., Chiba, T., Takahashi, S., Ishii, T., Igarashi, K., Katoh, Y., Oyake, T., Hayashi, N., Satoh, K., Hatayama, I.*, et al.* (1997). An Nrf2/small Maf heterodimer mediates the induction of phase II detoxifying enzyme genes through antioxidant response elements. Biochemical and biophysical research communications *236*, 313-322.

Itoh, K., Wakabayashi, N., Katoh, Y., Ishii, T., Igarashi, K., Engel, J.D., and Yamamoto, M. (1999). Keap1 represses nuclear activation of antioxidant responsive elements by Nrf2 through binding to the amino-terminal Neh2 domain. Genes & development *13*, 76-86.

Iwai, K., Drake, S.K., Wehr, N.B., Weissman, A.M., LaVaute, T., Minato, N., Klausner, R.D., Levine, R.L., and Rouault, T.A. (1998). Iron-dependent oxidation, ubiquitination, and degradation of iron regulatory protein 2: implications for degradation of oxidized proteins. Proceedings of the National Academy of Sciences of the United States of America *95*, 4924-4928.

Iwaki, T., Kume-Iwaki, A., Liem, R.K., and Goldman, J.E. (1989). Alpha B-crystallin is expressed in non-lenticular tissues and accumulates in Alexander's disease brain. Cell *57*, 71-78.

Iwaki, T., Wisniewski, T., Iwaki, A., Corbin, E., Tomokane, N., Tateishi, J., and Goldman, J.E. (1992). Accumulation of alpha B-crystallin in central nervous system glia and neurons in pathologic conditions. The American journal of pathology *140*, 345-356.

Iwakoshi, N.N., Lee, A.H., Vallabhajosyula, P., Otipoby, K.L., Rajewsky, K., and Glimcher, L.H. (2003). Plasma cell differentiation and the unfolded protein response intersect at the transcription factor XBP-1. Nature immunology *4*, 321-329.

Izawa, I., and Inagaki, M. (2006). Regulatory mechanisms and functions of intermediate filaments: a study using site- and phosphorylation state-specific antibodies. Cancer Sci *97*, 167-174.

Jaiswal, A.K. (2000). Regulation of genes encoding NAD(P)H:quinone oxidoreductases. Free radical biology & medicine *29*, 254-262.

Jana, M., Anderson, J.A., Saha, R.N., Liu, X., and Pahan, K. (2005). Regulation of inducible nitric oxide synthase in proinflammatory cytokine-stimulated human primary astrocytes. Free radical biology & medicine *38*, 655-664.

Janzer, R.C., and Friede, R.L. (1981). Do Rosenthal fibers contain glial fibrillary acid protein? Acta neuropathologica *55*, 75-76.

Jeon, S., Kim, S., Park, J.B., Suh, P.G., Kim, Y.S., Bae, C.D., and Park, J. (2002). RhoA and Rho kinase-dependent phosphorylation of moesin at Thr-558 in hippocampal neuronal cells by glutamate. The Journal of biological chemistry *277*, 16576-16584.

Jeong, S.Y., and David, S. (2003). Glycosylphosphatidylinositol-anchored ceruloplasmin is required for iron efflux from cells in the central nervous system. The Journal of biological chemistry *278*, 27144-27148.

Jeong, S.Y., and David, S. (2006). Age-related changes in iron homeostasis and cell death in the cerebellum of ceruloplasmin-deficient mice. The Journal of neuroscience : the official journal of the Society for Neuroscience *26*, 9810-9819.

Jian, B., Hsieh, C.H., Chen, J., Choudhry, M., Bland, K., Chaudry, I., and Raju, R. (2008). Activation of endoplasmic reticulum stress response following trauma-hemorrhage. Biochimica et biophysica acta *1782*, 621-626.

Johnson, A.B., and Bettica, A. (1989). On-grid immunogold labeling of glial intermediate filaments in epoxy-embedded tissue. The American journal of anatomy *185*, 335-341.

Johnson, K., Mintz-Hittner, H.A., Conley, Y.P., and Ferrell, R.E. (1996). X-linked exudative vitreoretinopathy caused by an arginine to leucine substitution (R121L) in the Norrie disease protein. Clinical genetics *50*, 113-115.

Johnston, J. (2006). The Aggresome: Proteasomes, Inclusion Bodies and Protein Aggression. In Protein Misfolding, Aggregation and Conformational Diseases

Part A: Protein Aggregration and Conformational Diseases, V. Uverski, and A. Fink, eds. (Springer Science and Business Media), pp. 175-222.

Kacem, K., Lacombe, P., Seylaz, J., and Bonvento, G. (1998). Structural organization of the perivascular astrocyte endfeet and their relationship with the endothelial glucose transporter: a confocal microscopy study. Glia *23*, 1-10.

Kakhlon, O., and Cabantchik, Z.I. (2002). The labile iron pool: characterization, measurement, and participation in cellular processes(1). Free radical biology & medicine *33*, 1037-1046.

Kalman, M. (2004). Glial Reactions and Reactive Glia. In The Nervous System: Function and Dysfunction, L. Hertz, ed., pp. 787-834.

Kanapin, A., Batalov, S., Davis, M.J., Gough, J., Grimmond, S., Kawaji, H., Magrane, M., Matsuda, H., Schonbach, C., Teasdale, R.D*., et al.* (2003). Mouse proteome analysis. Genome research *13*, 1335-1344.

Kaneko, K., Nakamura, A., Yoshida, K., Kametani, F., Higuchi, K., and Ikeda, S. (2002a). Glial fibrillary acidic protein is greatly modified by oxidative stress in aceruloplasminemia brain. Free radical research *36*, 303-306.

Kaneko, K., Yoshida, K., Arima, K., Ohara, S., Miyajima, H., Kato, T., Ohta, M., and Ikeda, S.I. (2002b). Astrocytic deformity and globular structures are characteristic of the brains of patients with aceruloplasminemia. Journal of neuropathology and experimental neurology *61*, 1069-1077.

Kaplan, J., and Kushner, J.P. (2000). Mining the genome for iron. Nature *403*, 711, 713.

Katoh, S., Zheng, Z., Oritani, K., Shimozato, T., and Kincade, P.W. (1995). Glycosylation of CD44 negatively regulates its recognition of hyaluronan. The Journal of experimental medicine *182*, 419-429.

Kaur, D., Lee, D., Ragapolan, S., and Andersen, J.K. (2009). Glutathione depletion in immortalized midbrain-derived dopaminergic neurons results in increases in the labile iron pool: implications for Parkinson's disease. Free radical biology & medicine *46*, 593-598.

Keene, S.D., Greco, T.M., Parastatidis, I., Lee, S.H., Hughes, E.G., Balice-Gordon, R.J., Speicher, D.W., and Ischiropoulos, H. (2009). Mass spectrometric and computational analysis of cytokine-induced alterations in the astrocyte secretome. Proteomics *9*, 768-782.

Kim, H.S., Bae, C.D., and Park, J. (2010). Glutamate receptor-mediated phosphorylation of ezrin/radixin/moesin proteins is implicated in filopodial protrusion of primary cultured hippocampal neuronal cells. Journal of neurochemistry *113*, 1565-1576.

Kim, I., Xu, W., and Reed, J.C. (2008). Cell death and endoplasmic reticulum stress: disease relevance and therapeutic opportunities. Nature reviews Drug discovery *7*, 1013-1030.

Kim, M.D., Cho, H.J., and Shin, T. (2004). Expression of osteopontin and its ligand, CD44, in the spinal cords of Lewis rats with experimental autoimmune encephalomyelitis. Journal of neuroimmunology *151*, 78-84.

Klomp, L.W., Farhangrazi, Z.S., Dugan, L.L., and Gitlin, J.D. (1996). Ceruloplasmin gene expression in the murine central nervous system. The Journal of clinical investigation *98*, 207-215.

Klomp, L.W., and Gitlin, J.D. (1996). Expression of the ceruloplasmin gene in the human retina and brain: implications for a pathogenic model in aceruloplasminemia. Human molecular genetics *5*, 1989-1996.

Knudson, C.B. (1993). Hyaluronan receptor-directed assembly of chondrocyte pericellular matrix. The Journal of cell biology *120*, 825-834.

Knudson, W., Bartnik, E., and Knudson, C.B. (1993). Assembly of pericellular matrices by COS-7 cells transfected with CD44 lymphocyte-homing receptor genes. Proceedings of the National Academy of Sciences of the United States of America *90*, 4003-4007.

Kohlschutter, A., and Eichler, F. (2011). Childhood leukodystrophies: a clinical perspective. Expert review of neurotherapeutics *11*, 1485-1496.

Kondo, S., Murakami, T., Tatsumi, K., Ogata, M., Kanemoto, S., Otori, K., Iseki, K., Wanaka, A., and Imaizumi, K. (2005). OASIS, a CREB/ATF-family member, modulates UPR signalling in astrocytes. Nature cell biology *7*, 186-194.

Kono, S. (2012). Aceruloplasminemia. Current drug targets *13*, 1190-1199.

Koopman, G., van Kooyk, Y., de Graaff, M., Meyer, C.J., Figdor, C.G., and Pals, S.T. (1990). Triggering of the CD44 antigen on T lymphocytes promotes T cell adhesion through the LFA-1 pathway. Journal of immunology *145*, 3589-3593.

Kovacs, W.J., Tape, K.N., Shackelford, J.E., Wikander, T.M., Richards, M.J., Fliesler, S.J., Krisans, S.K., and Faust, P.L. (2009). Peroxisome deficiency causes a complex phenotype because of hepatic SREBP/Insig dysregulation associated with endoplasmic reticulum stress. The Journal of biological chemistry *284*, 7232-7245.

Kozutsumi, Y., Segal, M., Normington, K., Gething, M.J., and Sambrook, J. (1988). The presence of malfolded proteins in the endoplasmic reticulum signals the induction of glucose-regulated proteins. Nature *332*, 462-464.

Kress, Y., Gaskin, F., Brosnan, C.F., and Levine, S. (1981). Effects of zinc on the cytoskeletal proteins in the central nervous system of the rat. Brain research *220*, 139-149.

Kyllerman, M., Rosengren, L., Wiklund, L.M., and Holmberg, E. (2005). Increased levels of GFAP in the cerebrospinal fluid in three subtypes of genetically confirmed Alexander disease. Neuropediatrics *36*, 319-323.

Lammich, S., Okochi, M., Takeda, M., Kaether, C., Capell, A., Zimmer, A.K., Edbauer, D., Walter, J., Steiner, H., and Haass, C. (2002). Presenilin-dependent intramembrane proteolysis of CD44 leads to the liberation of its intracellular domain and the secretion of an Abeta-like peptide. The Journal of biological chemistry *277*, 44754-44759.

Lavialle, M., Aumann, G., Anlauf, E., Prols, F., Arpin, M., and Derouiche, A. (2011). Structural plasticity of perisynaptic astrocyte processes involves ezrin and metabotropic glutamate receptors. Proceedings of the National Academy of Sciences of the United States of America *108*, 12915-12919.

Lee, A., Rayfield, A., Hryciw, D.H., Ma, T.A., Wang, D., Pow, D., Broer, S., Yun, C., and Poronnik, P. (2007a). Na+-H+ exchanger regulatory factor 1 is a PDZ scaffold for the astroglial glutamate transporter GLAST. Glia *55*, 119-129.

Lee, J.L., Wang, M.J., Sudhir, P.R., Chen, G.D., Chi, C.W., and Chen, J.Y. (2007b). Osteopontin promotes integrin activation through outside-in and inside-out mechanisms: OPN-CD44V interaction enhances survival in gastrointestinal cancer cells. Cancer research *67*, 2089-2097.

Lee, S., Park, J.Y., Lee, W.H., Kim, H., Park, H.C., Mori, K., and Suk, K. (2009). Lipocalin-2 is an autocrine mediator of reactive astrocytosis. The Journal of neuroscience : the official journal of the Society for Neuroscience *29*, 234-249.

Legg, J.W., and Isacke, C.M. (1998). Identification and functional analysis of the ezrin-binding site in the hyaluronan receptor, CD44. Current biology : CB *8*, 705-708.

Lemke, G. (1992). Myelin and Myelination. In Molecular neurobiology, Z. Hall, ed. (Sunderland, MA: Sinauer Associates), pp. 281-308.

Lesley, J., Hyman, R., and Kincade, P.W. (1993). CD44 and its interaction with extracellular matrix. Advances in immunology *54*, 271-335.

Levine, R.L., Oliver, C.N., Fulks, R.M., and Stadtman, E.R. (1981). Turnover of bacterial glutamine synthetase: oxidative inactivation precedes proteolysis. Proceedings of the National Academy of Sciences of the United States of America *78*, 2120-2124.

LeVine, S.M. (1991). Oligodendrocytes and myelin sheaths in normal, quaking and shiverer brains are enriched in iron. Journal of neuroscience research *29*, 413-419.

LeVine, S.M. (1997). Iron deposits in multiple sclerosis and Alzheimer's disease brains. Brain research *760*, 298-303.

LeVine, S.M., and Goldman, J.E. (1988). Spatial and temporal patterns of oligodendrocyte differentiation in rat cerebrum and cerebellum. The Journal of comparative neurology *277*, 441-455.

Li, R., Johnson, A.B., Salomons, G., Goldman, J.E., Naidu, S., Quinlan, R., Cree, B., Ruyle, S.Z., Banwell, B., D'Hooghe, M.*, et al.* (2005). Glial fibrillary acidic protein mutations in infantile, juvenile, and adult forms of Alexander disease. Annals of neurology *57*, 310-326.

Li, R., Johnson, A.B., Salomons, G.S., van der Knaap, M.S., Rodriguez, D., Boespflug-Tanguy, O., Gorospe, J.R., Goldman, J.E., Messing, A., and Brenner, M. (2006). Propensity for paternal inheritance of de novo mutations in Alexander disease. Human genetics *119*, 137-144.

Li, X.P., Xie, W.J., Zhang, Z., Kansara, S., Jankovic, J., and Le, W.D. (2012). A mechanistic study of proteasome inhibition-induced iron misregulation in dopamine neuron degeneration. Neuro-Signals *20*, 223-236.

Liedtke, W., Edelmann, W., Bieri, P.L., Chiu, F.C., Cowan, N.J., Kucherlapati, R., and Raine, C.S. (1996). GFAP is necessary for the integrity of CNS white matter architecture and long-term maintenance of myelination. Neuron *17*, 607-615.

Liem, R.K., and Messing, A. (2009). Dysfunctions of neuronal and glial intermediate filaments in disease. The Journal of clinical investigation *119*, 1814-1824.

Lin, W., Bailey, S.L., Ho, H., Harding, H.P., Ron, D., Miller, S.D., and Popko, B. (2007). The integrated stress response prevents demyelination by protecting oligodendrocytes against immune-mediated damage. The Journal of clinical investigation *117*, 448-456.

Liochev, S.I., and Fridovich, I. (1994). The role of O2.- in the production of HO.: in vitro and in vivo. Free radical biology & medicine *16*, 29-33.

Lipinski, B. (2011). Hydroxyl radical and its scavengers in health and disease. Oxidative medicine and cellular longevity *2011*, 809696.

Liu, Y., Han, S.S., Wu, Y., Tuohy, T.M., Xue, H., Cai, J., Back, S.A., Sherman, L.S., Fischer, I., and Rao, M.S. (2004). CD44 expression identifies astrocyte-restricted precursor cells. Developmental biology *276*, 31-46.

Lokeshwar, V.B., and Bourguignon, L.Y. (1991). Post-translational protein modification and expression of ankyrin-binding site(s) in GP85 (Pgp-1/CD44) and its biosynthetic precursors during T-lymphoma membrane biosynthesis. The Journal of biological chemistry *266*, 17983-17989.

Lokeshwar, V.B., Fregien, N., and Bourguignon, L.Y. (1994). Ankyrin-binding domain of CD44(GP85) is required for the expression of hyaluronic acid-mediated adhesion function. The Journal of cell biology *126*, 1099-1109.

Lopez-Egido, J., Cunningham, J., Berg, M., Oberg, K., Bongcam-Rudloff, E., and Gobl, A. (2002). Menin's interaction with glial fibrillary acidic protein and vimentin suggests a role for the intermediate filament network in regulating menin activity. Experimental cell research *278*, 175-183.

Luke, H.J., and Prehm, P. (1999). Synthesis and shedding of hyaluronan from plasma membranes of human fibroblasts and metastatic and non-metastatic melanoma cells. The Biochemical journal *343 Pt 1*, 71-75.

M, B., JE, G., RA, Q., and A., M. (2009). Alexander disease: a genetic disorder of astrocytes (New York: Springer).

Ma, Y., and Hendershot, L.M. (2004). ER chaperone functions during normal and stress conditions. Journal of chemical neuroanatomy *28*, 51-65.

Maisonneuve, E., Fraysse, L., Lignon, S., Capron, L., and Dukan, S. (2008). Carbonylated proteins are detectable only in a degradation-resistant aggregate state in Escherichia coli. Journal of bacteriology *190*, 6609-6614.

Malone, P.E., and Hernandez, M.R. (2007). 4-Hydroxynonenal, a product of oxidative stress, leads to an antioxidant response in optic nerve head astrocytes. Experimental eye research *84*, 444-454.

Mancini, R., Fagioli, C., Fra, A.M., Maggioni, C., and Sitia, R. (2000). Degradation of unassembled soluble Ig subunits by cytosolic proteasomes: evidence that retrotranslocation and degradation are coupled events. FASEB journal : official publication of the Federation of American Societies for Experimental Biology *14*, 769-778.

Marhaba, R., and Zoller, M. (2004). CD44 in cancer progression: adhesion, migration and growth regulation. Journal of molecular histology *35*, 211-231.

Markowitz, A.J., White, M.G., Kolson, D.L., and Jordan-Sciutto, K.L. (2007). Cellular interplay between neurons and glia: toward a comprehensive mechanism for excitotoxic neuronal loss in neurodegeneration. Cellscience *4*, 111-146.

Marks, F., Klingmüller, U., and Müller-Decker, K. (2009). Cellular signal processing : an introduction to the molecular mechanisms of signal transduction (New York: Garland Science).

Marques, C., Pereira, P., Taylor, A., Liang, J.N., Reddy, V.N., Szweda, L.I., and Shang, F. (2004). Ubiquitin-dependent lysosomal degradation of the HNE-modified proteins in lens epithelial cells. FASEB journal : official publication of the Federation of American Societies for Experimental Biology *18*, 1424-1426.

Marrero-Diaz, R., Bravo-Cordero, J.J., Megias, D., Garcia, M.A., Bartolome, R.A., Teixido, J., and Montoya, M.C. (2009). Polarized MT1-MMP-CD44 interaction and CD44 cleavage during cell retraction reveal an essential role for MT1-MMP in CD44-mediated invasion. Cell motility and the cytoskeleton *66*, 48-61.

Mastri, A.R., and Sung, J.H. (1973). Diffuse Rosenthal fiber formation in the adult: a report of four cases. Journal of neuropathology and experimental neurology *32*, 424-436.

Mathewson, A.J., and Berry, M. (1985). Observations on the astrocyte response to a cerebral stab wound in adult rats. Brain research *327*, 61-69.

Matsumoto, T., Imagama, S., Hirano, K., Ohgomori, T., Natori, T., Kobayashi, K., Muramoto, A., Ishiguro, N., and Kadomatsu, K. (2012). CD44 expression in astrocytes and microglia is associated with ALS progression in a mouse model. Neuroscience letters *520*, 115-120.

Maytin, E.V., Ubeda, M., Lin, J.C., and Habener, J.F. (2001). Stress-inducible transcription factor CHOP/gadd153 induces apoptosis in mammalian cells via p38 kinase-dependent and -independent mechanisms. Experimental cell research *267*, 193-204.

McCall, M.A., Gregg, R.G., Behringer, R.R., Brenner, M., Delaney, C.L., Galbreath, E.J., Zhang, C.L., Pearce, R.A., Chiu, S.Y., and Messing, A. (1996). Targeted deletion in astrocyte intermediate filament (Gfap) alters neuronal physiology. Proceedings of the National Academy of Sciences of the United States of America *93*, 6361-6366.

McCarthy, K.D., and de Vellis, J. (1980). Preparation of separate astroglial and oligodendroglial cell cultures from rat cerebral tissue. The Journal of cell biology *85*, 890-902.

McCord, J.M. (2004). Iron, free radicals, and oxidative injury. The Journal of nutrition *134*, 3171S-3172S.

McKee, C.M., Penno, M.B., Cowman, M., Burdick, M.D., Strieter, R.M., Bao, C., and Noble, P.W. (1996). Hyaluronan (HA) fragments induce chemokine gene expression in alveolar macrophages. The role of HA size and CD44. The Journal of clinical investigation *98*, 2403-2413.

McKie, A.T., and Barlow, D.J. (2004). The SLC40 basolateral iron transporter family (IREG1/ferroportin/MTP1). Pflugers Archiv : European journal of physiology *447*, 801-806.

McKie, A.T., Marciani, P., Rolfs, A., Brennan, K., Wehr, K., Barrow, D., Miret, S., Bomford, A., Peters, T.J., Farzaneh, F*., et al.* (2000). A novel duodenal iron-regulated transporter, IREG1, implicated in the basolateral transfer of iron to the circulation. Molecular cell *5*, 299-309.

Menzel, R., Vogel, F., Kargel, E., and Schunck, W.H. (1997). Inducible membranes in yeast: relation to the unfolded-protein-response pathway. Yeast *13*, 1211-1229.

Meplan, C., Richard, M.J., and Hainaut, P. (2000). Redox signalling and transition metals in the control of the p53 pathway. Biochemical pharmacology *59*, 25-33.

Messing, A. (1998). Transgenic studies of peripheral and central glia. The International journal of developmental biology *42*, 1019-1024.

Messing, A., Brenner, M., Feany, M.B., Nedergaard, M., and Goldman, J.E. (2012a). Alexander disease. The Journal of neuroscience : the official journal of the Society for Neuroscience *32*, 5017-5023.

Messing, A., Brenner, M., Johnson, A.B., and Goldman, J.E. (2001a). Update on white matter genetic disorders. Pediatric neurology *25*, 347-348; author reply 348.

Messing, A., and Goldman, J.E. (2004). Chapter 36 Alexander Disease. In Myelin Biology and Disorders, R.A. Lazzarini, ed., pp. 851-866.

Messing, A., Goldman, J.E., Johnson, A.B., and Brenner, M. (2001b). Alexander disease: new insights from genetics. Journal of neuropathology and experimental neurology *60*, 563-573.

Messing, A., Head, M.W., Galles, K., Galbreath, E.J., Goldman, J.E., and Brenner, M. (1998). Fatal encephalopathy with astrocyte inclusions in GFAP transgenic mice. The American journal of pathology *152*, 391-398.

Messing, A., Li, R., Naidu, S., Taylor, J.P., Silverman, L., Flint, D., van der Knaap, M.S., and Brenner, M. (2012b). Archetypal and new families with Alexander disease and novel mutations in GFAP. Archives of neurology *69*, 208-214.

Miyajima, H., Takahashi, Y., and Kono, S. (2003). Aceruloplasminemia, an inherited disorder of iron metabolism. Biometals *16*, 205-213.

Miyake, K., Underhill, C.B., Lesley, J., and Kincade, P.W. (1990). Hyaluronate can function as a cell adhesion molecule and CD44 participates in hyaluronate recognition. The Journal of experimental medicine *172*, 69-75.

Miyake, T., Hattori, T., Fukuda, M., Kitamura, T., and Fujita, S. (1988). Quantitative studies on proliferative changes of reactive astrocytes in mouse cerebral cortex. Brain research *451*, 133-138.

Moos, T. (1996). Immunohistochemical localization of intraneuronal transferrin receptor immunoreactivity in the adult mouse central nervous system. The Journal of comparative neurology *375*, 675-692.

Moos, T., and Morgan, E.H. (1998). Evidence for low molecular weight, non-transferrin-bound iron in rat brain and cerebrospinal fluid. Journal of neuroscience research *54*, 486-494.

Moos, T., and Morgan, E.H. (2000). Transferrin and transferrin receptor function in brain barrier systems. Cellular and molecular neurobiology *20*, 77-95.

Moos, T., and Morgan, E.H. (2001). Restricted transport of anti-transferrin receptor antibody (OX26) through the blood-brain barrier in the rat. Journal of neurochemistry *79*, 119-129.

Moos, T., Rosengren Nielsen, T., Skjorringe, T., and Morgan, E.H. (2007). Iron trafficking inside the brain. Journal of neurochemistry *103*, 1730-1740.

Mor-Vaknin, N., Punturieri, A., Sitwala, K., and Markovitz, D.M. (2003). Vimentin is secreted by activated macrophages. Nature cell biology *5*, 59-63.

Morath, D.J., and Mayer-Proschel, M. (2001). Iron modulates the differentiation of a distinct population of glial precursor cells into oligodendrocytes. Developmental biology *237*, 232-243.

Morath, D.J., and Mayer-Proschel, M. (2002). Iron deficiency during embryogenesis and consequences for oligodendrocyte generation in vivo. Developmental neuroscience *24*, 197-207.

Morita, H., Ikeda, S., Yamamoto, K., Morita, S., Yoshida, K., Nomoto, S., Kato, M., and Yanagisawa, N. (1995). Hereditary ceruloplasmin deficiency with hemosiderosis: a clinicopathological study of a Japanese family. Annals of neurology *37*, 646-656.

Morris, C.M., Candy, J.M., Oakley, A.E., Bloxham, C.A., and Edwardson, J.A. (1992). Histochemical distribution of non-haem iron in the human brain. Acta anatomica *144*, 235-257.

Moseley, R., Waddington, R.J., and Embery, G. (1997). Degradation of glycosaminoglycans by reactive oxygen species derived from stimulated polymorphonuclear leukocytes. Biochimica et biophysica acta *1362*, 221-231.

Murakami, D., Okamoto, I., Nagano, O., Kawano, Y., Tomita, T., Iwatsubo, T., De Strooper, B., Yumoto, E., and Saya, H. (2003). Presenilin-dependent gamma-secretase activity mediates the intramembranous cleavage of CD44. Oncogene *22*, 1511-1516.

Naghavi, M.H., Valente, S., Hatziioannou, T., de Los Santos, K., Wen, Y., Mott, C., Gundersen, G.G., and Goff, S.P. (2007). Moesin regulates stable microtubule formation and limits retroviral infection in cultured cells. The EMBO journal *26*, 41-52.

Naito, J., Kaji, H., Sowa, H., Hendy, G.N., Sugimoto, T., and Chihara, K. (2005). Menin suppresses osteoblast differentiation by antagonizing the AP-1 factor, JunD. The Journal of biological chemistry *280*, 4785-4791.

Namekawa, M., Takiyama, Y., Aoki, Y., Takayashiki, N., Sakoe, K., Shimazaki, H., Taguchi, T., Tanaka, Y., Nishizawa, M., Saito, K.*, et al.* (2002). Identification of GFAP gene mutation in hereditary adult-onset Alexander's disease. Annals of neurology *52*, 779-785.

Nappi, A.J., and Vass, E. (2002). Interactions of iron with reactive intermediates of oxygen and nitrogen. Developmental neuroscience *24*, 134-142.

Nawashiro, H., Messing, A., Azzam, N., and Brenner, M. (1998). Mice lacking GFAP are hypersensitive to traumatic cerebrospinal injury. Neuroreport *9*, 1691-1696.

Neame, P.J., and Barry, F.P. (1993). The link proteins. Experientia *49*, 393-402.

Nestl, A., Von Stein, O.D., Zatloukal, K., Thies, W.G., Herrlich, P., Hofmann, M., and Sleeman, J.P. (2001). Gene expression patterns associated with the metastatic phenotype in rodent and human tumors. Cancer research *61*, 1569-1577.

Nguyen-Legros, J., Bizot, J., Bolesse, M., and Pulicani, J.P. (1980a). ["Diaminobenzidine black" as a new histochemical demonstration of exogenous iron (author's transl)]. Histochemistry *66*, 239-244.

Nguyen-Legros, J., Cesaro, P., Berger, B., and Alvarez, C. (1980b). Demonstration of double-labelled branched neurons in the CNS of the rat by retrograde axonal transport of iron-dextran complex and HRP. An application to epoxy-embedded material. Folia Morphol (Praha) *28*, 246-250.

Nielsen, A.L., Holm, I.E., Johansen, M., Bonven, B., Jorgensen, P., and Jorgensen, A.L. (2002a). A new splice variant of glial fibrillary acidic protein, GFAP epsilon, interacts with the presenilin proteins. The Journal of biological chemistry *277*, 29983-29991.

Nielsen, A.L., Jorgensen, P., and Jorgensen, A.L. (2002b). Mutations associated with a childhood leukodystrophy, Alexander disease, cause deficiency in dimerization of the cytoskeletal protein GFAP. Journal of neurogenetics *16*, 175-179.

O'Hare, T., Wiens, G.D., Whitcomb, E.A., Enns, C.A., and Rittenberg, M.B. (1999). Cutting edge: proteasome involvement in the degradation of unassembled Ig light chains. Journal of immunology *163*, 11-14.

Ogata, M., Hino, S., Saito, A., Morikawa, K., Kondo, S., Kanemoto, S., Murakami, T., Taniguchi, M., Tanii, I., Yoshinaga, K.*, et al.* (2006). Autophagy is activated for cell survival after endoplasmic reticulum stress. Molecular and cellular biology *26*, 9220-9231.

Oide, T., Yoshida, K., Kaneko, K., Ohta, M., and Arima, K. (2006). Iron overload and antioxidative role of perivascular astrocytes in aceruloplasminemia. Neuropathology and applied neurobiology *32*, 170-176.

Okamoto, I., Kawano, Y., Matsumoto, M., Suga, M., Kaibuchi, K., Ando, M., and Saya, H. (1999a). Regulated CD44 cleavage under the control of protein kinase C, calcium influx, and the Rho family of small G proteins. The Journal of biological chemistry *274*, 25525-25534.

Okamoto, I., Kawano, Y., Tsuiki, H., Sasaki, J., Nakao, M., Matsumoto, M., Suga, M., Ando, M., Nakajima, M., and Saya, H. (1999b). CD44 cleavage induced by a membrane-associated metalloprotease plays a critical role in tumor cell migration. Oncogene *18*, 1435-1446.

Ortiz, E., Pasquini, J.M., Thompson, K., Felt, B., Butkus, G., Beard, J., and Connor, J.R. (2004). Effect of manipulation of iron storage, transport, or availability on myelin composition and brain iron content in three different animal models. Journal of neuroscience research *77*, 681-689.

Ouyang, Y.B., Xu, L.J., Emery, J.F., Lee, A.S., and Giffard, R.G. (2011). Overexpressing GRP78 influences Ca2+ handling and function of mitochondria in astrocytes after ischemia-like stress. Mitochondrion *11*, 279-286.

Owh, P., da Cruz, L.A., Ackerley, C.A., and Moscarello, M.A. (1997). Increased expression of CD44 on astrocytoma cells induced by binding myelin basic protein. European journal of cell biology *74*, 172-180.

Pall, T., Pink, A., Kasak, L., Turkina, M., Anderson, W., Valkna, A., and Kogerman, P. (2011). Soluble CD44 interacts with intermediate filament protein vimentin on endothelial cell surface. PloS one *6*, e29305.

Parry, D.A., and Steinert, P.M. (1992). Intermediate filament structure. Current opinion in cell biology *4*, 94-98.

Paschen, W., Hotop, S., and Aufenberg, C. (2003). Loading neurons with BAPTA-AM activates xbp1 processing indicative of induction of endoplasmic reticulum stress. Cell calcium *33*, 83-89.

Patel, B.N., and David, S. (1997). A novel glycosylphosphatidylinositol-anchored form of ceruloplasmin is expressed by mammalian astrocytes. The Journal of biological chemistry *272*, 20185-20190.

Peach, R.J., Hollenbaugh, D., Stamenkovic, I., and Aruffo, A. (1993). Identification of hyaluronic acid binding sites in the extracellular domain of CD44. The Journal of cell biology *122*, 257-264.

Pekny, M., Leveen, P., Pekna, M., Eliasson, C., Berthold, C.H., Westermark, B., and Betsholtz, C. (1995). Mice lacking glial fibrillary acidic protein display astrocytes devoid of intermediate filaments but develop and reproduce normally. The EMBO journal *14*, 1590-1598.

Pennypacker, K.R., Thai, L., Hong, J.S., and McMillian, M.K. (1994). Prolonged expression of AP-1 transcription factors in the rat hippocampus after systemic kainate treatment. The Journal of neuroscience : the official journal of the Society for Neuroscience *14*, 3998-4006.

Phatak, P.D., Ryan, D.H., Cappuccio, J., Oakes, D., Braggins, C., Provenzano, K., Eberly, S., and Sham, R.L. (2002). Prevalence and penetrance of HFE mutations in 4865 unselected primary care patients. Blood cells, molecules & diseases *29*, 41-47.

Pickart, C.M., and Cohen, R.E. (2004). Proteasomes and their kin: proteases in the machine age. Nature reviews Molecular cell biology *5*, 177-187.

Picker, L.J., Nakache, M., and Butcher, E.C. (1989). Monoclonal antibodies to human lymphocyte homing receptors define a novel class of adhesion molecules on diverse cell types. The Journal of cell biology *109*, 927-937.

Pleasure, D., Kim, S., and Silberberg, D. (1984). In vito studies of oligodendroglis lipid metabolism. In Oligodendroglia Advanced Neurochemistry, W.T. Norton, ed. (New York: Plenum Press), pp. 175-198.

Ponta, H., Sherman, L., and Herrlich, P.A. (2003). CD44: from adhesion molecules to signalling regulators. Nature reviews Molecular cell biology *4*, 33-45.

Ponta, H., Sleeman, J., Dall, P., Moll, J., Sherman, L., and Herrlich, P. (1994). CD44 isoforms in metastatic cancer. Invasion & metastasis *14*, 82-86.

Pridmore, C.L., Baraitser, M., Harding, B., Boyd, S.G., Kendall, B., and Brett, E.M. (1993). Alexander's disease: clues to diagnosis. Journal of child neurology *8*, 134-144.

Prust, M., Wang, J., Morizono, H., Messing, A., Brenner, M., Gordon, E., Hartka, T., Sokohl, A., Schiffmann, R., Gordish-Dressman, H.*, et al.* (2011). GFAP mutations, age at onset, and clinical subtypes in Alexander disease. Neurology *77*, 1287-1294.

Qian, Z.M., To, Y., Tang, P.L., and Feng, Y.M. (1999). Transferrin receptors on the plasma membrane of cultured rat astrocytes. Experimental brain research Experimentelle Hirnforschung Experimentation cerebrale *129*, 473-476.

Quackenbush, E.J., Cruz, T.F., Moscarello, M.A., and Letarte, M. (1985). Identification of three antigens in human brain associated with similar antigens on human leukaemic cells. The Biochemical journal *225*, 291-299.

Quinlan, R. (2001). Cytoskeletal catastrophe causes brain degeneration. Nature genetics *27*, 10-11.

Rae, T.D., Schmidt, P.J., Pufahl, R.A., Culotta, V.C., and O'Halloran, T.V. (1999). Undetectable intracellular free copper: the requirement of a copper chaperone for superoxide dismutase. Science *284*, 805-808.

Rajan, K.S., Colburn, R.W., and Davis, J.M. (1976). Distribution of metal ions in the subcellular fractions of several rat brain areas. Life Sci *18*, 423-431.

Rampon, C., Weiss, N., Deboux, C., Chaverot, N., Miller, F., Buchet, D., Tricoire-Leignel, H., Cazaubon, S., Baron-Van Evercooren, A., and Couraud, P.O. (2008). Molecular mechanism of systemic delivery of neural precursor cells to the brain: assembly of brain endothelial apical cups and control of transmigration by CD44. Stem cells *26*, 1673-1682.

Rankin, W.E., Hart, M.N., and Weisenburger, D.D. (1977). Thrombotic thrombocytopenic purpura in a child with Alexander's disease. Archives of pathology & laboratory medicine *101*, 655-657.

Ravikumar, B., Vacher, C., Berger, Z., Davies, J.E., Luo, S., Oroz, L.G., Scaravilli, F., Easton, D.F., Duden, R., O'Kane, C.J.*, et al.* (2004). Inhibition of mTOR induces autophagy and reduces toxicity of polyglutamine expansions in fly and mouse models of Huntington disease. Nature genetics *36*, 585-595.

Reeves, S.A., Helman, L.J., Allison, A., and Israel, M.A. (1989). Molecular cloning and primary structure of human glial fibrillary acidic protein. Proceedings of the National Academy of Sciences of the United States of America *86*, 5178-5182.

Reichard, E.A., Ball, W.S., Jr., and Bove, K.E. (1996). Alexander disease: a case report and review of the literature. Pediatric pathology & laboratory medicine : journal of the Society for Pediatric Pathology, affiliated with the International Paediatric Pathology Association *16*, 327-343.

Renkawek, K., Bosman, G.J., and Gaestel, M. (1993). Increased expression of heat-shock protein 27 kDa in Alzheimer disease: a preliminary study. Neuroreport *5*, 14-16.

Richardson, D.R., Lane, D.J., Becker, E.M., Huang, M.L., Whitnall, M., Suryo Rahmanto, Y., Sheftel, A.D., and Ponka, P. (2010). Mitochondrial iron trafficking and the integration of iron metabolism between the mitochondrion and cytosol. Proceedings of the National Academy of Sciences of the United States of America *107*, 10775-10782.

Ridet, J.L., Malhotra, S.K., Privat, A., and Gage, F.H. (1997). Reactive astrocytes: cellular and molecular cues to biological function. Trends in neurosciences *20*, 570-577.

Riggs, J.E., Schochet, S.S., Jr., and Nelson, J. (1988). Asymptomatic adult Alexander's disease: entity or nosological misconception? Neurology *38*, 152-154.

Rivera-Zengotita, M., and Yachnis, A.T. (2012). Gliosis versus glioma?: don't grade until you know. Advances in anatomic pathology *19*, 239-249.

Roelofs, R.F., Fischer, D.F., Houtman, S.H., Sluijs, J.A., Van Haren, W., Van Leeuwen, F.W., and Hol, E.M. (2005). Adult human subventricular, subgranular, and subpial zones contain astrocytes with a specialized intermediate filament cytoskeleton. Glia *52*, 289-300.

Ron, D., and Walter, P. (2007). Signal integration in the endoplasmic reticulum unfolded protein response. Nature reviews Molecular cell biology *8*, 519-529.

Rosenthal, W. (1898). Uber eine eigenthumliche, mit syringomyelie complicirte geshwulst des ruckenmarkds. Bietr Pathol Anat *23*, 111-143.

Roskams, A.J., and Connor, J.R. (1994). Iron, transferrin, and ferritin in the rat brain during development and aging. Journal of neurochemistry *63*, 709-716.

Rossi, D., Brambilla, L., Valori, C.F., Crugnola, A., Giaccone, G., Capobianco, R., Mangieri, M., Kingston, A.E., Bloc, A., Bezzi, P.*, et al.* (2005). Defective tumor necrosis factor-alpha-dependent control of astrocyte glutamate release in a transgenic mouse model of Alzheimer disease. The Journal of biological chemistry *280*, 42088-42096.

Rouault, T.A. (2006). The role of iron regulatory proteins in mammalian iron homeostasis and disease. Nature chemical biology *2*, 406-414.

Rouault, T.A., and Cooperman, S. (2006). Brain iron metabolism. Seminars in pediatric neurology *13*, 142-148.

Russo, L.S., Jr., Aron, A., and Anderson, P.J. (1976). Alexander's disease: a report and reappraisal. Neurology *26*, 607-614.

Sambrook, J.F. (1990). The involvement of calcium in transport of secretory proteins from the endoplasmic reticulum. Cell *61*, 197-199.

Sampson, P.M., Rochester, C.L., Freundlich, B., and Elias, J.A. (1992). Cytokine regulation of human lung fibroblast hyaluronan (hyaluronic acid) production. Evidence for cytokine-regulated hyaluronan (hyaluronic acid) degradation and human lung fibroblast-derived hyaluronidase. The Journal of clinical investigation *90*, 1492-1503.

Sayre, L.M., Zelasko, D.A., Harris, P.L., Perry, G., Salomon, R.G., and Smith, M.A. (1997). 4-Hydroxynonenal-derived advanced lipid peroxidation end products are increased in Alzheimer's disease. Journal of neurochemistry *68*, 2092-2097.

Schenck, J.F., and Zimmerman, E.A. (2004). High-field magnetic resonance imaging of brain iron: birth of a biomarker? NMR in biomedicine *17*, 433-445.

Scheuner, D., Song, B., McEwen, E., Liu, C., Laybutt, R., Gillespie, P., Saunders, T., Bonner-Weir, S., and Kaufman, R.J. (2001). Translational control is required for the unfolded protein response and in vivo glucose homeostasis. Molecular cell *7*, 1165-1176.

Schipper, H.M. (2004). Heme oxygenase expression in human central nervous system disorders. Free radical biology & medicine *37*, 1995-2011.

Schipper, H.M., Vininsky, R., Brull, R., Small, L., and Brawer, J.R. (1998). Astrocyte mitochondria: a substrate for iron deposition in the aging rat substantia nigra. Experimental neurology *152*, 188-196.

Schmidt-Ott, K.M., Mori, K., Li, J.Y., Kalandadze, A., Cohen, D.J., Devarajan, P., and Barasch, J. (2007). Dual action of neutrophil gelatinase-associated lipocalin. Journal of the American Society of Nephrology : JASN *18*, 407-413.

Schroder, M., Chang, J.S., and Kaufman, R.J. (2000). The unfolded protein response represses nitrogen-starvation induced developmental differentiation in yeast. Genes & development *14*, 2962-2975.

Schroder, M., and Kaufman, R.J. (2005). ER stress and the unfolded protein response. Mutat Res *569*, 29-63.

Schulz, K., Kroner, A., and David, S. (2012). Iron efflux from astrocytes plays a role in remyelination. The Journal of neuroscience : the official journal of the Society for Neuroscience *32*, 4841-4847.

Schwankhaus, J.D., Parisi, J.E., Gulledge, W.R., Chin, L., and Currier, R.D. (1995). Hereditary adult-onset Alexander's disease with palatal myoclonus, spastic paraparesis, and cerebellar ataxia. Neurology *45*, 2266-2271.

Screaton, G.R., Bell, M.V., Jackson, D.G., Cornelis, F.B., Gerth, U., and Bell, J.I. (1992). Genomic structure of DNA encoding the lymphocyte homing receptor CD44 reveals at least 12 alternatively spliced exons. Proceedings of the National Academy of Sciences of the United States of America *89*, 12160-12164.

Seil, F.J., Schochet, S.S., Jr., and Earle, K.M. (1968). Alexander's disease in an adult. Report of a case. Archives of neurology *19*, 494-502.

Shcherbina, A., Bretscher, A., Kenney, D.M., and Remold-O'Donnell, E. (1999). Moesin, the major ERM protein of lymphocytes and platelets, differs from ezrin in its insensitivity to calpain. FEBS letters *443*, 31-36.

Sherman, L., Sleeman, J., Herrlich, P., and Ponta, H. (1994). Hyaluronate receptors: key players in growth, differentiation, migration and tumor progression. Current opinion in cell biology *6*, 726-733.

Shibuki, K., Gomi, H., Chen, L., Bao, S., Kim, J.J., Wakatsuki, H., Fujisaki, T., Fujimoto, K., Katoh, A., Ikeda, T.*, et al.* (1996). Deficient cerebellar long-term depression, impaired eyeblink conditioning, and normal motor coordination in GFAP mutant mice. Neuron *16*, 587-599.

Shinohara, H., Inaguma, Y., Goto, S., Inagaki, T., and Kato, K. (1993). Alpha B crystallin and HSP28 are enhanced in the cerebral cortex of patients with Alzheimer's disease. Journal of the neurological sciences *119*, 203-208.

Shiroma, N., Kanazawa, N., Kato, Z., Shimozawa, N., Imamura, A., Ito, M., Ohtani, K., Oka, A., Wakabayashi, K., Iai, M.*, et al.* (2003). Molecular genetic study in Japanese patients with Alexander disease: a novel mutation, R79L. Brain & development *25*, 116-121.

Siegel, S.J., Bieschke, J., Powers, E.T., and Kelly, J.W. (2007). The oxidative stress metabolite 4-hydroxynonenal promotes Alzheimer protofibril formation. Biochemistry *46*, 1503-1510.

Sloane, B.F., Sameni, M., Podgorski, I., Cavallo-Medved, D., and Moin, K. (2006). Functional imaging of tumor proteolysis. Annual review of pharmacology and toxicology *46*, 301-315.

Sloane, J.A., Batt, C., Ma, Y., Harris, Z.M., Trapp, B., and Vartanian, T. (2010). Hyaluronan blocks oligodendrocyte progenitor maturation and remyelination through TLR2. Proceedings of the National Academy of Sciences of the United States of America *107*, 11555-11560.

Soffer, D., and Horoupian, D.S. (1979). Rosenthal fibers formation in the central nervous system. Its relation to Alexander's disease. Acta neuropathologica *47*, 81-84.

Sonnenberg, A., and Liem, R.K. (2007). Plakins in development and disease. Experimental cell research *313*, 2189-2203.

Sosunov, A.A., Guilfoyle, E., Wu, X., McKhann 2nd, G.M., and Goldman, J.E. (2013). Phenotypic Conversions of “Protoplasmic” to “Reactive” Astrocytes in Alexander Disease. Journal of Neuroscience *33*, 7439-7450.

Sotelo, J., Toh, B.H., Lolait, S.J., Yildiz, A., Osung, O., and Holborow, E.J. (1980). Cytoplasmic intermediate filaments in cultured glial cells. Neuropathology and applied neurobiology *6*, 291-298.

Soum, E., and Drapier, J.C. (2003). Nitric oxide and peroxynitrite promote complete disruption of the [4Fe-4S] cluster of recombinant human iron regulatory protein 1. Journal of biological inorganic chemistry : JBIC : a publication of the Society of Biological Inorganic Chemistry *8*, 226-232.

Springer, S., Erlewein, R., Naegele, T., Becker, I., Auer, D., Grodd, W., and Krageloh-Mann, I. (2000). Alexander disease--classification revisited and isolation of a neonatal form. Neuropediatrics *31*, 86-92.

Stamenkovic, I., Aruffo, A., Amiot, M., and Seed, B. (1991). The hematopoietic and epithelial forms of CD44 are distinct polypeptides with different adhesion potentials for hyaluronate-bearing cells. The EMBO journal *10*, 343-348.

Steinert, P.M., and Roop, D.R. (1988). Molecular and cellular biology of intermediate filaments. Annual review of biochemistry *57*, 593-625.

Stemmer-Rachamimov, A.O., Gonzalez-Agosti, C., Xu, L., Burwick, J.A., Beauchamp, R., Pinney, D., Louis, D.N., and Ramesh, V. (1997). Expression of NF2-encoded merlin and related ERM family proteins in the human central nervous system. Journal of neuropathology and experimental neurology *56*, 735-742.

Stumpf, E., Masson, H., Duquette, A., Berthelet, F., McNabb, J., Lortie, A., Lesage, J., Montplaisir, J., Brais, B., and Cossette, P. (2003). Adult Alexander disease with autosomal dominant transmission: a distinct entity caused by mutation in the glial fibrillary acid protein gene. Archives of neurology *60*, 1307-1312.

Su, W., Xing, R., Foster, S., Acevedo, S., Raber, J., and Sherman, L.S. (2010). CD44 and hyaluronan regulate adult hippocampal neurogenesis In Soceiety for Neuroscience (San Diego: Program #

31.1/C18).

Takamiya, A., Takeda, M., Yoshida, A., and Kiyama, H. (2002). Inflammation induces serine protease inhibitor 3 expression in the rat pineal gland. Neuroscience *113*, 387-394.

Takanashi, J., Sugita, K., Tanabe, Y., and Niimi, H. (1998). Adolescent case of Alexander disease: MR imaging and MR spectroscopy. Pediatric neurology *18*, 67-70.

Takewaka, T., Zimmer, T., Hirata, A., Ohta, A., and Takagi, M. (1999). Null mutation in IRE1 gene inhibits overproduction of microsomal cytochrome P450Alk1 (CYP 52A3) and proliferation of the endoplasmic reticulum in Saccharomyces cerevisiae. Journal of biochemistry *125*, 507-514.

Tammi, R., Rilla, K., Pienimaki, J.P., MacCallum, D.K., Hogg, M., Luukkonen, M., Hascall, V.C., and Tammi, M. (2001). Hyaluronan enters keratinocytes by a novel endocytic route for catabolism. The Journal of biological chemistry *276*, 35111-35122.

Tanaka, H., Katoh, A., Oguro, K., Shimazaki, K., Gomi, H., Itohara, S., Masuzawa, T., and Kawai, N. (2002). Disturbance of hippocampal long-term potentiation after transient ischemia in GFAP deficient mice. Journal of neuroscience research *67*, 11-20.

Tang, G., Perng, M.D., Wilk, S., Quinlan, R., and Goldman, J.E. (2010). Oligomers of mutant glial fibrillary acidic protein (GFAP) Inhibit the proteasome system in alexander disease astrocytes, and the small heat shock protein alphaB-crystallin reverses the inhibition. The Journal of biological chemistry *285*, 10527-10537.

Tang, G., Xu, Z., and Goldman, J.E. (2006). Synergistic effects of the SAPK/JNK and the proteasome pathway on glial fibrillary acidic protein (GFAP) accumulation in Alexander disease. The Journal of biological chemistry *281*, 38634-38643.

Tang, G., Yue, Z., Talloczy, Z., Hagemann, T., Cho, W., Messing, A., Sulzer, D.L., and Goldman, J.E. (2008). Autophagy induced by Alexander disease-mutant GFAP accumulation is regulated by p38/MAPK and mTOR signaling pathways. Human molecular genetics *17*, 1540-1555.

Thomas, L., Byers, H.R., Vink, J., and Stamenkovic, I. (1992). CD44H regulates tumor cell migration on hyaluronate-coated substrate. The Journal of cell biology *118*, 971-977.

Thompson, K., Menzies, S., Muckenthaler, M., Torti, F.M., Wood, T., Torti, S.V., Hentze, M.W., Beard, J., and Connor, J. (2003). Mouse brains deficient in H-ferritin have normal iron concentration but a protein profile of iron deficiency and increased evidence of oxidative stress. Journal of neuroscience research *71*, 46-63.

Thyagarajan, D., Chataway, T., Li, R., Gai, W.P., and Brenner, M. (2004). Dominantly-inherited adult-onset leukodystrophy with palatal tremor caused by a mutation in the glial fibrillary acidic protein gene. Movement disorders : official journal of the Movement Disorder Society *19*, 1244-1248.

Tian, R., Gregor, M., Wiche, G., and Goldman, J.E. (2006). Plectin regulates the organization of glial fibrillary acidic protein in Alexander disease. The American journal of pathology *168*, 888-897.

Tian, R., Wu, X., Hagemann, T.L., Sosunov, A.A., Messing, A., McKhann, G.M., and Goldman, J.E. (2010). Alexander disease mutant glial fibrillary acidic protein compromises glutamate transport in astrocytes. Journal of neuropathology and experimental neurology *69*, 335-345.

Tihen, W.S. (1972). Central pontine myelinolysis and Rosenthal fibers of the brainstem. Association with emaciation and prolonged intravenous hyperalimentation. Neurology *22*, 710-716.

Todorich, B., Pasquini, J.M., Garcia, C.I., Paez, P.M., and Connor, J.R. (2009). Oligodendrocytes and myelination: the role of iron. Glia *57*, 467-478.

Tomokane, N., Iwaki, T., Tateishi, J., Iwaki, A., and Goldman, J.E. (1991). Rosenthal fibers share epitopes with alpha B-crystallin, glial fibrillary acidic protein, and ubiquitin, but not with vimentin. Immunoelectron microscopy with colloidal gold. The American journal of pathology *138*, 875-885.

Tong, W.H., and Rouault, T.A. (2007). Metabolic regulation of citrate and iron by aconitases: role of iron-sulfur cluster biogenesis. Biometals *20*, 549-564.

Toole, B.P. (2004). Hyaluronan: from extracellular glue to pericellular cue. Nature reviews Cancer *4*, 528-539.

Tout, S., Dreher, Z., Chan-Ling, T., and Stone, J. (1993). Contact-spacing among astrocytes is independent of neighbouring structures: in vivo and in vitro evidence. The Journal of comparative neurology *332*, 433-443.

Towfighi, J., Young, R., Sassani, J., Ramer, J., and Horoupian, D.S. (1983). Alexander's disease: further light-, and electron-microscopic observations. Acta neuropathologica *61*, 36-42.

Townsend, J.J., Wilson, J.F., Harris, T., Coulter, D., and Fife, R. (1985). Alexander's disease. Acta neuropathologica *67*, 163-166.

Tsukita, S., Oishi, K., Sato, N., Sagara, J., Kawai, A., and Tsukita, S. (1994). ERM family members as molecular linkers between the cell surface glycoprotein CD44 and actin-based cytoskeletons. The Journal of cell biology *126*, 391-401.

Uchida, K. (2003). 4-Hydroxy-2-nonenal: a product and mediator of oxidative stress. Progress in lipid research *42*, 318-343.

Ueda, F., Raja, K.B., Simpson, R.J., Trowbridge, I.S., and Bradbury, M.W. (1993). Rate of 59Fe uptake into brain and cerebrospinal fluid and the influence thereon of antibodies against the transferrin receptor. Journal of neurochemistry *60*, 106-113.

Underhill, C.B., Thurn, A.L., and Lacy, B.E. (1985). Characterization and identification of the hyaluronate binding site from membranes of SV-3T3 cells. The Journal of biological chemistry *260*, 8128-8133.

Valko, M., Morris, H., and Cronin, M.T. (2005). Metals, toxicity and oxidative stress. Current medicinal chemistry *12*, 1161-1208.

van der Knaap, M.S., Barth, P.G., Vrensen, G.F., and Valk, J. (1996). Histopathology of an infantile-onset spongiform leukoencephalopathy with a discrepantly mild clinical course. Acta neuropathologica *92*, 206-212.

van der Knaap, M.S., Naidu, S., Breiter, S.N., Blaser, S., Stroink, H., Springer, S., Begeer, J.C., van Coster, R., Barth, P.G., Thomas, N.H.*, et al.* (2001). Alexander disease: diagnosis with MR imaging. AJNR American journal of neuroradiology *22*, 541-552.

van der Knaap, M.S., Valk, J., Barth, P.G., Smit, L.M., van Engelen, B.G., and Tortori Donati, P. (1995). Leukoencephalopathy with swelling in children and adolescents: MRI patterns and differential diagnosis. Neuroradiology *37*, 679-686.

van der Voorn, J.P., Pouwels, P.J., Salomons, G.S., Barkhof, F., and van der Knaap, M.S. (2009). Unraveling pathology in juvenile Alexander disease: serial quantitative MR imaging and spectroscopy of white matter. Neuroradiology *51*, 669-675.

van Weering, D.H., Baas, P.D., and Bos, J.L. (1993). A PCR-based method for the analysis of human CD44 splice products. PCR methods and applications *3*, 100-106.

Vassiliev, V., Harris, Z.L., and Zatta, P. (2005). Ceruloplasmin in neurodegenerative diseases. Brain research Brain research reviews *49*, 633-640.

Vembar, S.S., and Brodsky, J.L. (2008). One step at a time: endoplasmic reticulum-associated degradation. Nature reviews Molecular cell biology *9*, 944-957.

Vermot-Desroches, C., Wijdenes, J., Valmu, L., Roy, C., Pigott, R., Nortamo, P., and Gahmberg, C.G. (1995). A CD44 monoclonal antibody differentially regulates CD11a/CD18 binding to intercellular adhesion molecules CD54, CD102 and CD50. Eur J Immunol *25*, 2460-2464.

Visvader, J.E., and Lindeman, G.J. (2008). Cancer stem cells in solid tumours: accumulating evidence and unresolved questions. Nature reviews Cancer *8*, 755-768.

Vogel, F.S., and Hallervorden, J. (1962). Leukodystrophy with Diffuse Rosenthal Fiber Formation. Acta neuropathologica, 126-143.

Voskuhl, R.R., Peterson, R.S., Song, B., Ao, Y., Morales, L.B., Tiwari-Woodruff, S., and Sofroniew, M.V. (2009). Reactive astrocytes form scar-like perivascular barriers to leukocytes during adaptive immune inflammation of the CNS. The Journal of neuroscience : the official journal of the Society for Neuroscience *29*, 11511-11522.

Vulpe, C.D., Kuo, Y.M., Murphy, T.L., Cowley, L., Askwith, C., Libina, N., Gitschier, J., and Anderson, G.J. (1999). Hephaestin, a ceruloplasmin homologue implicated in intestinal iron transport, is defective in the sla mouse. Nature genetics *21*, 195-199.

Walls, T.J., Jones, R.A., Cartlidge, N., and Saunders, M. (1984). Alexander's disease with Rosenthal fibre formation in an adult. Journal of neurology, neurosurgery, and psychiatry *47*, 399-403.

Wang, J., and Pantopoulos, K. (2011). Regulation of cellular iron metabolism. The Biochemical journal *434*, 365-381.

Wang, L., Colodner, K.J., and Feany, M.B. (2011). Protein misfolding and oxidative stress promote glial-mediated neurodegeneration in an Alexander disease model. The Journal of neuroscience : the official journal of the Society for Neuroscience *31*, 2868-2877.

Wang, X., Messing, A., and David, S. (1997). Axonal and nonneuronal cell responses to spinal cord injury in mice lacking glial fibrillary acidic protein. Experimental neurology *148*, 568-576.

Wang, X.S., Ong, W.Y., and Connor, J.R. (2002). A light and electron microscopic study of divalent metal transporter-1 distribution in the rat hippocampus, after kainate-induced neuronal injury. Experimental neurology *177*, 193-201.

Wang, X.Z., Lawson, B., Brewer, J.W., Zinszner, H., Sanjay, A., Mi, L.J., Boorstein, R., Kreibich, G., Hendershot, L.M., and Ron, D. (1996). Signals from the stressed endoplasmic reticulum induce C/EBP-homologous protein (CHOP/GADD153). Molecular and cellular biology *16*, 4273-4280.

Ward, C.L., and Kopito, R.R. (1994). Intracellular turnover of cystic fibrosis transmembrane conductance regulator. Inefficient processing and rapid degradation of wild-type and mutant proteins. The Journal of biological chemistry *269*, 25710-25718.

Weigel, J.A., and Weigel, P.H. (2003). Characterization of the recombinant rat 175-kDa hyaluronan receptor for endocytosis (HARE). The Journal of biological chemistry *278*, 42802-42811.

Welch, K.D., Davis, T.Z., Van Eden, M.E., and Aust, S.D. (2002). Deleterious iron-mediated oxidation of biomolecules. Free radical biology & medicine *32*, 577-583.

Werner, E.D., Brodsky, J.L., and McCracken, A.A. (1996). Proteasome-dependent endoplasmic reticulum-associated protein degradation: an unconventional route to a familiar fate. Proceedings of the National Academy of Sciences of the United States of America *93*, 13797-13801.

Wiggins, R.C., Benjamins, J.A., Krigman, M.R., and Morell, P. (1974). Synthesis of myelin proteins during starvation. Brain research *80*, 345-349.

Wilhelmsson, U., Bushong, E.A., Price, D.L., Smarr, B.L., Phung, V., Terada, M., Ellisman, M.H., and Pekny, M. (2006). Redefining the concept of reactive astrocytes as cells that remain within their unique domains upon reaction to injury. Proceedings of the National Academy of Sciences of the United States of America *103*, 17513-17518.

Williams, B.L., and Lipkin, W.I. (2006). Endoplasmic reticulum stress and neurodegeneration in rats neonatally infected with borna disease virus. Journal of virology *80*, 8613-8626.

Wippold, F.J., 2nd, Perry, A., and Lennerz, J. (2006). Neuropathology for the neuroradiologist: Rosenthal fibers. AJNR American journal of neuroradiology *27*, 958-961.

Wiranowska, M., Ladd, S., Smith, S.R., and Gottschall, P.E. (2006). CD44 adhesion molecule and neuro-glial proteoglycan NG2 as invasive markers of glioma. Brain cell biology *35*, 159-172.

Wohlwill, F.J., Bernstein, J., and Yakovlev, P.I. (1959). Dysmyelinogenic leukodystrophy; report of a case of a new, presumably familial type of leukodystrophy with megalobarencephaly. Journal of neuropathology and experimental neurology *18*, 359-383.

Wohlwill, F.J., and Paine, R.S. (1958). Progressive demyelinating leukoencephalopathy. Neurology *8*, 285-295.

Wu, J., Hua, Y., Keep, R.F., Nakamura, T., Hoff, J.T., and Xi, G. (2003). Iron and iron-handling proteins in the brain after intracerebral hemorrhage. Stroke; a journal of cerebral circulation *34*, 2964-2969.

Wu, L.L., Zhang, L., Shao, J., Qin, Y.F., Yang, R.W., and Zhao, Z.Y. (2008). Effect of perinatal iron deficiency on myelination and associated behaviors in rat pups. Behavioural brain research *188*, 263-270.

Wu, T., and Hua, X. (2011). Menin represses tumorigenesis via repressing cell proliferation. American journal of cancer research *1*, 726-739.

Yang, D.D., Kuan, C.Y., Whitmarsh, A.J., Rincon, M., Zheng, T.S., Davis, R.J., Rakic, P., and Flavell, R.A. (1997). Absence of excitotoxicity-induced apoptosis in the hippocampus of mice lacking the Jnk3 gene. Nature *389*, 865-870.

Yang, J., Goetz, D., Li, J.Y., Wang, W., Mori, K., Setlik, D., Du, T., Erdjument-Bromage, H., Tempst, P., Strong, R.*, et al.* (2002). An iron delivery pathway mediated by a lipocalin. Molecular cell *10*, 1045-1056.

Yeh, K.Y., Yeh, M., Mims, L., and Glass, J. (2009). Iron feeding induces ferroportin 1 and hephaestin migration and interaction in rat duodenal epithelium. American journal of physiology Gastrointestinal and liver physiology *296*, G55-65.

Yonemura, S., Hirao, M., Doi, Y., Takahashi, N., Kondo, T., Tsukita, S., and Tsukita, S. (1998). Ezrin/radixin/moesin (ERM) proteins bind to a positively charged amino acid cluster in the juxta-membrane cytoplasmic domain of CD44, CD43, and ICAM-2. The Journal of cell biology *140*, 885-895.

Yoritaka, A., Hattori, N., Uchida, K., Tanaka, M., Stadtman, E.R., and Mizuno, Y. (1996). Immunohistochemical detection of 4-hydroxynonenal protein adducts in Parkinson disease. Proceedings of the National Academy of Sciences of the United States of America *93*, 2696-2701.

Yu, W.H., Woessner, J.F., Jr., McNeish, J.D., and Stamenkovic, I. (2002). CD44 anchors the assembly of matrilysin/MMP-7 with heparin-binding epidermal growth factor precursor and ErbB4 and regulates female reproductive organ remodeling. Genes & development *16*, 307-323.

Yu, Z., Luo, H., Fu, W., and Mattson, M.P. (1999). The endoplasmic reticulum stress-responsive protein GRP78 protects neurons against excitotoxicity and apoptosis: suppression of oxidative stress and stabilization of calcium homeostasis. Experimental neurology *155*, 302-314.

Zahs, K.R., Bigornia, V., and Deschepper, C.F. (1993). Characterization of "plasma proteins" secreted by cultured rat macroglial cells. Glia *7*, 121-133.

Zamanian, J.L., Xu, L., Foo, L.C., Nouri, N., Zhou, L., Giffard, R.G., and Barres, B.A. (2012). Genomic analysis of reactive astrogliosis. The Journal of neuroscience : the official journal of the Society for Neuroscience *32*, 6391-6410.

Zecca, L., Gallorini, M., Schunemann, V., Trautwein, A.X., Gerlach, M., Riederer, P., Vezzoni, P., and Tampellini, D. (2001). Iron, neuromelanin and ferritin content in the substantia nigra of normal subjects

at different ages: consequences for iron storage and neurodegenerative processes. Journal of neurochemistry *76*, 1766-1773.

Zelenika, D., Grima, B., Brenner, M., and Pessac, B. (1995). A novel glial fibrillary acidic protein mRNA lacking exon 1. Brain research Molecular brain research *30*, 251-258.

Zimmer, T., Ogura, A., Ohta, A., and Takagi, M. (1999). Misfolded membrane-bound cytochrome P450 activates KAR2 induction through two distinct mechanisms. Journal of biochemistry *126*, 1080-1089.